

*TIM Lee*

NUREG/CR-3046  
PNL-4385  
Vol. 4

---

---

# COBRA/TRAC - A Thermal-Hydraulics Code for Transient Analysis of Nuclear Reactor Vessels and Primary Coolant Systems

Developmental Assessment and Data Comparisons

---

---

Prepared by M. J. Thurgood, T. E. Guidotti, G. A. Sly,  
J. M. Kelly, R. J. Kohrt, K. R. Crowell,  
C. A. Wilkins, J. M. Cuta, S. H. Bian

**Pacific Northwest Laboratory**  
Operated by  
Battelle Memorial Institute

Prepared for  
**U.S. Nuclear Regulatory  
Commission**

## NOTICE

This report was prepared as an account of work sponsored by an agency of the United States Government. Neither the United States Government nor any agency thereof, or any of their employees, makes any warranty, expressed or implied, or assumes any legal liability of responsibility for any third party's use, or the results of such use, of any information, apparatus, product or process disclosed in this report, or represents that its use by such third party would not infringe privately owned rights.

### Availability of Reference Materials Cited in NRC Publications

Most documents cited in NRC publications will be available from one of the following sources:

1. The NRC Public Document Room, 1717 H Street, N.W.  
Washington, DC 20555
2. The NRC/GPO Sales Program, U.S. Nuclear Regulatory Commission,  
Washington, DC 20555
3. The National Technical Information Service, Springfield, VA 22161

Although the listing that follows represents the majority of documents cited in NRC publications, it is not intended to be exhaustive.

Referenced documents available for inspection and copying for a fee from the NRC Public Document Room include NRC correspondence and internal NRC memoranda; NRC Office of Inspection and Enforcement bulletins, circulars, information notices, inspection and investigation notices; Licensee Event Reports; vendor reports and correspondence; Commission papers; and applicant and licensee documents and correspondence.

The following documents in the NUREG series are available for purchase from the NRC/GPO Sales Program: formal NRC staff and contractor reports, NRC-sponsored conference proceedings, and NRC booklets and brochures. Also available are Regulatory Guides, NRC regulations in the *Code of Federal Regulations*, and *Nuclear Regulatory Commission Issuances*.

Documents available from the National Technical Information Service include NUREG series reports and technical reports prepared by other federal agencies and reports prepared by the Atomic Energy Commission, forerunner agency to the Nuclear Regulatory Commission.

Documents available from public and special technical libraries include all open literature items, such as books, journal and periodical articles, and transactions. *Federal Register* notices, federal and state legislation, and congressional reports can usually be obtained from these libraries.

Documents such as theses, dissertations, foreign reports and translations, and non-NRC conference proceedings are available for purchase from the organization sponsoring the publication cited.

Single copies of NRC draft reports are available free upon written request to the Division of Technical Information and Document Control, U.S. Nuclear Regulatory Commission, Washington, DC 20555.

Copies of industry codes and standards used in a substantive manner in the NRC regulatory process are maintained at the NRC Library, 7920 Norfolk Avenue, Bethesda, Maryland, and are available there for reference use by the public. Codes and standards are usually copyrighted and may be purchased from the originating organization or, if they are American National Standards, from the American National Standards Institute, 1430 Broadway, New York, NY 10018.

---

---

# COBRA/TRAC - A Thermal-Hydraulics Code for Transient Analysis of Nuclear Reactor Vessels and Primary Coolant Systems

Developmental Assessment and Data Comparisons

---

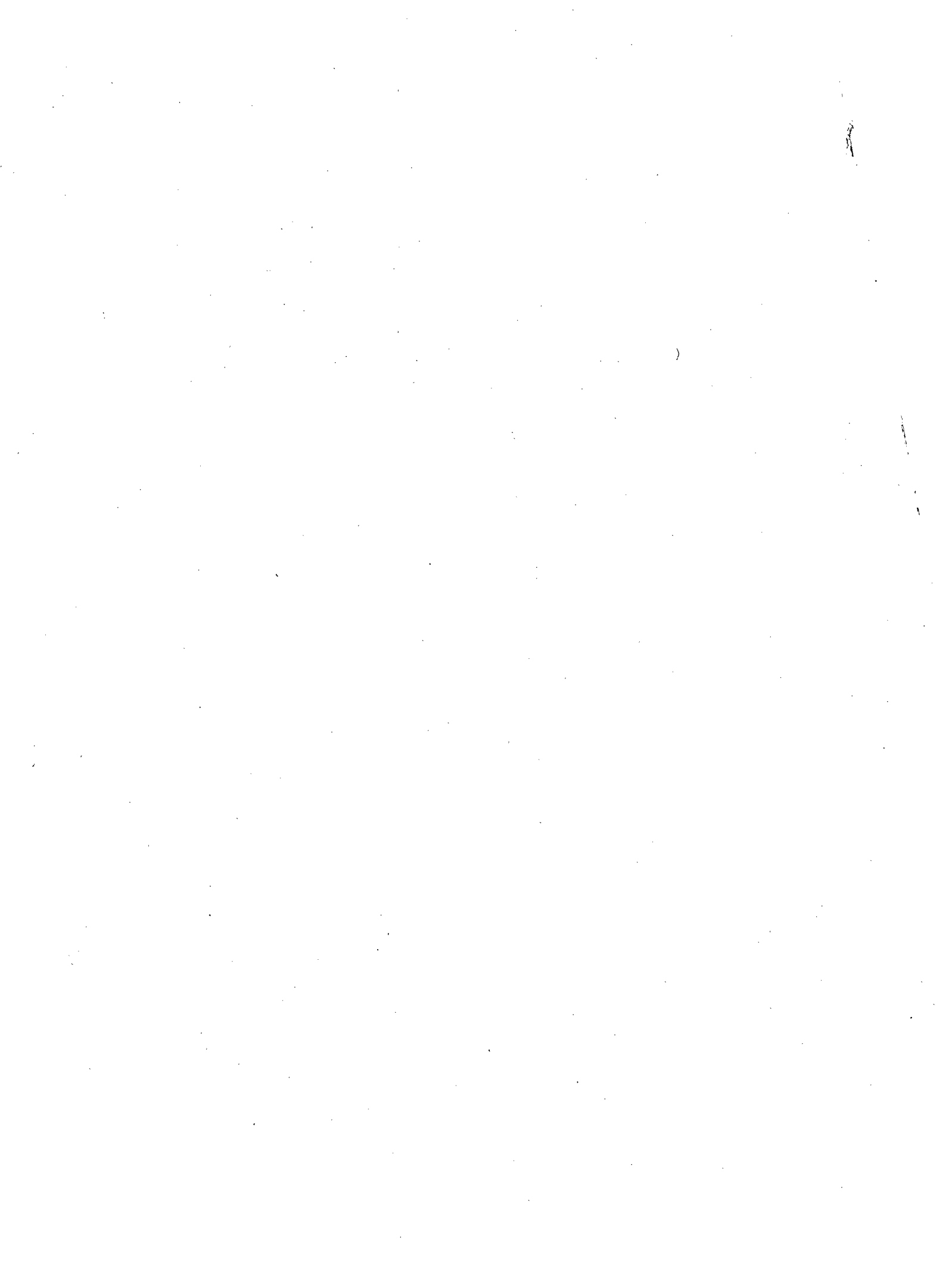
---

Manuscript Completed: November 1982  
Date Published: March 1983

Prepared by  
M. J. Thurgood, T. E. Guidotti, G. A. Sly,  
J. M. Kelly, R. J. Kohrt, K. R. Crowell  
C. A. Wilkins, J. M. Cuta, S. H. Bian

Pacific Northwest Laboratory  
Richland, WA 99352

Prepared for  
Division of Accident Evaluation  
Office of Nuclear Regulatory Research  
U.S. Nuclear Regulatory Commission  
Washington, D.C. 20555  
NRC FIN B2391



## ABSTRACT

The COBRA/TRAC computer program has been developed to predict the thermal-hydraulic response of nuclear reactor primary coolant systems to small and large break loss-of-coolant accidents and other anticipated transients. The code solves the compressible three-dimensional, two-fluid, three-field equations for two-phase flow in the reactor vessel. The three fields are the vapor field, the continuous liquid field, and the liquid drop field. A five-equation drift flux model is used to model fluid flow in the primary system piping, pressurizer, pumps, and accumulators. The heat generation rate of the core is specified by input and no reactor kinetics calculations are included in the solution. This volume documents the major data comparisons made with COBRA/TRAC during the process of code development. These data comparisons were extremely useful in detecting programming errors and defining deficiencies in the code's physical models. The data comparisons presented in this volume document the results obtained on developmental versions of the code. A separate document will be released at a later date containing data comparisons run on the final released version of the code.



## CONTENTS

ACKNOWLEDGEMENTS.....	xix
1.0 INTRODUCTION.....	1.1
2.0 DATA COMPARISONS PERFORMED WITH DEVELOPMENTAL VERSIONS OF COBRA/TRAC .....	2.1
2.1 DARTMOUTH COUNTERCURRENT FLOW TUBE FLOODING EXPERIMENTS.....	2.3
2.1.1 Description of Experiment.....	2.3
2.1.2 COBRA/TRAC Model .....	2.4
2.1.3 Discussion of Results.....	2.6
2.2 NORTHWESTERN UNIVERSITY ORIFICE PLATE FLOODING EXPERIMENT.....	2.8
2.2.1 Description of Experiment.....	2.8
2.2.2 COBRA/TRAC Model Description.....	2.9
2.2.3 Discussion of Results.....	2.10
2.3. CREARE 1/15th SCALE DOWNCOMER ECC BYPASS EXPERIMENTS.....	2.11
2.3.1 Description of Experiment.....	2.12
2.3.2 COBRA/TRAC Model Description.....	2.13
2.3.3 Discussion of Results.....	2.14
2.4 BATTELLE COLUMBUS 2/15ths SCALE DOWNCOMER TRANSIENT ECC BYPASS EXPERIMENT.....	2.15
2.4.1 Description of Experiment.....	2.18
2.4.2 COBRA/TRAC Model Description.....	2.19
2.4.3 Discussion of Results.....	2.22
2.5 FEBA FORCED BOTTOM REFLOOD EXPERIMENT.....	2.25
2.5.1 Description of Experiment.....	2.25
2.5.2 COBRA/TRAC Model Description.....	2.29

2.5.3	Discussion of Results.....	2.31
2.6	FLECHT LOW FLOODING RATE COSINE TEST SERIES.....	2.37
2.6.1	Description of Experiment.....	2.37
2.6.2	COBRA/TRAC Model Description.....	2.39
2.6.3	Discussion of Results.....	2.43
2.7	STANDARD PROBLEM NO. 9.....	2.50
2.7.1	Experimental Description.....	2.57
2.7.2	COBRA/TRAC Model Description.....	2.60
2.7.3	Discussion of Results.....	2.62
2.8	NRU NUCLEAR FUEL ROD FORCED REFLOOD EXPERIMENT.....	2.74
2.8.1	Experimental Description.....	2.74
2.8.2	COBRA/TRAC Model Description.....	2.78
2.8.3	Discussion of Results.....	2.80
2.9	PKL GRAVITY REFLOOD EXPERIMENT K9.....	2.91
2.9.1	Description of Experiment.....	2.91
2.9.2	COBRA/TRAC Model Description.....	2.93
2.9.3	Discussion of Results.....	2.95
2.10	CYLINDRICAL CORE TEST FACILITY GRAVITY REFLOOD.....	2.105
2.10.1	Description of Experiment.....	2.105
2.10.2	COBRA/TRAC Model Description.....	2.108
2.10.3	Discussion of Results.....	2.108
2.11	NORTHWESTERN UNIVERSITY COUNTERCURRENT FLOW FILM CONDENSATION EXPERIMENT.....	2.122
2.11.1	Description of Experiment.....	2.122
2.11.2	COBRA/TRAC Model Description.....	2.124
2.11.3	Discussion of Results.....	2.126

2.12	RPI FLAT PLATE PHASE DISTRIBUTION EXPERIMENT.....	2.127
2.12.1	Description of Experiment.....	2.127
2.12.2	COBRA/TRAC Model Description.....	2.129
2.12.3	Discussion of Results.....	2.129
2.13	BENNETT TUBE CRITICAL HEAT FLUX EXPERIMENTS.....	2.136
2.13.1	Description of Experiment.....	2.136
2.13.2	COBRA/TRAC Model Description.....	2.137
2.13.3	Discussion of Results.....	2.138
2.14	FRIGG FORCED CONVECTION TESTS.....	2.151
2.14.1	Description of Experiment.....	2.151
2.14.2	COBRA/TRAC Model Description.....	2.152
2.14.3	Discussion of Results.....	2.153
2.15	FRIGG NATURAL CIRCULATION TESTS.....	2.157
2.15.1	Description of Experiment.....	2.157
2.15.2	COBRA/TRAC Model Description.....	2.159
2.15.3	Discussion of Results.....	2.159
2.16	SEMISCALE MOD3 TEST S-07-6.....	2.164
2.16.1	Description of Experiment.....	2.164
2.16.2	COBRA/TRAC Model Description.....	2.165
2.16.3	Discussion of Results.....	2.169
2.17	SEMISCALE MOD2A TEST S-UT-2.....	2.173
2.17.1	Description of Experiment.....	2.173
2.17.2	COBRA/TRAC Model Description.....	2.176
2.17.3	Discussion of Results.....	2.178
2.18	WESTINGHOUSE UPPER HEAD DRAIN TEST.....	2.188
2.18.1	Description of Experiment.....	2.188

2.18.2 COBRA/TRAC Model Description.....2.189  
2.18.3 Discussion of Results.....2.190  
REFERENCES .....R.1  
APPENDIX A .....A.1

## FIGURES

2.1-1	Experimental Setup for Flooding in Large Tubes.....	2.5
2.1-2	Liquid Penetration in 2-in. Tube.....	2.7
2.1-3	Liquid Penetration in 10-in. Tube.....	2.7
2.2-1	COBRA/TRAC Model of Northwestern University CCFL Experimental Facility.....	2.9
2.2-2	Liquid Penetration - $DBUB_{MAX} = \text{Hydraulic Diameter}$ .....	2.11
2.2-3	Liquid Penetration - $DBUB_{MAX} = 2*(\text{hydraulic diameter})$ .....	2.12
2.3-1	Schematic of CREARE Downcomer Vessel.....	2.13
2.3-2	COBRA/TRAC Model of CREARE Downcomer.....	2.14
2.3-3	Downcomer Penetration Curve - Saturated ECC Water at 30 GPM....	2.16
2.3-4	Downcomer Penetration Curve - Saturated ECC Water at 120 GPM...	2.16
2.3-5	Downcomer Penetration Curve - Subcooled ECC Water at 30 GPM....	2.17
2.3-6	Downcomer Penetration Curve - Subcooled ECC Water at 120 GPM...	2.17
2.4-1	Diagram of Battelle Columbus 2/15th Scale Downcomer Vessel.....	2.19
2.4-2	COBRA/TRAC Model of BCL Downcomer.....	2.20
2.4-3	Lower Plenum Liquid Volume vs. Time for Test 404.....	2.23
2.4-4	Lower Plenum Liquid Volume vs. Time for Test 501.....	2.23
2.4-5	Lower Plenum Pressure vs. Time for Test 501.....	2.24
2.4-6	Net Condensation Rate in the Vessel vs. Time for Test 404.....	2.24
2.5-1	Schematic of FEBA Test Facility.....	2.26
2.5-2	Cross Section of FEBA 5x5 Test Section Bundle Representative Heater Rod.....	2.28
2.5-3	Axial Power Profile and Grid Spacer Locations for FEBA Test Section.....	2.28
2.5-4	Power Decay Curve for FEBA Test Run 216.....	2.29
2.5-5	COBRA/TRAC Model of FEBA Test Section.....	2.30
2.5-6	COBRA/TRAC Initial Rod Temperatures vs. Axial Position.....	2.32

2.5-7	Test Section Axial Power Profile and COBRA/TRAC Model of the Axial Power Profile.....	2.32
2.5-8	COBRA/TRAC Predicted Rod Temperatures at 0.8m for FEBA Test 216.....	2.33
2.5-9	COBRA/TRAC Predicted Rod Temperatures at 1.3m for FEBA Test 216.....	2.33
2.5-10	COBRA/TRAC Predicted Rod Temperatures at 1.9m for FEBA Test 216.....	2.34
2.5-11	COBRA/TRAC Predicted Rod Temperatures at 2.4m for FEBA Test 216.....	2.34
2.5-12	COBRA/TRAC Predicted Rod Temperatures at 3.0m for FEBA Test 216.....	2.35
2.5-13	COBRA/TRAC Predicted Rod Temperatures at 3.5m for FEBA Test 216.....	2.35
2.5-14	Collapsed Liquid Level vs. Time for FEBA Test 216.....	2.36
2.6-1	FLECHT Test Bundle Cross Section.....	2.38
2.6-2	FLECHT Test Section Axial Power Profile and Grid Elevations....	2.39
2.6-3	COBRA/TRAC Model of FLECHT Test Section.....	2.41
2.6-4	Temperature at 2-ft Elevation - FLECHT 00904.....	2.44
2.6-5	Temperature at 4-ft Elevation - FLECHT 00904.....	2.44
2.6-6	Temperature at 6-ft Elevation - FLECHT 00904.....	2.45
2.6-7	Temperature at 7-ft Elevation - FLECHT 00904.....	2.45
2.6-8	Temperature at 9-ft Elevation - FLECHT 00904.....	2.46
2.6-9	Temperature at 10-ft Elevation - FLECHT 00904.....	2.46
2.6-10	Vapor Fraction at 0 to 2-ft Elevation for FLECHT 00904.....	2.47
2.6-11	Vapor Fraction at 2 to 4-ft Elevation for FLECHT 00904.....	2.47
2.6-12	Vapor Fraction at 4 to 6-ft Elevation for FLECHT 00904.....	2.48
2.6-13	Vapor Fraction at 6 to 8-ft Elevation for FLECHT 00904.....	2.48
2.6-14	Vapor Fraction at 8 to 10-ft Elevation for FLECHT 00904.....	2.49
2.6-15	Vapor Fraction at 10 to 12-ft Elevation for FLECHT 00904.....	2.49

2.6-16	Temperature at 2-ft Elevation--FLECHT 04444.....	2.51
2.6-17	Temperature at 4-ft Elevation--FLECHT 04444.....	2.51
2.6-18	Temperature at 6-ft Elevation--FLECHT 04444.....	2.52
2.6-19	Temperature at 7-ft Elevation--FLECHT 04444.....	2.52
2.6-20	Temperature at 8-ft Elevation--FLECHT 04444.....	2.53
2.6-21	Temperature at 9-ft Elevation--FLECHT 04444.....	2.53
2.6-22	Temperature at 10-ft Elevation--FLECHT 04444.....	2.54
2.6-23	Vapor Fraction at 0 to 2-ft Elevation--FLECHT 04444.....	2.54
2.6-24	Vapor Fraction at 2 to 4-ft Elevation--FLECHT 04444.....	2.55
2.6-25	Vapor Fraction at 4 to 6-ft Elevation--FLECHT 04444.....	2.55
2.6-26	Vapor Fraction at 6 to 8-ft Elevation--FLECHT 04444.....	2.56
2.6-27	Vapor Fraction at 8 to 10-ft Elevation--FLECHT 04444.....	2.56
2.6-28	Vapor Fraction at 10 to 12-ft Elevation--FLECHT 04444.....	2.57
2.7-1	FLECHT-SEASET Bundle Cross-Section.....	2.58
2.7-2	FLECHT-SEASET Axial Power Profile and Grid Locations.....	2.59
2.7-3	COBRA/TRAC Model of FLECHT-SEASET for Standard Problem No. 9...	2.61
2.7-4	Temperatures at 2-ft Elevation for Low Reflood Rate (Test 31805).....	2.63
2.7-5	Temperatures at 4-ft Elevation for Low Reflood Rate (Test 31805).....	2.63
2.7-6	Temperatures at 6-ft Elevation for Low Reflood Rate (Test 31805).....	2.64
2.7-7	Temperatures at 10-ft Elevation for Low Reflood Rate (Test 31805).....	2.64
2.7-8	Temperatures at 11-ft Elevation for Low Reflood Rate (Test 31805).....	2.65
2.7-9	Vapor Fraction at 0 to 1-ft Elevation for Low Reflood Rate (Test 31805).....	2.65
2.7-10	Vapor Fraction at 1 to 2-ft Elevation for Low Reflood Rate (Test 31805).....	2.66

2.7-11	Vapor Fraction at 2- to 3-ft Elevation for Low Reflood Rate (Test 31805).....	2.66
2.7-12	Vapor Fraction at 3 to 4-ft Elevation for Low Reflood Rate (Test 31805).....	2.67
2.7-13	Vapor Fraction at 4 to 5-ft Elevation for Low Reflood Rate (Test 31805).....	2.67
2.7-14	Vapor Fraction at 5 to 6-ft Elevation for Low Reflood Rate (Test 31805).....	2.68
2.7-15	Vapor Fraction at 6 to 7-ft Elevation for Low Reflood Rate (Test 31805).....	2.68
2.7-16	Vapor Fraction at 7 to 8-ft Elevation for Low Reflood Rate (Test 31805).....	2.69
2.7-17	Vapor Fraction at 8 to 9-ft Elevation for Low Reflood Rate (Test 31805).....	2.69
2.7-18	Vapor Fraction at 9 to 10-ft Elevation for Low Reflood Rate (Test 31805).....	2.70
2.7-19	Vapor Fraction at 10 to 11-ft Elevation for Low Reflood Rate (Test 31805).....	2.70
2.7-20	Vapor Fraction at 11 to 12-ft Elevation for Low Reflood Rate (Test 31805).....	2.71
2.7-21	Temperatures at 2-ft Elevation for High Reflood Rate (Test 31701).....	2.71
2.7-22	Temperatures at 4-ft Elevation for High Reflood Rate (Test 31701).....	2.72
2.7-23	Temperatures at 6-ft Elevation for High Reflood Rate (Test 31701).....	2.72
2.7-24	Temperatures at 10-ft Elevation for High Reflood Rate (Test 31701).....	2.73
2.7-25	Temperatures at 11-ft Elevation for High Reflood Rate (Test 31701).....	2.73
2.8-1	Vertical Test Train Configuration for NRU Reflood Experiments..	2.75
2.8-2	NRU Test Bundle Cross-Section.....	2.76
2.8-3	COBRA/TRAC Model of NRU Test Section.....	2.79
2.8-4	Temperatures at the 1.12-ft Elevation (Test PTH110).....	2.81

2.8-5	Temperatures at the 3.0-ft Elevation (Test PTH110).....	2.81
2.8-6	Temperatures at the 4.0-ft Elevation (Test PTH110).....	2.82
2.8-7	Temperatures at the 5.0-ft Elevation (Test PTH110).....	2.82
2.8-8	Temperatures at the 6.0-ft Elevation (Test PTH110).....	2.83
2.8-9	Temperatures at the 7-ft Elevation (Test PTH110).....	2.83
2.8-10	Temperatures at the 8.0-ft Elevation (Test PTH110).....	2.84
2.8-11	Temperatures at the 10.0-ft Elevation (Test PTH110).....	2.84
2.8-12	Temperatures at the 1.12-ft Elevation (Test TH214).....	2.86
2.8-13	Temperatures at the 3.0-ft Elevation (Test TH214).....	2.86
2.8-14	Temperatures at the 4.0-ft Elevation (Test TH214).....	2.87
2.8-15	Temperatures at the 5.0-ft Elevation (Test TH214).....	2.87
2.8-16	Temperatures at the 6.0-ft Elevation (Test TH214).....	2.88
2.8-17	Temperatures at the 7-ft Elevation (Test TH214).....	2.88
2.8-18	Temperatures at the 8.0-ft Elevation (Test TH214).....	2.89
2.8-19	Temperatures at the 10.0-ft Elevation (Test TH214).....	2.89
2.8-20	Collapsed Liquid Level vs. Time (Test TH214).....	2.90
2.9-1	Diagram of PKL System.....	2.92
2.9-2	COBRA/TRAC Model of PKL Test Facility.....	2.94
2.9-3	Schematic of COBRA/TRAC Model of PKL Pressure Vessel and Downcomer.....	2.94
2.9-4	Pressure in the Upper Plenum (Channels 5-8).....	2.96
2.9-5	Pressure in the Break Pipe.....	2.96
2.9-6	Collapsed Water Level in the Core.....	2.98
2.9-7	Flow Rate in the Downcomer (Averaged Over Length of Channel 10).....	2.98
2.9-8	Flow Rate in the Downcomer at the Lower Boundary Node.....	2.99
2.9-9	Rod Surface Temperature at Level 1.....	2.99
2.9-10	Rod Surface Temperature at Level 2.....	2.100

2.9-11	Rod Surface Temperature at Level 3.....	2.100
2.9-12	Rod Surface Temperature at Level 4.....	2.101
2.9-13	Rod Surface Temperature at Level 42.....	2.101
2.9-14	Rod Surface Temperature at Level 51.....	2.102
2.9-15	Rod Surface Temperature at Level 7.....	2.102
2.9-16	Quench Front Envelope.....	2.103
2.9-17	Void Fraction in the Core, (Channel 3, Nodes 3-5).....	2.103
2.9-18	Void Fraction in the Core, (Channels 3-4, Node 5-9,2).....	2.104
2.9-19	Void Fraction in the Core.....	2.104
2.10-1	Schematic of Cylindrical Core Test Facility.....	2.106
2.10-2	Diagram of CCTF Pressure Vessel.....	2.109
2.10-3	Cross-Section of CCTF Core.....	2.110
2.10-4	Axial Power Profile and Thermocouple Elevations for Heater Rods in CCTF Core.....	2.111
2.10-5	Schematic of COBRA/TRAC Model of CCTF.....	2.113
2.10-6	Vessel Mesh for CCTF.....	2.113
2.10-7	Differential Pressure in the Lower Plenum.....	2.114
2.10-8	Differential Pressure Between the 0 and 2-ft Elevations in the Core.....	2.114
2.10-9	Differential Pressure Between 2 and 4-ft Elevations in the Core.....	2.115
2.10-10	Differential Pressure Between 4 and 5-ft Elevations in the Core.....	2.115
2.10-11	Differential Pressure Between 6 and 8-ft Elevations in the Core.....	2.116
2.10-12	Differential Pressure Between 8 and 10-ft Elevations in the Core.....	2.116
2.10-13	Differential Pressure Between 10 and 12-ft Elevations in the Core.....	2.117
2.10-14	Differential Pressure in the Upper Plenum.....	2.117

2.10-15	Temperature at 0.38 m Elevation.....	2.118
2.10-16	Temperature at 1.015 m Elevation.....	2.118
2.10-17	Temperature at 1.83 m Elevation.....	2.119
2.10-18	Temperature at 2.44 m Elevation.....	2.119
2.10-19	Temperature at 3.05 m Elevation.....	2.120
2.11-1	Vertical Test Apparatus for CounterCurrent Flow Film Condensation Experiments.....	2.123
2.11-2	COBRA/TRAC Model for NWU CCFF Condensation Tests.....	2.125
2.11-3	Steam Flow Rate as a Function of Axial Position.....	2.126
2.12-1	RPI Phase Separation Experimental Apparatus.....	2.128
2.12-2	COBRA/TRAC Model of the RPI Phase Separation Experiment Test Section.....	2.130
2.12-3	Void Distribution for RPI Test #8 Predicted by COBRA/TRAC without the Turbulence Model.....	2.131
2.12-4	Void Distribution for RPI Test #10 Predicted by COBRA/TRAC without the Turbulence Model.....	2.132
2.12-5	Void Distribution for RPI Test #8 Predicted by COBRA/TRAC with the Turbulence Model.....	2.133
2.12-6	Void Distribution for RPI Test #10, Predicted by COBRA/TRAC with the Turbulence Model.....	2.134
2.13-1	COBRA/TRAC Mesh for Bennett Tests.....	2.138
2.13-2	Entrained Liquid in Bennett Test No. 5373.....	2.140
2.13-3	Bennett Test Critical Heat Flux vs. Equilibrium Quality (at Mass Flux = $2.84 \times 10^6$ lbm/hr-ft <sup>2</sup> ).....	2.141
2.13-4	Bennett Test Critical Heat Flux vs. Equilibrium Quality (at Mass Flux = $1.0 \times 10^6$ lbm/hr-ft <sup>2</sup> ).....	2.141
2.13-5	Bennett Test Critical Heat Flux vs. Equilibrium Quality (at Mass Flux = $0.49 \times 10^6$ lbm/hr-ft <sup>2</sup> ).....	2.142
2.13-6	Bennett Test Critical Heat Flux vs. Equilibrium Quality (at Mass Flux = $0.29 \times 10^6$ lbm/hr-ft <sup>2</sup> ).....	2.142
2.13-7	Bennett Test 5359 Axial Temperature Profile.....	2.145
2.13-8	Bennett Test 5336 Axial Temperature Profile.....	2.145

2.13-9	Bennett Test 5273 Axial Temperature Profile.....	2.146
2.13-10	Bennett Test 5250 Axial Temperature Profile.....	2.146
2.13-11	Bennett Test 5294 Axial Temperature Profile.....	2.147
2.13-12	Bennett Test 5313 Axial Temperature Profile.....	2.147
2.13-13	Bennett Test 5310 Axial Temperature Profile.....	2.148
2.13-14	Bennett Test 5379 Axial Temperature Profile.....	2.148
2.13-15	Bennett Test 5397 Axial Temperature Profile.....	2.149
2.14-1	Simplified Diagram of FRIGG Forced Convection Loop.....	2.152
2.14-2	COBRA/TRAC Model of FRIGG Forced Convection Loop.....	2.153
2.14-3	FRIGG Forced Convection Test 313018.....	2.155
2.14-4	FRIGG Forced Convection Test 313020.....	2.155
2.14-5	FRIGG Forced Convection Test 313016.....	2.156
2.15-1	Simplified Diagram of FRIGG Natural Circulation Loop.....	2.158
2.15-2	COBRA/TRAC Model of FRIGG Natural Circulation Loop.....	2.160
2.15-3	FRIGG Natural Circulation Test 313030.....	2.162
2.15-4	FRIGG Natural Circulation Test 313034.....	2.162
2.15-5	FRIGG Natural Circulation Test 313037.....	2.163
2.15-6	FRIGG Natural Circulation Mass Velocities.....	2.163
2.16-1	COBRA/TRAC Model of Semiscale MOD3 System.....	2.166
2.16-2	COBRA/TRAC Model of Semiscale Pressure Vessel and Downcomer for Test S-07-6.....	2.168
2.16-3	Upper Plenum Pressure.....	2.170
2.16-4	Density at Top of Core.....	2.170
2.16-5	Density in Upper Head.....	2.171
2.17-1	Semiscale MOD2A System for Small Break LOCA.....	2.174
2.17-2	Detail of Small Break Orifice in Test S-UT-2.....	2.175
2.17-3	COBRA/TRAC Model of Semiscale MOD2A System.....	2.177

2.17-4	COBRA/TRAC Model of Semiscale Pressure Vessel and Downcomer for Test S-UT-2.....	2.179
2.17-5	COBRA/TRAC Noding of Break Nozzle.....	2.180
2.17-6	System Pressure.....	2.182
2.17-7	Collapsed Liquid Level in Semiscale Downcomer Pipe.....	2.183
2.17-8	Collapsed Liquid Level in Semiscale Core.....	2.183
2.17-9	Collapsed Liquid Level in Upper Head.....	2.184
2.17-10	Upper Head Fluid Temperature.....	2.184
2.17-11	Rod Temperature at the Core Mid-Plane.....	2.185
2.17-12	Rod Temperature Near Top of Core.....	2.185
2.18-1	COBRA/TRAC Model of Westinghouse Upper Head Test Section.....	2.190
2.18-2	Westinghouse Drain Test #5; Upper Head Liquid Level vs. Time.....	2.191
2.18-3	Westinghouse Drain Test #5; Fluid Temperature at Top of Support Columns.....	2.191
2.18-4	Westinghouse Drain Test #5; Pressure at Top of Guide Tube....	2.192

## TABLES

2.1	Battelle Columbus 2/15th Scale Downcomer Test Conditions.....	2.21
2.2	Reverse Core Steam Flow Rate Ramps for BCL 2/15th Scale Downcomer Tests.....	2.21
2.3	Boundary Conditions for FEBA Test 216.....	2.29
2.4	Initial Conditions for FLECHT Cosine Series Tests.....	2.40
2.5	FLECHT Initial Cladding Temperatures.....	2.42
2.6	Test Parameters for Standard Problem No. 9.....	2.59
2.7	Initial Design Parameters for NRU Tests PTH110 and TH214.....	2.77
2.8	Component Scaled Dimensions for Cylindrical Core Test Facility.....	2.107
2.9	Summary of Conditions for CCTF Test C1-2.....	2.112
2.10	Execution Speeds and Average Time Steps for Calculations of RPI Phase Separation Tests.....	2.136
2.11	Summary of Bennett Test Conditions and Results of Dryout Point Calculations.....	2.139
2.12	Summary of FRIGG Forced Convection Test Conditions.....	2.154
2.13	Summary of FRIGG Natural Circulation Test Conditions.....	2.160
2.14	Initial Conditions for Semiscale Test S-07-2.....	2.169
2.15	Initial Conditions for Semiscale Test S-UT-2.....	2.182

## ACKNOWLEDGEMENTS

COBRA/TRAC is the result of the efforts of a number of people. We wish to acknowledge the main contributors and to express our appreciation to those who have offered their advice and suggestions.

The main contributors to the program are listed below.

Fluid Dynamics:	M. J. Thurgood, T. L. George, and T. E. Guidotti
Heat Transfer	J. M. Kelly, R. J. Kohrt
Turbulence Model	K. R. Crowell
Graphics and Programming:	A. S. Koontz
Simulations:	K. L. Basehore, S. H. Bian, J. M. Cuta, R. J. Kohrt, G. A. Sly and C. A. Wilkins
One-Dimensional Components and Code Architecture:	Members of the TRAC-PIA Code Development Group at LANL

We wish to thank Dr. S. Fabric of the U.S. Nuclear Regulatory Commission for his patience, support and suggestions during this large undertaking. We also wish to thank Drs. Tong, Shotkin, Han and Zuber of the U.S. Nuclear Regulatory Commission and members of the Advanced Code Review Group for their many helpful suggestions. We also express our gratitude to our manager, Dr. D. S. Trent, for his support, and Cathy Darby and Peggy Snyder for their lead roles in typing this report.



COBRA/TRAC - A THERMAL-HYDRAULICS CODE FOR TRANSIENT ANALYSIS  
OF NUCLEAR REACTOR VESSELS AND PRIMARY COOLANT SYSTEMS  
VOLUME 4: DEVELOPMENTAL ASSESSMENT AND DATA COMPARISONS

1.0 INTRODUCTION

The COBRA/TRAC computer program was developed to predict the thermal-hydraulic response of nuclear reactor primary coolant systems to small and large break loss-of-coolant accidents and other anticipated transients. It is derived from the merging of COBRA-TF and TRAC-PD2 (Ref. 1).

The COBRA-TF computer code provides a two-fluid, three-field representation of two-phase flow. Each field is treated in three-dimensions and is compressible. The three fields are, continuous vapor, continuous liquid and entrained liquid drops. The conservation equations for each of the three fields and for heat transfer from and within the solid structures in contact with the fluid are solved using a semi-implicit finite-difference numerical technique on an Eulerian mesh. COBRA-TF features extremely flexible noding for both the hydrodynamic mesh and the heat transfer solution. This flexibility enables modeling of the wide variety of geometries encountered in vertical components of nuclear reactor primary systems.

TRAC-PD2 is a systems code designed to model the behavior of the entire reactor primary system. It features special models for each component in the system. These include accumulators, pumps, valves, pipes, pressurizers, steam generators and the reactor vessel. With the exception of the reactor vessel, the thermal-hydraulic response of the components to transients is treated with a five-equation drift flux representation of two-phase flow. The TRAC vessel component is somewhat restricted in the geometries modeled and cannot treat the entrainment of liquid drops from the continuous liquid phase directly.

The TRAC vessel module has been removed and COBRA-TF implemented as the new vessel component. The resulting code is COBRA/TRAC. The vessel component in COBRA/TRAC has both the extended capabilities provided by the three-field representation of two-phase flow and the flexible noding. The code was

assessed against a variety of two-phase flow data from experiments conducted to simulate important phenomena anticipated during postulated accidents and transients in light water reactors.

The documentation of the COBRA/TRAC program is contained in five separate volumes. Volume 1 contains the equations and constitutive models from COBRA-TF used in the vessel component. Volume 2 describes the finite-difference equations for the vessel and the numerical techniques used to solve these equations. The coupling between the TRAC-PD2 equations and the COBRA-TF vessel equations is also described. Volume 3 is the users' manual, containing line-by-line input instructions for COBRA/TRAC and guidelines for the user. Volume 4 is the developmental assessment manual. It contains the results of simulations run to assess the performance of the code. Volume 5 is the programmers' manual.

This volume documents the major data comparisons made with COBRA/TRAC during the process of code development. Many data comparisons were run to verify the accuracy and applicability of various models as they were installed in the code. These data comparisons were extremely useful in detecting programming errors and defining deficiencies in the code's physical models. Data comparisons were rerun on progressively more advanced versions of the code until the code could successfully predict the observed behavior, within experimental error and known limitations of the models. Constraints of time and manpower make it impossible to rerun the data comparisons with the final released version of the code before the date for final release. Therefore, the data comparisons presented in this volume document the results obtained on developmental versions of the code. A separate document will be released at a later date containing data comparisons run on the final released version of the code.

In general, the data comparisons are very good and demonstrate that COBRA/TRAC is capable of simulating the major phenomena of interest during a loss-of-coolant accident in a PWR. However, the code developers recommend that users conduct their own independent assessment of the code to satisfy themselves that the code will provide adequate answers for their particular needs. This is especially true if the code is to be applied to types of problems or phenomena not covered by the developmental assessment.

## 2.0 DATA COMPARISONS PERFORMED WITH DEVELOPMENTAL VERSIONS OF COBRA/TRAC

This section discusses the data comparisons made during the development of COBRA/TRAC. The great majority were run on later versions of the code, notably cycles 8, 10 and 11 (the released version is cycle 13). (See Appendix A for a description of code cycles.)

The developmental assessment simulations fall into three main categories:

- basic tests
- separate effects tests
- integral systems tests

These tests include a large variety of two-phase flow and heat transfer phenomena important in reactor safety. The code has been compared with data for the following phenomena:

countercurrent flow limiting (CCFL)  
downcomer ECC bypass with condensation, hot wall and transient effects  
top and bottom reflood  
condensation  
phase separation (lateral void drift)  
CHF and post-CHF  
subcooled boiling  
natural circulation  
nucleate boiling (axial void profile and two-phase  $\Delta P$ )  
uncovering/recovery  
upper head draining  
system simulations

The basic tests performed include:

RPI phase distribution  
University of Houston tube CCFL  
Dartmouth tube CCFL  
NWU orifice plate CCFL  
Bennett CHF and post-CHF heat transfer  
NWU condensation on a falling liquid film

Separate effects tests include:

- Forced bottom reflood
  - FLECHT low flooding rate cosine series
  - FLECHT-SEASET
  - NRU nuclear fuel rods
  - FEBA
- Top reflood:
  - Westinghouse G2
- Core thermal hydraulics:
  - FRIGG forced flow subcooled boiling
  - FRIGG natural circulation
  - THTF upflow film boiling
  - THTF uncovering/recovery
- Upper head hydraulics:
  - Westinghouse drain test
- Downcomer
  - BCL 2/15th scale downcomer ECC bypass
  - CREARE 1/15th scale downcomer ECC bypass

COBRA/TRAC simulations of integral tests include:

- Semiscale S-07-6
- Semiscale Mod 2A S-UT-2
- Cylindrical core test facility test C1-2
- PKL gravity reflood test K9

The mesh chosen for the COBRA/TRAC model of each simulation was based on the following objectives:

- The mesh size must be comparable to that expected to be used to model similar structures in the reactor vessel. (This was done to determine if the relatively coarse mesh required to model a vessel with a realistic number of cells would provide reliable results. Mesh cells in all simulations were on the order of 1/2 to 2 feet long).

- A sufficient number of mesh cells must be used to model the physical geometry of the experiment and to capture the dominant physical phenomena. (In most simulations, a one-dimensional mesh was sufficient.)
- The number of mesh cells must be minimized to reduce computation costs as much as possible while maintaining a sufficient degree of accuracy.

The selection of a mesh that satisfies these criteria requires the code user to exercise his judgment. Experience and familiarity with the modeling techniques used in COBRA/TRAC will be helpful, but the user may also have to experiment with different meshes before selecting the most suitable one for a given problem.

The meshes chosen for the simulations contained in this document are the result of the experienced judgment of the code developers and early users. They should be used as guidelines in setting up models for other simulations. They should not be considered as perfect nor as an all-inclusive list of possible meshes.

## 2.1 DARTMOUTH COUNTERCURRENT FLOW TUBE FLOODING EXPERIMENTS

Simulations were made of the Dartmouth College (Ref. 2) air-water countercurrent flow flooding experiments in vertical tubes. There were three main objectives in performing these simulations. First and foremost was to evaluate the physical models for entrainment of drops from a falling liquid film by the countercurrent vapor (or in this case, air) flow. Secondly, this data provided a means to evaluate the models for interfacial shear between the air and liquid film. Finally, this simulation provided experience in determining the best mesh to model a liquid pool above a tube or orifice.

### 2.1.1 Description of Experiment

The test facility consisted of a vertical, 40 or 48-in. tubular test section connecting an upper and lower plenum. Three different test sections with diameters of 2, 6, and 10 in. were used. The upper plenum was a 55-gallon drum. Water was introduced into the upper plenum through a 2-in. pipe at rates up to about 250 gpm and an overflow maintained a pool height of 18-20 in. Air was injected in the lower plenum through a 10-in. pipe. The

liquid penetration rate was determined by measuring the liquid accumulation rate in the lower plenum. A schematic of the test section is shown in Figure 2.1-1.

The experimental procedure was as follows:

- Airflow was set at a high enough value to stop all liquid penetration into the flooding tube.
- The water supply was then turned on, and a liquid pool was allowed to form in the upper plenum.
- Airflow was decreased, allowing water to penetrate the tube.
- Water accumulation in the lower plenum was measured.
- Airflow was checked for constancy.

#### 2.1.2 COBRA/TRAC Model

In reactor safety applications, injected cooling water must penetrate tubes or orifice plates against countercurrent steam flow. The accumulation of water above tie plates results in the formation of a liquid pool. It is therefore essential to model the flow in the liquid pool correctly to obtain accurate inlet conditions for the flooding tube or orifice. The most important aspects to model are the velocity and void fraction distributions in the pool. When a high-velocity vapor enters a pool from a tube or orifice, it can be expected that a high-velocity, high-void fraction region will exist in the pool directly above the tube or orifice, while the fluid in the pool surrounding the inlet tube or orifice remains at low velocity and low void fraction. One might expect a two-phase jet consisting of vapor and water drops at higher vapor velocities or water and vapor bubbles at lower vapor velocities. Liquid in the two-phase jet above the inlet should be rising while that surrounding the inlet may be falling.

The void and velocity distribution in the pool can be modeled by two-fluid computer codes if a sufficiently small mesh is used to resolve the gradients. However, this would require a very large number of mesh cells to model the liquid pool in the upper plenum of a PWR, which has several vapor jets entering the pool through orifices in the top nozzles of the fuel assemblies.

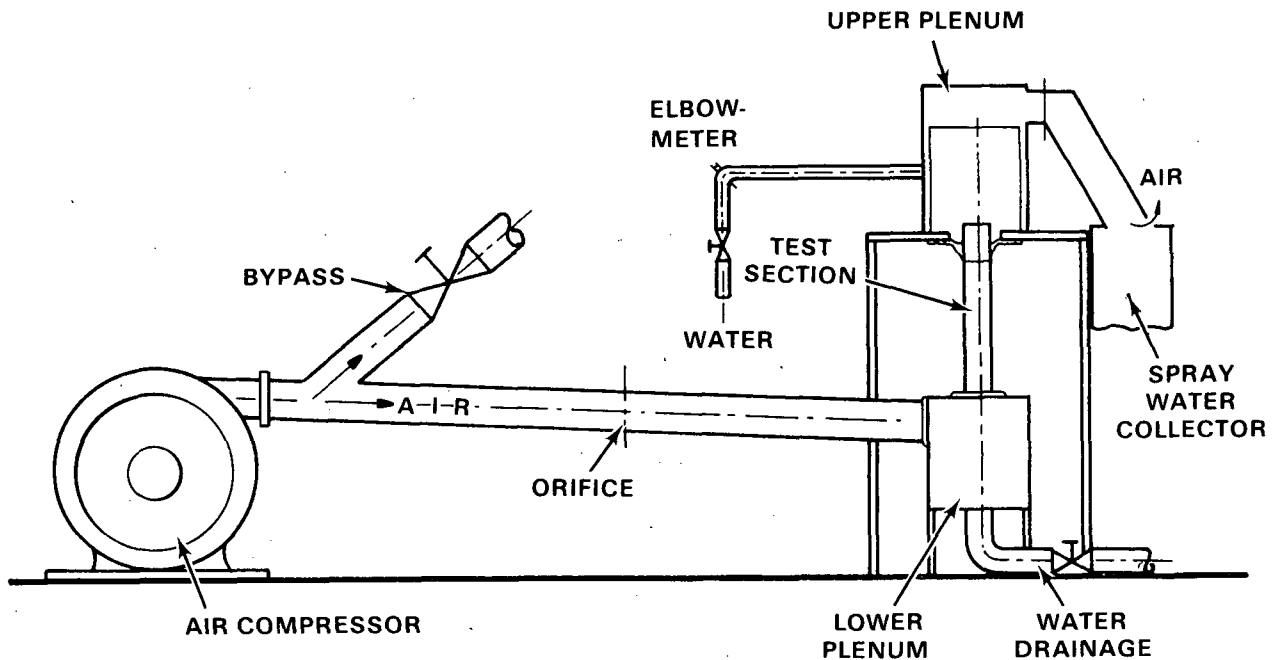


FIGURE 2.1-1. Experimental Setup for Flooding in Large Tubes

The optional subchannel formulation of the momentum equation and channel-splitting capability available in COBRA/TRAC can be used to model the pool with a reasonable number of nodes. This is done by modeling the pool in each region of the upper plenum with two subchannels; one for the area directly above the holes and the other for the area surrounding the holes. The channel directly above the holes has the same flow area and hydraulic diameter as the holes. This provides a two-region model of the pool, that has been successfully used to predict CCFL in a variety of geometries.

The test section was modeled with a single column 10 mesh cells high. The bottom two mesh cells were used to model the collection of water in the lower plenum. The upper plenum was modeled with two columns of mesh cells (i.e., two channels). One channel was located directly above the test section and had the same flow area and hydraulic diameter as the tube. The second channel modeled the flow area in the remainder of the upper plenum. The subchannel formulation of the momentum equation was used for the cross-flow between these two channels. Air was modeled with steam at a suitable pressure (~30 psi) to give a density equivalent to that of the air used in the

experiment. (This was done because only the equation of state for steam, not air, is available in the code.) The steam was injected into the third mesh cell of the lower plenum. Water was injected in the first cell of the upper plenum. The overflow was modeled with a pressure boundary condition in the fourth cell of the upper plenum, which provided the correct liquid head in the pool. A node length of 6 in. was used in this simulation.

### 2.1.3 Discussion of Results

Experimental results were presented on plots of dimensionless gas flux,  $(j_g^*)^{1/2}$ , as a function of dimensionless liquid penetration flux,  $(j_l^*)^{1/2}$ , where for the *i*th phase:

$$j_i^* = \frac{\rho_i^{1/2} j_i}{[gD(\rho_f - \rho_g)]^{1/2}} \quad (2.1)$$

where *D* is the diameter of the test section, *j* is the phase superficial velocity, *g* is the acceleration of gravity and  $\rho$  is the density.

COBRA/TRAC predictions of the 2-in. tube experimental results are shown in Figure 2.1-2. The comparison is quite reasonable. At high airflow rates, film stability and entrainment in the test section or at the tube inlet limited the rate at which liquid could penetrate to the lower plenum. At lower airflow rates, liquid penetration was limited by the bubbly flow in the pool above the test section inlet. COBRA/TRAC predictions of the 10-in. tube experimental data are shown in Figure 2.1-3. The comparison is very reasonable and the limiting behavior was similar to that for the 2-in. test section.

This simulation was run on cycle 8 of COBRA/TRAC. Significant deviations in the prediction would be unlikely if the simulation were rerun on the final code version. Some minor changes in the interpolation between the small and large bubble flow regimes may affect the results as may the modification of the unstable film friction factor.

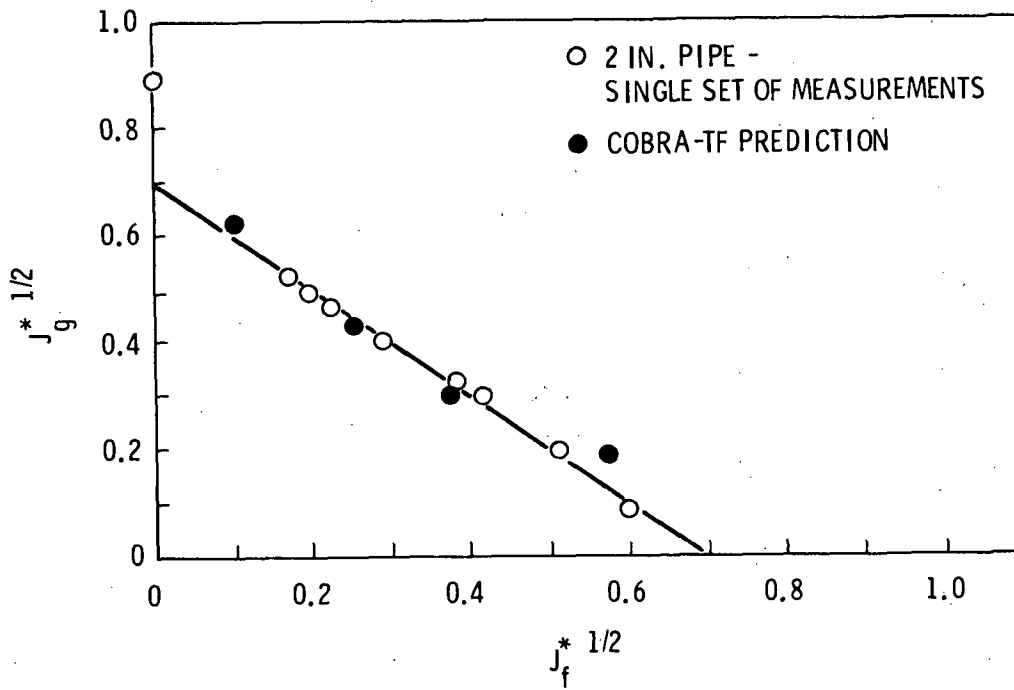


FIGURE 2.1-2. Liquid Penetration in 2-in. Tube

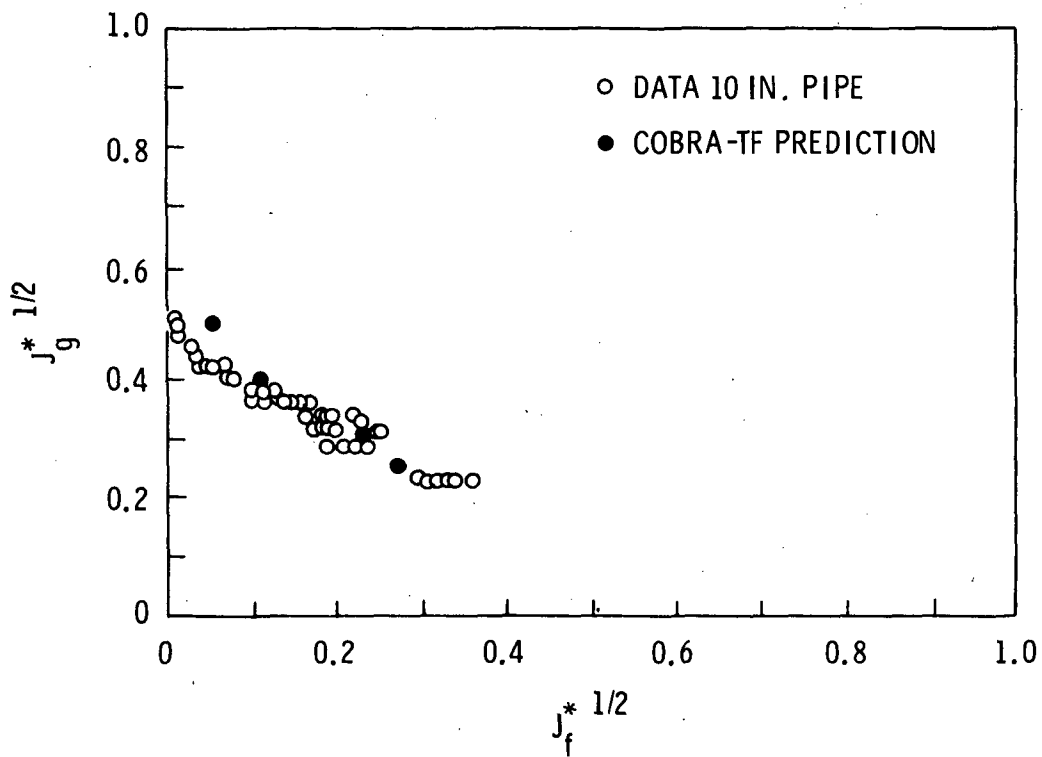


FIGURE 2.1-3. Liquid Penetration in 10-in. Tube

## 2.2 NORTHWESTERN UNIVERSITY ORIFICE PLATE FLOODING EXPERIMENT

Air-water countercurrent flow experiments in a vertical test section containing an orifice plate were conducted at Northwestern University (Ref. 3). The experiments studied the penetration of liquid through the holes of the orifice plate against the upflow of air. This experiment was simulated with COBRA/TRAC to assess the applicability of the nodalization developed for a liquid pool above a tube (described in Section 2.1) to the pool above an orifice plate. This simulation demonstrated the capability to predict the correct liquid penetration through the orifice plate at various air (vapor) velocities.

### 2.2.1 Description of Experiment

The experimental test section consisted of a vertical, rectangular box made of brass with a Lexan front and back to allow observation of the flow during the experiment. An orifice plate divided the test section into an upper and lower section. Air was injected into the lower section at a specified rate while water was injected into the upper section. The water was injected through a vertical tube that was sealed off on the end and had several small holes drilled around its perimeter to minimize the effects of momentum of the injected liquid. Orifice plates with various hole sizes and numbers of holes were investigated. An overflow pipe was connected to the upper plenum to maintain a constant pool height. An air outlet pipe was connected above that. A schematic of the test facility is shown in Figure 2.2-1.

Experiments were performed for different orifice plates, liquid injection nozzle elevations, and water flow rates. The experimental procedure was as follows:

- Water flow was initiated in the upper plenum.
- Air flow was adjusted to the desired rate.
- The liquid penetration rate was measured.

The procedure was repeated with higher air flow rates.

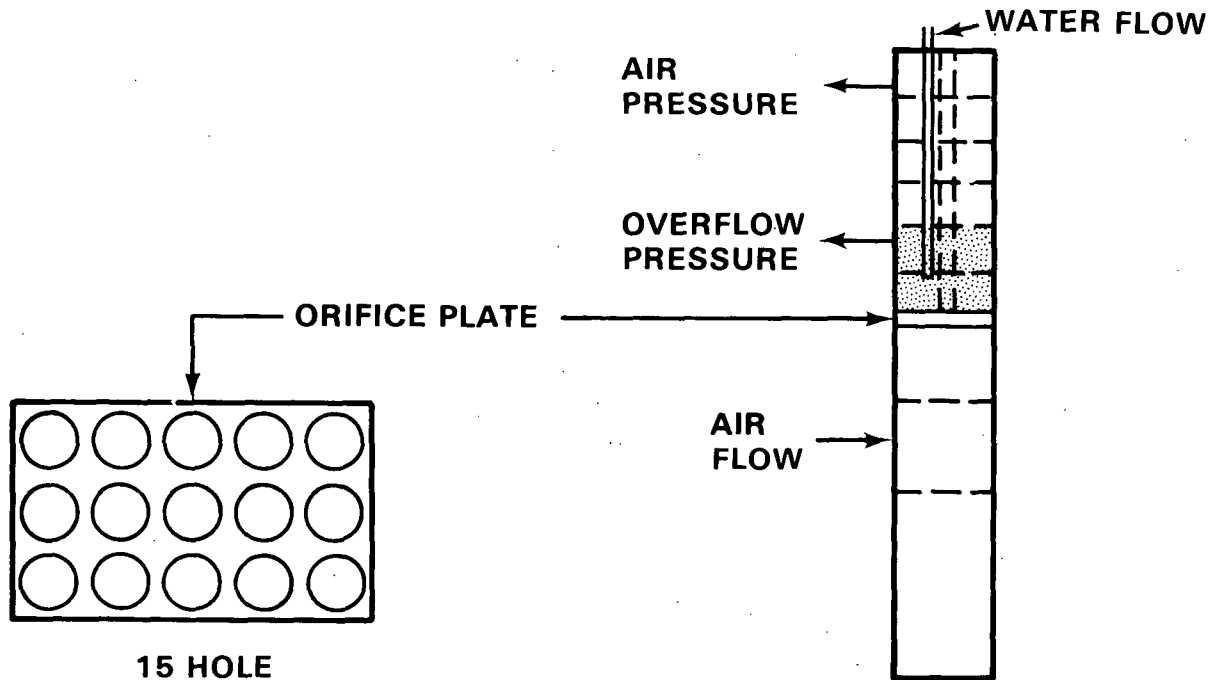


FIGURE 2.2-1. COBRA/TRAC Model of Northwestern University CCFL Experimental Facility

### 2.2.2 COBRA/TRAC Model Description

A test containing an orifice plate with fifteen 10.5 mm holes arranged in a 3x5 rectangular array was selected for this simulation. The liquid pool above the orifice plate was modeled with two columns of mesh cells using a subchannel approximation for the lateral flow between the two. This was done to model the void and velocity profiles in the pool as described in Section 2.1. The first channel had a flow area equal to the total area of the 15 holes and a hydraulic diameter equal to the diameter of a single hole. The second channel modeled the area surrounding the holes. A node length of 5 in. was used.

Two channels were used below the orifice plate. The lower one served as a liquid collection volume, and the top one modeled the region below the orifice plate into which air was injected. Liquid was injected into the fifth axial node in the upper plenum. Since the liquid was injected from the side, it was assumed for the COBRA/TRAC model that the injected fluid had no vertical component of momentum.

### 2.2.3 Discussion of Results

Experimental results were presented on plots of dimensionless gas flux,  $H_g^{*1/2}$ , as a function of dimensionless liquid penetration flux,  $H_l^{*1/2}$ , where for the  $i$ th phase

$$H_i^* = \frac{\rho_i^{1/2} j_i}{[g W_8 (\rho_l - \rho_g)]^{1/2}} \quad (2.2)$$

where  $W_8$  is a characteristic dimension that is an interpolation between  $D_H$  used in  $J^*$  scaling and the wave length of the Taylor instability,  $[\sigma/[g(\rho_f - \rho_g)]]^{1/2}$ , used in  $k^*$  scaling.

The following definitions hold for the above equation:

$$W_8 = D_H^{(1-\psi)} [\sigma/g (\rho_f - \rho_g)]^{\psi/2} \quad (2.3)$$

$$\psi = \tanh [(K D_H) (A_h)/A_T] \quad (2.4)$$

$D_H$  = hydraulic diameter of the hole in the perforated plate

$\psi$  = interpolation function between  $J^*$  and  $k^*$  scaling

$A_h$  = total area of holes in perforated plate

$A_T$  = total area of test cross section

$K$  = wave number (plate thickness/2)

COBRA/TRAC data predictions are shown in Figure 2.2-2. The predictions are quite reasonable, with bubbly flow in the pool limiting liquid penetration at all vapor velocities. At lower vapor velocities less liquid penetration was predicted than was measured experimentally.

The bubble size is limited in the calculation to the hydraulic diameter of the holes. With holes located so close together it is probable that bubbles coalesced and that larger bubble diameters are possible. The limit on bubble sizes was arbitrarily set to twice the hole diameter and the

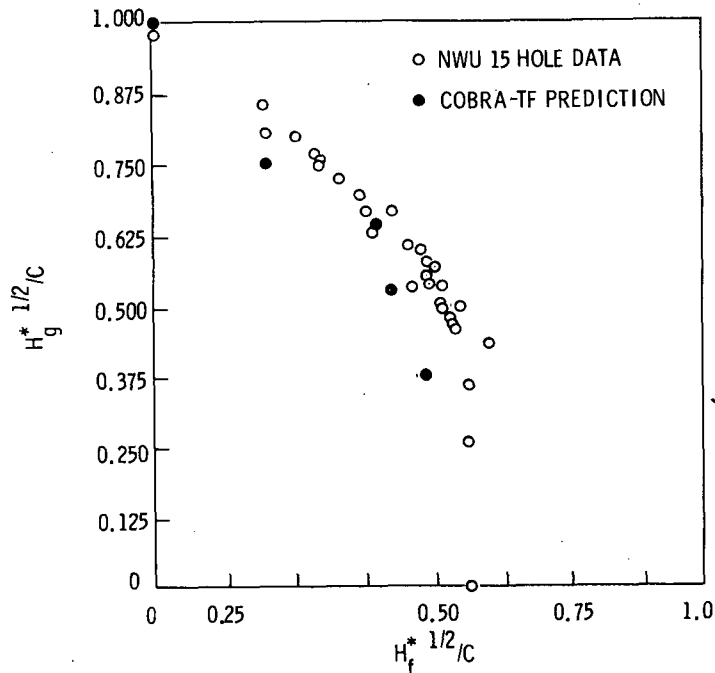


FIGURE 2.2-2. Liquid Penetration -  $DBUB_{MAX}$  = Hydraulic Diameter

calculation was repeated. As can be seen in Figure 2.2-3, this change improved the data comparison. This simulation was run on cycle 8 of COBRA/TRAC.

### 2.3 CREARE 1/15th SCALE DOWNCOMER ECC BYPASS EXPERIMENTS

Countercurrent flow experiments were conducted at CREARE, Inc., to evaluate the downward penetration of emergency core cooling water against the up-flow of steam in a PWR downcomer. The effects of countercurrent flow, lower plenum voiding, superheated downcomer walls and condensation were investigated separately and in combination. Test conditions included elevated pressures, transient steam flows and a range of geometric parameters (Ref. 4). Tests that used steady steam flow, unheated walls and injection of emergency coolant at saturated and subcooled conditions were selected for simulation. These simulations were made to assess the applicability of flow pattern selection logic to the geometry of a PWR downcomer, and verify physical models for interfacial drag, wall shear, entrainment and interfacial heat transfer.

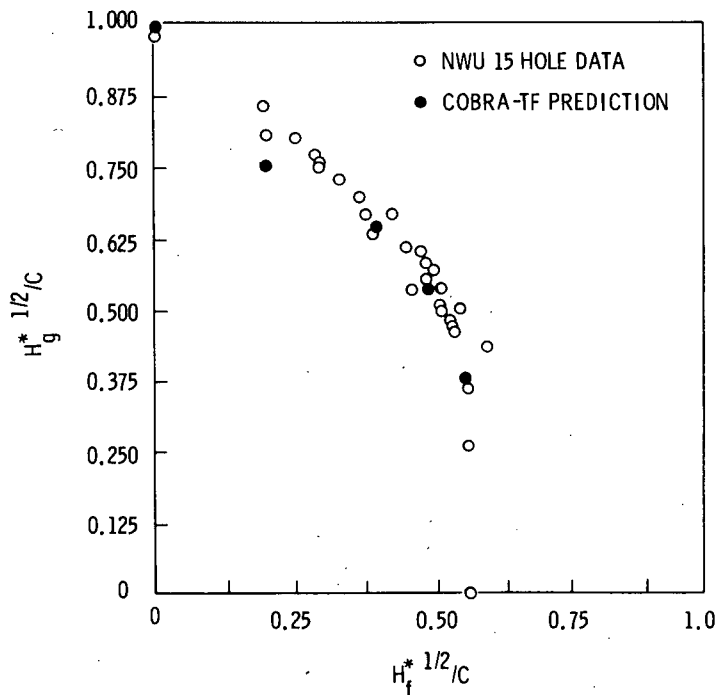


FIGURE 2.2-3. Liquid Penetration -  $DBUB_{MAX} = 2*$  (hydraulic diameter)

### 2.3.1 Description of Experiment

The test apparatus consisted of a cylindrical vessel containing a 1/15-scale PWR downcomer and an extended lower plenum. Figure 2.3-1 shows a diagram of the test section. The downcomer gap and circumference were 0.5 in. and 34.6 in., respectively. Three intact cold legs and one broken cold leg were connected to the top of the downcomer. Emergency core cooling water was injected into each of the three intact cold legs. The broken cold leg was connected to a separator. Steam was injected in the top of the vessel on the inside of the core barrel to simulate reverse core steam flow.

Tests were run by first injecting a constant steam flow rate through the vessel, purging the vessel of air, and then injecting water at a constant rate through the intact cold legs into the downcomer. The flow was then allowed to achieve dynamic equilibrium, and the liquid penetration rate into the lower plenum was measured. This procedure was repeated at different steam flow rates for each liquid injection rate and temperature, covering the range from complete bypass of the injected liquid out the broken cold leg to complete penetration of the liquid into the lower plenum.

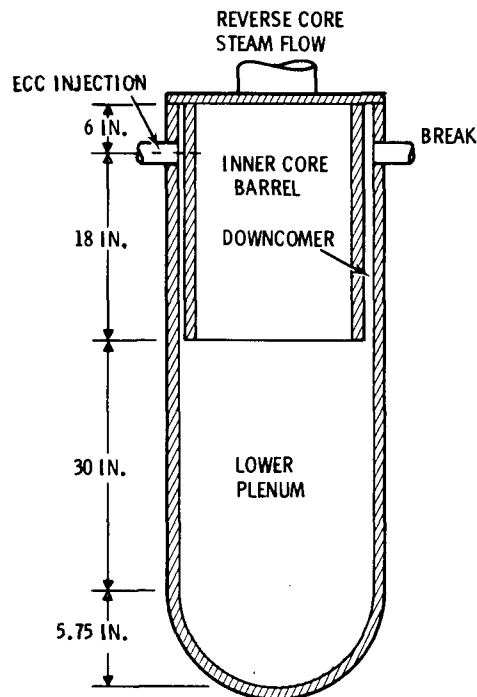


FIGURE 2.3-1. Schematic CREARE Downcomer Vessel

### 2.3.2 COBRA/TRAC Model Description

The test vessel was simulated using a two-section, six-subchannel model with 34 hydrodynamic mesh cells. A diagram of the model is shown in Figure 2.3-2. A pressure boundary condition was modeled on the broken cold leg using a BREAK component. Liquid flow boundary conditions were specified at each of the three intact cold legs. Reverse core steam flows were specified at the top of channel 2 over the range of values used in the experiment. The downcomer was modeled using four azimuthal channels having six vertical nodes each, and the lower plenum was modeled using a single channel with four axial nodes. Four channels in the downcomer with six vertical nodes each was felt to be the minimum number required to model void and velocity profiles in the downcomer and to allow connections with three intact cold legs and one broken cold leg.

The calculation was initiated by specifying a reverse core steam flow rate high enough to cause complete bypass of the emergency core cooling (ECC) liquid. Once the initial steam flow reached a steady state, ECC liquid

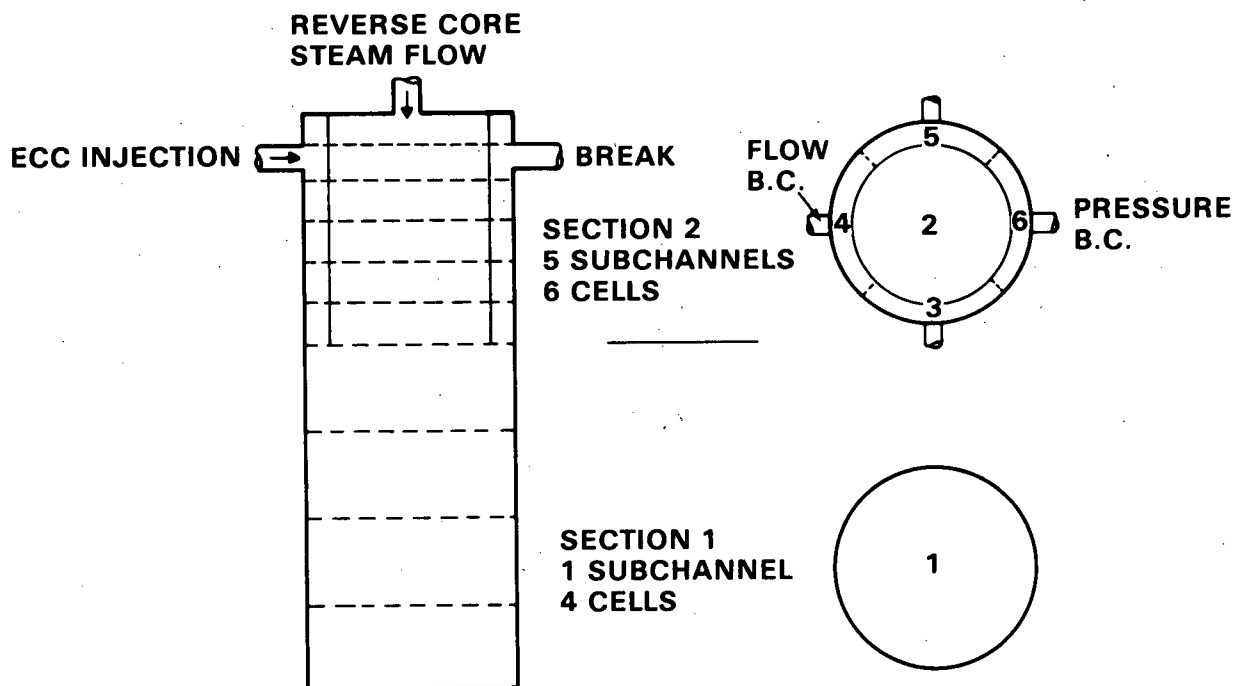


FIGURE 2.3-2. COBRA/TRAC Model of CREARE Downcomer

injection was initiated and allowed to establish a quasi-steady state. The rate of liquid accumulation in the lower plenum was then calculated and compared with the experimentally measured value. This procedure was repeated for several steam flow rates at different ECC flow rates and subcoolings.

### 2.3.3 Discussion of Results

The data comparisons are presented as penetration curves of the dimensionless countercurrent steam flow,  $J_{gc}^*$ , versus the dimensionless water flow delivered to the lower plenum,  $J_{fd}^*$ . These quantities are defined as follows:

$$J_{gc}^* = \frac{j_g \rho_g^{1/2}}{[g_w (\rho_f - \rho_g)]^{1/2}} \quad (2-3)$$

and

$$J_{fd}^* = \frac{j_f \rho_f^{1/2}}{[gw (\rho_f - \rho_g)]^{1/2}} \quad (2-4)$$

where  $j_g$  and  $j_f$  are the vapor and liquid volumetric fluxes at the base of the downcomer,  $\rho_g$  and  $\rho_f$  are the vapor and liquid densities, and  $w$  is the downcomer circumference.

Figures 2.3-3 and 2.3-4 show the penetration curves for ECC injection of saturated water at injection rates of 30 and 120 gpm, respectively. At 30 gpm, the experimental data indicate that complete bypass occurs for dimensionless steam flows greater than 0.18, partial penetration between 0.18 and 0.04, and complete penetration below 0.04. COBRA/TRAC slightly overpredicts the penetration rate; however, this data comparison is acceptable. The data comparison for the 120 gpm penetration curve is good. Liquid begins to penetrate the downcomer at  $J_{fd}^* = 0.18$  with COBRA/TRAC slightly underpredicting the filling rate until a transition occurs at  $J_{fd}^* = 0.11$ . This occurred as the liquid reached the bottom of the downcomer on the side opposite the break, allowing a sudden increase in liquid penetration.

These saturated ECC penetration curves assessed the code's ability to predict the momentum transfer in the downcomer. The subcooled ECC injection tests assessed the condensation heat transfer in the downcomer. Figures 2.3-5 and 2.3-6 show the penetration curves when liquid at 100°F (~115°F subcooled) is injected at 30 and 120 gpm. At both flow rates COBRA/TRAC predicts the transition from complete bypass to complete penetration very well. Partial penetration at high ECC subcoolings is actually a time average of periods of complete bypass and periods of complete penetration (periodic downcomer filling and dumping). These simulations were run with cycle 8.

#### 2.4 BATTELLE COLUMBUS 2/15th SCALE DOWNCOMER TRANSIENT ECC BYPASS EXPERIMENT

Two transient Battelle Columbus downcomer tests were simulated. These experiments were part of the Steam-Water Mixing and System Hydrodynamics program conducted at Battelle in Columbus, Ohio (Ref. 5,6,7). The purpose was

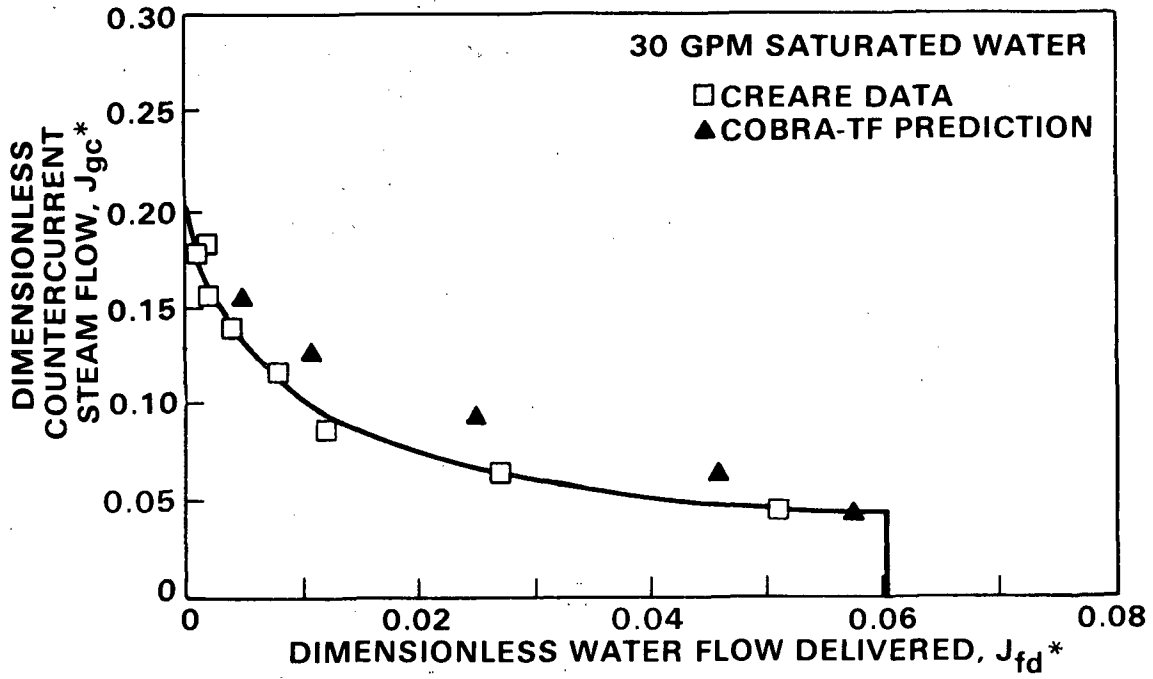


FIGURE 2.3-3. Downcomer Penetration Curve - Saturated ECC Water at 30 GPM

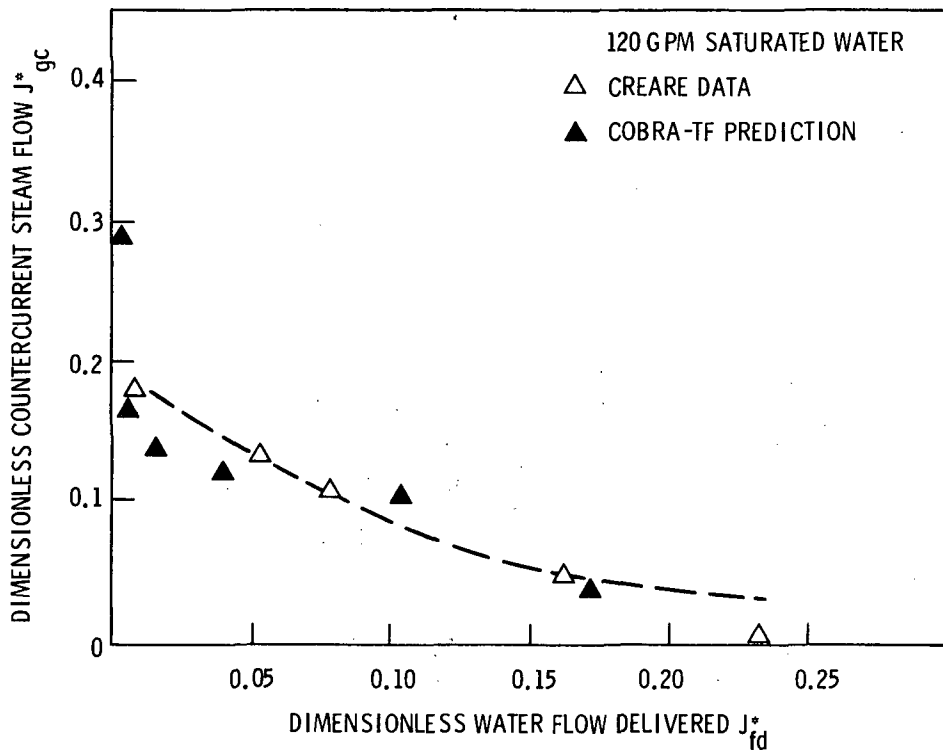


FIGURE 2.3-4. Downcomer Penetration Curve - Saturated ECC Water at 120 GPM

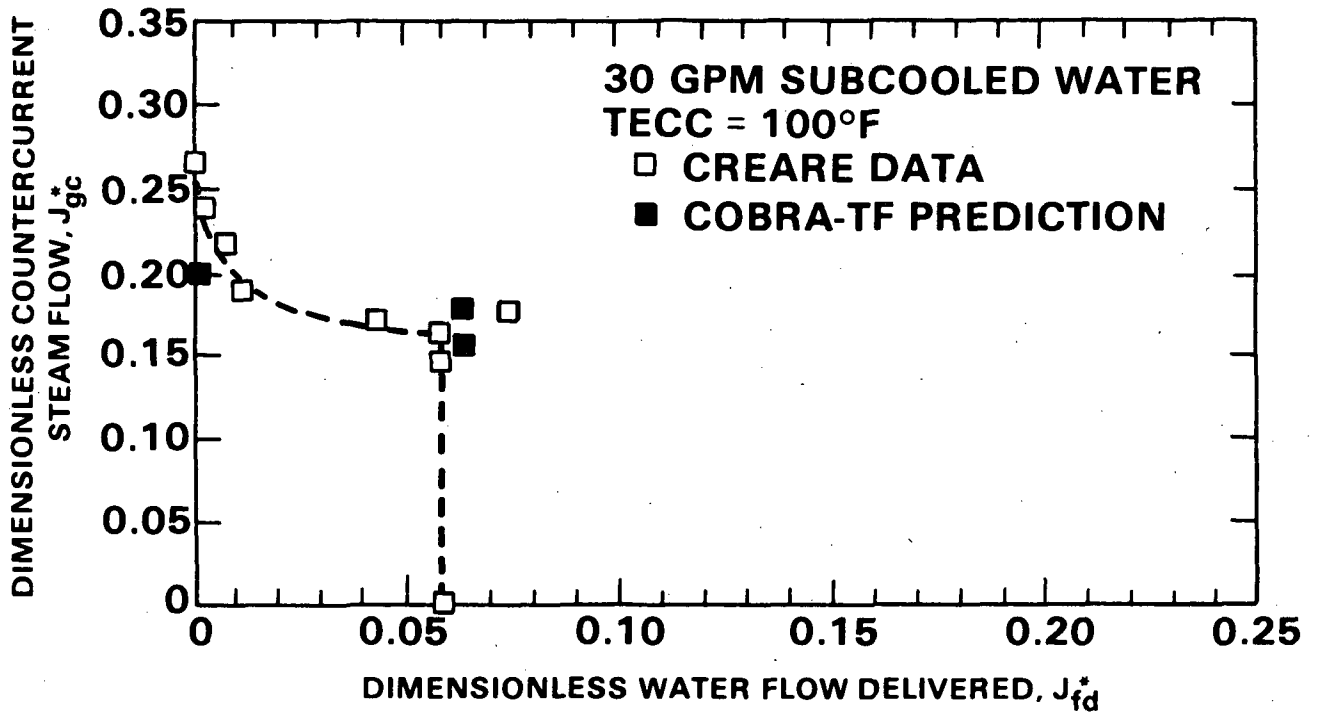


FIGURE 2.3-5. Downcomer Penetration Curve - Subcooled ECC Water at 30 GPM

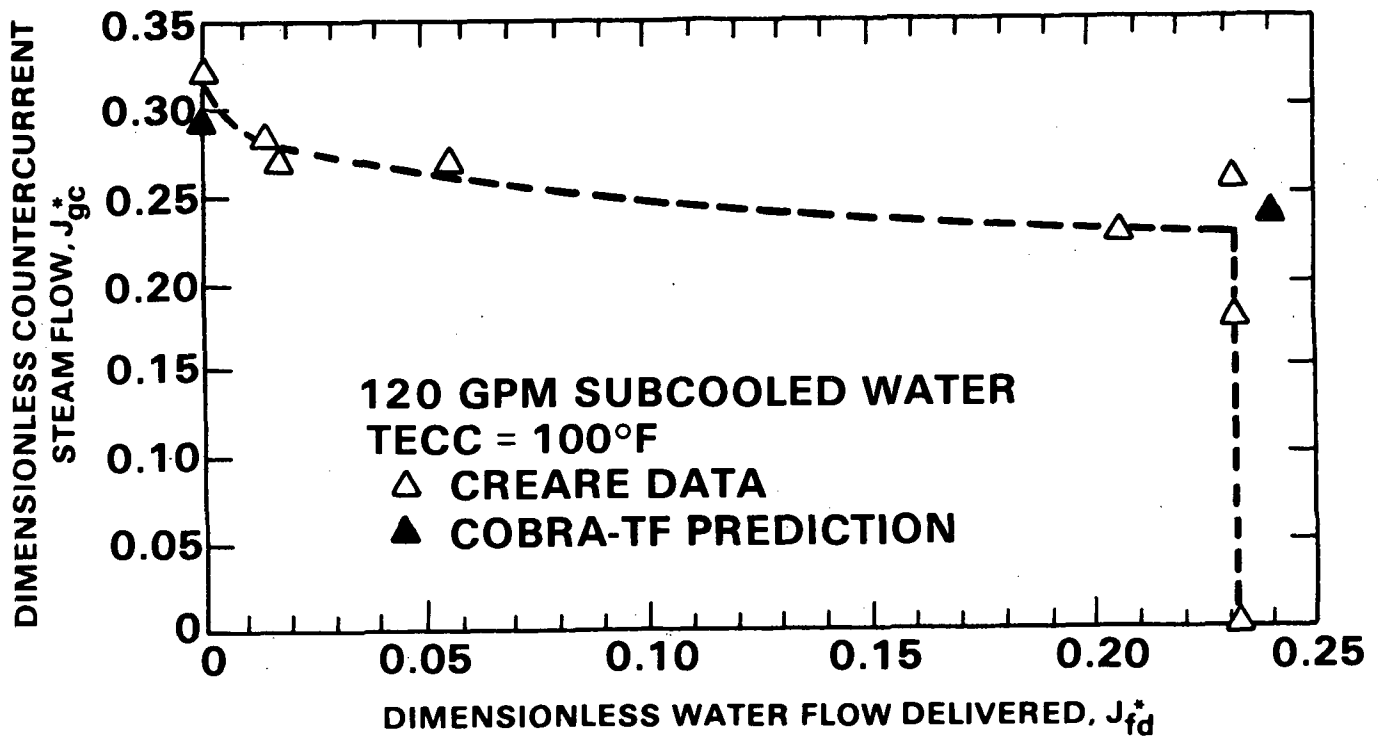


FIGURE 2.3-6. Downcomer Penetration Curve - Subcooled ECC Water at 120 GPM

to study the interactions between steam and the ECC fluid within the primary system. Of particular interest here are the tests concerned with the ECC bypass behavior in the downcomer annulus. These calculations assessed COBRA/TRAC's ability to predict the combined effects of ramped reverse core steam flow, subcooled emergency core cooling (ECC) water, and hot walls on the ECC bypass behavior during countercurrent flow in a downcomer.

#### 2.4.1 Description of Experiment

The test vessel was a 2/15th-scale PWR downcomer with an extended lower plenum. Four cold legs were arranged in a 60° to 120° orientation with a hot leg plug (7.84 in. O.D.) located in the center of the two 120° arcs. Each of the three intact cold legs modeled the loop piping from the steam generator exit to the vessel and included the pump suction piping and a simulated pump. The broken cold leg discharged into a pressure controlled containment tank. The principle dimensions of the vessel are shown in Figure 2.4-1. The downcomer was 41 in. high, had a circumference of 72.6 in. and a downcomer gap width of 1.23 in.

Steam was injected in the top of the vessel at a prescribed rate. It flowed into the lower plenum, up the downcomer and out the broken leg to the containment vessel. ECC water was injected at a constant rate in each of the intact loops. Depending on the instantaneous steam and ECC flow rate, the subcooling of the ECC water and the initial temperature of the downcomer walls, liquid would either bypass the downcomer and be carried by the steam out the break or penetrate the downcomer and flow into the lower plenum. Because the tests all had decreasing steam ramps, the behavior was initially complete bypass, then as the steam flow rate decreased, partial bypass and finally complete penetration to the lower plenum.

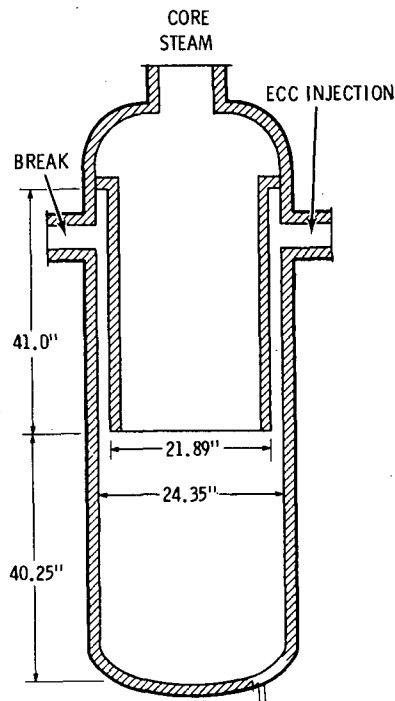


FIGURE 2.4-1. Diagram of Battelle Columbus 2/15-th Scale Downcomer Vessel

The test procedure used in the ramped steam flow rate, hot wall tests was as follows:

- Using steam, the vessel was heated to the required wall temperature.
- The ECC water injection rate and initial reverse core steam flow rate were established by routing these flows to the ECC supply tank and containment vessel, respectively.
- Simultaneously, the steam and ECC flows were switched to the vessel and the decreasing steam ramp was initiated.

Pressures, temperatures and liquid levels were recorded during the tests.

#### 2.4.2 COBRA/TRAC Model Description

The COBRA/TRAC vessel nodalization to model the BCL downcomer test is shown in Figure 2.4-2. It consists of 57 hydrodynamic cells in 9 channels and 2 sections. Section 1 models the lower plenum using 1 channel and 4 axial levels spaced 10 in. apart. Channel 2 models the region beneath the downcomer and connects to channels 4 through 9 above. Section 2 models the downcomer

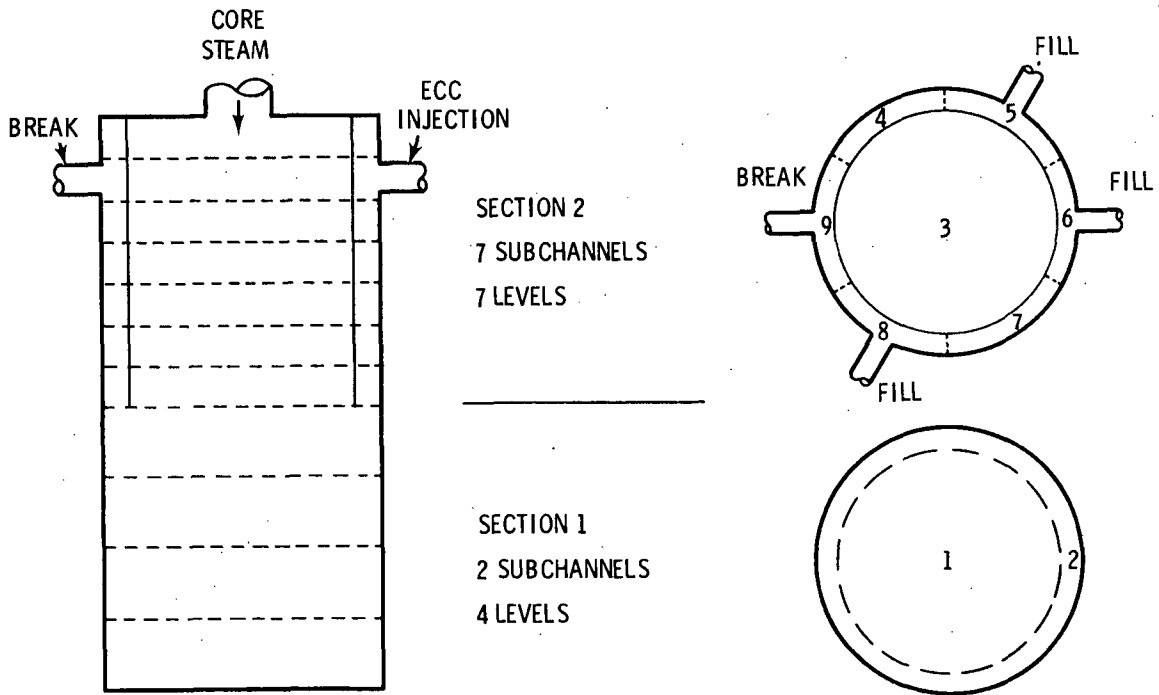


FIGURE 2.4-2. COBRA/TRAC Model of BCL Downcomer

and inner core barrel using 7 axial cells, each 6 in. high. The reverse core steam flow rate versus time was specified at the top of channel 3 using a mass flow rate boundary condition. ECC injection rates in the sixth level of channels 5, 6 and 8 were also specified using boundary conditions. The pressure boundary condition at the broken cold leg was modeled using PIPE and BREAK components. The hot leg plugs were simulated by applying zero flow rate boundary conditions at each face of the sixth hydrodynamic cell in channels 4 and 7. Six channels were used in the downcomer to model velocity and void profiles, the four cold leg connections and the hot leg plugs.

The physical structure of the test section was modeled with 12 rods, each representing a fraction of the downcomer circumference seen by the channels. The conduction heat transfer model was used to calculate the effects of stored energy in the vessel and downcomer walls.

Two tests, 404 and 501, were simulated. Table 2.1 summarizes the test conditions. The ramps used on the reverse core steam flow rate (Ref. 7) are given in Table 2.2. Test 501 was run at a higher pressure and initial wall

TABLE 2.1. Battelle Columbus 2/15th Scale Downcomer Test Conditions

<u>Test Number</u>	<u>Initial Wall Temp. (°F)</u>	<u>Initial ECC Subcooling Temperature (°F)</u>	<u>Initial Steam Flow Rate, (lbm/sec)</u>	<u>ECC Injection Rate, (gpm)</u>	<u>Initial Containment Pressure (psia)</u>
404	355	121	5.55	243	28.3
501	550	105	3.28	412	81.9

TABLE 2.2. Reverse Core Steam Flow Rate Ramps for BCL 2/15th Scale

Downcomer Tests			
Test 404		Test 501	
<u>Time (sec)</u>	<u>Fraction of Initial Flow</u>	<u>Time (sec)</u>	<u>Fraction of Initial Flow</u>
0.0	1.0000	0.0	1.0000
1.0	1.0000	1.0	1.0000
2.111	0.9817	1.909	0.9926
3.222	0.7740	2.818	0.9850
4.333	0.6092	3.727	0.9813
5.444	0.4597	4.636	0.9552
6.556	0.3154	5.546	0.9291
7.667	0.1911	6.455	0.8956
8.778	0.1215	7.364	0.8735
9.889	0.0962	8.273	0.8582
11.000	0.0841	9.182	0.8432
12.110	0.0778	10.090	0.8358
13.220	0.0713	11.000	0.8286
14.330	0.0582	11.910	0.8360
15.440	0.0517	12.820	0.8397
16.560	0.0440	13.730	0.8435
		14.640	0.8547

temperature than 404. It also had a larger ECC injection rate, and a smaller steam flow rate. Therefore, it should allow a faster filling rate than test 404.

### 2.4.3 Discussion of Results

Figures 2.4-3 and 2.4-4 show the lower plenum liquid volume versus time for the ramped steam hot wall tests 404 and 501. (ECC injection began at 1 sec.) The data comparison is good. COBRA/TRAC predicted the initial delay time to within 1 sec. The filling rate for test 404 was in excellent agreement. A slightly higher filling rate occurred in test 501, because the containment pressure used in COBRA/TRAC was too high. During periods of condensation, the containment pressure was greater than the lower plenum pressure and reverse break flow was predicted.

The condensation led to flow oscillations in the downcomer. During periods of condensation the pressure in the lower plenum decreased and the rate of liquid delivery increased. This is shown in Figure 2.4-5 a plot of the lower plenum pressure, and Figure 2.4-6, a graph of the net condensation rate in the vessel. For example, the condensation rate at 15 sec is high (nearly 6.0 lbm/sec), while the pressure is low (about 18 psia). This caused the lower plenum filling rate to increase as shown in Figure 2.4-3. As the condensation increased and decreased, the rate of liquid delivery to the lower plenum oscillated.

Most of the delivery occurred on the side of the downcomer opposite the broken cold leg. Starting from the bottom of the downcomer and moving up, the flow pattern was: film flow, then inverted pool where the liquid fraction typically increased from 0.05 to 0.8, and finally bubbly flow. Generally, the farther around the downcomer circumference from the break, the lower the transition to inverted pool occurred. As a result, the film to bubble interface was tilted with the lower side opposite the broken cold leg.

COBRA/TRAC's predictions of the lower plenum filling rate agrees well with the data. This implies that the physical models for phase interfacial drag and heat transfer in the film, inverted pool and bubbly flow regimes are properly representing the ECC bypass behavior in the downcomer. This simulation was run on cycle 8 of COBRA/TRAC.

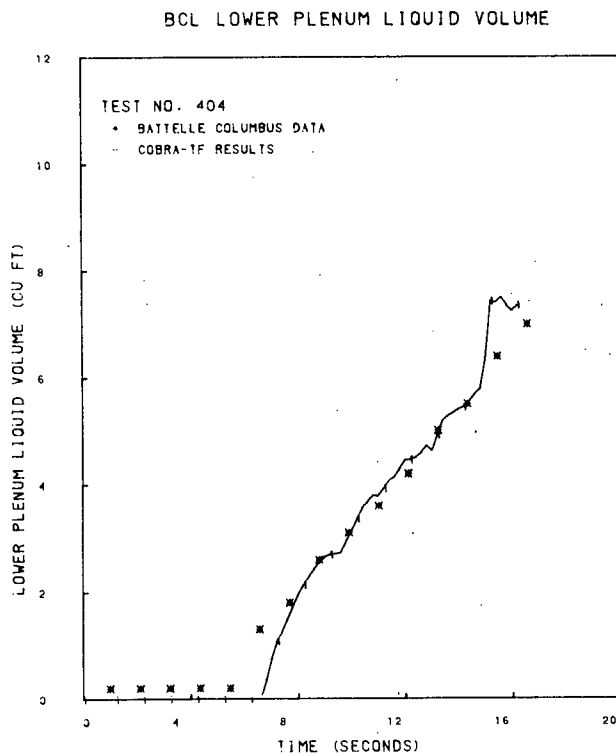


**FIGURE 2.4-3. Lower Plenum Liquid Volume vs. Time for Test 404**

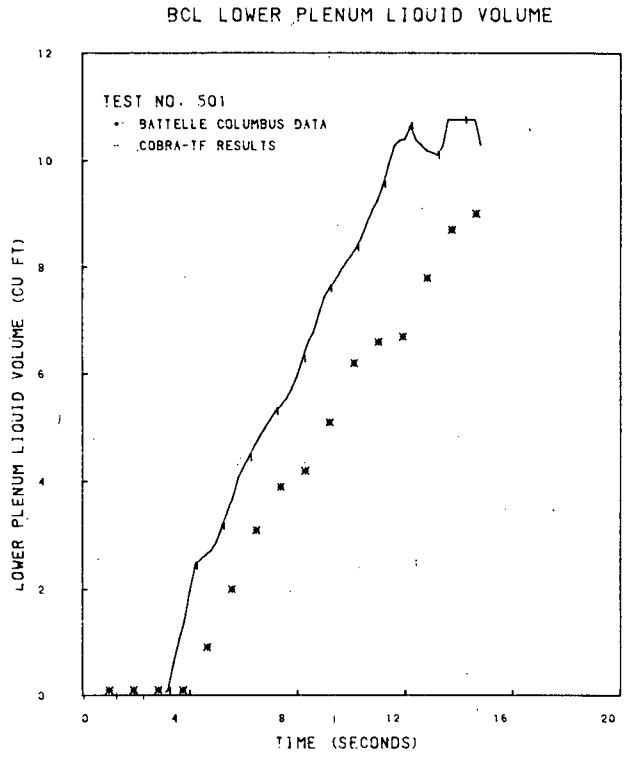


**FIGURE 2.4-4. Lower Plenum Liquid Volume vs. Time for Test 501**

BCL LOWER PLENUM PRESSURE

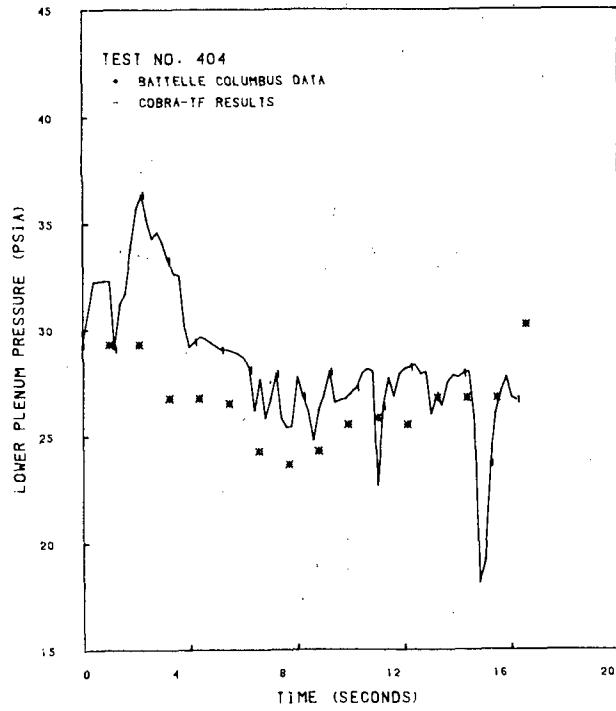


FIGURE 2.4-5. Lower Plenum Pressure vs. Time for Test 404

BCL CONDENSATION RATE VS. TIME

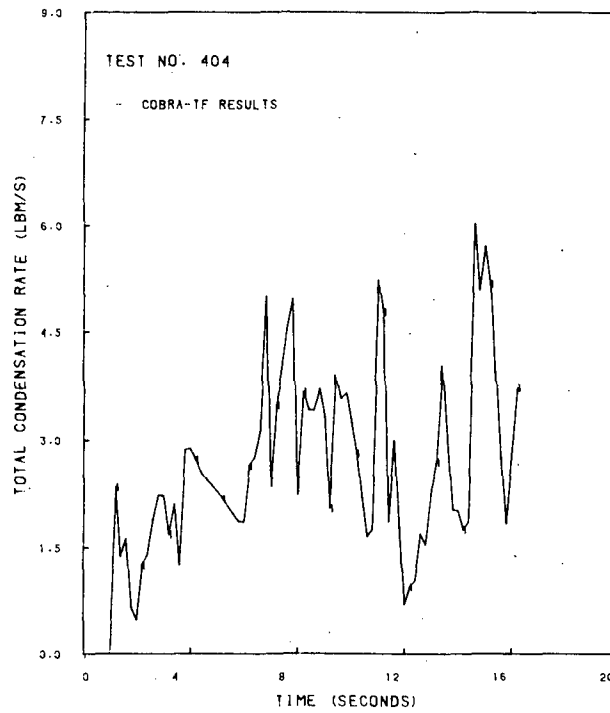


FIGURE 2.4-6. Net Condensation Rate in the Vessel vs. Time for Test 404

## 2.5 FEBA FORCED BOTTOM REFLOOD EXPERIMENT

Forced flow bottom reflood experiments were performed in the Flooding Experiments in Blocked Arrays (FEBA) test assembly in Karlsruhe, West Germany (Ref. 8,9). The purpose of these experiments was to determine the effects of grid spacers and flow blockages on reflood heat transfer. This was done by performing a series of tests with different grid spacer and blockage configurations. These included tests with normal grid spacers, tests with a single grid spacer removed, and tests with sleeve blockages attached to heater rods.

The test with normal grid spacers and no blockage was simulated with COBRA/TRAC to assess the models used for reflood heat transfer and reflood hydrodynamics.

### 2.5.1 Description of Experiment

The FEBA test facility, shown schematically in Figure 2.5-1, was originally designed to simulate idealized reflood conditions in a German PWR core with constant forced bottom reflood, system pressure and test section geometry. The experimental test loop consisted of a lower plenum, a test section with a 5x5 electrically heated rod bundle, an upper plenum, buffer tank and associated piping.

During test operations, coolant was pumped from a storage tank into the lower plenum of the test assembly. The water was regulated at a prescribed level in the lower plenum and the heater rod and housing were heated to the prescribed initial temperatures. Reflood water injection was then initiated. Water entering the test section generated vapor as a result of heat transfer from the heated rods. Steam and entrained water droplets were transported upward through the test section and impinged on a steam/water separator in the upper plenum. The separated water droplets were moved away from the top of the heated length, reducing the amount of water fallback into the test section. The steam flowed through the steam/water separator and into a steam buffer tank. The buffer tank regulated the system pressure and exit steam temperature. A square test section housing enclosed the test section and connected the lower plenum to the upper plenum. The housing was insulated to reduce heat losses to the environment.

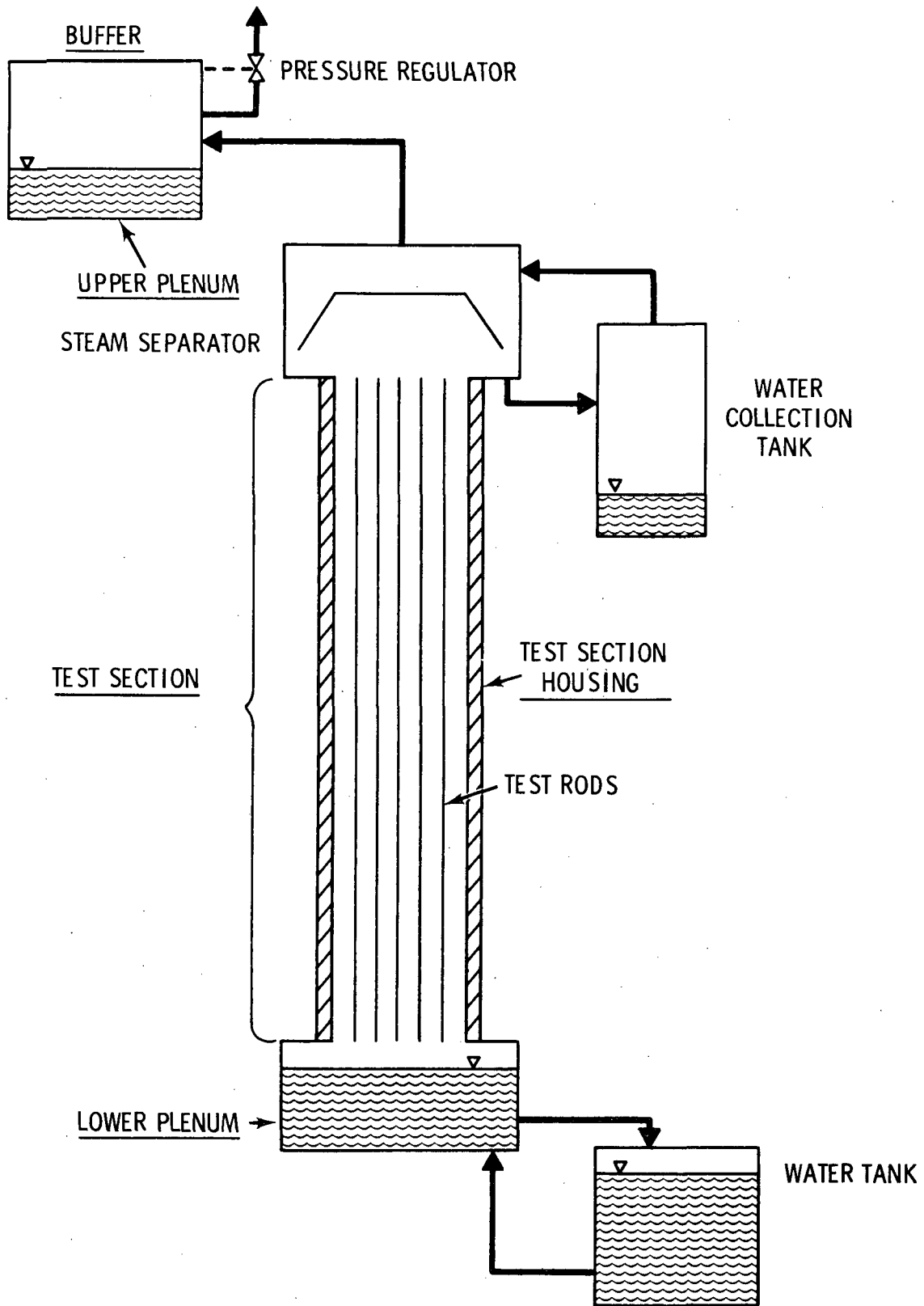


FIGURE 2.5-1. Schematic of FEBA Test Facility

The test section consisted of a 5x5 square array of electrical heater rods. A cross-sectional view of the test section and one representative heater rod are shown in Figure 2.5-2. The test section wall thickness was 6.5 mm. The rod pitch was 14.3 mm. The rod outside cladding diameter was 10.75 mm with a diametral clad thickness of 2.1 mm. The outside diameter of the heater element was 8.55 mm. The upper ends of the heater rods were bolted to the top of the test assembly while the lower ends were allowed to hang free, permitting axial movement. Horizontal movement and/or bowing of the rods was restricted by seven typical KWU-PWR grid spacers every 545 mm and centered on the test section midplane.

The electrical heater rods were constructed of spiral-wound heating elements embedded in magnesium oxide insulators. The cosine power profile of nuclear fuel was approximated by a seven-step power profile. The length of each power step and the peak-to-average power factors are shown in Figure 2.5-3.

The test assembly was initially heated by radiation from the heater rods for about 2 hours prior to reflood. During this heat-up phase the heater rods were at a low power level and surrounded by stagnant steam. These test conditions were maintained until the desired peak cladding temperatures were reached.

Reflood was initiated after the cladding temperatures reached the required initial temperature. Water was injected into the lower plenum with a constant flow rate of 3.5 cm/sec, an inlet temperature of 40°C, and at a pressure of 4 bars. When the rising water reached the lower end of the heated length, the rod power was increased to the ANS + 20% decay heat level corresponding to 40 seconds after scram. The power was then decreased according to the ANS +20% curve during the remainder of the test. The temporal power decay curve used for test run 216, normalized to  $P_0$ , where  $P_0$  was the peak power at time zero is shown in Figure 2.5-4. The initial test parameters for test 216 have been tabulated in Table 2.3.

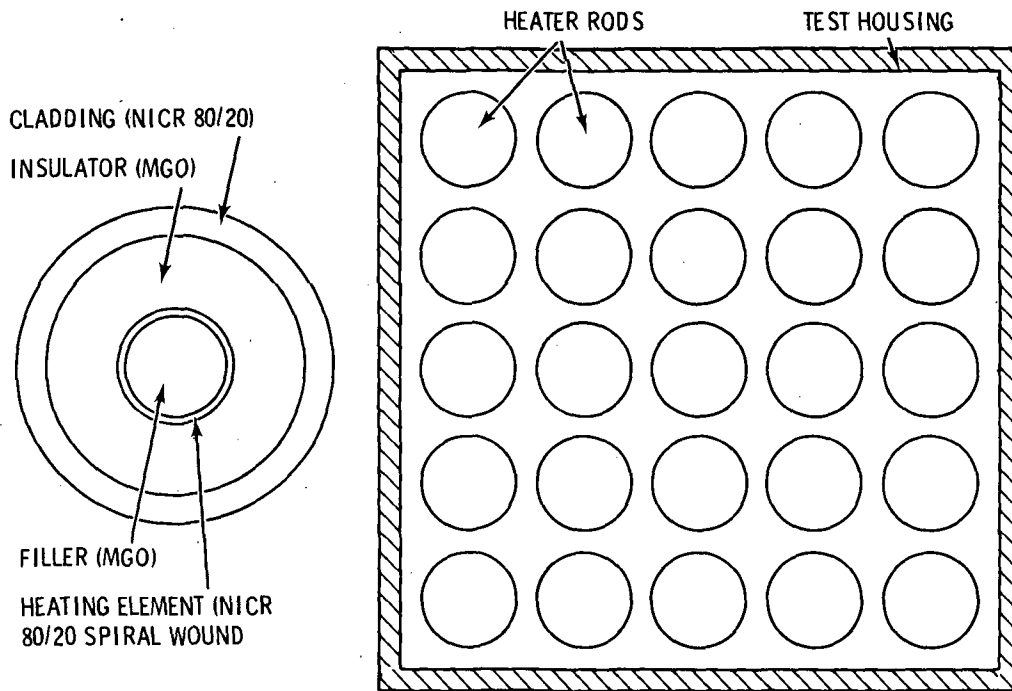


**FIGURE 2.5-2.** Cross Section of FEBA Test Section 5x5 Bundle and Representative Heater Rod

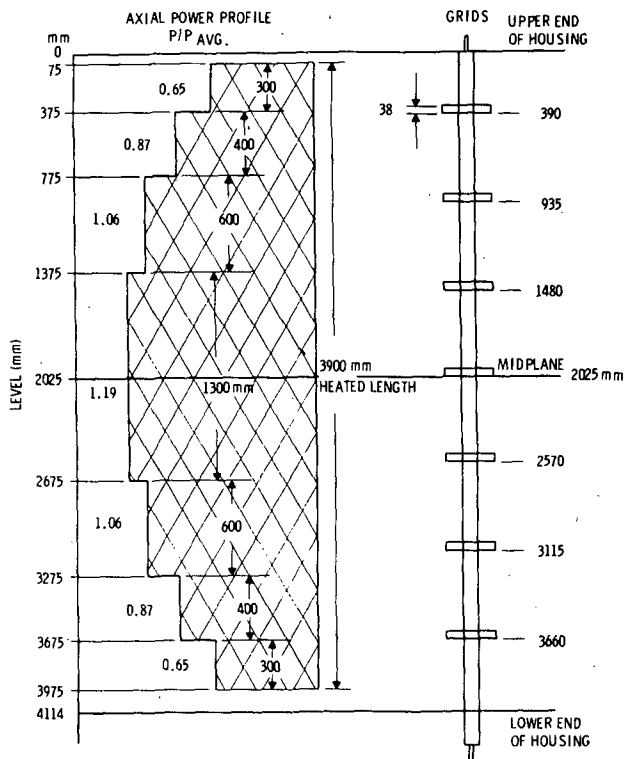


**FIGURE 2.5-3.** Axial Power Profile and Grid Spacer Locations for FEBA Test Section

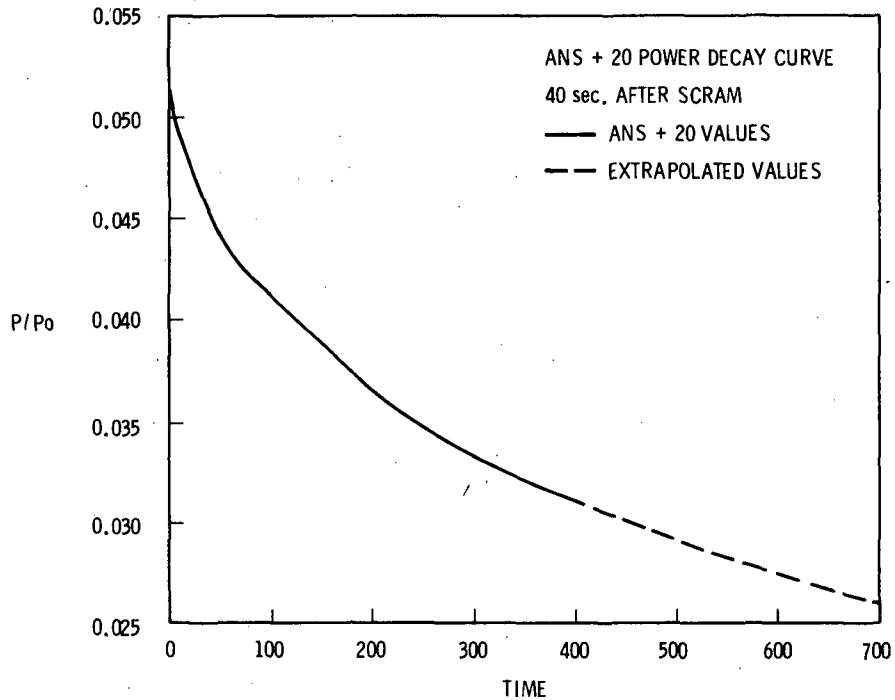


FIGURE 2.5-4. Power Decay Curve for FEBA Test Run 216

TABLE 2.3. Boundary Conditions for FEBA Test 216

Initial peak rod temperature	800°C
Peak rod power	0.8 kW/ft
Constant flow rate	3.5 cm/sec
Inlet coolant temperature	40°C
System pressure	4 bars

### 2.5.2 COBRA/TRAC Model Description

The FEBA test facility was modeled with three components: a one-dimensional vessel component with mass injection at the bottom boundary; a PIPE component connected to the top of the vessel; and a BREAK component connected to the pipe. The COBRA/TRAC nodalization schematic is shown in Figure 2.5-5. The vessel component modeled the lower plenum, test section and upper plenum. The total fluid flow area (38.9 cm<sup>2</sup>) was modeled using four channels; one channel for the lower plenum and three for the heated length and

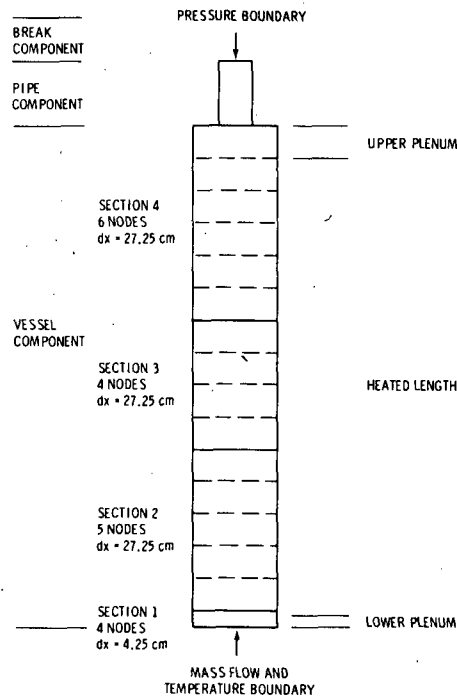


FIGURE 2.5-5. COBRA/TRAC Model of FEBA Test Section

upper plenum. Three channels were used in the heated length so that the mesh size could be reduced in the grid spacer vicinity so that the effect of grids on heat transfer could be studied in later simulations. There were 19 fluid nodes in the four channels. The 25 heater rods were modeled using a single average rod. The test section housing was modeled with a tube rod with an inside heat transfer surface and an insulated outer surface. A one-dimensional nodalization was used since it was not believed that any significant radial distribution would occur in the experiment. The vertical node length was chosen to coincide with measurement locations.

The vessel, pipe and break components were initialized with saturated steam at 2.8 bars. A constant flow boundary of 3.5 cm/sec at 54°C was specified at the bottom of the vessel. At the break, a pressure boundary of 2.8 bars was specified. The break boundary condition simulated the effects of the pressure buffer.

The test pin rod was initialized with an axial temperature profile having a maximum cladding temperature of 800°C and a step power profile with a maximum peak power of 0.8 kW/ft. The rod modeling the housing was initialized

with an axial temperature profile and zero power generation. Both temperature profiles were symmetric about the test section midplane. The initial rod and housing temperatures used in the simulation have been plotted in Figure 2.5-6. Figure 2.5-7 shows the seven step axial power profile and the power profile as modeled in COBRA/TRAC. The original power profile was modified to fit the fluid cell boundaries with reference to the original power profile step changes. The total power to the test section has been conserved in the power profile.

The reflood transient was run from a standing start, with the boundary conditions described in Table 2-3, and the ANS +20% rod power decay. The simulation continued until 75% of the heated rod was quenched.

### 2.5.3 Discussion of Results

The COBRA/TRAC prediction of temperature histories at six elevations in the rod bundle are compared with the experimental data in Figures 2.5-8 through 2.5-13. The FEBA temperature data for several rods were averaged to obtain an average temperature for each elevation. The vertical bars indicate the maximum variation in measured temperatures between rods on a given level. COBRA/TRAC does a satisfactory job of predicting the peak temperatures and quench times at all elevations. This implies that the amount of desuperheating of the steam due to the existing grid spacer model is of the proper magnitude. Further examination of Figures 2.5-8 through 2.5-13 shows that the calculated quench times become increasingly greater than the experimental as the axial elevation increases. This difference has been attributed to the underprediction of the liquid content of the flow in the upper portions of the bundle.

The bundle collapsed liquid levels as a function of time are compared in Figure 2.5-14. The experimental values for collapsed liquid level were calculated from full bundle differential pressure measurements. The computed values for collapsed liquid level were calculated by summing the liquid fraction multiplied by the node length for all nodes, then dividing by the total section length. The comparison between the COBRA/TRAC and experimental collapsed liquid levels is reasonable in the early portion of the transient. This is also where the best data comparison between peak rod temperatures and



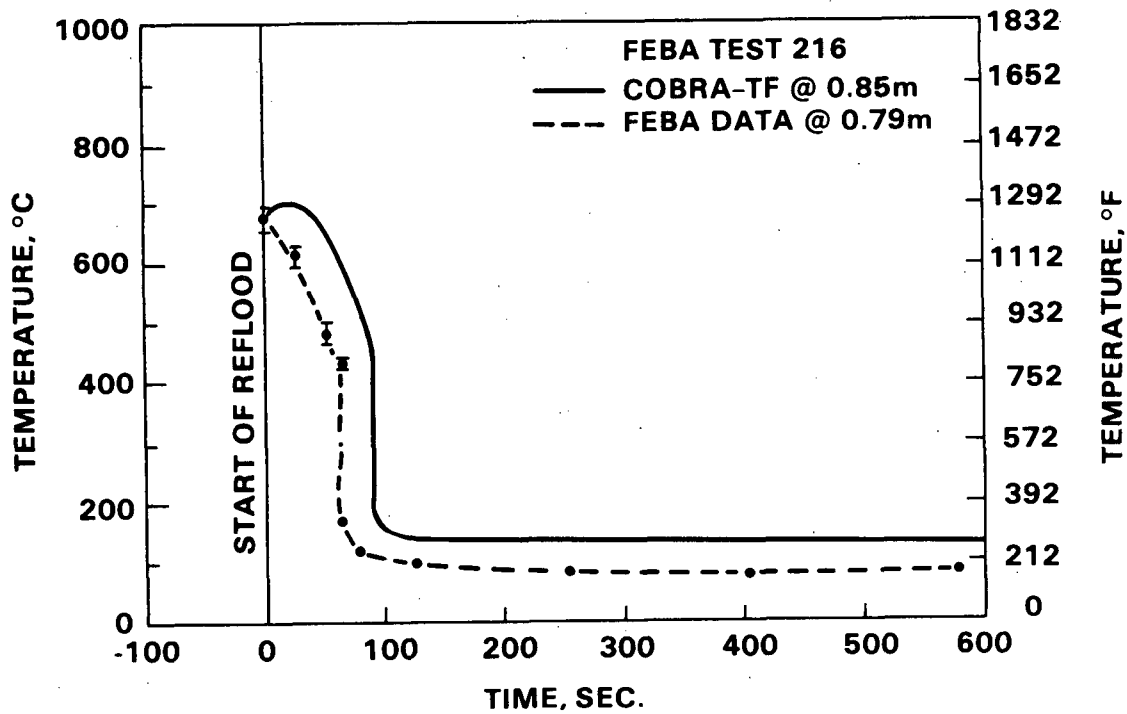


FIGURE 2.5-8. COBRA/TRAC Predicted Rod Temperatures at 0.8m for FEBA Test 216

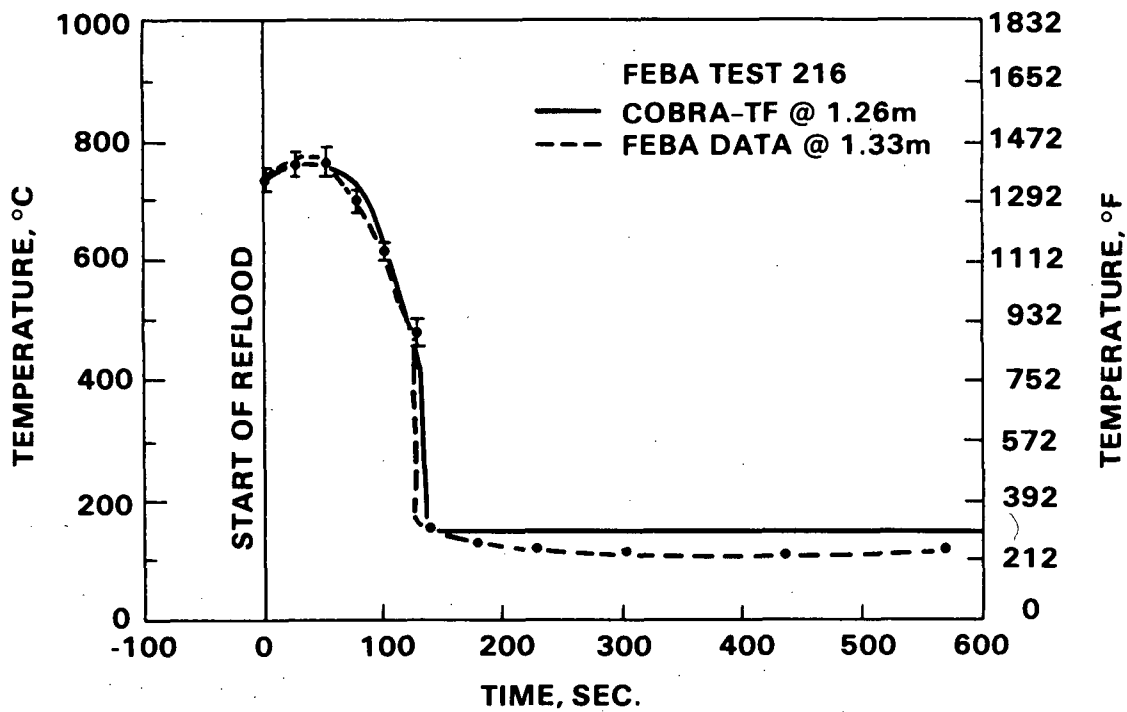


FIGURE 2.5-9. COBRA/TRAC Predicted Rod Temperatures at 1.3m for FEBA Test 216

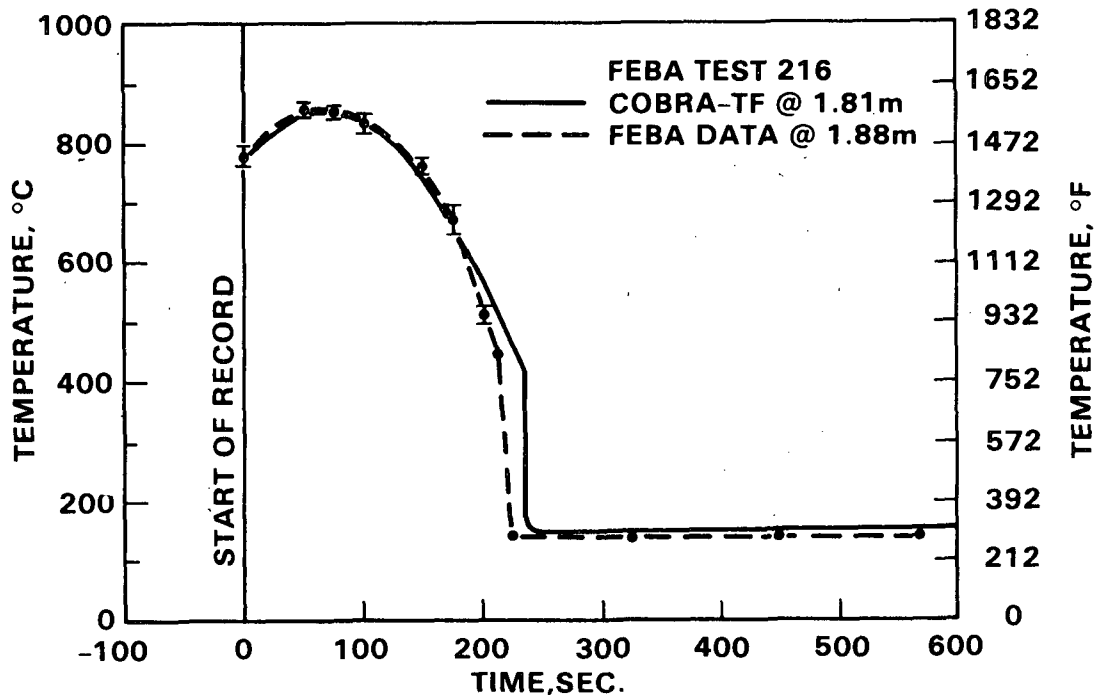


FIGURE 2.5-10. COBRA/TRAC Predicted Rod Temperatures at 1.9m for FEBA Test 216

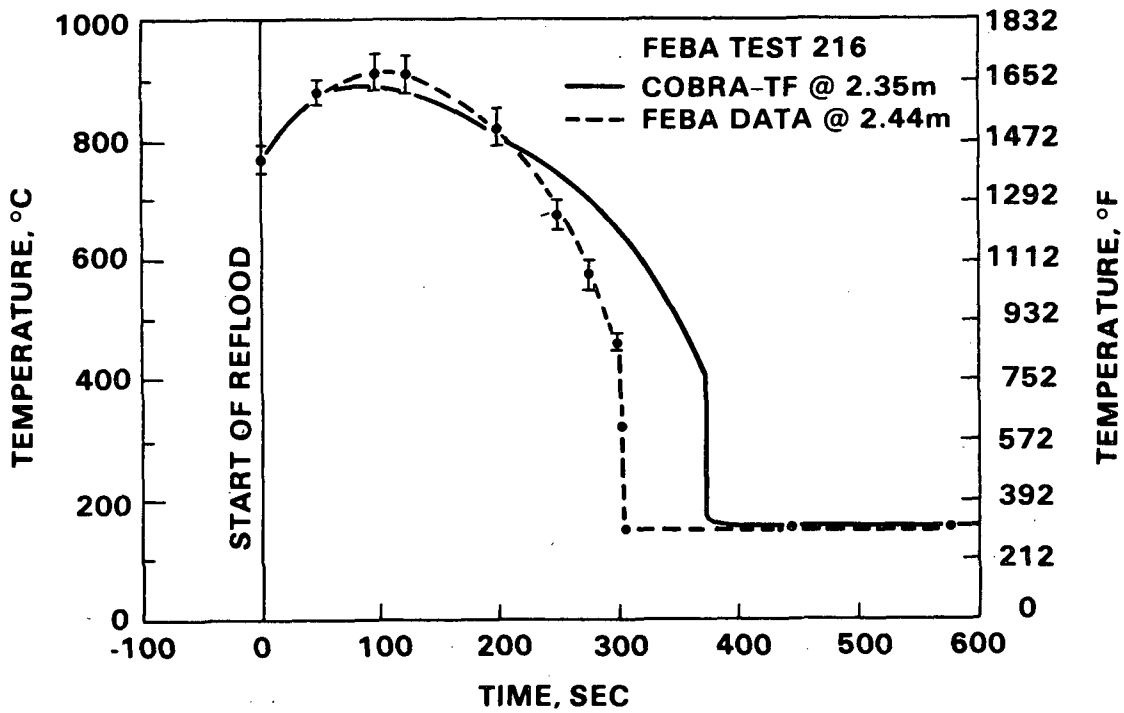


FIGURE 2.5-11. COBRA/TRAC Predicted Rod Temperatures at 2.4m for FEBA Test 216

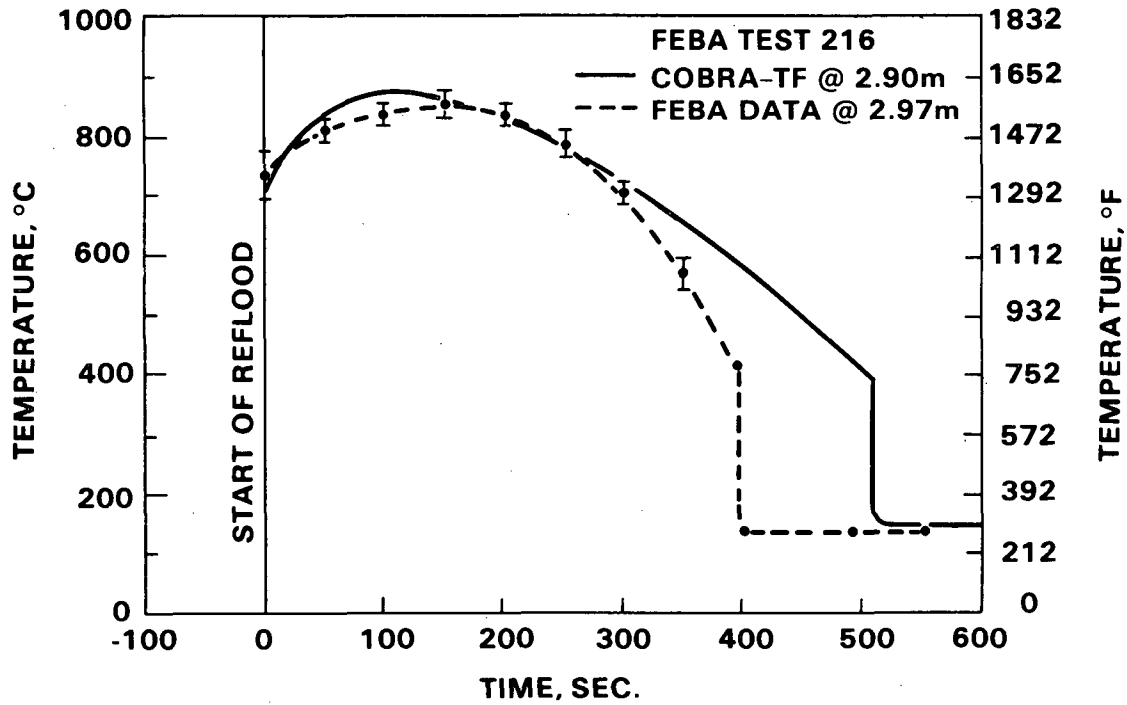


FIGURE 2.5-12. COBRA/TRAC Predicted Rod Temperatures at 3.0m for FEBA Test 216

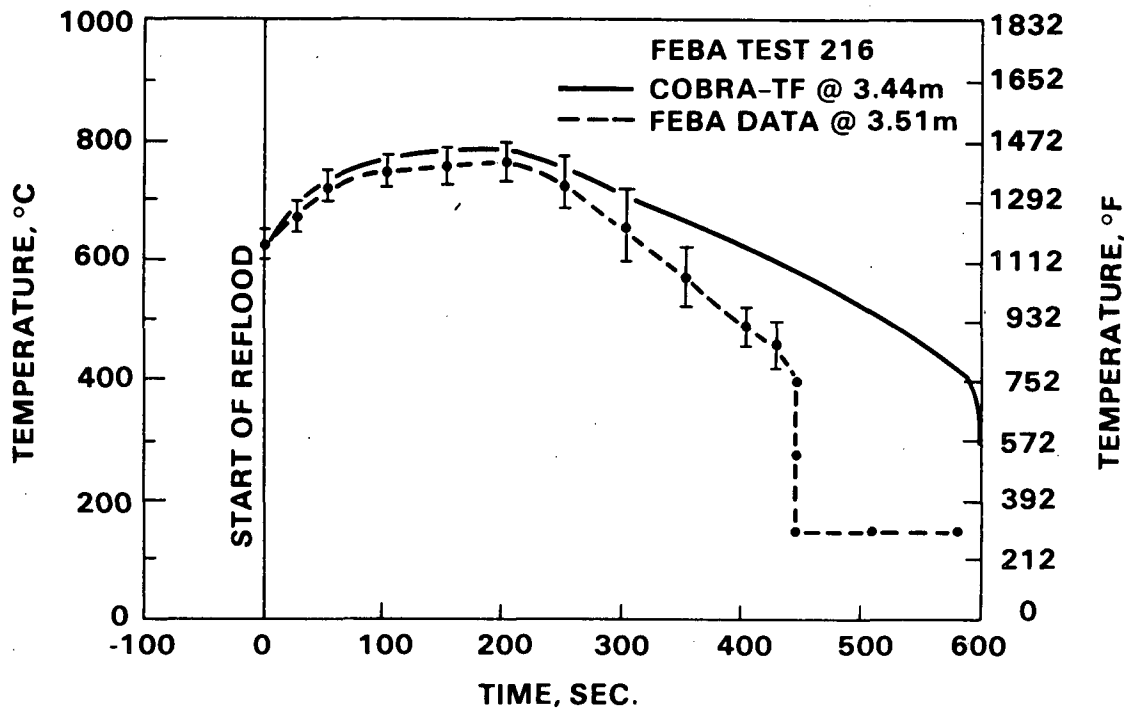


FIGURE 2.5-13. COBRA/TRAC Predicted Rod Temperatures at 3.5m for FEBA Test 216

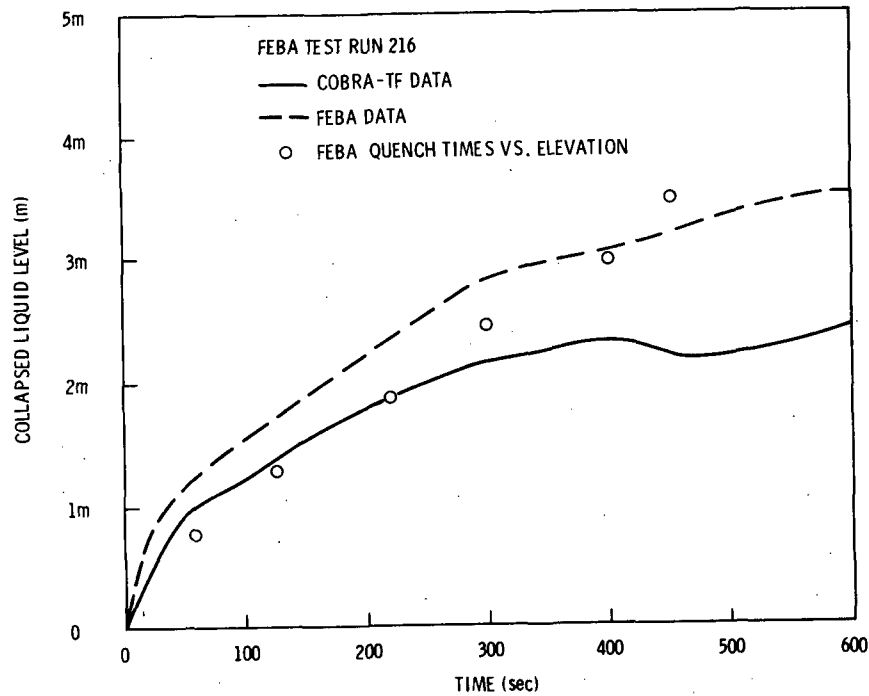


FIGURE 2.5-14. Collapsed Liquid Level vs. Time for FEBA Test 216

quench times occur. The computed liquid level drops significantly below the measure level later in time, when the calculated temperatures are higher than the experimental values.

The actual quench time for six axial elevations has also been included in Figure 2.5-14. By comparing these quench times with the collapsed liquid level, it could be concluded that a significant amount of water existed above the quench front in the experiment at all elevations, while less water content was predicted by COBRA/TRAC. It should also be noted that the closer the quench times are to the computed liquid level, the closer the computed peak temperatures and quench times are to the experimental values.

Since the amount of liquid in the test section is underpredicted, the quench time will be later. This effect is seen in the temperature plots. The results of this and other reflood simulations indicate that more work needs to be done on defining the froth region above the quench front. The froth region is a transition region between the bubbly flow below the quench front and the dispersed droplet flow above the quench front.

Although some discrepancies have been noted between the predicted and experimental results, a satisfactory job was done of predicting the peak temperatures and quench times in the test section. A better prediction of the liquid level would probably improve the prediction of the quench times in the upper portions of the bundle.

This simulation was run on cycle 8.

## 2.6 FLECHT LOW FLOODING RATE COSINE TEST SERIES

COBRA/TRAC has been run against a number of forced flow bottom reflood tests with a variety of constant flooding rates. The runs presented here, FLECHT 00904 and FLECHT 04444, (Ref. 10,11) evaluate COBRA/TRAC's thermal and hydraulic calculational capabilities against a medium and a high constant flooding rate bottom reflood test. The purpose of these simulations was to assess the heat transfer selection logic, heat transfer correlations, rezoning heat transfer logic, interfacial heat transfer for dispersed flow, interfacial drag correlations for hot wall and normal flow regimes and the reflood entrainment rate model.

### 2.6.1 Description of Experiment

There were two major objectives in the FLECHT (Full Length Emergency Cooling Heat Transfer) low flooding rate cosine tests. The first was to provide experimental data for use in reflood model development. The second was to evaluate the heat transfer capabilities of a PWR emergency core cooling system during a postulated loss-of-coolant accident. Only the test section was modeled with COBRA/TRAC, using known inlet and outlet boundary conditions from system measurements. The remainder of the system was not modeled.

The FLECHT low flooding rate cosine test series rod bundle, shown in Figure 2.6-1, consisted of 91 electrical heater rods arranged in a 10x10 square array, simulating a quarter section of a 15x15 PWR fuel assembly. The rod diameter was 0.422 in. and the rod pitch was 0.563 in. The bundle contained eight control rod thimbles of 0.545 in. O.D. and one instrument tube of 0.463 in. O.D. The test section was enclosed by a square housing with internal cross sectional dimensions of 5.889 x 5.889 in. and a wall thickness of 0.02 in. Horizontal movement and/or bowing of the heater rods was

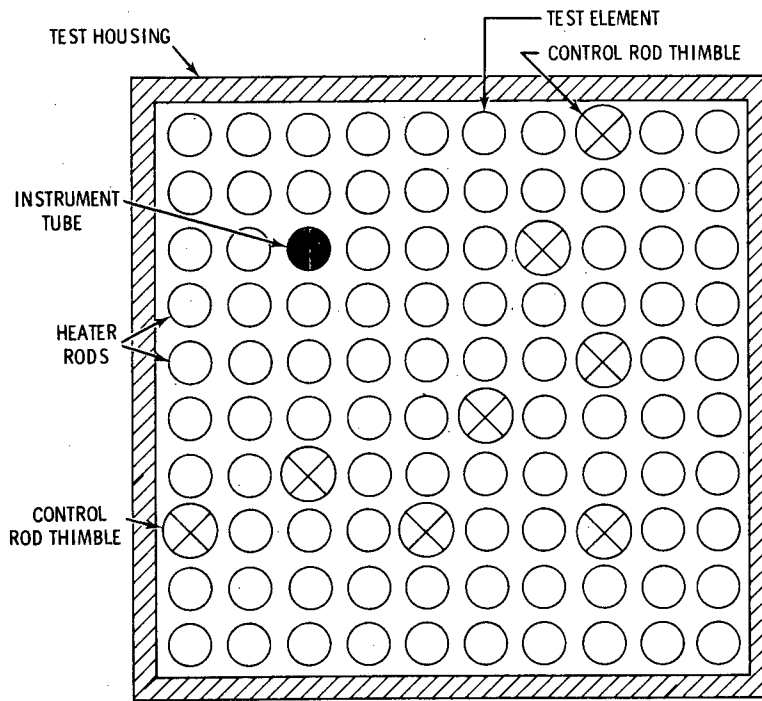


FIGURE 2.6-1. FLECHT Test Bundle Cross Section

restricted by eight typical Westinghouse PWR grid spacers located at 20.5 in. intervals, starting at the beginning of the heated length.

The electrical heater rods in the test section were constructed of a spiral-wound heating element embedded in a magnesium oxide insulator. A seven-step power profile approximated a chopped cosine power profile. The power profile and locations of the eight grid spacers are shown in Figure 2.6-2.

Prior to the start of reflood, the test assembly was heated by radiation from the heater rods and by external strip heaters. These test conditions were maintained until the desired initial cladding and housing temperature distributions were achieved. During this heat-up phase the heater rods were surrounded by stagnant steam. When the desired axial cladding and housing temperature profiles were reached, the housing strip heaters were shut off and reflood was initiated at the predetermined flow rate, temperature and pressure. When the water reached the bottom of the heated length the rod power followed the ANS +20% decay heat rate for zero time delay after a

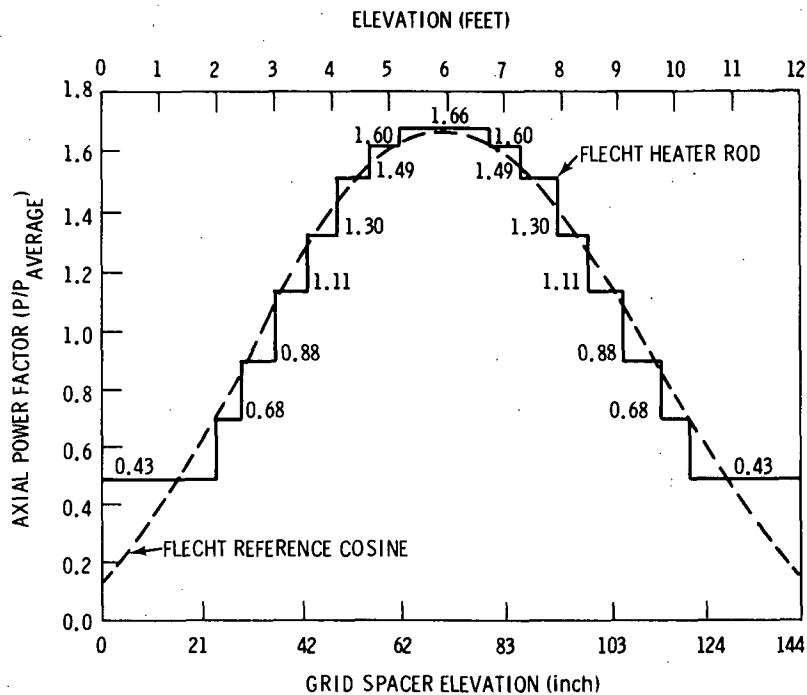


FIGURE 2.6-2. FLECHT Test Section Axial Power Profile and Grid Elevations

reactor shut down condition. The initial conditions for the transients are listed in Table 2.4. The axial housing temperatures in Table 2.4 are those obtained from thermocouple readings on the housing. Table 2.4 lists the initial clad temperature profiles for the heater rod in each experiment. The initial peak clad temperature was obtained by averaging the maximum temperature reading from all the thermocouples at the 6-ft level.

### 2.6.2 COBRA/TRAC Model Description

The FLECHT test bundle was modeled with three one-dimensional COBRA/TRAC components; a VESSEL component with constant mass injection and enthalpy at the bottom boundary, a PIPE component connected to the top of the vessel, and a BREAK component at the end of the pipe. The COBRA/TRAC noding diagram is shown in Figure 2.6-3. The vessel component modeled the heated length and upper plenum. A cross-sectional fluid flow area of 19.92 in.<sup>2</sup> was used over the total length. Three fluid channels were used to model the FLECHT test bundle; two for the heated length and one for the upper plenum. The two channels in the heated length were necessary to shift the temperature printout locations one-half of one fluid node. This allowed a direct comparison of

TABLE 2.4. Initial Condition for FLECHT Cosine Series Tests

	<u>Medium Flooding Rate</u> Run No. 00904	<u>High Flooding Rate</u> Run No. 04444
Upper Plenum Pressure (psia)	40	58
Initial Clad Temperature at 6 ft (°F)	998	1815
Rod Peak Power (kW/ft)	0.85	1.22
Flooding Rate (in./sec)	1.48	5.8
Coolant Temperature (°F)	128	155
Initial Housing Temperatures (°F)		
0 ft	135	273
2 ft	396	433
4 ft	562	533
5.5 ft	594	555
6 ft	606	617
6.5 ft	540	509
7 ft	533	510
7.5 ft	533	506
8 ft	539	504
10 ft	409	441
12 ft	277	295
lower plenum	115	150
upper plenum	282	358

predicted temperatures to the experimental temperatures for all locations above the 2-ft elevation, while keeping the bottom node at the bottom of the experimental heated length. There were 14 fluid nodes in the vessel component. A one-dimensional mesh was used in the test section since radial distributions were believed to be insignificant. The node length was chosen to allow comparison with measured data and yet maximize the time step size allowed by the Courant limitations.

The 91 electrical heater rods were modeled by one average rod with the average properties of all the heater rods. The test section housing was modeled with a second rod with an inside heat transfer surface and an

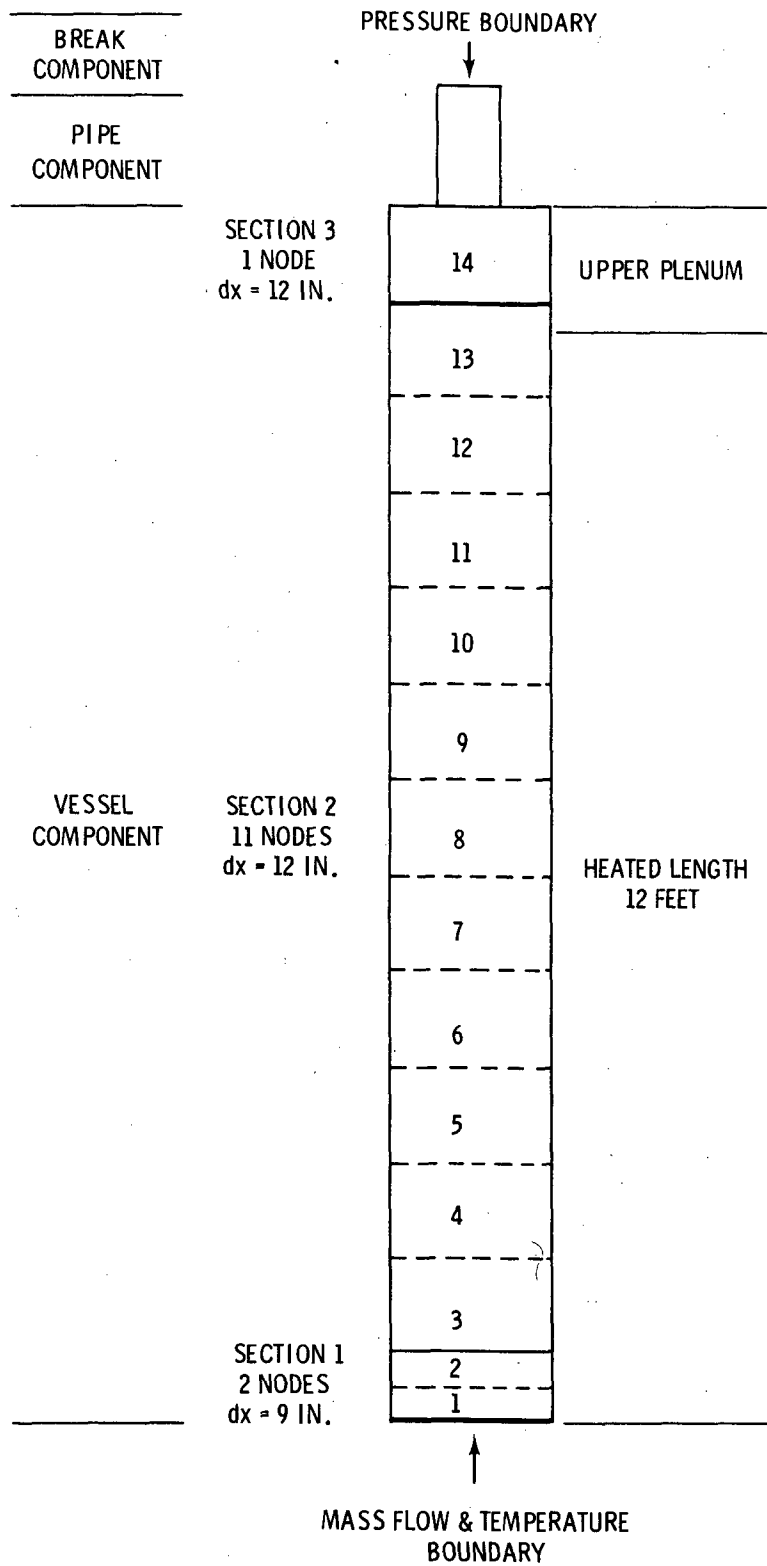


FIGURE 2.6-3. COBRA/TRAC Model of FLECHT Test Section

insulated outer surface. The test rod was initialized with the axial power profile shown in Figure 2.6-2 and the axial cladding temperature profile shown in Table 2.5. The values in Table 2.5 were obtained by averaging all the initial thermocouple readings (for a given elevation) presented in WCAP-8651 (Ref. 10). The housing was initialized with the axial temperature profile presented in Table 2.4 and zero power generation. The vessel, pipe and break components were initialized with saturated steam at the upper plenum pressure and zero flow. A constant inlet flow and enthalpy boundary was applied at the bottom of the vessel component. A pressure equal to the upper plenum pressure given in Table 2.4 was specified for the break component at the top of the vessel.

The reflood transient was run from a standing start with the initial conditions mentioned above and the ANS +20% power decay curve as a forcing function on the power level. The simulation continued until all levels in the heated section were quenched.

TABLE 2.5. FLECHT Initial Cladding Temperatures

<u>Elevation (Ave)</u> <u>ft</u>	<u>Medium Reflood Rate</u> <u>Run No. 00904</u> <u>°F</u>	<u>High Reflood Rate</u> <u>Run No. 04444</u> <u>°F</u>
0.0	270	516
0.5	404	730
1.0	447	760
1.5	500	769
2.0	614	1031
3.0	760	1293
4.0	893	1557
6.0	994	1742
6.5	975	1716
7.0	945	1638
8.0	879	1507
9.0	744	1170
10.0	636	931
11.0	420	628
12.0	277	277

### 2.6.3 Discussion of Results

#### Medium Reflood (FLECHT Test No. 00904)

Temperature versus time plots comparing COBRA/TRAC calculations with the experimental measurements for six axial levels are presented in Figures 2.6-4 through 2.6-9. The predictions for rod temperature are bundle radially averaged values. The thermocouple values are for a single rod at each axial level. COBRA/TRAC does a good job of predicting the overall temperature profile and quench time in lower elevations of the test section. But for higher elevations, COBRA/TRAC underpredicts the temperature for the earlier part of the transient and then overpredicts both the temperature and quench times in later portions of the transient. By comparing the measured quench time for the 9-ft elevation (~300 sec) with the quench time for the 10-ft elevation (~210 sec) it is obvious that a top-down quench front is developing. COBRA/TRAC underpredicts the velocity of this top quench front. This is probably a result of insufficient heat transfer near the minimum film boiling temperature when the entrained drops begin to wet the wall. Later data comparisons show an improved prediction of the top quench front. These data comparisons will be published in a later report.

Figures 2.6-10 through 2.6-15 indicate that the vapor fractions are predicted reasonably well. The void fractions below 8 ft are generally underpredicted while those above 8 ft are overpredicted. The lower liquid content at the higher elevations shows that the height of the froth front is underpredicted, indicating that further work may be required on the interfacial shear model for the hot wall flow regime.

The underprediction of the temperatures at the higher elevations is more difficult to explain. According to the vapor fraction plots, more entrainment is needed to correct the liquid levels in the lower portion of the test section. But increased entrainment would desuperheat the steam more, causing the rod temperatures to decrease further. A parametric study was performed to determine the sensitivity of the results to the effect of grids and the correlations for interfacial drag between vapor and drops. The results were insensitive to both of these parameters.

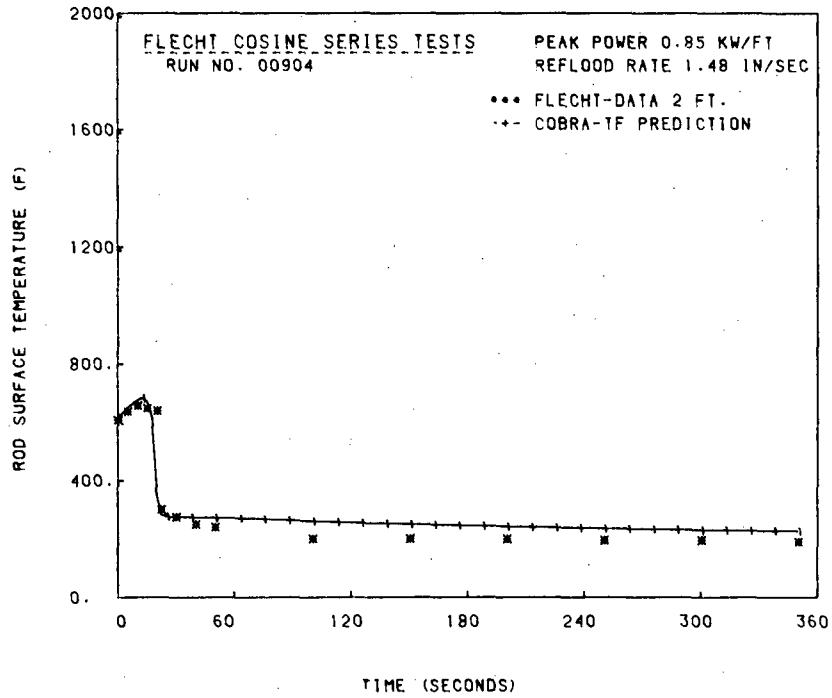


FIGURE 2.6-4. Temperature at 2-ft Elevation - FLECHT 00904

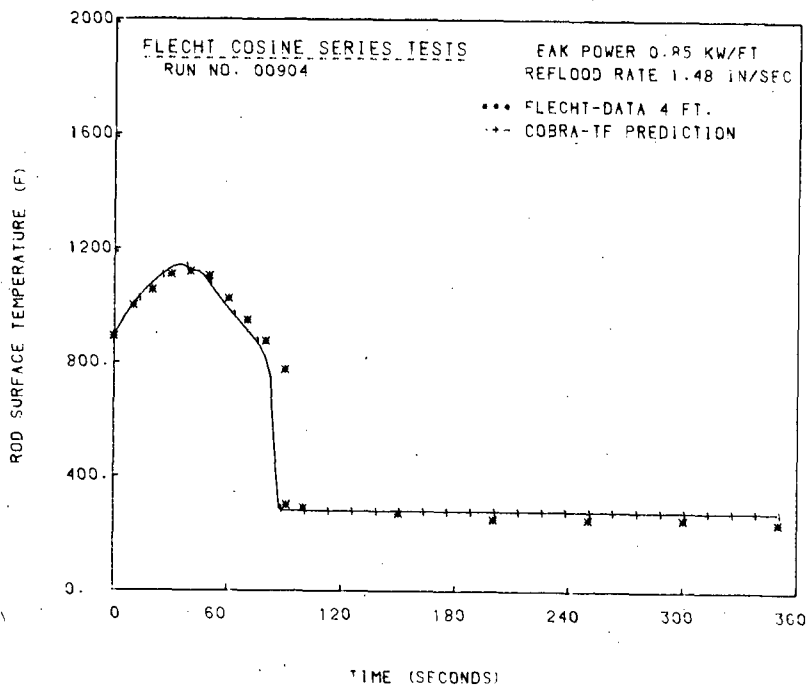
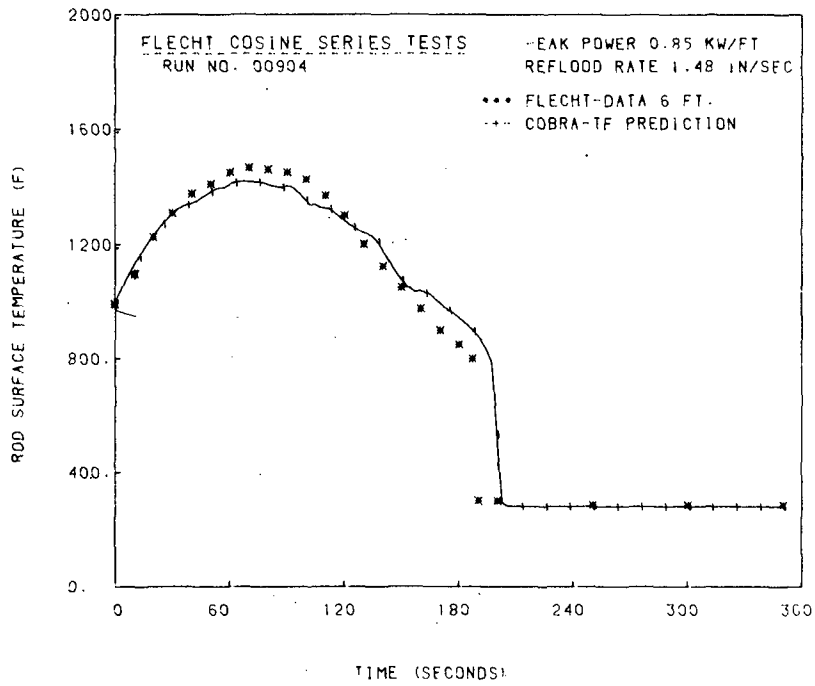
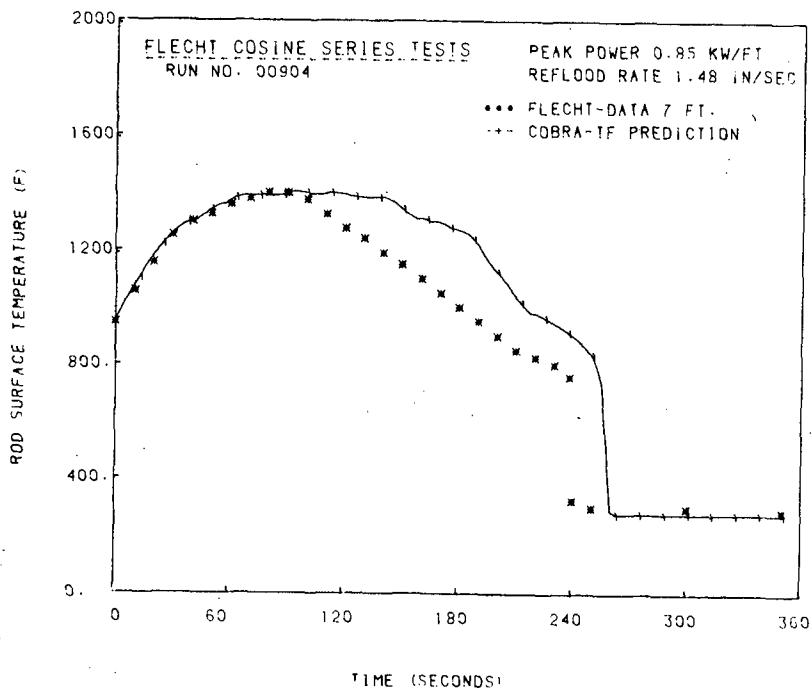


FIGURE 2.6-5. Temperature at 4-ft Elevation - FLECHT 00904



**FIGURE 2.6-6.** Temperature at 6-ft Elevation - FLECHT 00904



**FIGURE 2.6-7.** Temperature at 7-ft Elevation - FLECHT 00904

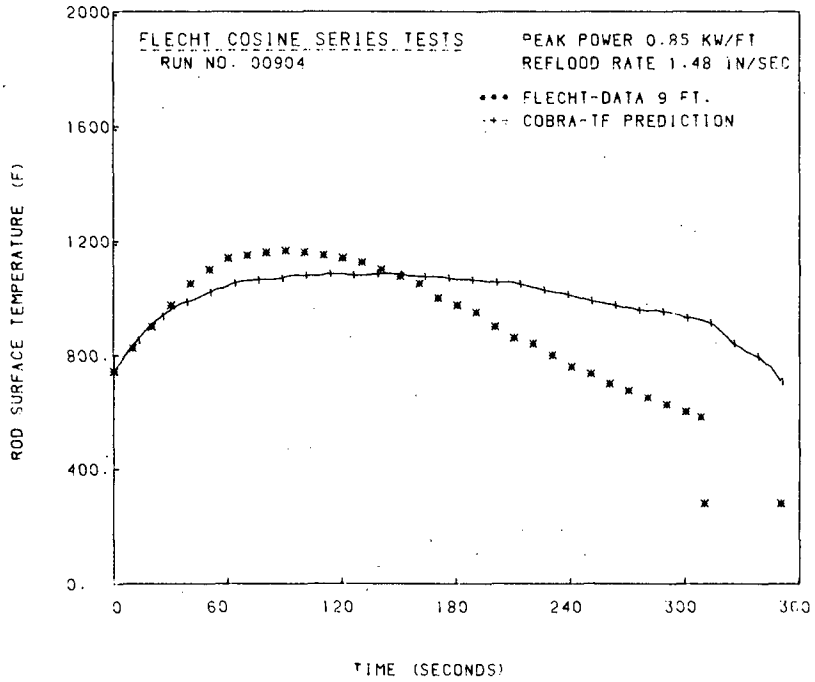


**FIGURE 2.6-8.** Temperature at 9-ft Elevation - FLECHT 00904

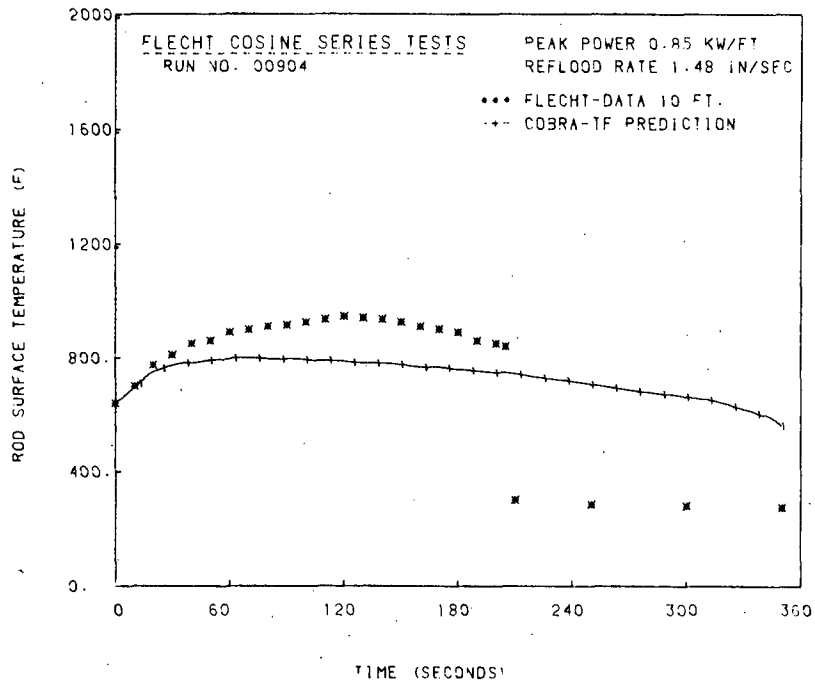


**FIGURE 2.6-9.** Temperature at 10-ft Elevation - FLECHT 00904

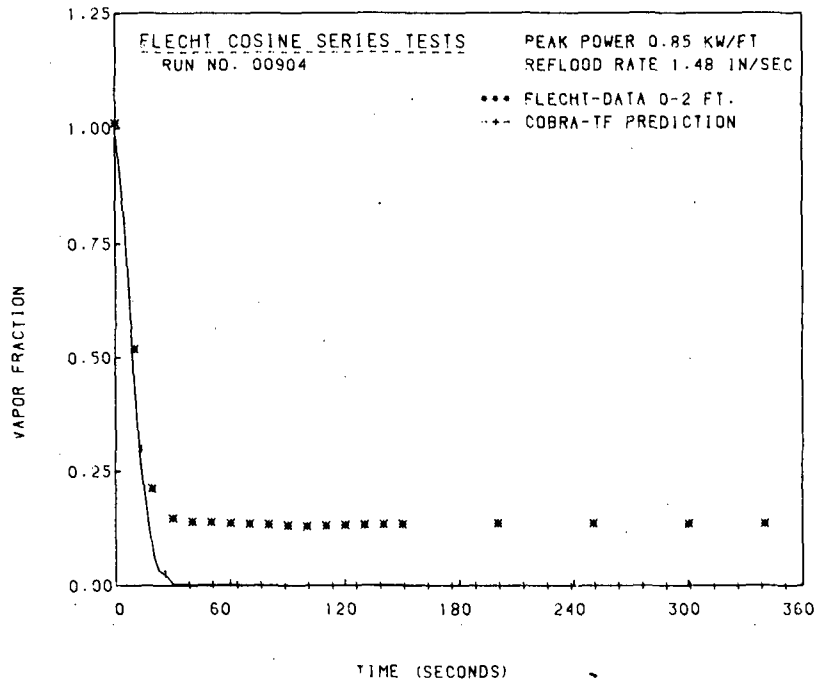


FIGURE 2.6-10. Vapor Fraction at 0 to 2-ft Elevation for FLECHT 00904

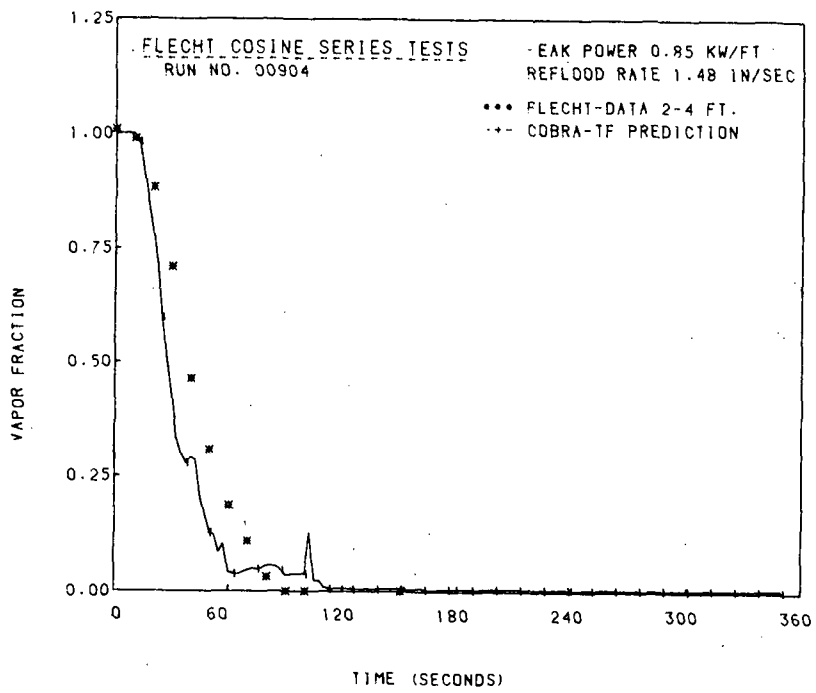
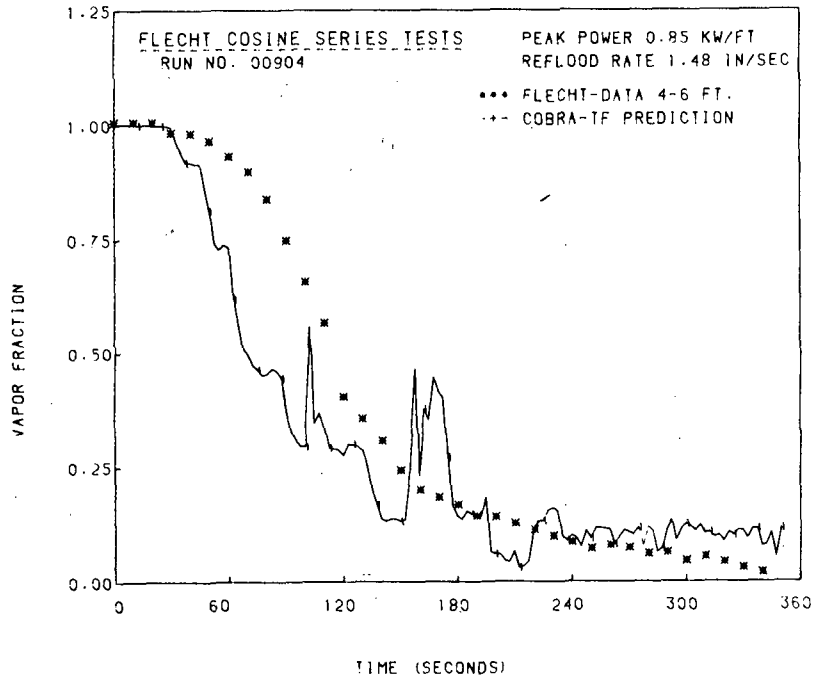
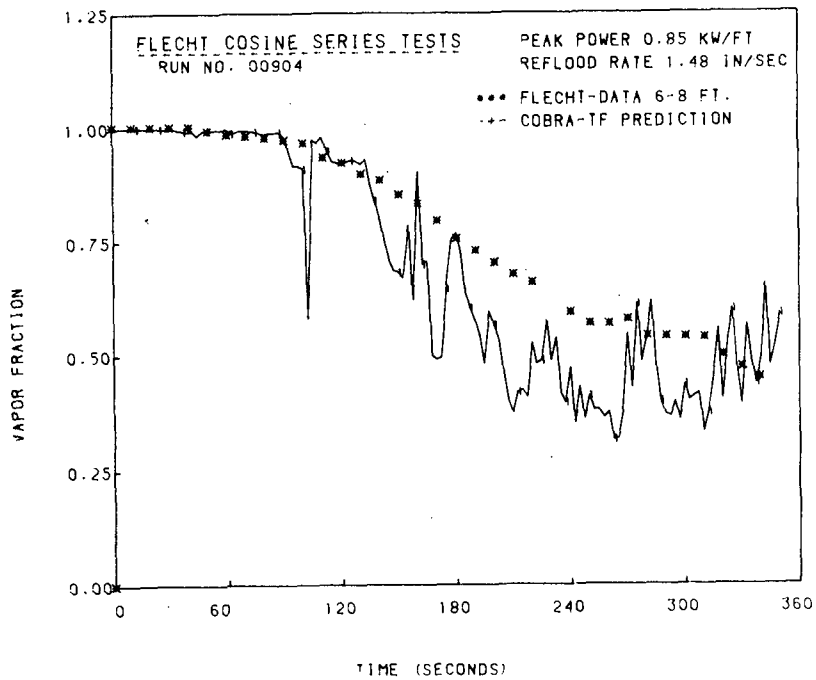


FIGURE 2.6-11 Vapor Fraction at 2 to 4-ft Elevation for FLECHT 00904



**FIGURE 2.6-12.** Vapor Fraction at 4 to 6-ft Elevation for FLECHT 00904



**FIGURE 2.6-13.** Vapor Fraction at 6 to 8-ft Elevation for FLECHT 00904

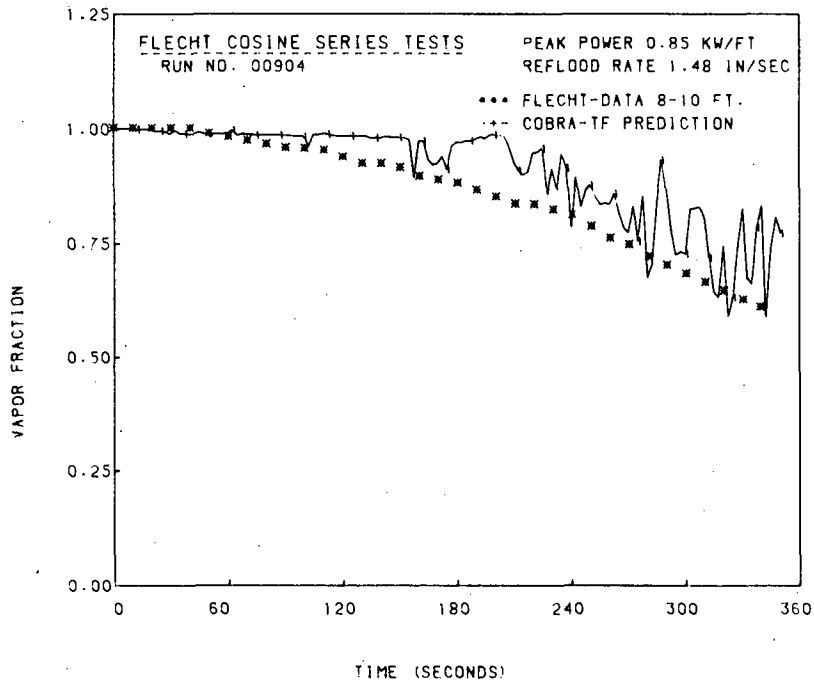


FIGURE 2.6-14. Vapor Fraction at 8 to 10-ft Elevation for FLECHT 00904

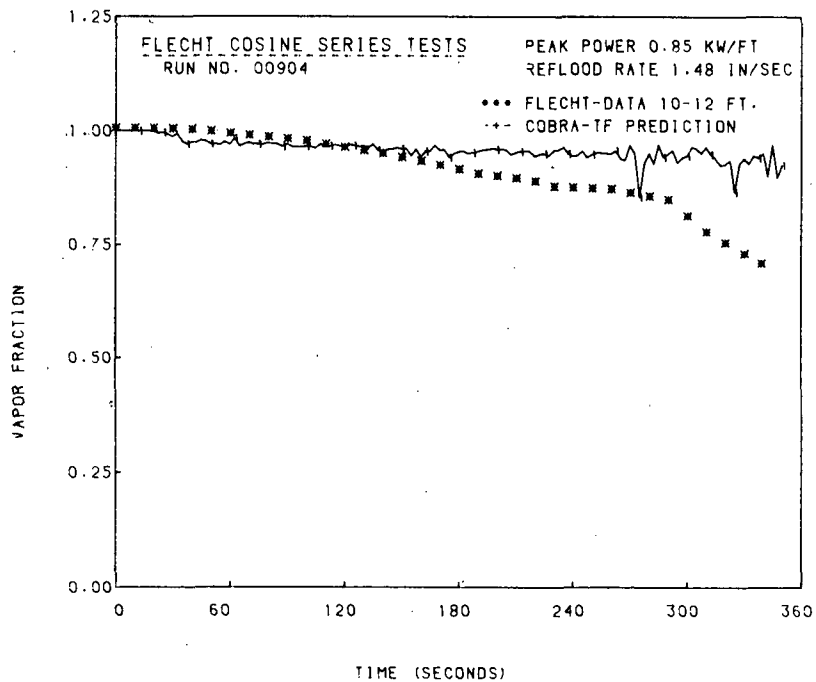


FIGURE 2.6-15. Vapor Fraction at 10 to 12-ft Elevation for FLECHT 00904

### High Reflood (FLECHT Test No. 04444)

Temperature versus time plots for the COBRA/TRAC predictions of test 04444 are shown in Figures 2.6-16 through 2.6-22. The temperature profiles are well predicted at all elevations, except that they tend to flatten out prior to quenching, causing a relatively large error in the quench time. This is caused by an insufficient amount of heat transfer near the minimum film boiling temperature. Increasing the heat transfer rate in this region by adding Hsu's transition boiling correlation to the film boiling heat flux results in correct prediction of the quench time at all elevations. This approach, however, gives poorer results for lower flooding rates. It appears that a better model for the wall-to-liquid heat transfer is needed near the minimum film boiling temperature. Void fraction predictions are shown in Figures 2.6-23 through 2.6-28. The predictions are very good at all elevations until the minimum film boiling temperature is reached. At that point the void fractions are overpredicted since the rods do not quench and continue to cause boiling. This increased the void fractions.

In general, the data comparisons indicate a need for more study of heat transfer near the quench front, heat transfer in the dispersed flow regime, and a better hydrodynamic model for the froth front above the quench front.

These simulations were run on cycle 10.

### 2.7 STANDARD PROBLEM NO. 9

COBRA/TRAC predictions were compared with two separate effects reflood tests conducted in the FLECHT-SEASET facility that are designated as Standard Problem Nine (Ref. 12,13). The two tests are constant forced flooding rate tests powered by 161 full length (12-ft) electrical heater rods. The purpose of these simulations was to assess the reflood heat transfer and hydrodynamic models for a low and high reflood rate.

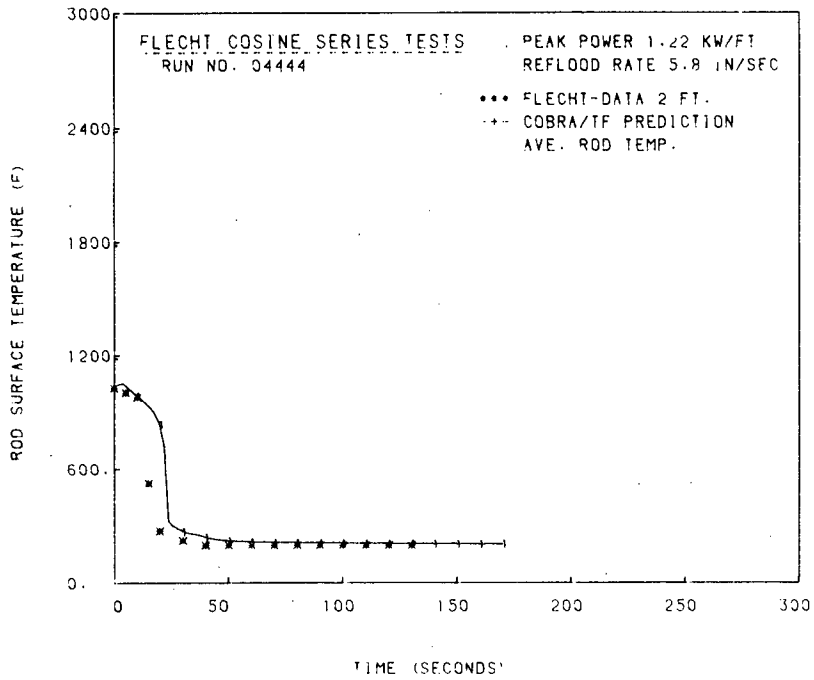


FIGURE 2.6-16. Temperature at 2-ft Elevation--FLECHT 04444

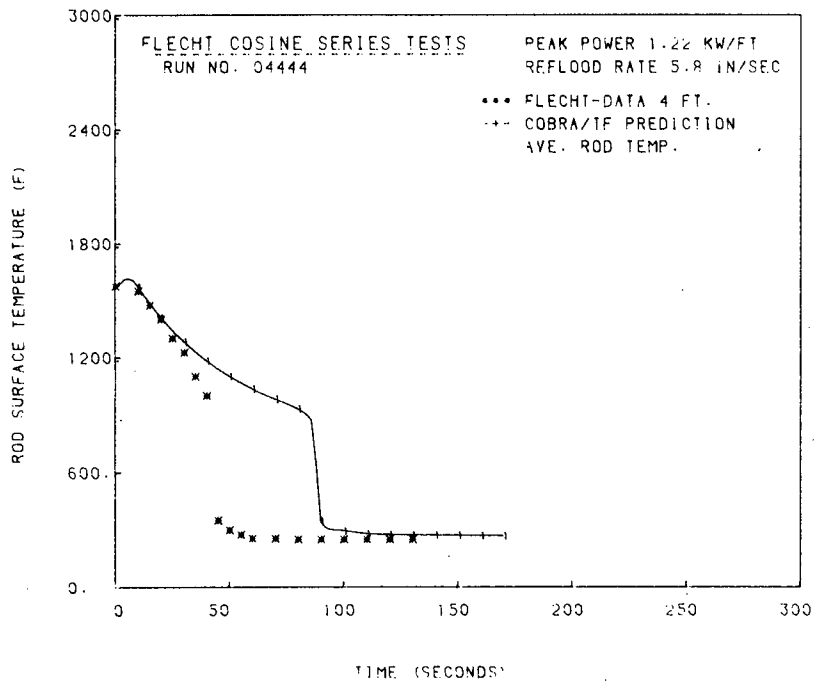
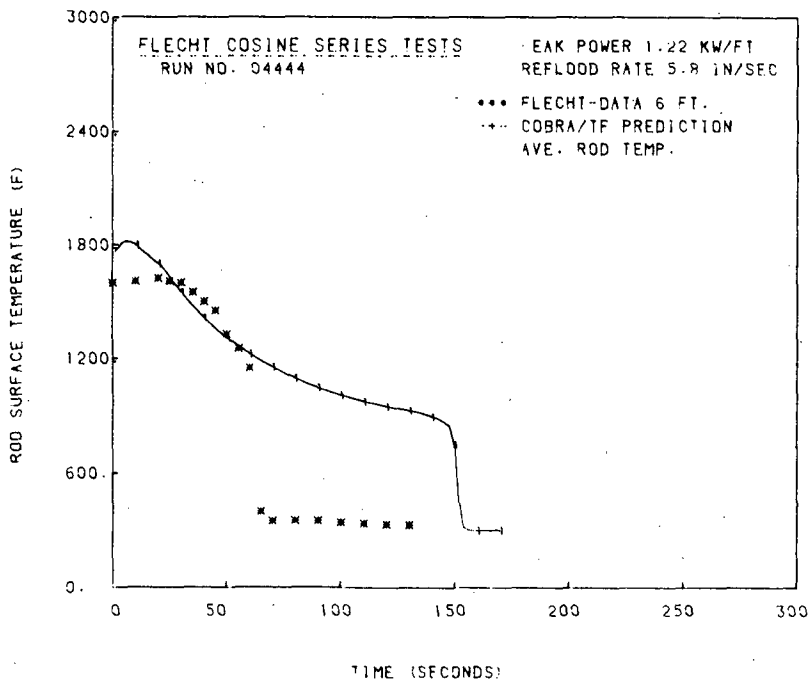
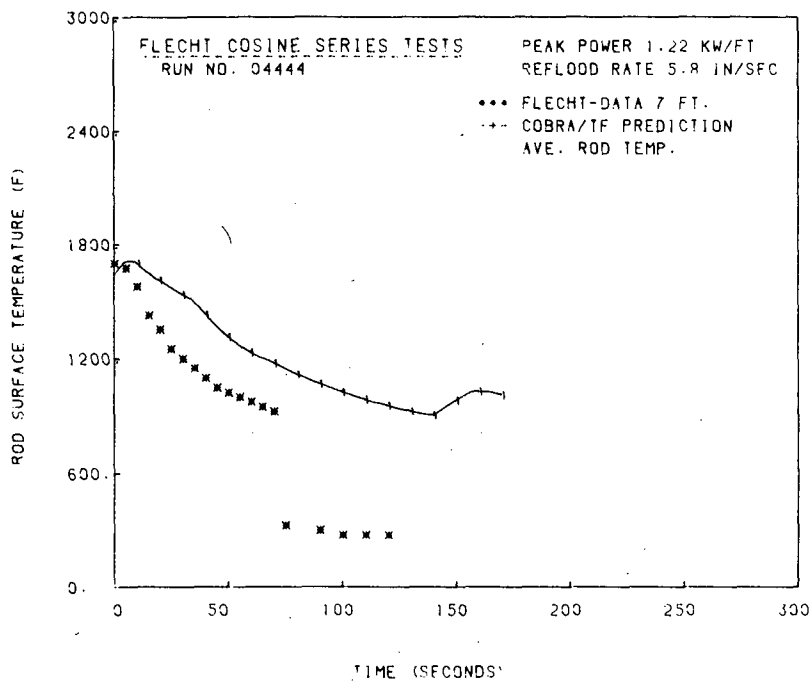


FIGURE 2.6-17. Temperature at 4-ft Elevation--FLECHT 04444



**FIGURE 2.6-18. Temperature at 6-ft Elevation--FLECHT 04444**



**FIGURE 2.6-19. Temperature at 7-ft Elevation--FLECHT 04444**

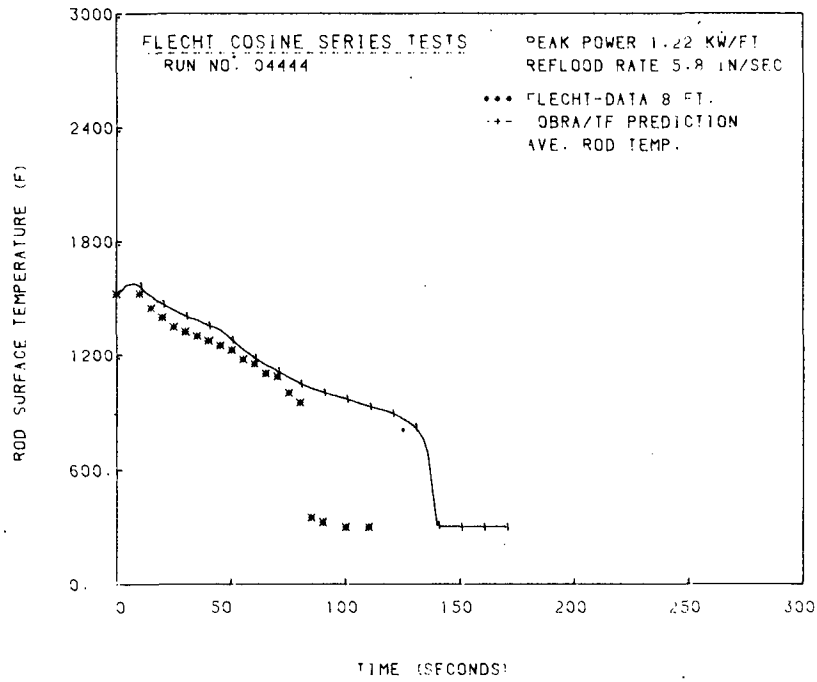


**FIGURE 2.6-20. Temperature at 8-ft Elevation--FLECHT 04444**

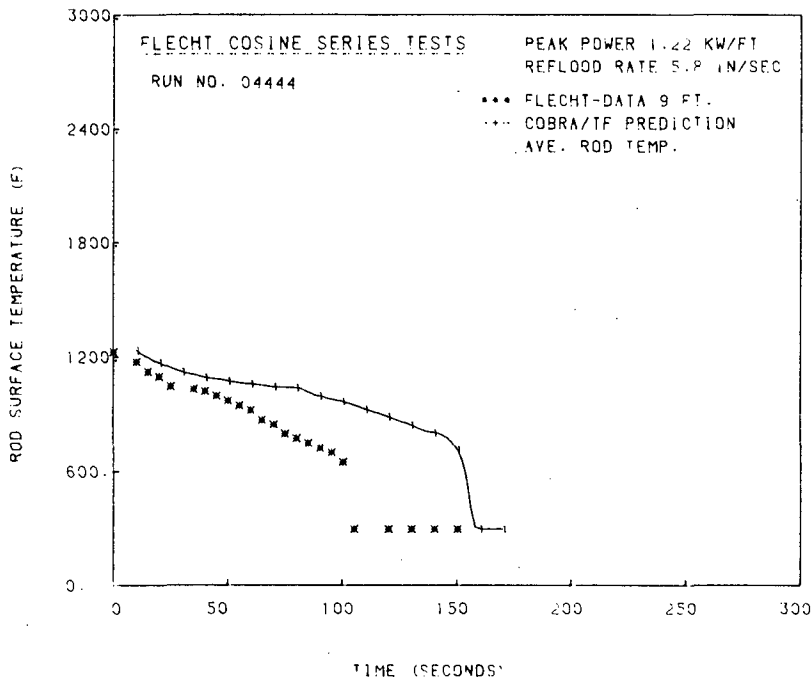


**FIGURE 2.6-21. Temperature at 9-ft Elevation--FLECHT 04444**

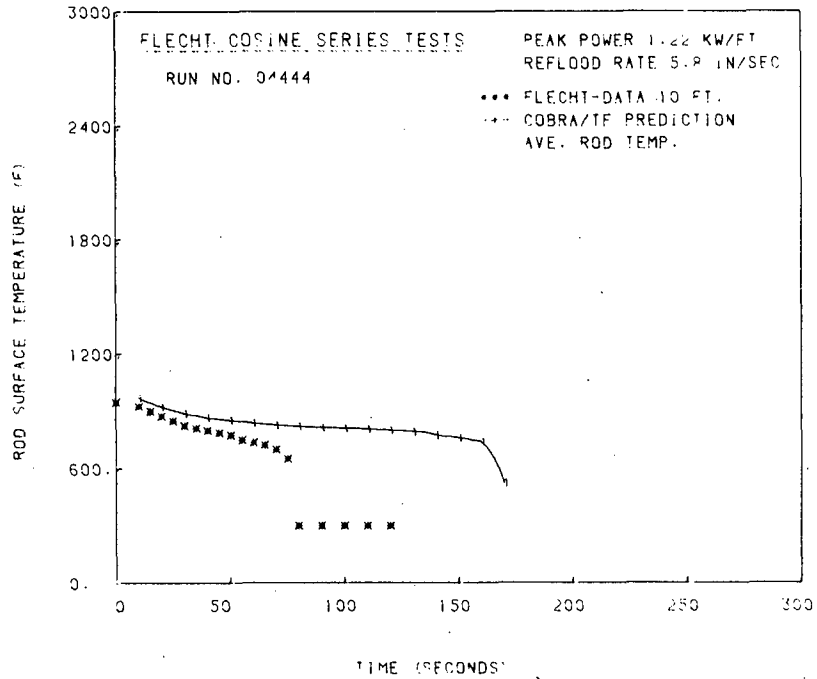


**FIGURE 2.6-22. Temperature at 10-ft Elevation--FLECHT 04444**

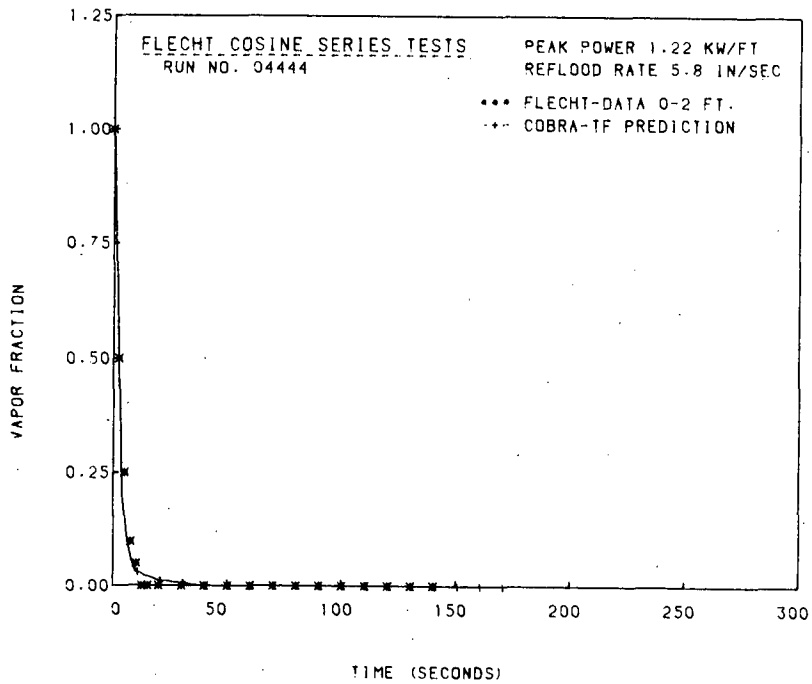


**FIGURE 2.6-23. Vapor Fraction at 0 to 1-ft Elevation--FLECHT 04444**

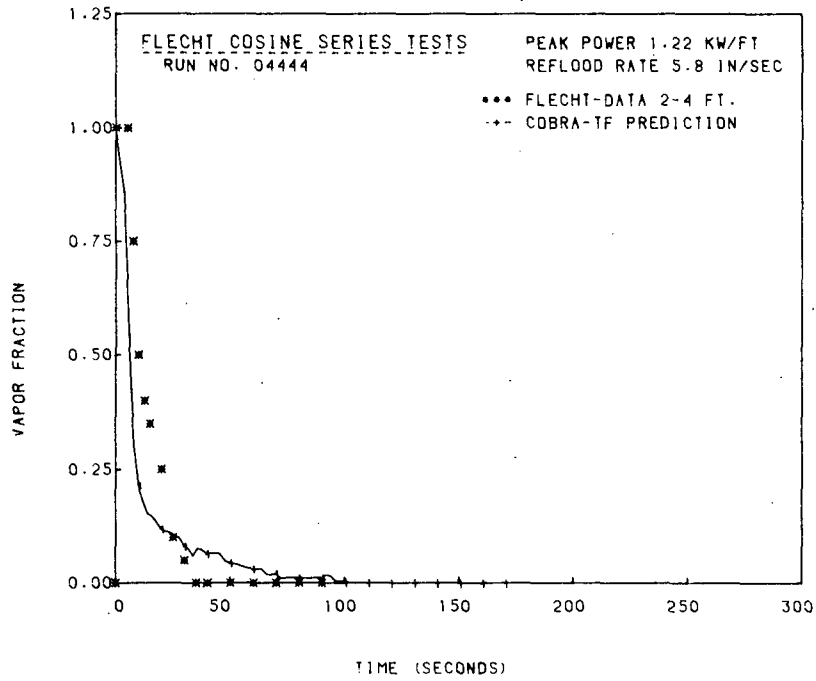


FIGURE 2.6-24. Vapor Fraction at 2 to 4-ft Elevation--FLECHT 04444

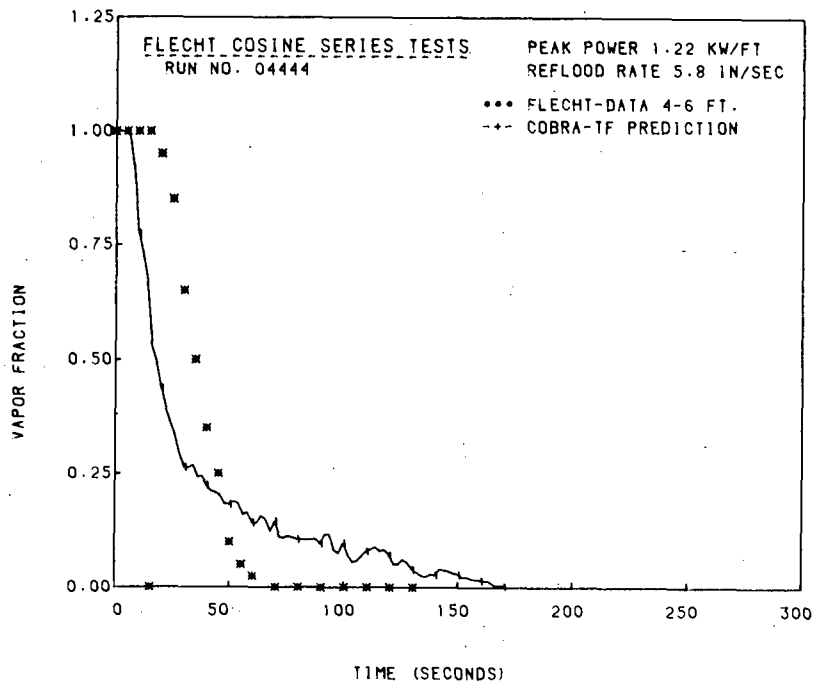


FIGURE 2.6-25. Vapor Fraction at 4 to 6-ft Elevation--FLECHT 04444

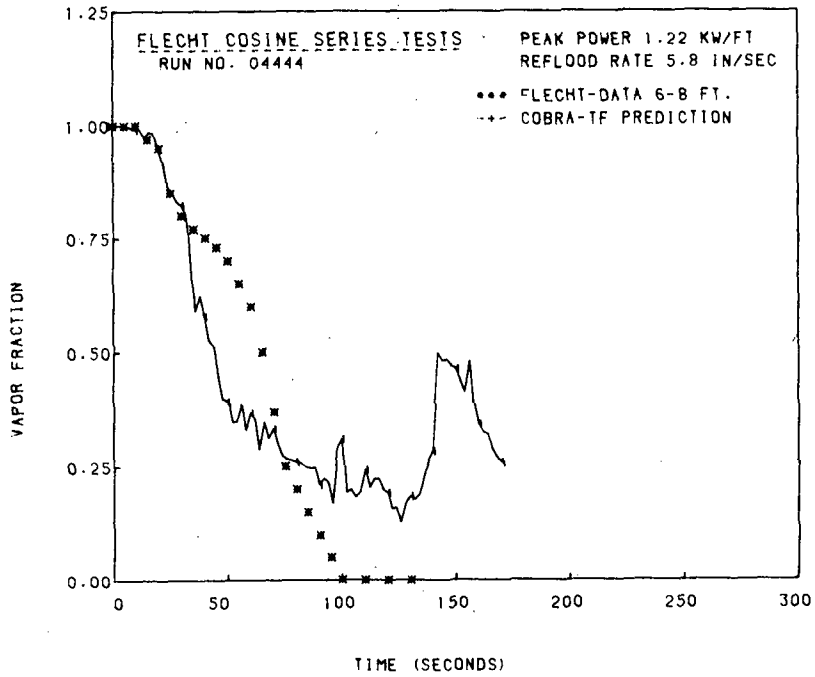


FIGURE 2.6-26. Vapor Fraction at 6 to 8-ft Elevation--FLECHT 04444

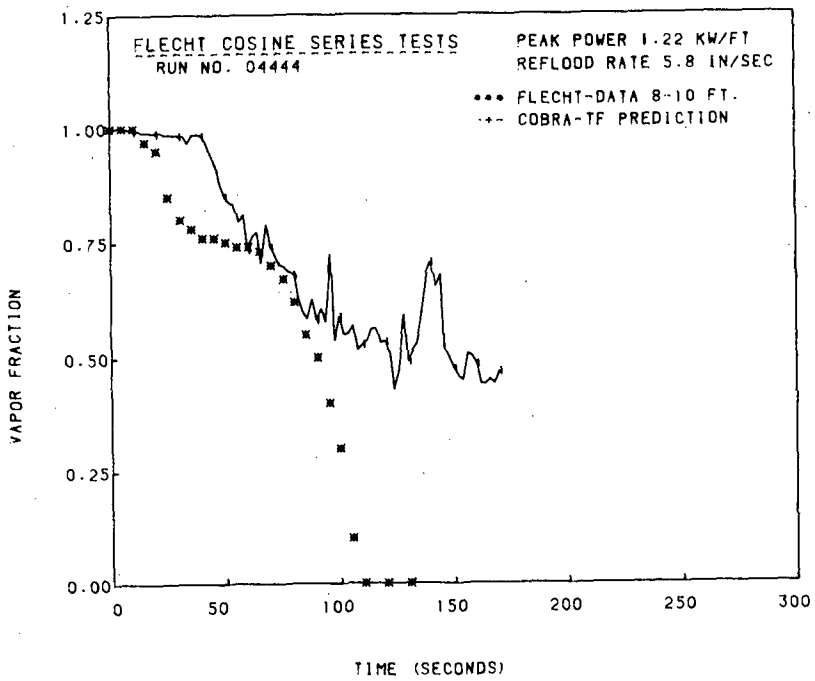


FIGURE 2.6-27. Vapor Fraction at 8 to 10-ft Elevation--FLECHT 04444

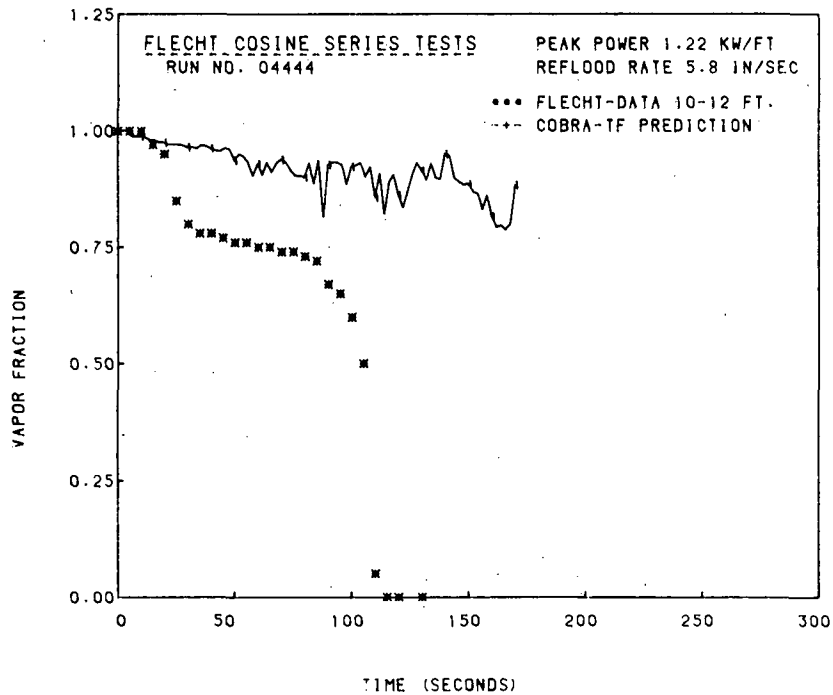


FIGURE 2.6-28. Vapor Fraction at 10 to 12-ft Elevation--FLECHT 04444

### 2.7.1 Experimental Description

A diagram of the FLECHT-SEASET test bundle is shown in Figure 2.7-1. The test section consisted of 161 electrical heater rods arranged in a square pitch with dimensions comparable to 17x17-in. PWR fuel rod arrays. The rod diameter was 0.374 in. and the rod pitch was 0.496 in. The bundle also contained 16 control rod guide tubes of 0.484 in. diameter and 8 solid filler rods. The triangular filler rods reduced the excess flow area to within 5% of the power/flow area ratio of a PWR fuel assembly. The test section was enclosed by a cylindrical stainless steel housing and was connected to an upper and lower plenum. The housing has an inside diameter of 7.625 in. and was insulated from the outside air to reduce the heat losses to the environment. The bundle flow area was 23.945 in.<sup>2</sup>. The upper ends of both the housing and test rods were bolted to the top of the test assembly. The lower ends were allowed to hang free permitting axial movement. Horizontal movement and/or bowing of the heater rods was restricted by 8 typical PWR grid spacers located at 20.5 in. intervals, starting at the beginning of the heated length.

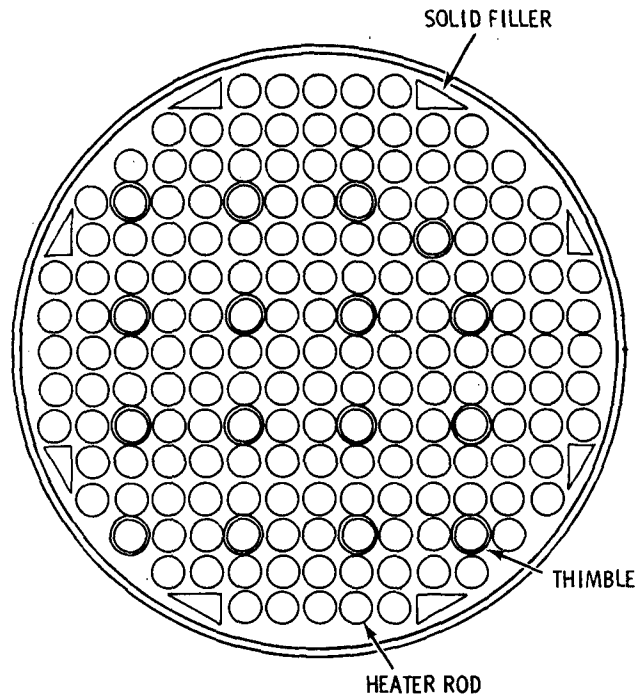


FIGURE 2.7-1. FLECHT-SEASET Bundle Cross-Section

The electrical heater rods were constructed of a spiral-wound heating element embedded in a magnesium oxide insulator. A chopped cosine power profile was approximated by a seven-step power profile. The length of each power step and the peak to average power factors are shown in Figure 2.7-2 along with the location of the 8 grid spacers.

The test assembly was initially heated by radiation from the heater rods for more than an hour prior to reflood. During this heat-up phase the rods were surrounded by stagnant steam and all rods had a constant peak power of 0.8 kW/ft. These conditions were maintained until the desired peak clad temperature of 1600°F was obtained. Water was injected into the lower plenum with a constant flow rate, an inlet temperature of 127°F, and a pressure of 40 psia. When the rising water reached the beginning of the heated length, the constant rod power was converted to the ANS +20% decay heat rate for the reflood portion of a LOCA. The initial test parameters for both the high and low flooding rate experiments have been tabulated in Table 2.6.

The initial temperatures for all axial levels were computed by averaging the thermocouple temperatures at a given elevation. Two heater rods were

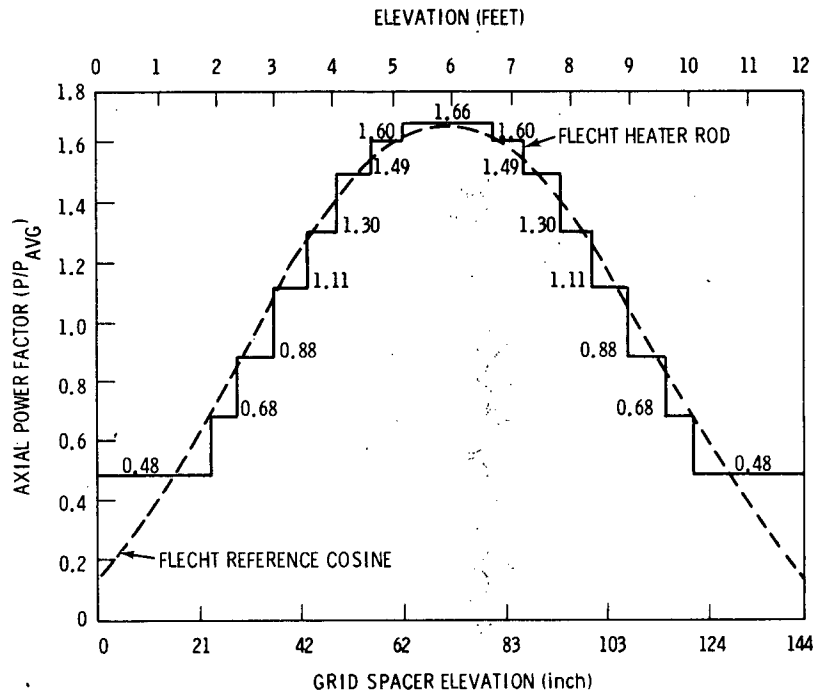


FIGURE 2.7-2. FLECHT-SEASET Axial Power Profile and Grid Locations

TABLE 2.6. Test Parameters for Standard Problem No. 9

	High Flooding (Run No. 31701)	Low Flooding (Run No. 31805)
Forced injection rate into bundle	6 in./sec	0.8 in./sec
Pressure at top of bundle	40 psia	40 psia
Injection water temperature	127°F	127°F
Initial power at 6 ft elevation	0.7 kW/ft	0.7 kW/ft
Initial rod temperatures (ave)	0 ft - 430°F 2 ft - 747°F 4 ft - 1275°F 6 ft - 1561°F 8 ft - 1327°F 10 ft - 836°F 12 ft - 600°F	0 ft - 430°F 2 ft - 751°F 4 ft - 1274°F 6 ft - 1560°F 8 ft - 1324°F 10 ft - 839°F 12 ft - 600°F

inoperative during the entire transient, therefore the rod temperature in the immediate vicinity of the unpowered rods and those near the housing were eliminated from the initial temperature averaging.

### 2.7.2 COBRA/TRAC Model Description

The FLECHT-SEASET test assembly was modeled with three COBRA/TRAC components; a one-dimensional VESSEL component with mass injection at the bottom boundary, a PIPE component connected to the top of the vessel, and a BREAK component on the end of the pipe. The COBRA/TRAC nodalization is shown in Figure 2.7-3. The vessel component modeled the heated length and upper plenum. A fluid flow area of 24.16 in.<sup>2</sup> was used for the simulation. (This area was calculated from pretest information and was approximately 0.6% greater than the actual flow area of 23.945 in.<sup>2</sup>.) The vessel was modeled using three channels, two for the heated length and one for the upper plenum. Two channels in the heated length were necessary to match the COBRA/TRAC temperature output locations with those presented in the experimental data. There were 14 fluid nodes in the vessel component. The 159 functioning heater rods were modeled with one average rod. The test section housing was modeled by a tube rod with an inside heat transfer surface and an insulated outer surface. A one-dimensional mesh was used since it was thought that no significant radial profiles existed in the experiment. This turned out to be an erroneous assumption for the low flooding test since significant radial vapor temperature distributions were measured in the experiment.

The COBRA/TRAC heater rod was initialized with the axial temperature profile of Table 2.6 and the axial power profile of Figure 2.7-2. The peak power was 0.7 kW/ft. The housing was initialized with the axial temperature profile and zero power generation. The vessel, pipe and break components were initialized with saturated steam at 40 psia. A constant flow boundary condition of 127°F water was specified at the bottom of the vessel. At the break, a pressure boundary of 40 psia was specified.

The reflood transient was run from a standing start, with the initial conditions listed in Table 2.6 and the ANS +20% power decay curve. The simulation continued until all levels of the heated section were quenched.

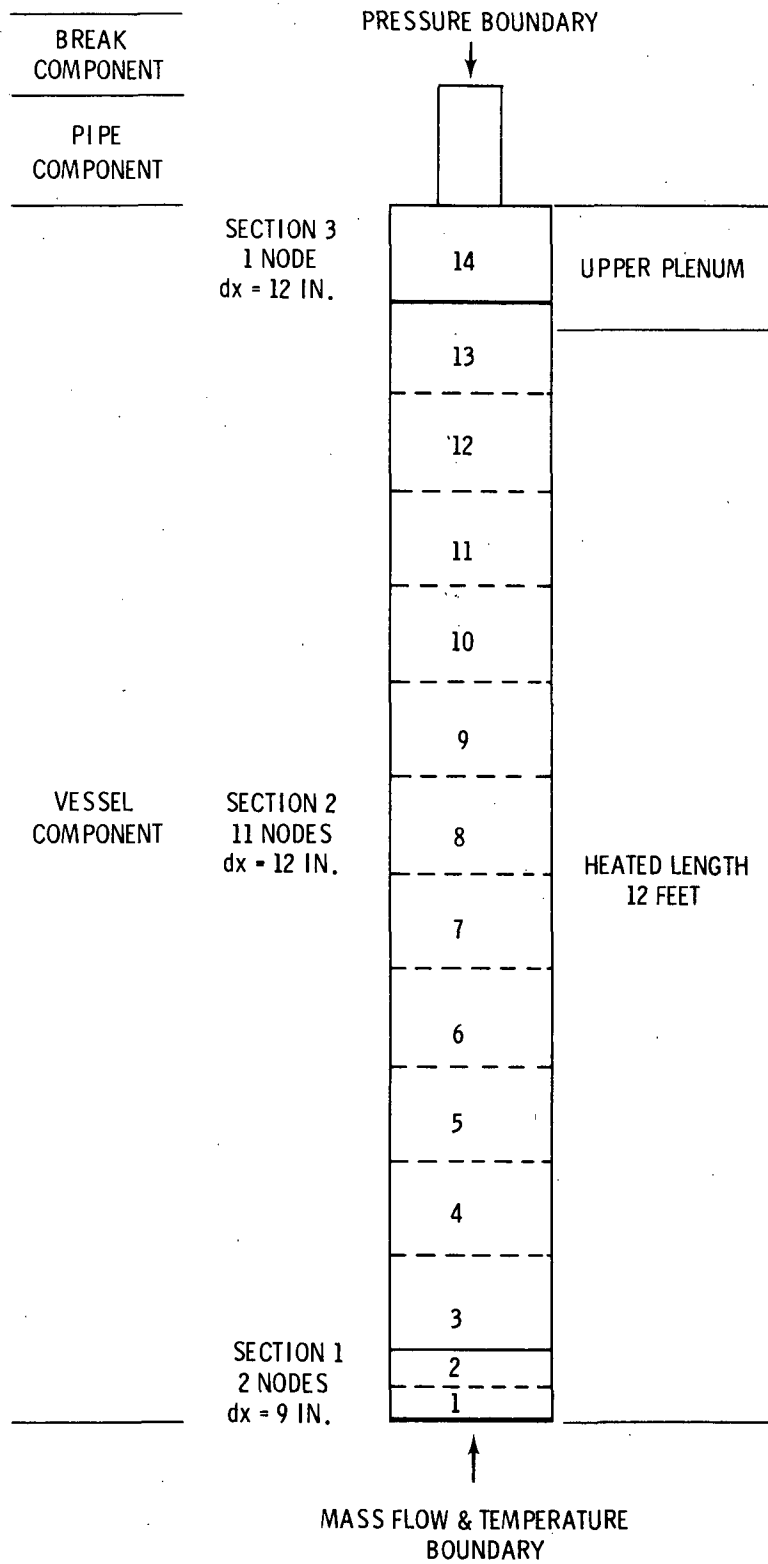


FIGURE 2.7-3. COBRA/TRAC Model of FLECHT-SEASET for Standard Problem No. 9

### 2.7.3 Discussion of Results

#### Low Reflood (FLECHT-SEASET Test No. 31805)

Temperature versus time plots comparing the COBRA/TRAC predictions at the various axial levels are shown in Figures 2.7-4 through 2.7-8. Temperatures calculated by COBRA/TRAC are compared to the measurements for one rod (this was the only data available). The temperature plots show that COBRA/TRAC does a good job of predicting the temperatures in the lower end of the test section, but temperatures are underpredicted in the higher elevations. More recent simulations have shown that radial temperature distributions have a significant effect on clad temperatures in the upper part of the bundle and a much better data comparison can be obtained by using more than one channel to model the test section. Void fraction comparisons are shown in Figures 2.7-9 through 2.7-20. The predictions are very good at all elevations, indicating that the models for liquid entrainment and interfacial shear are reasonably accurate.

#### High Reflood (FLECHT-SEASET Test No. 31701)

Temperatures versus time plots comparing the COBRA/TRAC prediction at the measured data at five axial levels are presented in Figures 2.7-21 through 2.7-25. No experimental data were available for this report, but they seem to follow the same general trends as those for FLECHT 04444 (Section 2.6), a test with approximately the same test conditions. The higher reflood rate, (6 in./sec) quenches all elevations in less than 150 seconds. If the same trends as those for FLECHT 04444 hold for the FLECHT-SEASET high reflood rate, COBRA/TRAC should be able to predict the peak temperatures at all elevations, but with an increasing overprediction for quench times at the higher axial elevations. The quench time predictions would probably improve if the simulation was rerun with the heat transfer improvements to the minimum film boiling temperature region.

These simulations were run on cycle 10 of COBRA/TRAC.

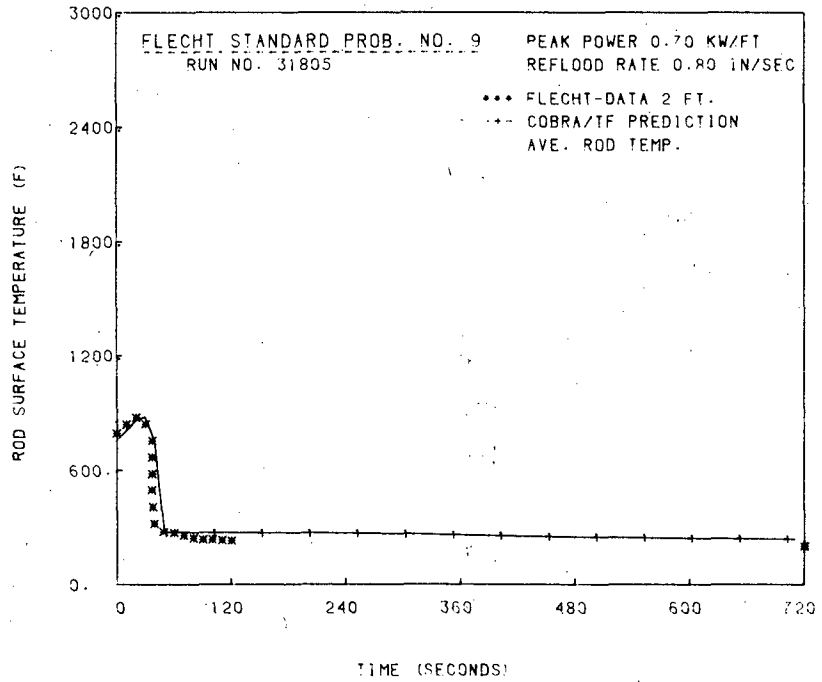


**FIGURE 2.7-4. Temperatures at 2 ft Elevation for Low Reflood Rate (Test 31805)**

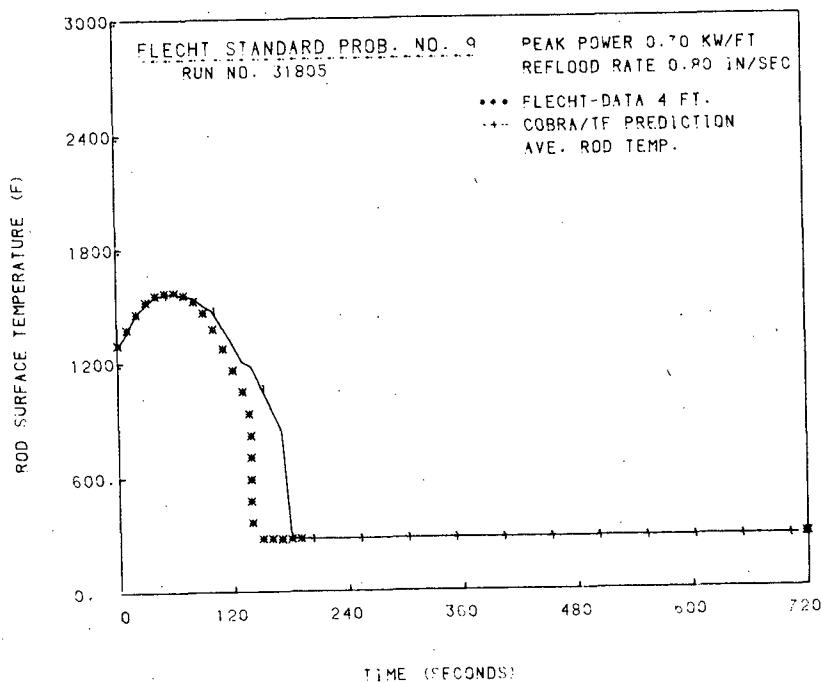


**FIGURE 2.7-5. Temperatures at 4 ft Elevation for Low Reflood Rate (Test 31805)**

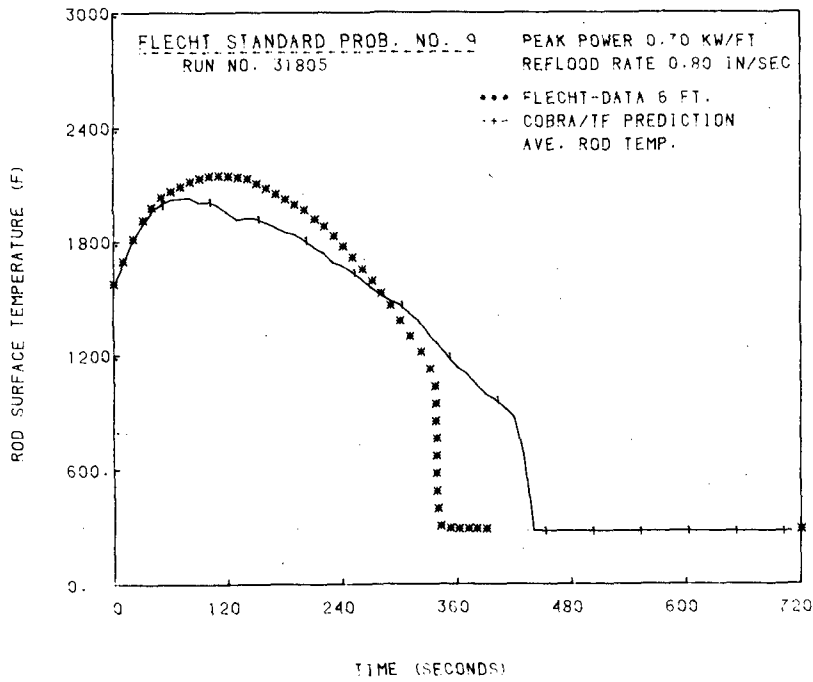


**FIGURE 2.7-6. Temperatures at 6-ft Elevation for Low Reflood Rate (Test 31805)**

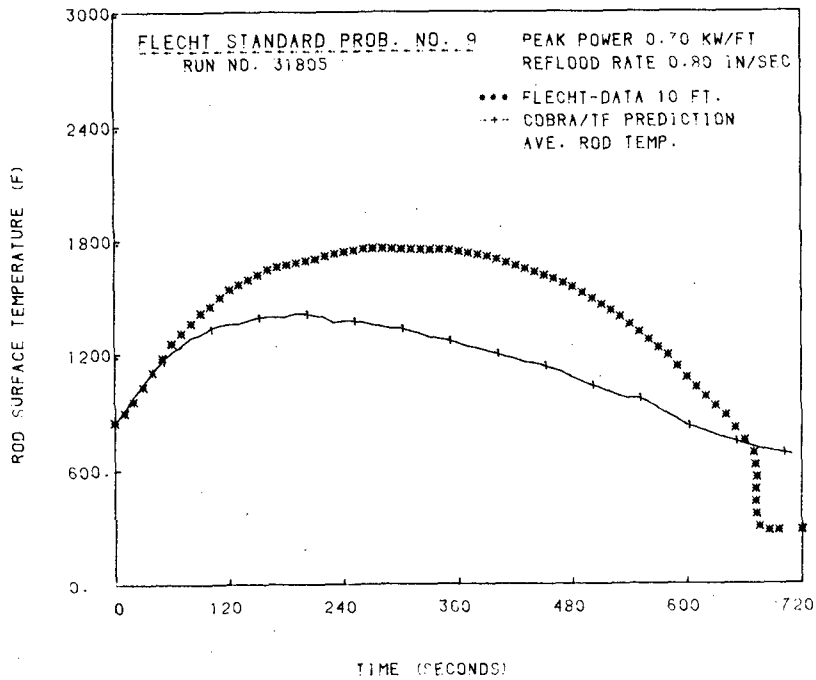


**FIGURE 2.7-7. Temperatures at 10-ft Elevation for Low Reflood Rate (Test 31805)**

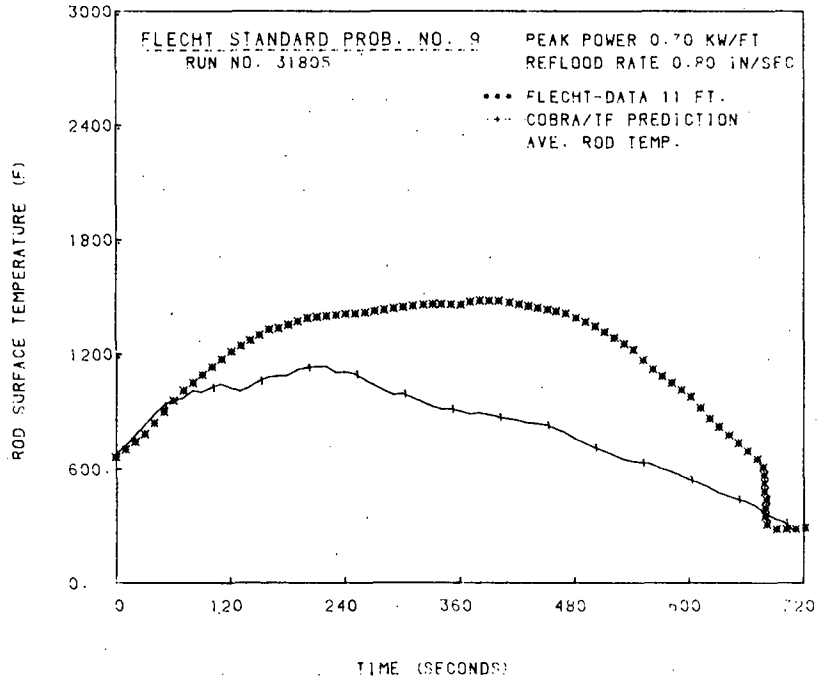


**FIGURE 2.7-8. Temperatures at 11-ft Elevation for Low Reflood Rate (Test 31805)**

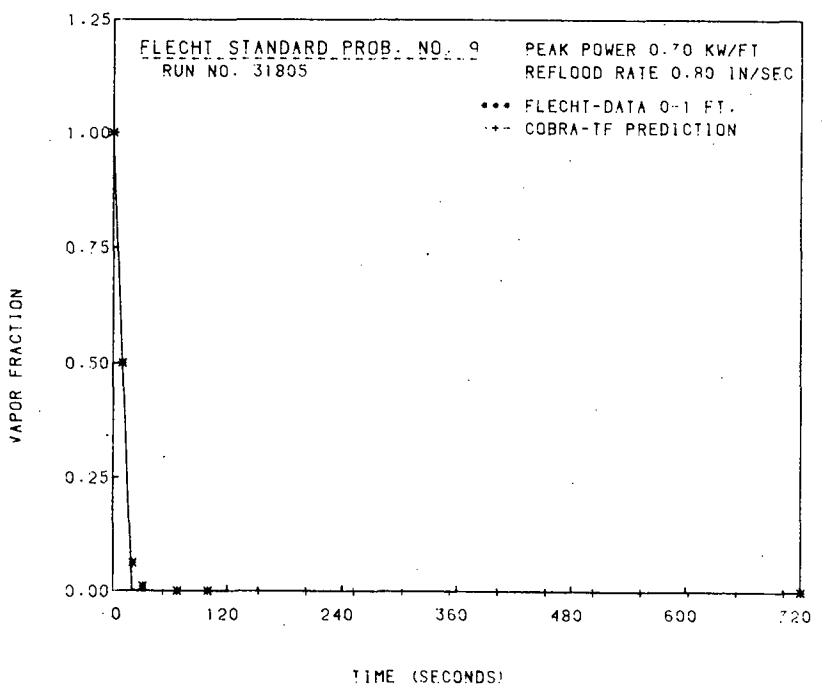


**FIGURE 2.7-9. Vapor Fraction at 0 to 1-ft Elevation for Low Reflood Rate (Test 31805)**

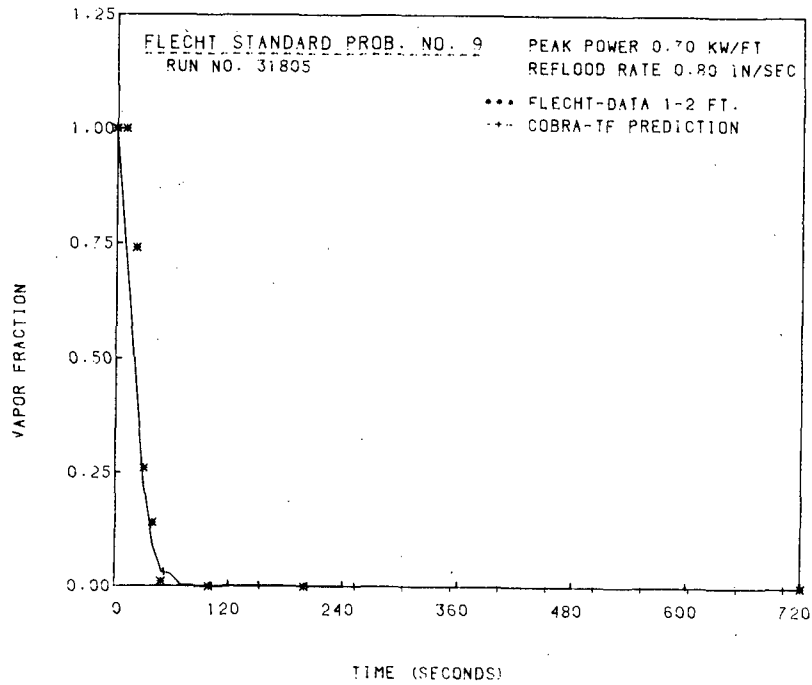


**FIGURE 2.7-10.** Vapor Fraction at 1 to 2-ft Elevation for Low Reflood Rate (Test 31805)

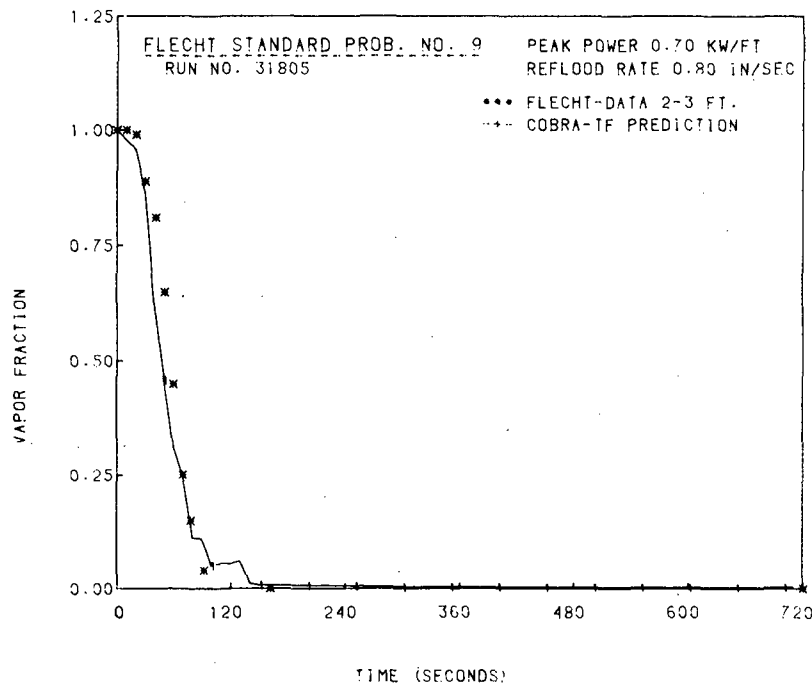


**FIGURE 2.7-11.** Vapor Fraction at 2 to 3-ft Elevation for Low Reflood Rate (No. 31805)

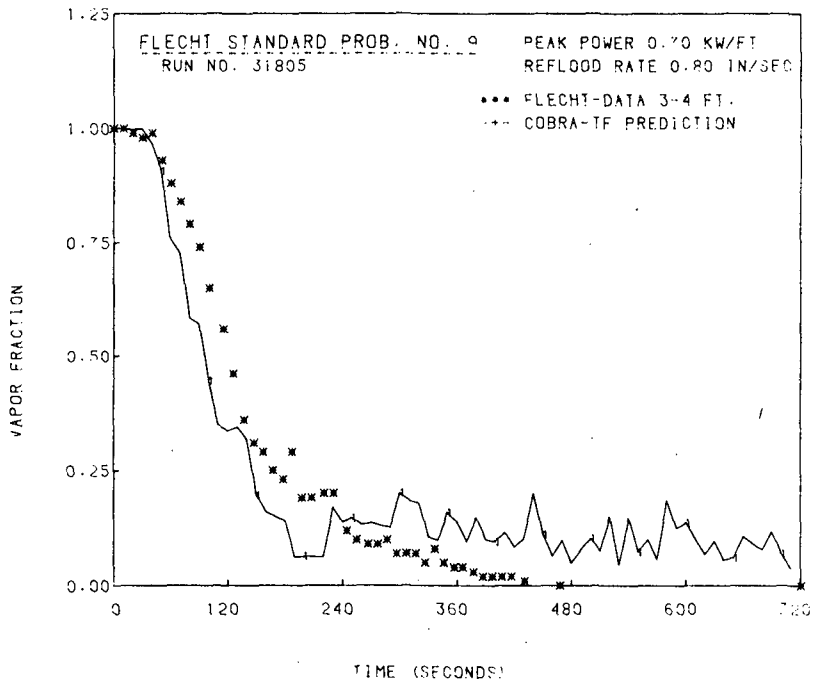


**FIGURE 2.7-12.** Vapor Fraction at 3 to 4-ft Elevation for Low Reflood Rate (Test 31805)

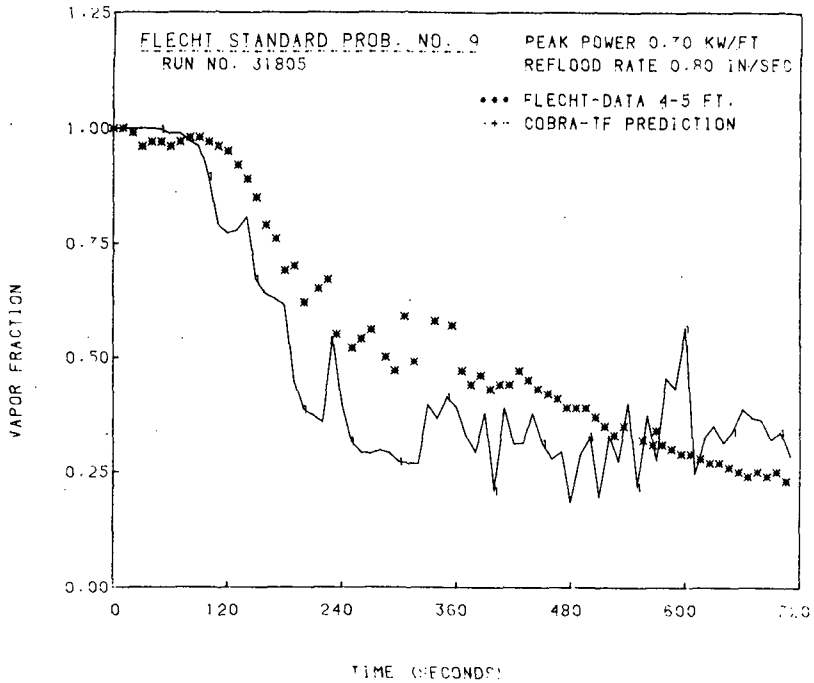


**FIGURE 2.7-13.** Vapor Fraction at 4 to 5-ft Elevation for Low Reflood Rate (Test 31805)

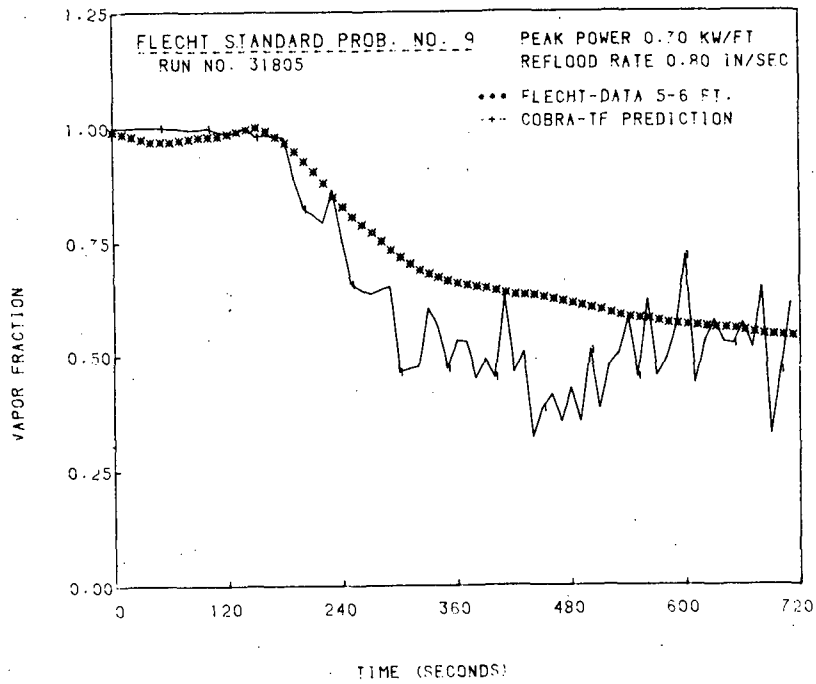


**FIGURE 2.7-14.** Vapor Fraction at 5 to 6-ft Elevation for Low Reflood Rate (Test 31805)

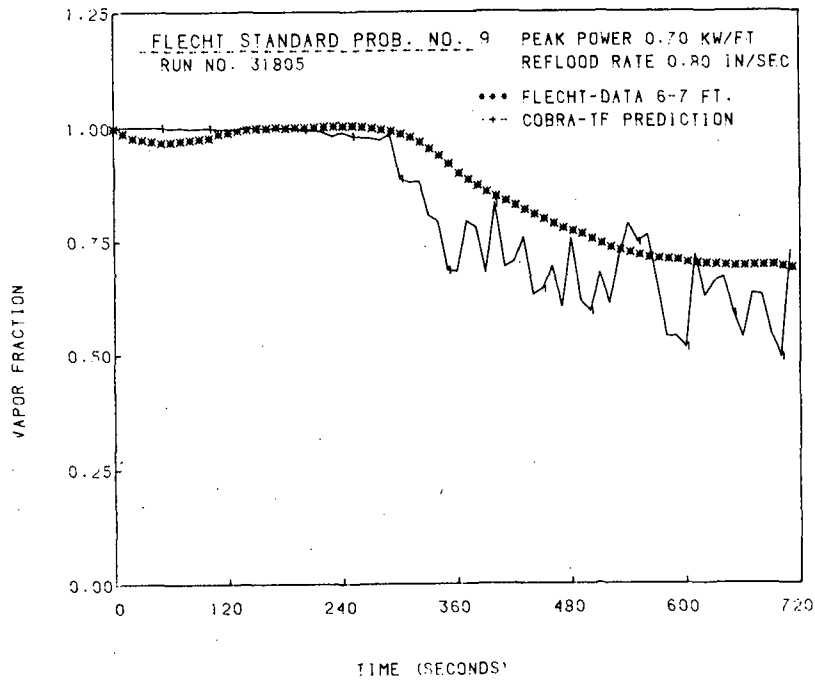


**FIGURE 2.7-15.** Vapor Fraction at 6 to 7-ft Elevation for Low Reflood Rate (Test 31805)

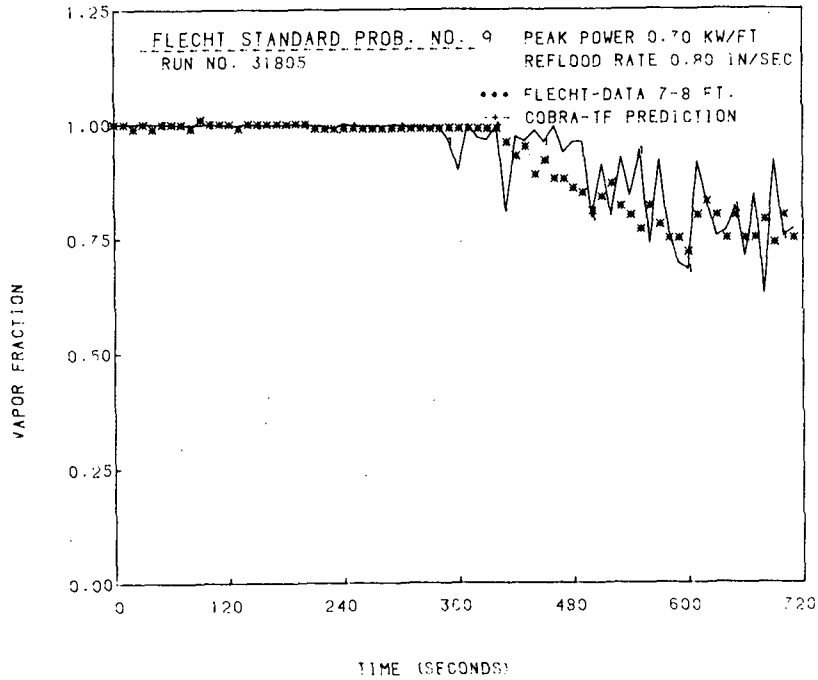


FIGURE 2.7-16. Vapor Fraction at 7 to 8-ft Elevation for Low Reflood Rate (Test 31805)

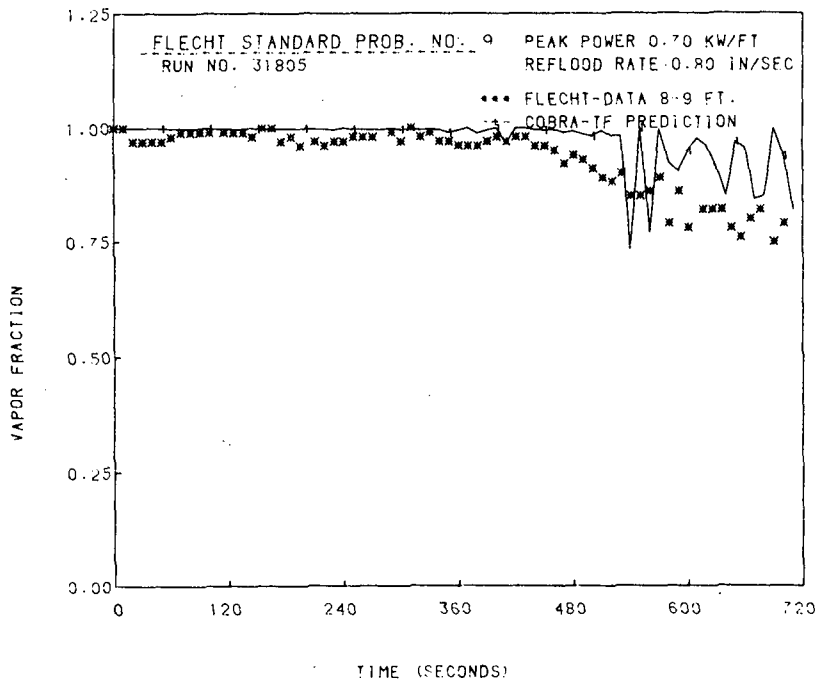
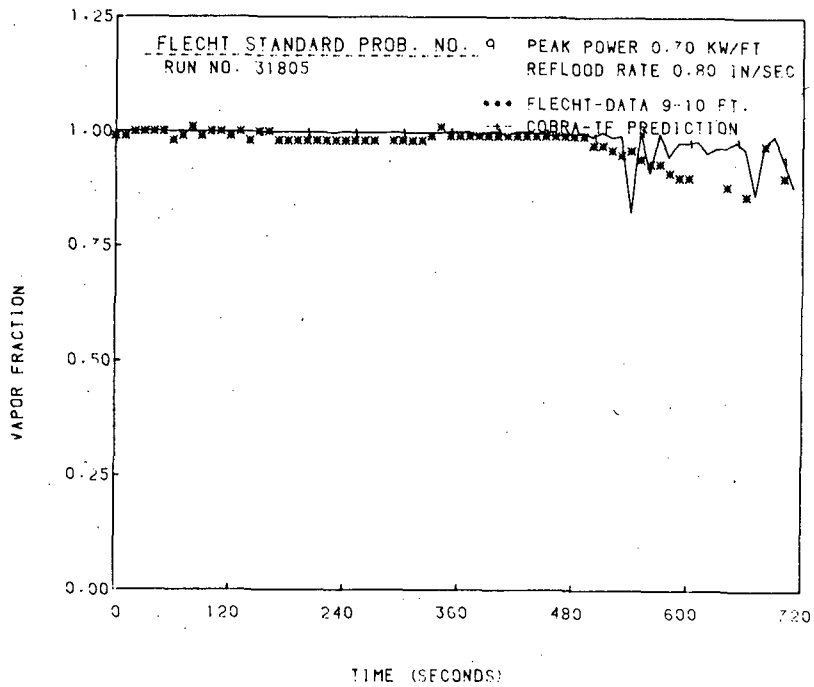
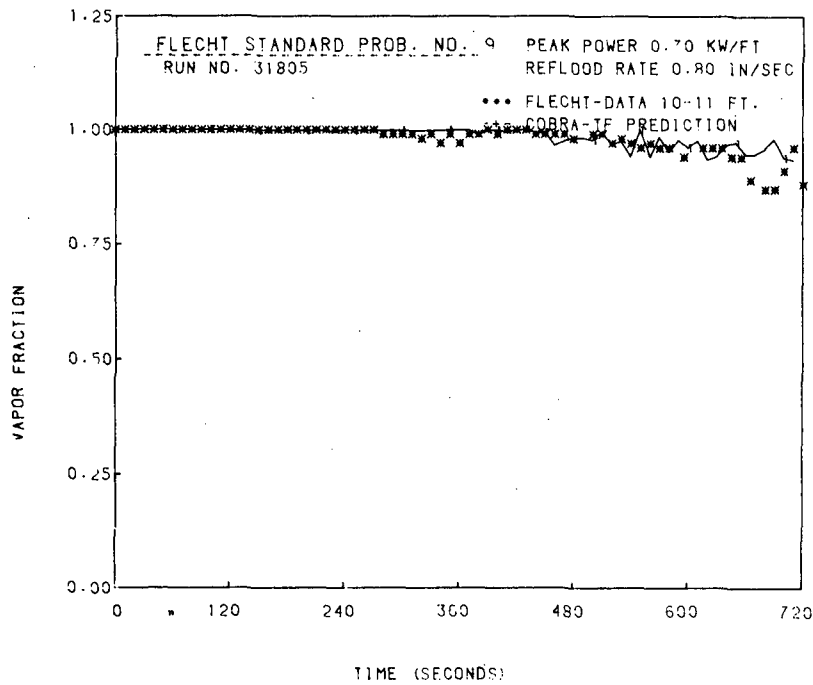


FIGURE 2.7-17. Vapor Fraction at 8 to 9-ft Elevation for Low Reflood Rate (Test 31805)



**FIGURE 2.7-18.** Vapor Fraction at 9 to 10-ft Elevation for Low Reflood Rate (Test 31805)



**FIGURE 2.7-19.** Vapor Fraction at 10 to 11-ft Elevation for Low Reflood Rate (Test 31805)

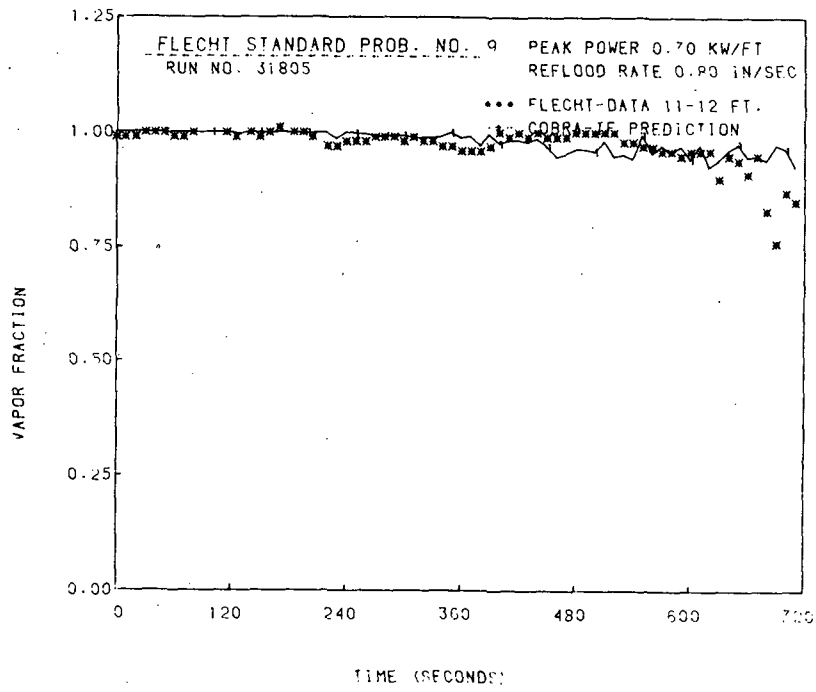


**FIGURE 2.7-20.** Vapor Fraction at 11 to 12-ft Elevations for Low Reflood Rate (Test 31805)

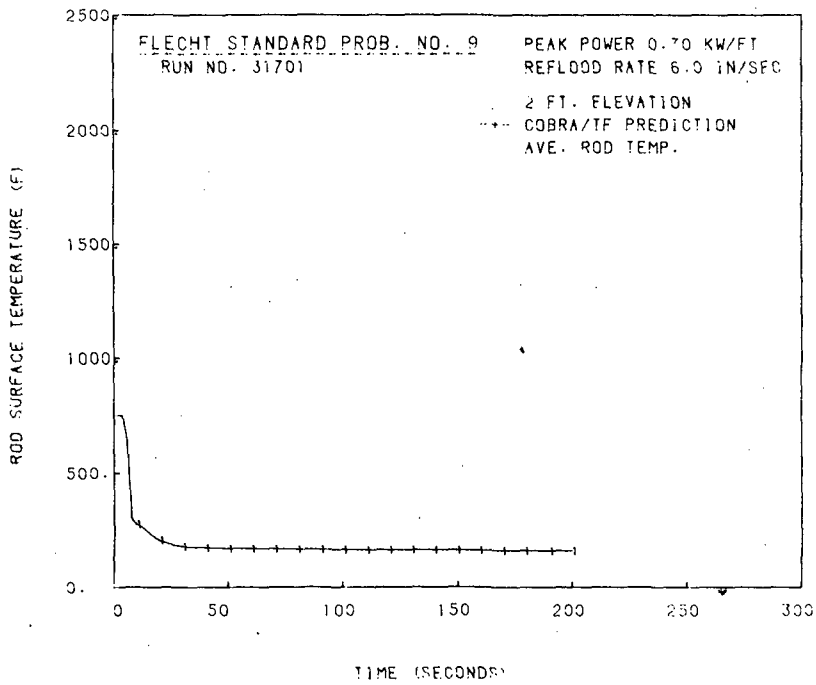


**FIGURE 2.7-21.** Temperatures at 2-ft Elevation for High Reflood Rate (Test 31701)

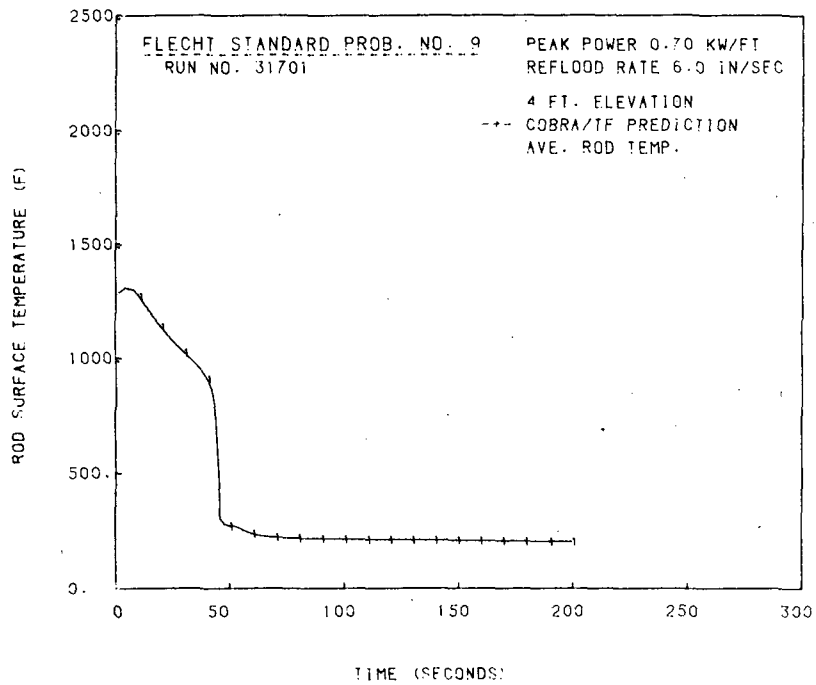


**FIGURE 2.7-22.** Temperatures at 4-ft Elevation for High Reflood Rate (Test 31701)

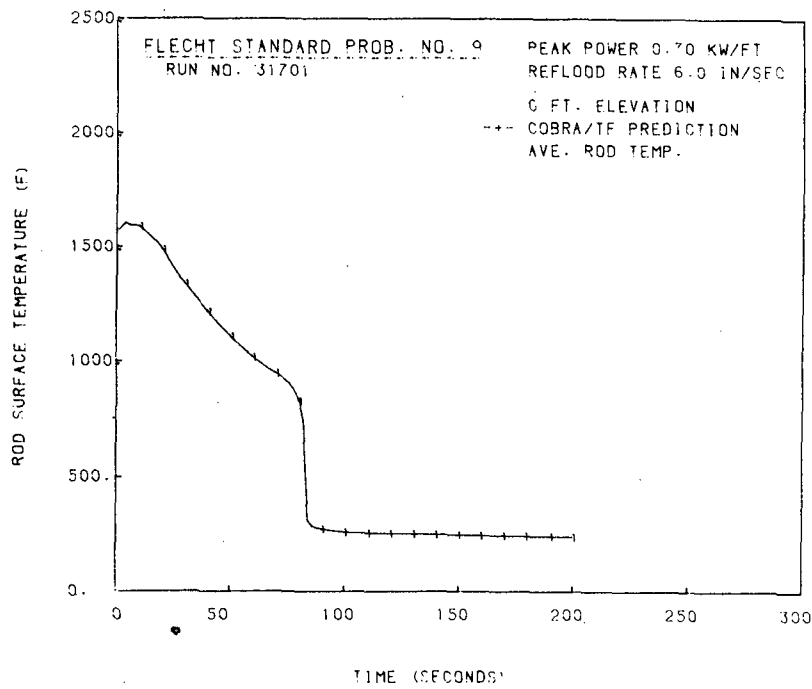


**FIGURE 2.7-23.** Temperatures at 6-ft Elevations for High Reflood Rate (Test 31701)

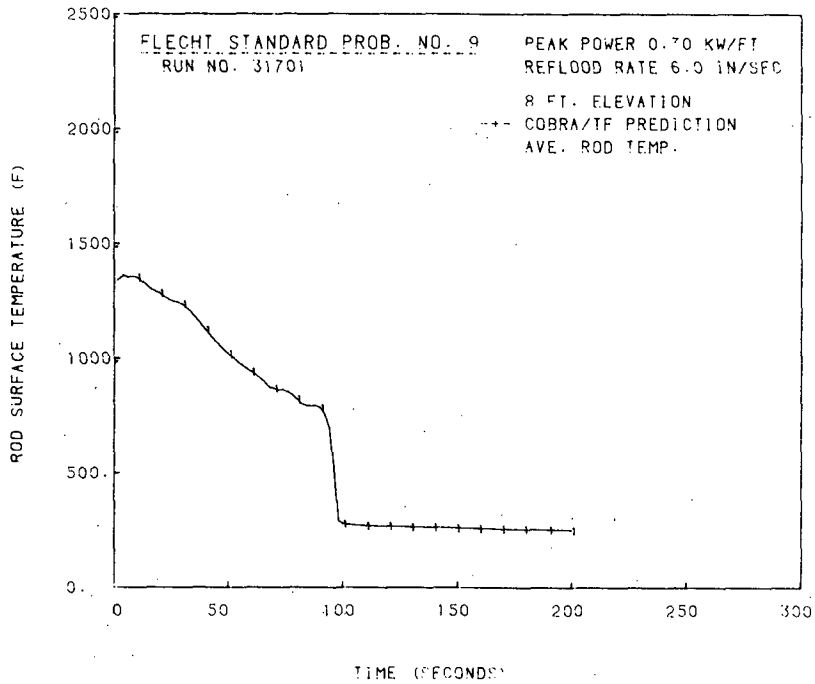


**FIGURE 2.7-24. Temperatures at 8-ft Elevation for High Reflood Rate (Test 31701)**

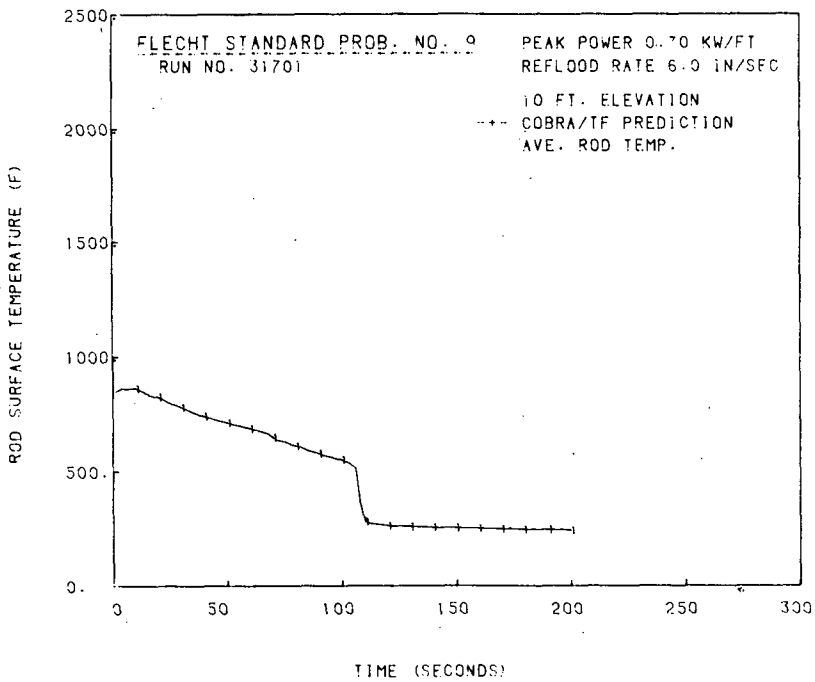


**FIGURE 2.7-25. Temperatures at 10-ft Elevation for High Reflood Rate (Test 31701)**

## 2.8 NRU NUCLEAR FUEL ROD FORCED REFLOOD EXPERIMENT

This LOCA test series was run in the National Research Universal (NRU) reactor at Chalk River, Ontario, Canada. The tests were conducted by PNL for the NRC to evaluate the thermal-hydraulic and mechanical deformation behavior of a full-length nuclear rod bundle during the heatup, reflood, and quench phases of a loss-of-coolant accident (LOCA). Two tests, PTH110 and TH214, (Ref. 14,15) were selected for COBRA/TRAC simulation to assess the applicability of the heat transfer and hydrodynamic models in the code (including the fuel rod gap conductance model) to reflood in nuclear fuel bundles. Test PTH110 was a constant forced bottom reflood experiment and test TH214 was a variable flow rate bottom reflood experiment. These two tests are representative of the approximately 55 experimental tests conducted in the NRU facility.

### 2.8.1 Experimental Description

The NRU test train was 30 ft 1-1/2 in. in length and consisted of six major sections; the inlet region, test bundle, shroud, outlet region, hanger and closure head. The entire test train was inserted into a 25-ft pressure tube inside the NRU reactor. The closure region provided the pressure boundary between the test train and the NRU pressure tube. A schematic of the NRU test train is shown in Figure 2.8-1. The hanger tube suspended the test bundle and shroud from the closure head. The 14-ft long stainless steel shroud, constructed from two halves clamped together at 7-in. intervals, supported the test bundle.

The fuel bundle consisted of a 6x6 segment of a 17x17 PWR assembly design with the four corner rods removed for easier insertion in the shroud. A cross-section of the test section is shown in Figure 2.8-2. The outer ring of 16 rods plus the corner rods of the next inner ring served as guard rod heaters during the tests. The central 11 rods and instrument thimble (inside the dotted line in Figure 2.8-2) arranged in a cruciform pattern were the test rods of interest. All rods were unpressurized for both tests. The nuclear fuel rods had a cladding O.D. of 0.379 in. and pellet diameter of 0.325 in. The rod-to-rod pitch was 0.502 in. and the chopped cosine power profile had a peak power of 0.55 kW/ft at the 6-ft elevation.

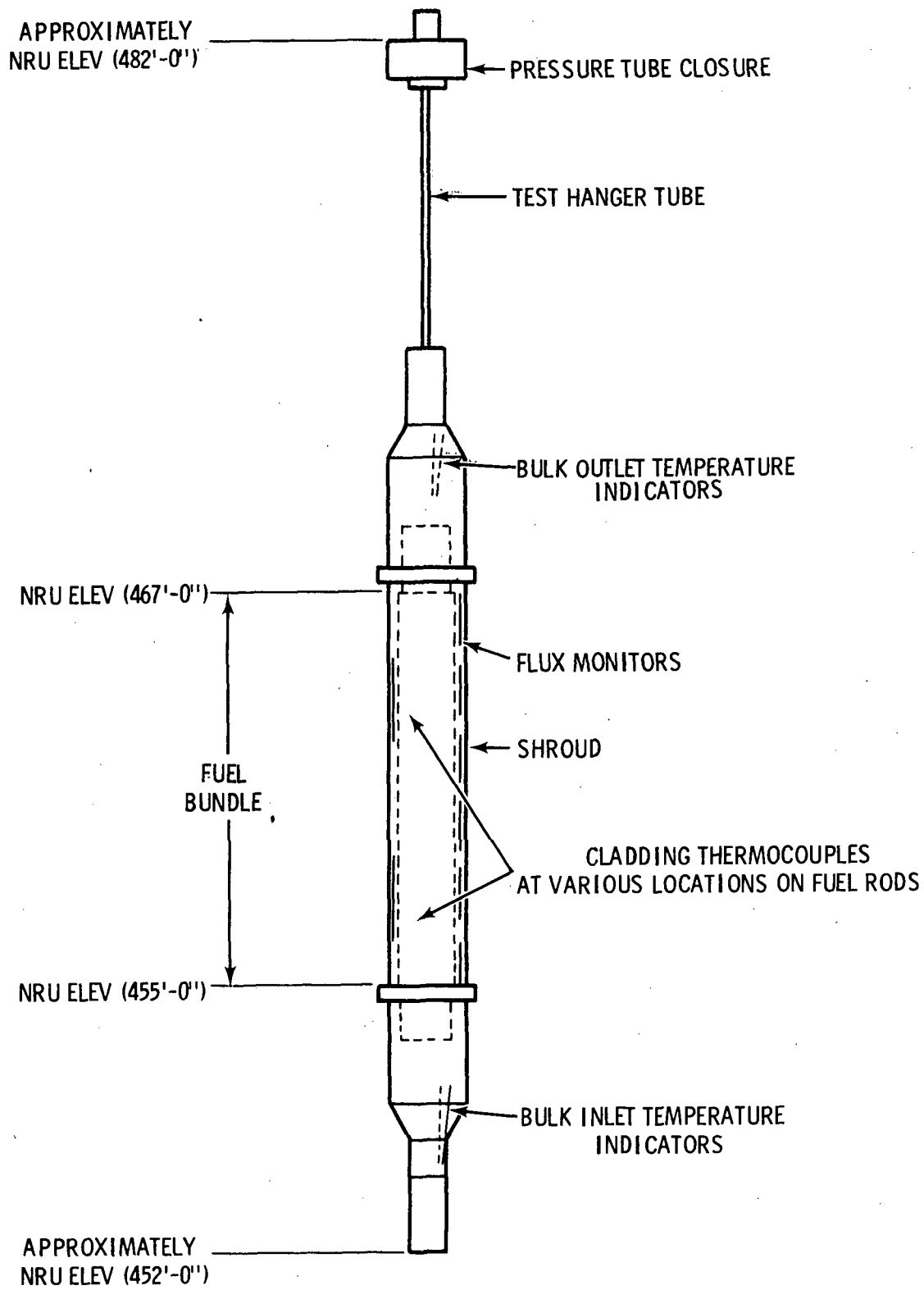
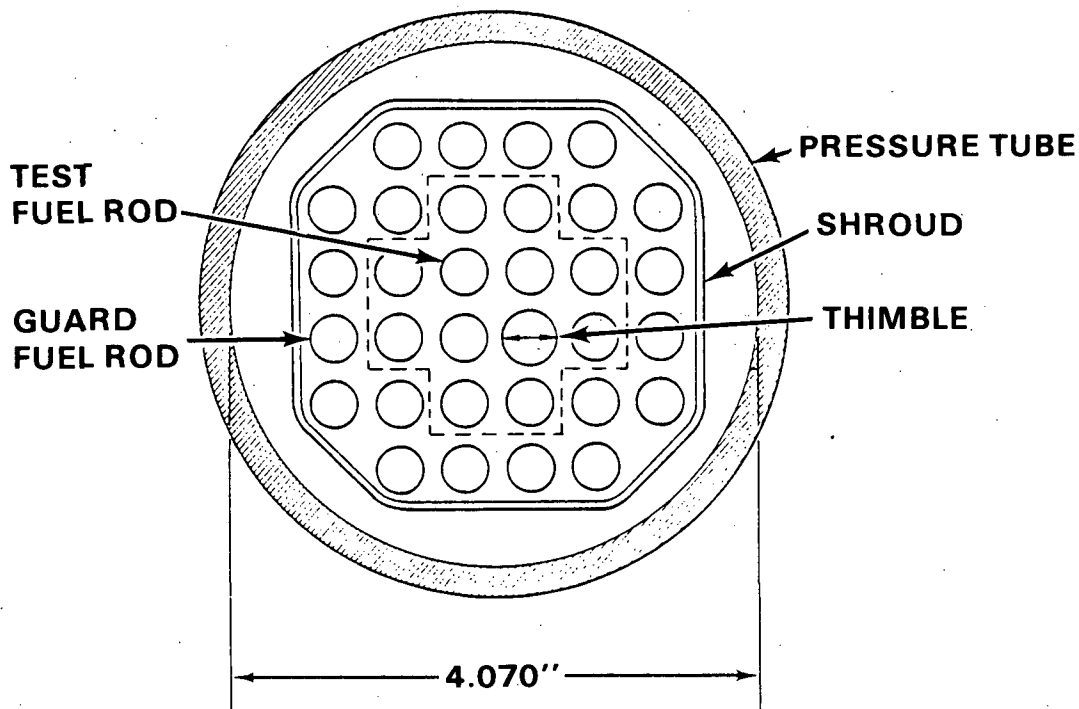


FIGURE 2.8-1. Vertical Test Train Configuration for NRU Reflood Experiments



**FIGURE 2.8-2. NRU Test Bundle Cross-Section**

Horizontal movement and/or bowing was restricted by seven typical PWR grid spacers at 21-in. intervals, starting at the beginning of the heated length. The shroud was insulated on the outer surface to reduce the amount of heat loss to the environment.

The experimental test conditions were obtained in two steps: a steady-state phase and a transient phase. During the steady-state phase, the rod power was slowly increased to the desired value for the particular test while the dry steam coolant flow rate was decreased to produce a peak cladding temperature of 800°F. The steady-state conditions were maintained at these values until the thermocouple readings stabilized. The transient was then initiated. The steam coolant flow was stopped as quickly as possible, then reflood was started at the desired flow rate. The time period between steam shut-off and reflood initiation was an adiabatic heatup period and was allowed to continue until the specified maximum peak cladding temperature was reached.

When the injected water reached the bottom of the heated length of the fuel rods, a quench front formed with significant vapor generation. The steam

and entrained water droplets flowing through the test section provided adequate cooling for the test assembly. This two-phase mixture of steam and droplets continued out the top of the heated length and into the hanger region. Here the drops de-entrained and a top-down quench front could develop if the right conditions existed. The de-entrained liquid remained directly above the test bundle and could fall back into the bundle if the vapor velocities were sufficiently low. Reflood was continued until all levels of the heated length had quenched. The test parameters for PTH110 and TH214 (Ref. 16,17) have been tabulated in Table 2.7.

TABLE 2.7. Initial and Boundary Conditions for NRU Tests PTH110 and TH214

	<u>PTH110</u>	<u>TH214</u>
Initial Peak Rod Temp. (Start of Transient) °F	848	800
Peak Rod Power kW/ft	0.55	0.55
Reflood Rate in./sec (Duration Time) sec	Constant 2.1	Variable (computer controlled) 2.18 for (54) sec 1.42 for (15) sec 0.89 for (24) sec 1.36 for (16) sec 0.54 for (136) sec 0.74 for (14) sec 0.51 for (72) sec
Inlet Coolant Temperature °F	~100	~127
Reflood Delay Time sec	32	7
System Pressure psia	40	40

## 2.8.2 COBRA/TRAC Model Description

The NRU test assembly, from the closure head to the bottom of the heated length, was modeled with three one-dimensional COBRA/TRAC components; a vessel component with mass injection at the bottom boundary, a PIPE component that connected to the top of the vessel, and a BREAK component connected to the end of the pipe. The COBRA/TRAC noding diagram is shown in Figure 2.8-3.

The vessel component was used to model the entire test train. The test assembly was divided into four vertical regions to facilitate modeling the cross-sectional area changes. Each region contained one fluid channel and the representative heat transfer surfaces. Twenty-seven vertical nodes were used. Two 9-in. and eleven 1-ft nodes were used to model the inlet and test section. This nodalization was selected so that the calculated temperatures were located as close as possible to the locations where the temperatures were measured. The outlet region and hanger regions were modeled with one 6-in. node and thirteen 1-ft nodes. The cross-sectional fluid flow areas were 5.582 in.<sup>2</sup>, 9.192 in.<sup>2</sup> and 9.868 in.<sup>2</sup> for the test section, outlet region and hanger region, respectively. The region above the test section was modeled because it was possible for de-entrained droplets to fall back into the test section.

The 11 test rods and one instrument rod were modeled by a single average fuel rod. The remaining 20 guard rods were modeled by a second average rod. Both rods were given the material properties of UO<sub>2</sub> fuel and Zr cladding. The shroud, hanger and pressure tube were modeled as three unheated conductors. The shroud extended over the heated length and the outlet regions, while the hanger and pressure tube extended only over the hanger region. The shroud and pressure tube were modeled as tube rods with internal heat transfer surfaces, zero power generation and insulated outer surfaces. The hanger was modeled as a tube with heat transfer surfaces on both the inside and outside surface. The seven grid spacers were each located in the fluid node that most closely approximated the vertical elevation of the grid.

The initial rod temperature profiles approximated the chopped cosine power profile. The peak cladding surface temperatures for the guard rods were

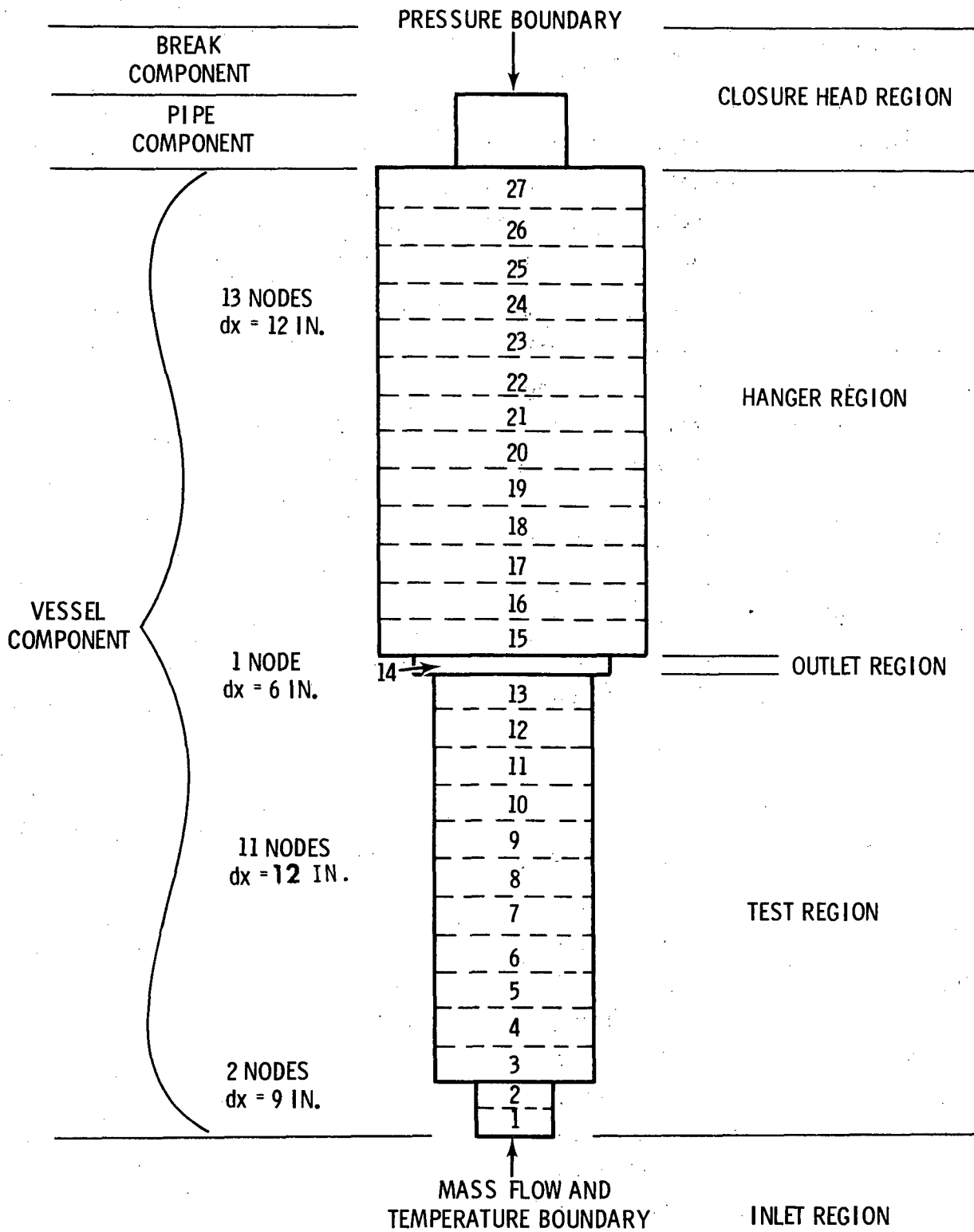


FIGURE 2.8-3. COBRA/TRAC Model of NRU Test Section

1321°F for test PTH110 and 990°F for test TH214. The peak central test rod temperatures were initialized at 1330°F for test PTH110 and 945°F for TH214. The shroud temperature increased linearly from the 275°F at the inlet region to 595°F at the outlet region, and the hanger and pressure tube temperatures were initialized at the test bundle outlet steam temperature of 596°F.

The vessel, pipe and break were all initialized with saturated steam at 40 psia. A constant average power with a chopped cosine power profile was applied to all rods. The appropriate flow boundary conditions were applied at the bottom of the vessel component. The simulation was run until all elevations had quenched.

### 2.8.3 Discussion of Results

#### Constant Reflood Rate Test (PTH110)

Figures 2.8-4 through 2.8-11 show the computed and experimental guard rod temperatures plotted versus time for eight axial locations. The NRU temperature data was averaged for all guard rod thermocouples at a particular axial location. Where the axial node locations in the computational model did not coincide exactly with axial temperature measurement locations, the COBRA/TRAC results were compared to the nearest thermocouple locations. In all cases the measured locations were within 4 to 6 in. of the computed levels. Computations for the 7-ft elevation were compared against measurements at both the 6.4-ft and 8.1-ft elevations. The COBRA/TRAC 7-ft values for temperatures and quench time were of the proper magnitude.

At nearly all elevations the prediction is within 50°F of the average guard rod peak temperature and within 100°F of the individual rod temperature, over the heated length. Exceptions to this are the 6-ft elevation, (compared in Figure 2.8-8 to the 6.36-ft NRU data) and the prediction at the 10-ft elevation, (compared in Figure 2.8-11 to the 9.86-ft NRU data) where the predicted temperatures differ somewhat from the NRU data. The early quench predicted at the 6-ft elevation is probably due to using a lower elevation in the calculation than the thermocouple's position, because comparisons at both the 5-ft and 7-ft elevations are very good. The inability to predict the

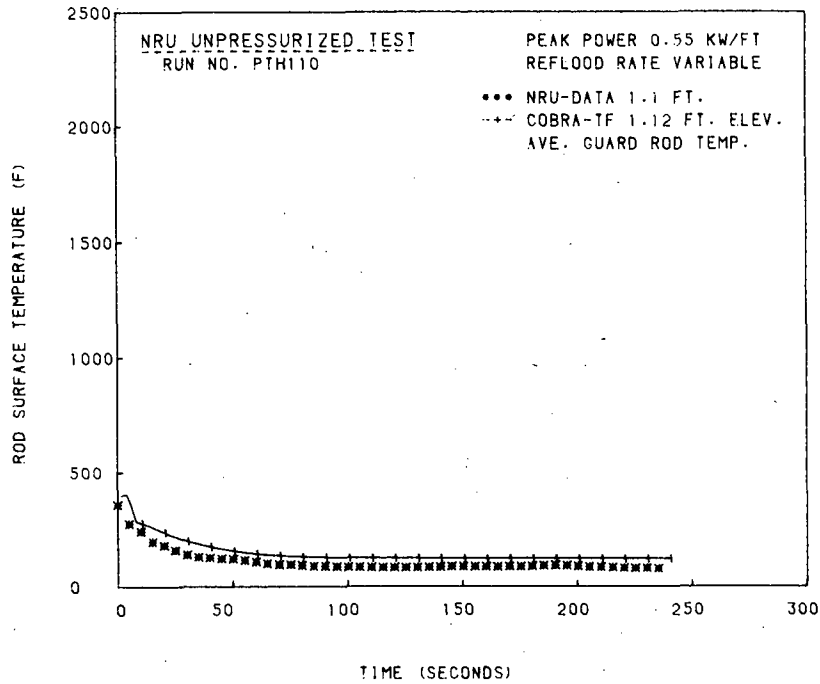


FIGURE 2.8-4. Temperatures at the 1.12-ft Elevation (Test PTH110)

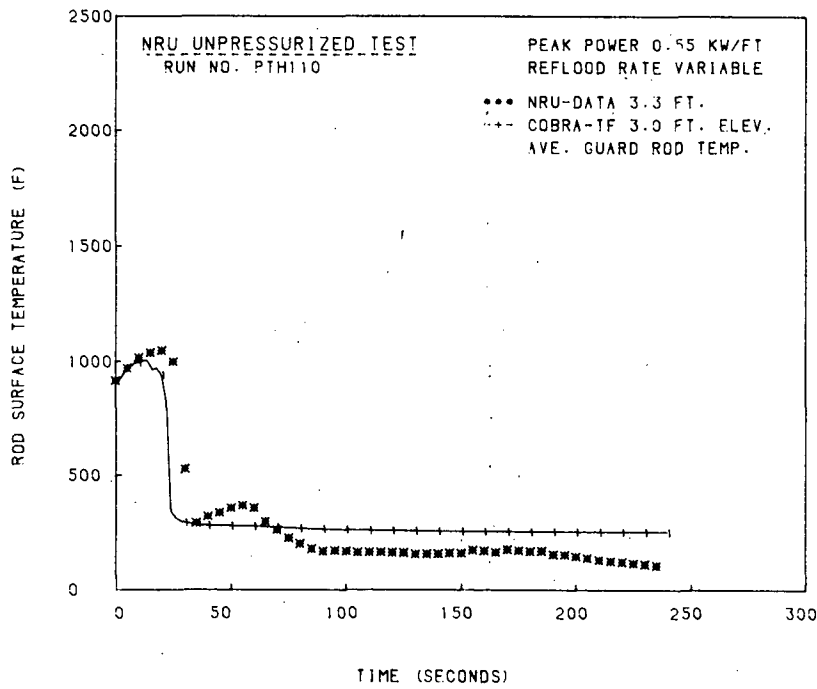


FIGURE 2.8-5. Temperatures at the 3.0-ft Elevation (Test PTH110)

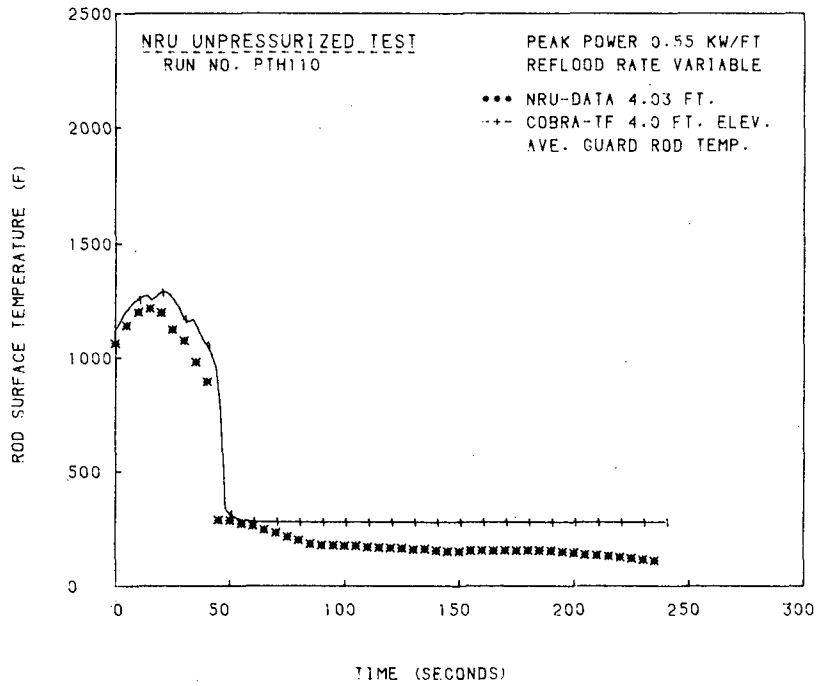


FIGURE 2.8-6. Temperatures at the 4.0-ft Elevation (Test PTH110)

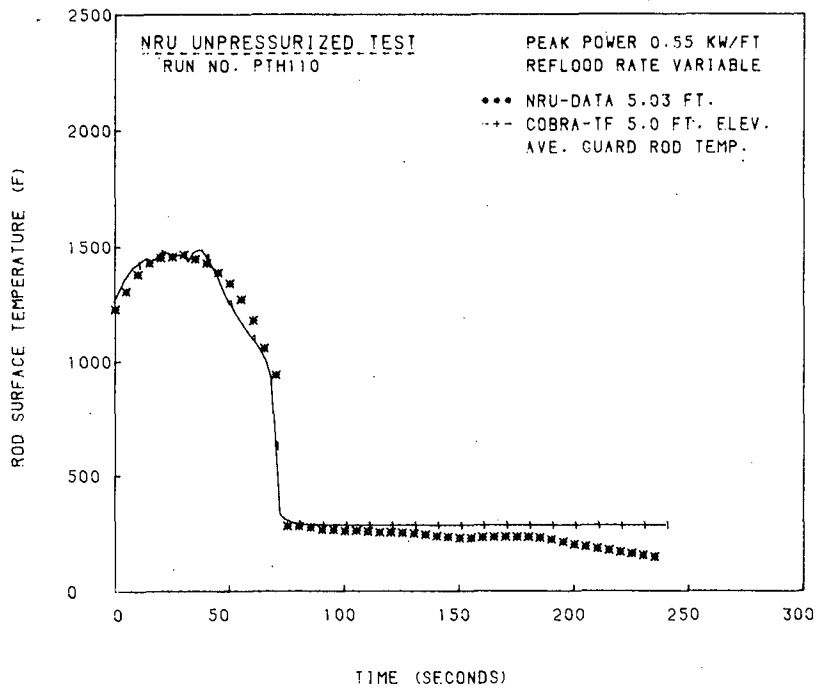


FIGURE 2.8-7. Temperatures at the 5.0-ft Elevation (Test PTH110)

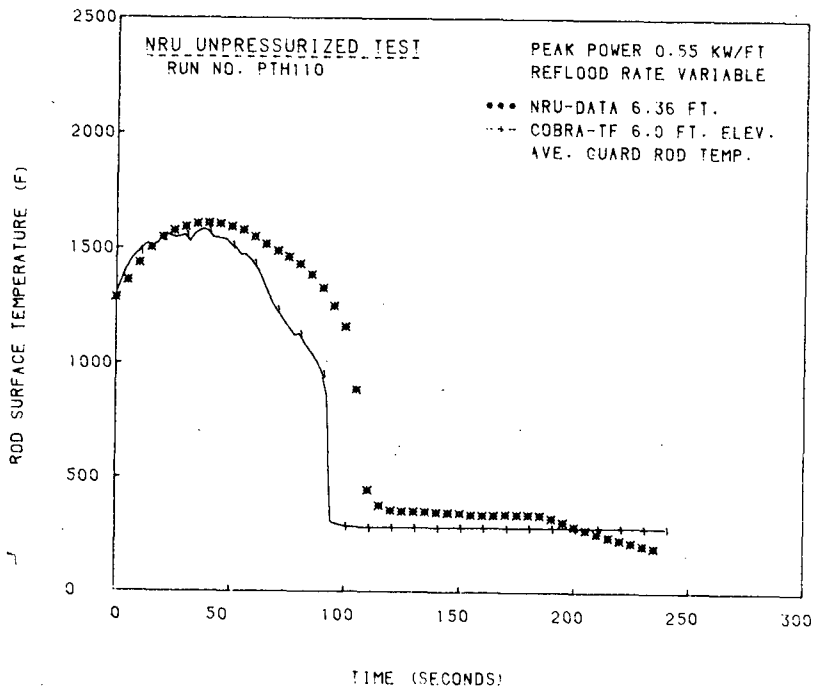


FIGURE 2.8-8. Temperatures at the 6.0-ft Elevation (Test PTH110)

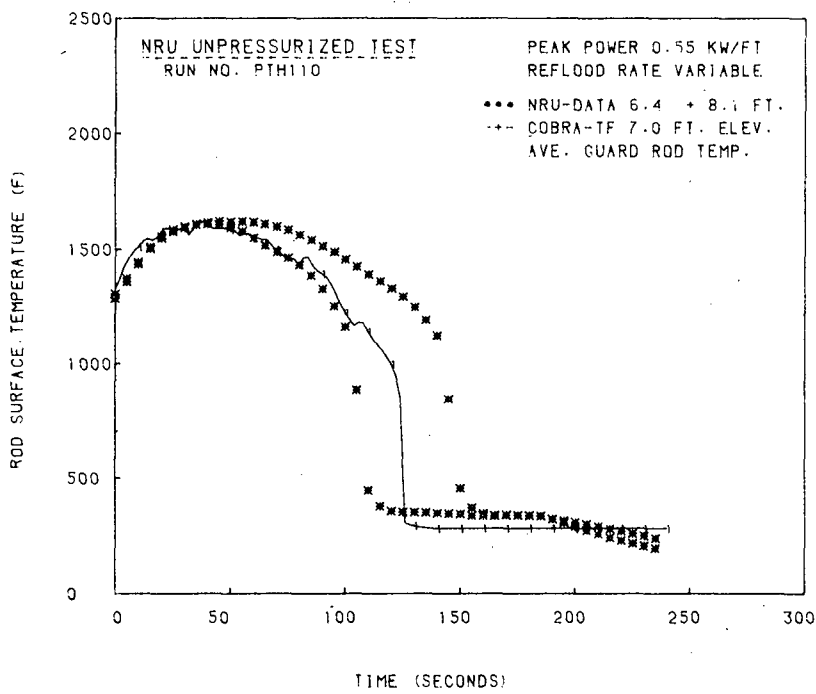
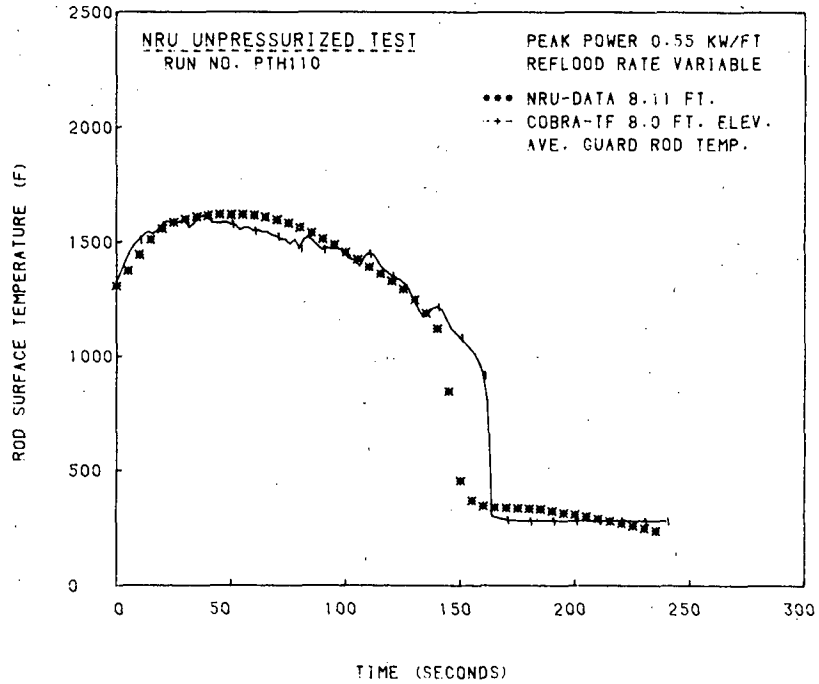
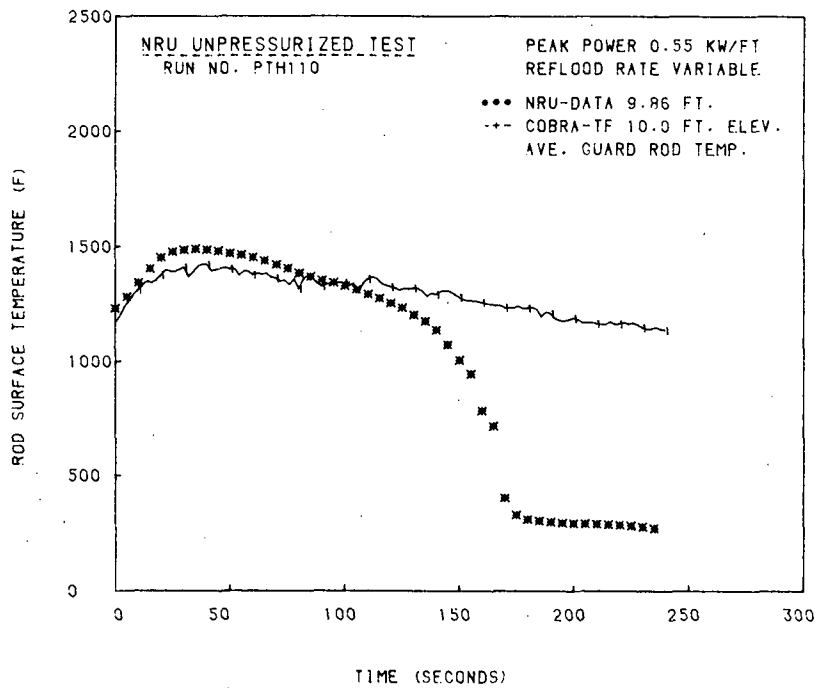


FIGURE 2.8-9. Temperatures at the 7-ft Elevation (Test PTH110)



**FIGURE 2.8-10.** Temperatures at the 8.0-ft Elevation (Test PTH110)



**FIGURE 2.8-11.** Temperatures at the 10.0-ft Elevation (Test PTH110)

quench time and temperature at the 10-ft elevation has been attributed to the absence of an accurate top-down quench model. A recent simulation using an improved top quench front model shows a markedly improved comparison at the 10 ft elevation. This simulation will be presented in a later report.

As was seen in the temperature profiles, COBRA/TRAC predicts the quench times for all elevations, except the 10-ft elevation, to within 10 to 15 sec of the NRU predictions. The results presented above are excellent for bottom reflood and quenching in a nuclear fuel bundle.

#### Variable Reflood Rate Test (TH214)

The plots of computed and experimental rod temperatures versus time for the same 8 axial locations as for test PTH110 are presented in Figures 2.8-12 through 2.8-19. As was the case with PTH110, all the NRU data is average guard rod information. COBRA/TRAC underpredicts the temperature profile and quench times in the 3- to 5-ft region ( Figures 2.8-13 through 2.8-15). The code underpredicts the peak temperatures while overpredicting the quench time for the 6-ft elevation (Figure 2.8-16). The uncertainty in the magnitude of the rapidly varying inlet flow rate and temperature is partially responsible for the poor data comparison in the test region below 6 ft.

Figure 2.8-17 compares the 7-ft prediction against the 6.4-ft and the 8.1-ft NRU test results. The fact that the 6.4-ft elevation quenched and 8.1-ft elevation did not quench indicates that the quench front stabilized somewhere between the two data locations. Therefore, if the COBRA/TRAC inlet condition was different than actual inlet conditions, a stable quench front would occur at a different location. By comparing the COBRA/TRAC results for the 6-ft to the 7-ft elevation, it appears that the predicted quench front stabilized closer to the 6-ft elevation rather than the 6.5 to 8.0-ft elevation presented by the data. Even though the quench front location was underpredicted, this had little effect on the temperatures above the 7-ft elevation, which would indicate that the entrainment rate and interfacial heat transfer is of the proper order of magnitude. Figures 2.8-17 through 2.8-19 show that the predictions are within 10% of the experimental data out to 250 sec, at which point the reactor was scrammed.

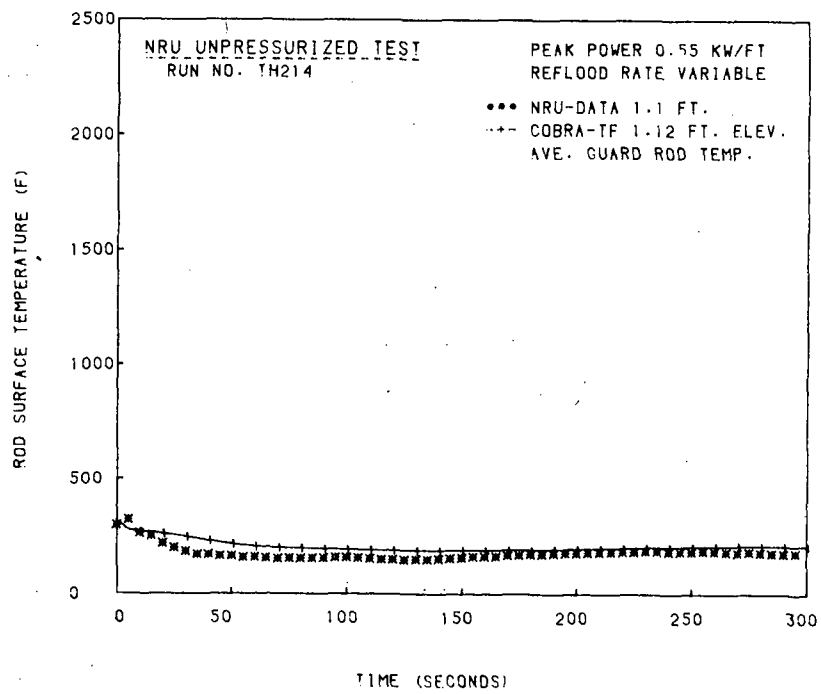


FIGURE 2.8-12. Temperatures at the 1.12-ft Elevation (Test TH214)

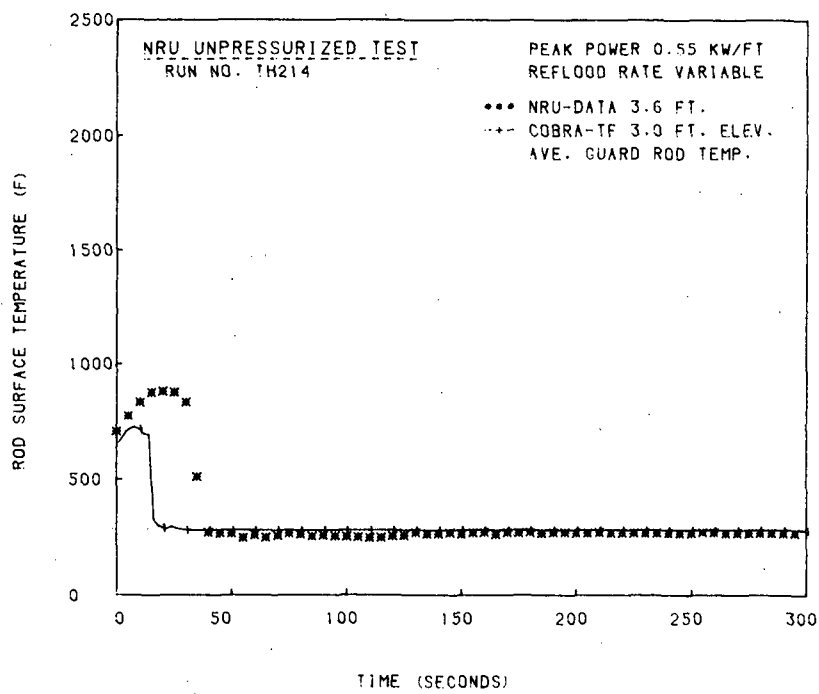
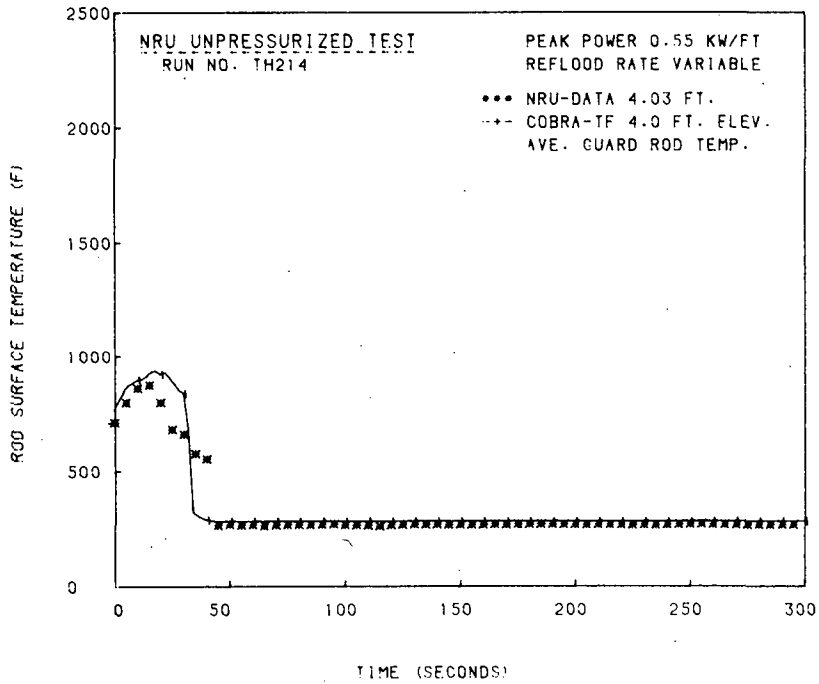
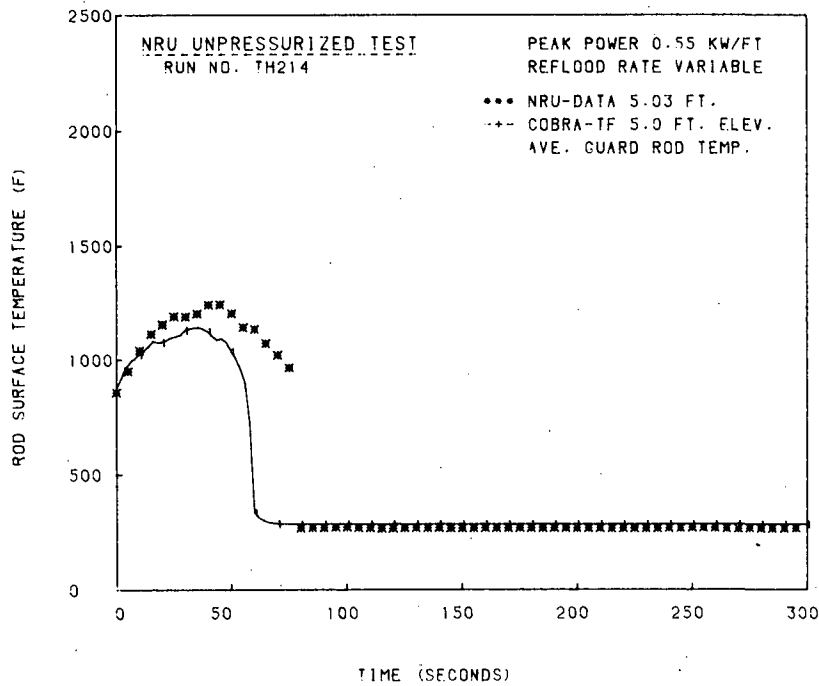


FIGURE 2.8-13. Temperatures at the 3.0-ft Elevation (Test TH214)



**FIGURE 2.8-14. Temperatures at the 4.0-ft Elevation (Test TH214)**



**FIGURE 2.8-15. Temperatures at the 5.0-ft Elevation (Test TH214)**

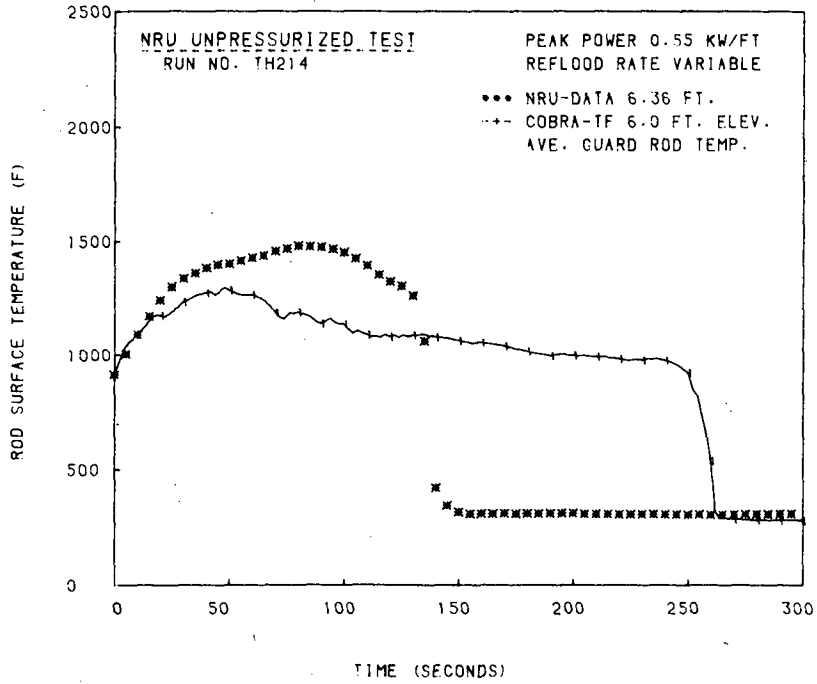


**FIGURE 2.8-16.** Temperatures at the 6.0-ft Elevation (Test TH214)

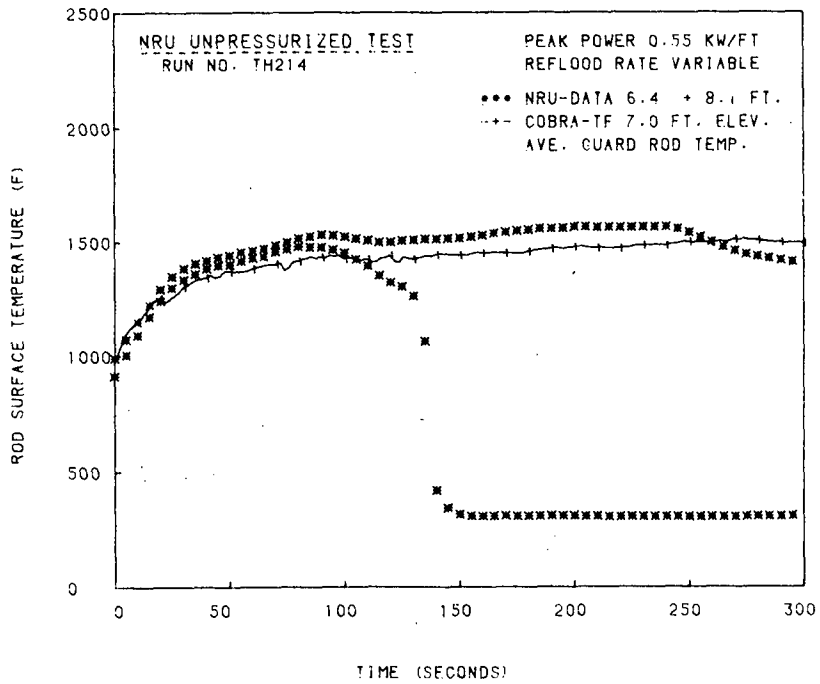


**FIGURE 2.8-17.** Temperatures at the 7-ft Elevation (Test TH214)

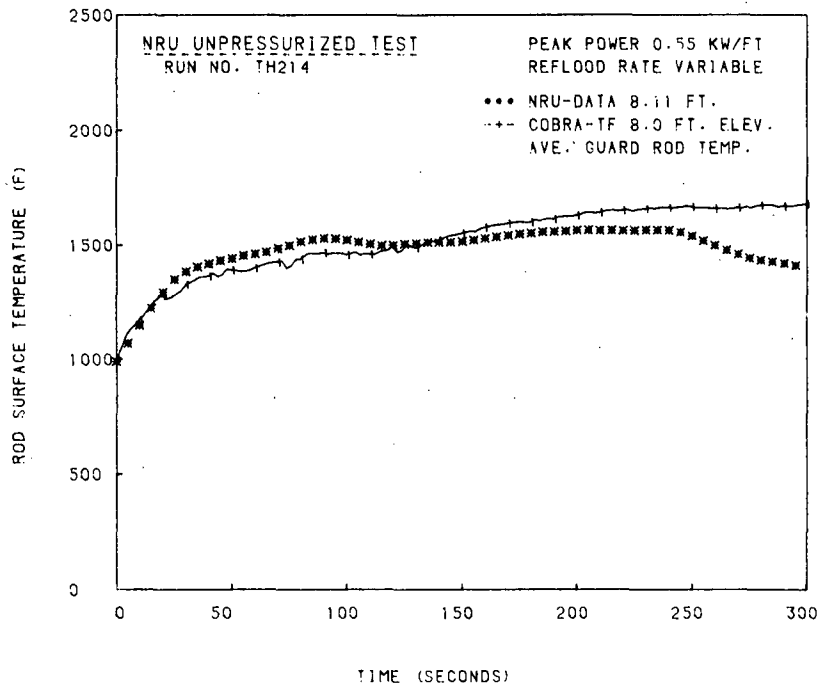


**FIGURE 2.8-18. Temperatures at the 8.0-ft Elevation (Test TH214)**

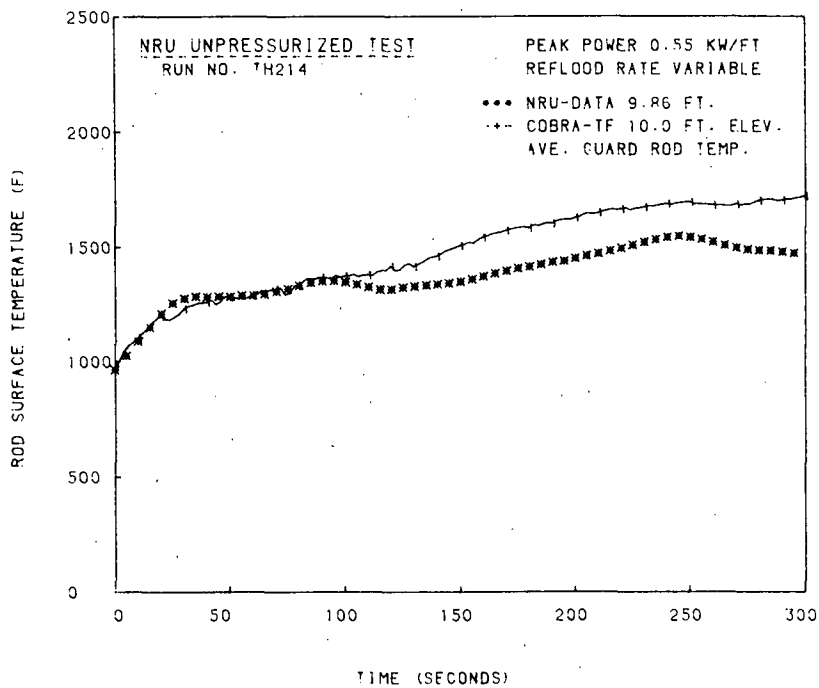


**FIGURE 2.8-19. Temperatures at the 10.0-ft Elevation (Test TH214)**

The predicted collapsed liquid level supports the ideas presented above, since it shows that the collapsed liquid level increased rapidly up to the 6-ft elevation and then stabilized there at about 125 sec (Figure 2.8-20). Then the liquid level decreased to ~5.5 ft. The decrease in collapsed liquid level at 125 sec should cause the rod temperatures at the higher elevations to increase after that time, and they do.

COBRA/TRAC does an excellent job of predicting the PTH110 and TH214 transients. Some problems did occur in trying to simulate the actual reflood conditions of TH214 and the top down quench front. These two simulations, PTH110 and TH214, are just two of the approximately 55 experimental NRU tests, and further simulations of this type are needed before a definite conclusion can be made about COBRA/TRAC's calculational abilities. The results presented here indicated that COBRA/TRAC does an acceptable job of predicting forced bottom reflood in nuclear fuel bundles.

Both simulations were run on cycle 10 of COBRA/TRAC.

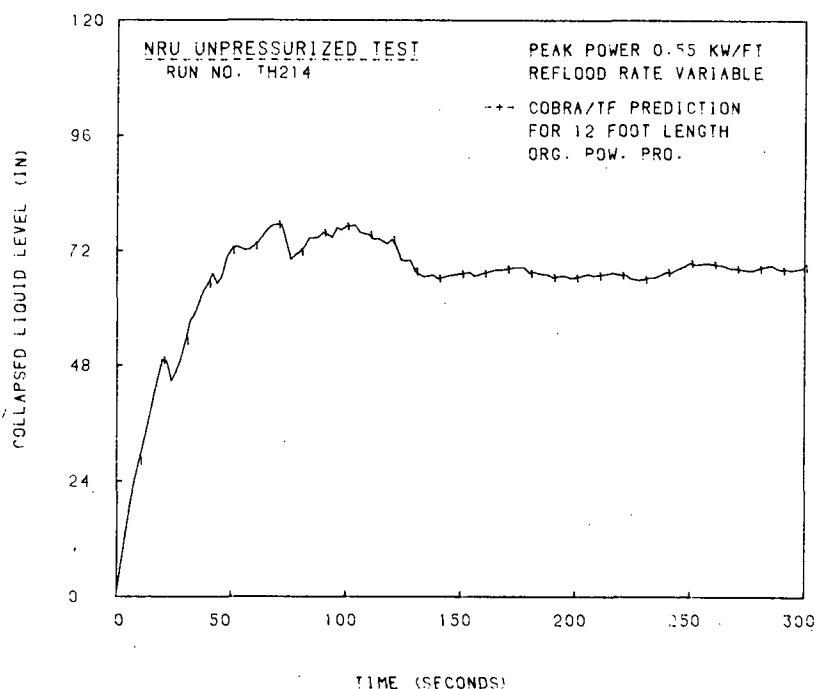


FIGURE 2.8-20. Collapsed Liquid Level vs. Time (Test TH214)

## 2.9 PKL GRAVITY REFLOOD EXPERIMENT K9

Experiments simulating the refill and reflood procedure after a loss-of-coolant accident (LOCA) in a 1300 MW PWR primary coolant system were performed at the KWU test facility in Erlangen, Germany (Ref. 18).<sup>(a)</sup> COBRA/TRAC was used to model experiment K9 of the PKL series (completed December 1979). PKL-K9 was characterized by a double-ended guillotine break in the cold leg with emergency core cooling water injected into the cold legs. This simulation assessed the code's ability to predict gravity feed reflood hydrodynamic and heat transfer phenomena.

### 2.9.1 Description of Experiment

The test facility was designed to simulate a 1300 MW PWR. The main components were a vessel (approximately 30 ft high and 1.6 ft in diameter), an external pipe downcomer (0.66 ft in diameter), and three primary coolant loops (one with double capacity). Each coolant loop contained a U-tube steam generator and a cold leg pump resistance. An orifice plate was used to model the pump rotor resistance in the broken loop.

The pressure vessel contained a rod bundle of 340 rods, of which 337 were electrically heated with a flat radial power profile. Upper and lower plenums with associated internals were also present. A separate pipe downcomer was attached to the vessel at the lower plenum. The hot leg of each coolant loop connected to a steam generator. The intact loop piping extended from the steam generator through a pump resistance to the top of the downcomer. The broken loop hot leg terminated in the pressurized containment tank (4.2 bar initially). The broken cold leg was also attached to the pressurized containment tank. The pressurized containment tank was partially filled with saturated water. Emergency core cooling water was injected into the cold legs at the downcomer, as well as directly into the downcomer. A diagram of the system is shown in Figure 2.9-1.

<sup>(a)</sup> The experimental work was sponsored by the German Ministry of Research and Technology to probe system interactions during refill and reflood.

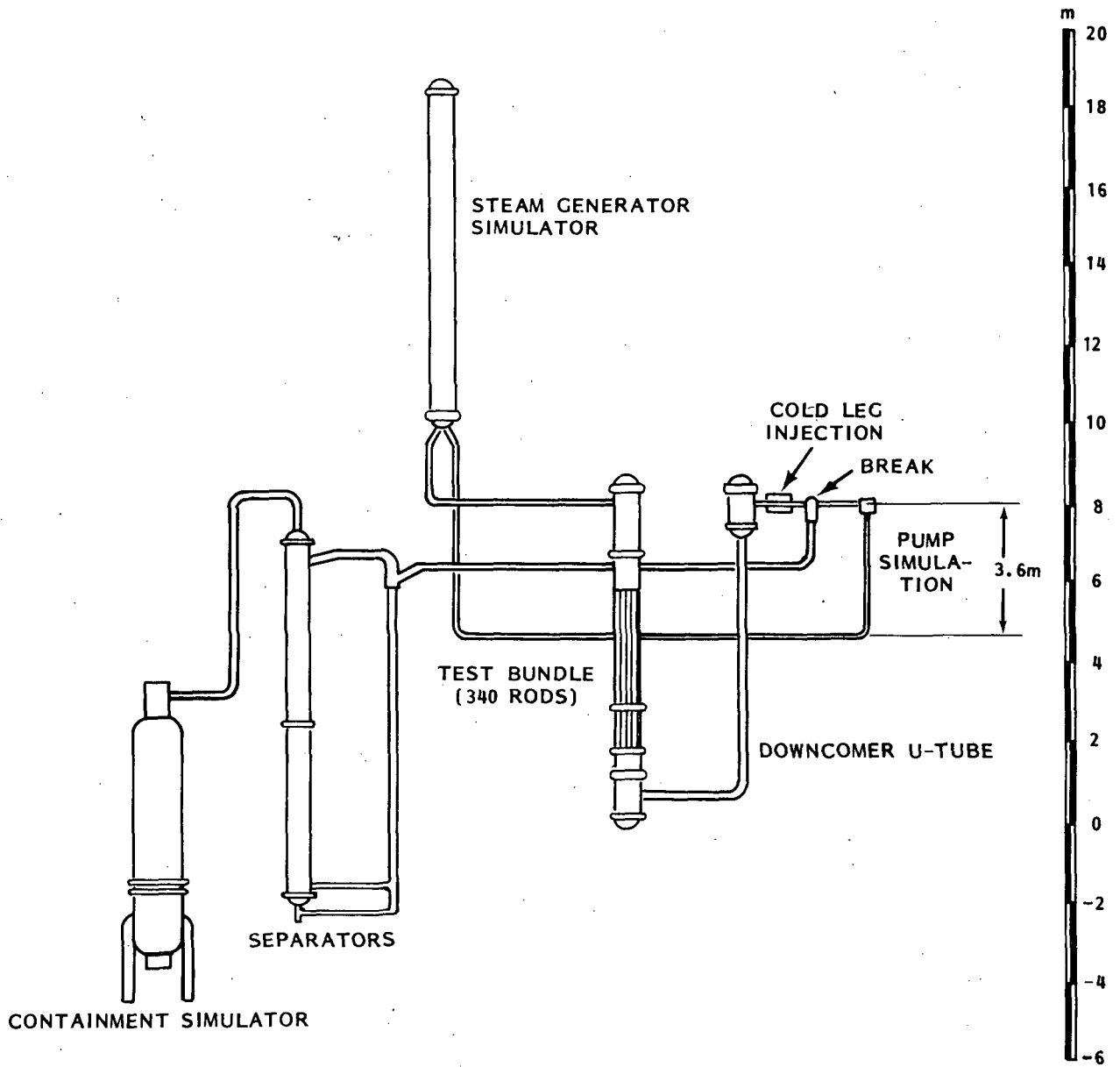


FIGURE 2.9-1. Diagram of PKL System

## 2.9.2 COBRA/TRAC Model Description

A COBRA/TRAC system component schematic for PKL-K9 is illustrated in Figure 2.9-2. The vessel and downcomer were modeled with the vessel component (component 1). The hot and cold leg pipes and the steam generators were simulated with the appropriate one-dimensional components.

A detailed diagram of the COBRA/TRAC model of the pressure vessel and downcomer is shown in Figure 2.9-3. This part of the facility was modeled with the three-dimensional vessel component. The vessel component contained five vertical sections. Section one modeled the bottom half of the lower plenum and the downcomer pipe connection. Section two modeled the top half of the lower plenum and the corresponding piece of the downcomer. The core and downcomer were simulated by sections three and four. Section five modeled the upper plenum and the top of the downcomer. Fourteen channels in five sections provided 82 mesh cells. One average heater rod, with a heated length of 12.67 ft located in core channels 3 and 4 (14.79 ft), was used to model the 337 heated rods in the core. A one-dimensional nodalization was used to minimize computation time. The vertical node length was chosen to coincide with measurement locations.

The three coolant loops of PKL-K9 were modeled with two equivalent loops that consisted of the flow area of the three loops. The broken cold leg (pipe 7) and the broken hot leg (pipe 4) were connected to break components 6 and 5 respectively. These break components modeled the containment pressure history described in the PKL documents (Ref. 18, 19 and 20). The intact cold leg (pipe 10), ECC injection, and broken cold leg (pipe 7) connect to the downcomer at nodes 4, 5, and 6, as illustrated in Figure 2.9-3. This configuration simulated the PKL-K9 test where ECC injection was into the intact loop cold legs.

The initial conditions for fluid state and rod temperatures were obtained from the PKL documents (Ref. 18,19). The vessel, the primary sides of the steam generators, and all pipes were initially filled with saturated steam. The secondary sides of the steam generators were filled with water to a height of 7.5 m. Initial flows in the system were zero. The initial vessel pressure was set to the specified pressure of 4.6 bars.

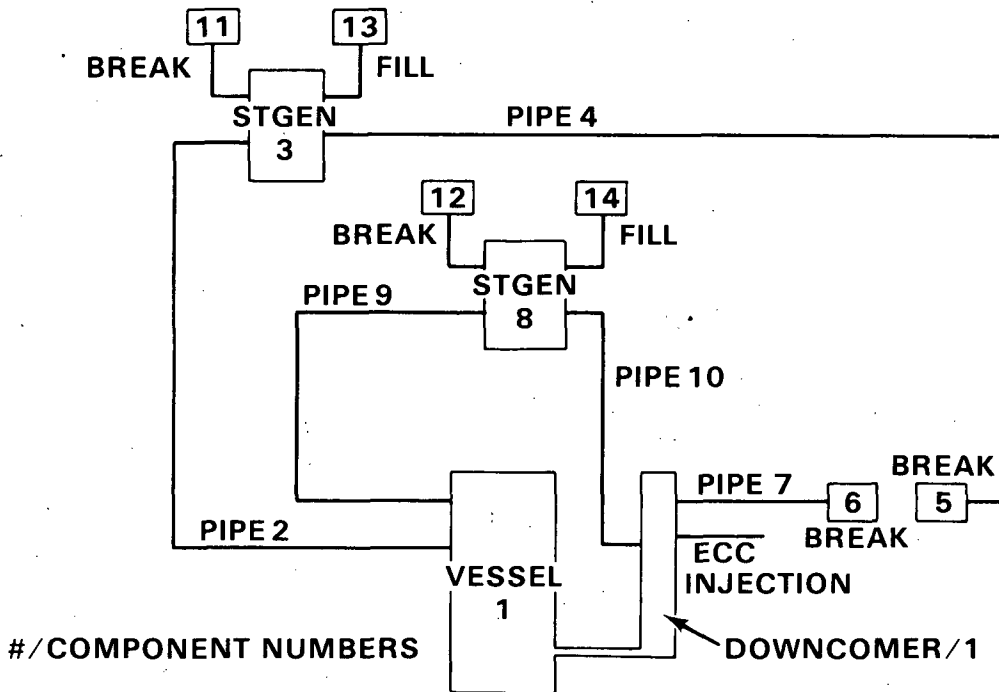


FIGURE 2.9-2. COBRA/TRAC Model of PKL Test Facility

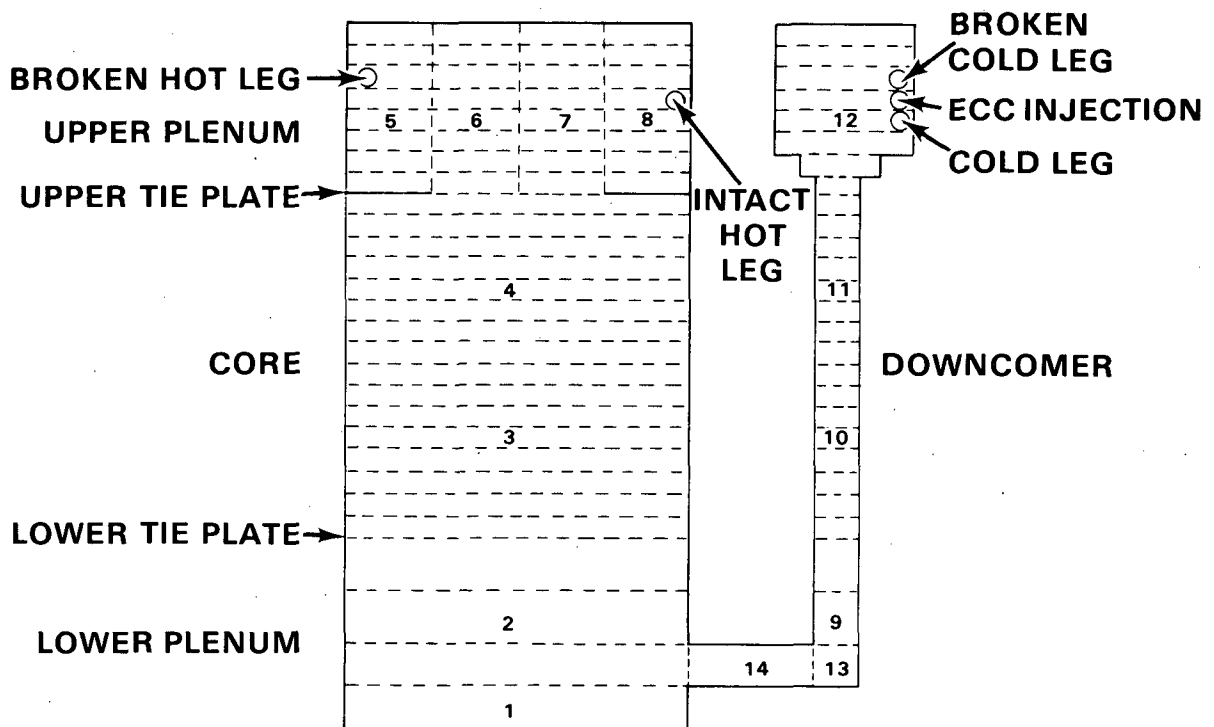


FIGURE 2.9-3. Schematic of COBRA/TRAC Model of PKL Pressure Vessel and Downcomer

The transient was initiated by the depressurization of BREAKs 5 and 6 at time zero. ECC injection began 0.001 seconds later. The transient was terminated after 220 seconds.

### 2.9.3 Discussion of Results

The simulation began with a double-ended guillotine break in one cold leg. ECC water condensed steam in the downcomer. This decreased the vessel pressure and drew steam in from both ends of the break. Since a pressure boundary condition simulating the containment back pressure was applied on both sides of the break, flow in the broken loop was forced toward the vessel from both directions. This resulted in reversed flow in the broken loop and normal directional flow in the intact loop. Normal directional flow in both loops was re-established when the lower plenum was filled and cooling began in the core at about 24 seconds. Figures 2.9-4 and 2.9-5 show that this corresponds to the time at which upper plenum pressure exceeded the break pressure.

COBRA/TRAC predicted a fairly stable broken cold leg pressure profile until approximately 145 seconds. Small oscillations were then evidenced. The pressure there was higher than the PKL measurements before 30 and after 70 seconds. The pressure in the upper plenum was oscillatory and a bit high after 25 seconds. Neither pressure prediction showed the initial pressure plunge similar to the reported data. This was probably due to the modeling method. While the COBRA/TRAC model of the containment as a pressure boundary condition allowed an unlimited steam supply, the small PKL containment provided a limited flow into the vessel. This is manifest in the steep pressure drop. The pressure oscillations probably were related to the flow oscillations predicted in the core and downcomer.

Forced flow oscillations continued throughout the test. These were due to the varying rates of steam production in the core. Steam production increased the pressure in the core, forcing liquid into the downcomer. Then diminished vapor generation in the core, coupled with hydrostatic head in the downcomer, forced liquid back into the core.

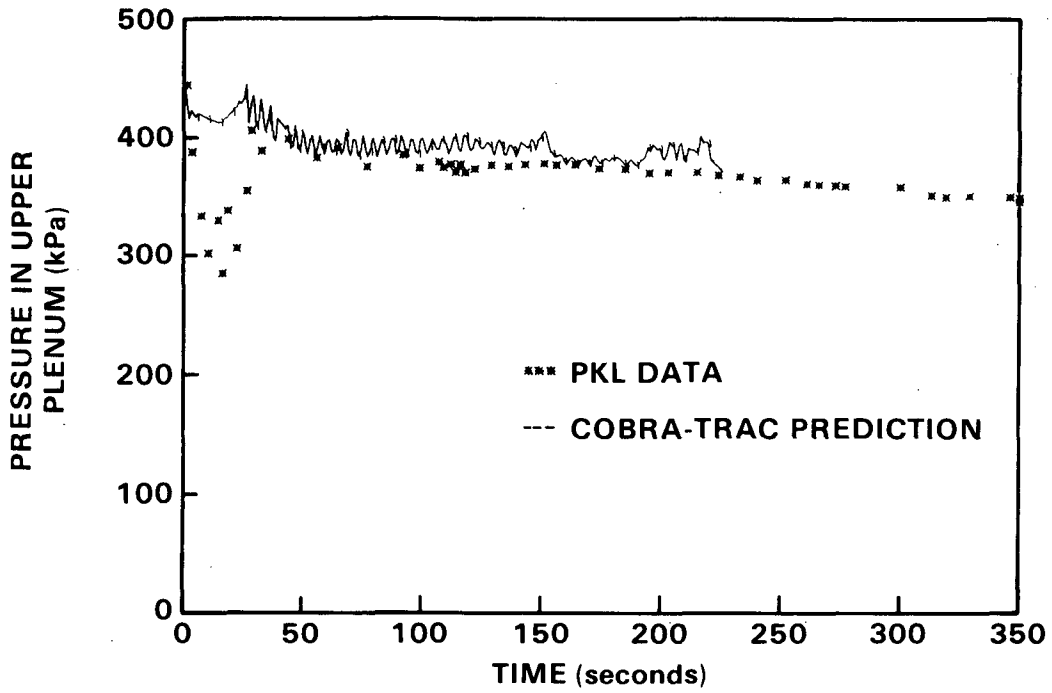


FIGURE 2.9-4. Pressure in the Upper Plenum (Channels 5-8)

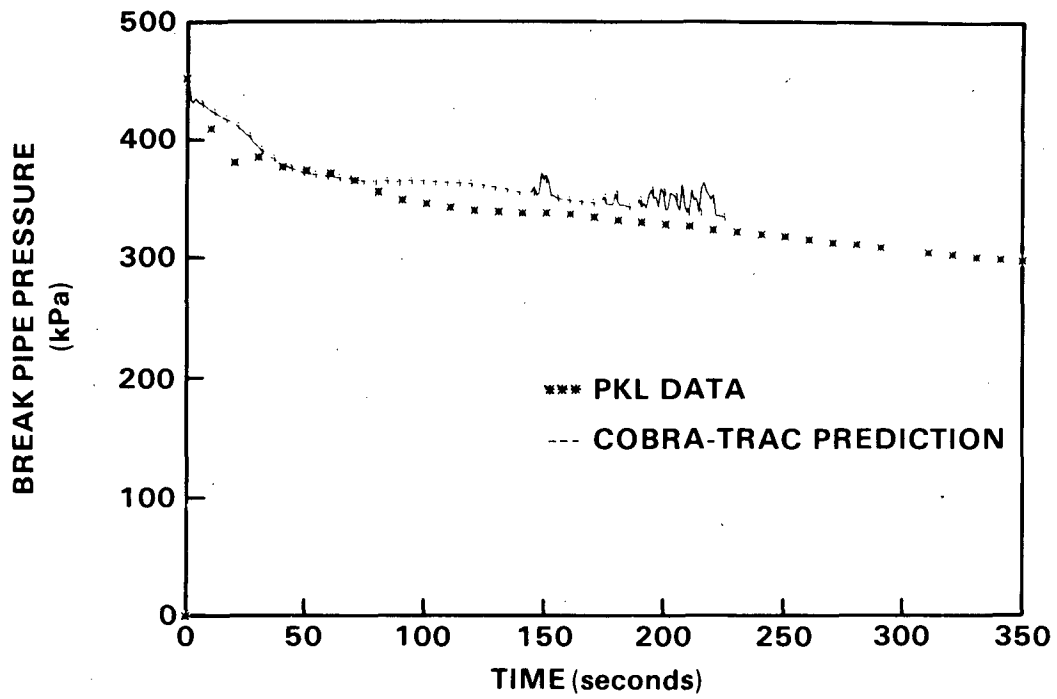


FIGURE 2.9-5. Pressure in the Break Pipe

Collapsed water level measurements agreed well with the PKL reported data (Figure 2.9-6) but following 150 seconds the water level appeared low.

The downcomer mass flow rate also oscillated. Figures 2.9-7 and 2.9-8 show downcomer flow rates in channel 10, the former averaged over the entire channel while the latter was taken at the lower node boundary. (The PKL measurement was at a similar location.) It appears that the COBRA/TRAC prediction follows the correct trend.

Clad temperature profiles at several elevations in the core are shown in Figures 2.9-9 through 2.9-15. Peak clad temperatures occur about 25 seconds after the start of the transient. This was when the lower plenum was filled with water and the bottom of the core was beginning reflood. Quench fronts through level four (~6.4 ft) were well predicted by COBRA/TRAC. Above level 4 the code underpredicted the heat transfer associated with top down quenching and consequently did not predict quench time at these elevations. A plot of the quench front envelope is shown in Figure 2.9-16.

The void fractions, shown Figures 2.9-17 through 2.9-19, also fluctuated. The severe oscillations may have been driven by the critical heat flux switching logic. The damping effects of a turbine flow meter in the power part of the downcomer possibly should have been modeled with a loss coefficient.

In summary, COBRA/TRAC predicted the temperature profiles in PKL in the lower half of the core well. It had difficulty with quench front in the core upper half because it did not correctly predict the falling film heat transfer. It is believed that the new top quench front model will improve data comparisons in the upper half of the core. Upper plenum pressure, break pressure and collapsed water level in the core predictions agreed fairly well with the measured data. Something is awry in the void fraction and downcomer velocity predictions. This simulation was run on cycle 10 of COBRA/TRAC.

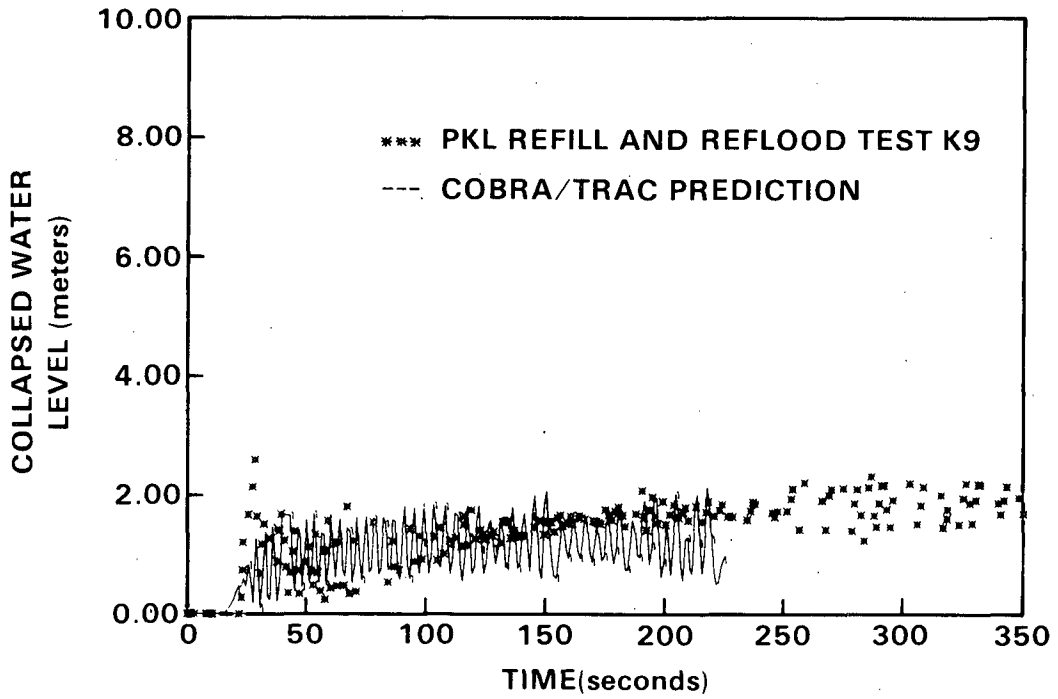


FIGURE 2.9-6. Collapsed Water Level in the Core

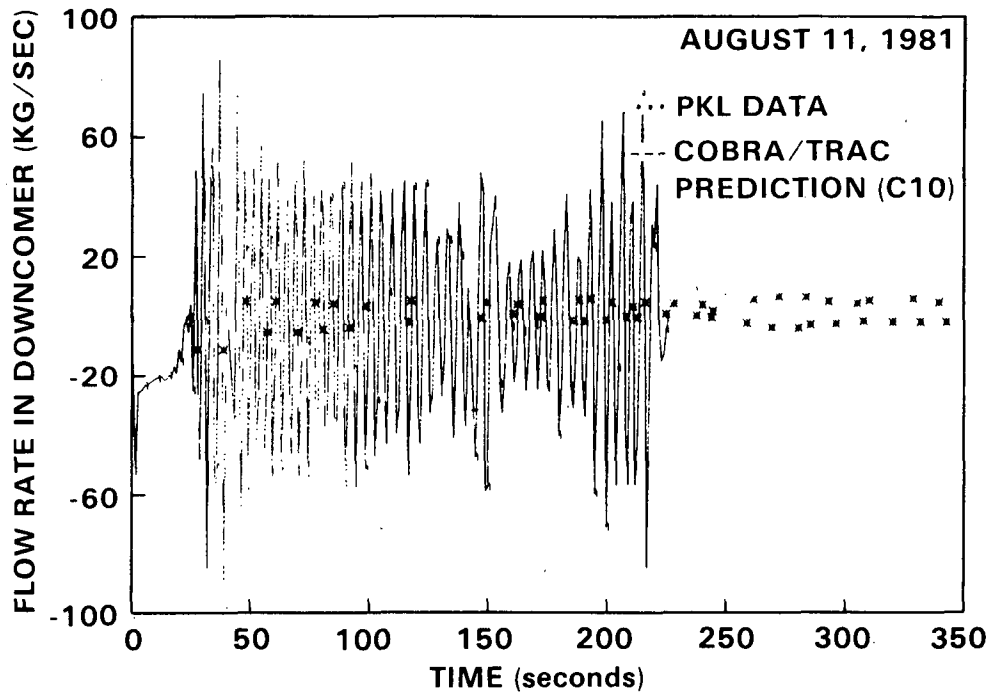


FIGURE 2.9-7. Flow Rate in the Downcomer (Averaged Over Length of Channel 10)

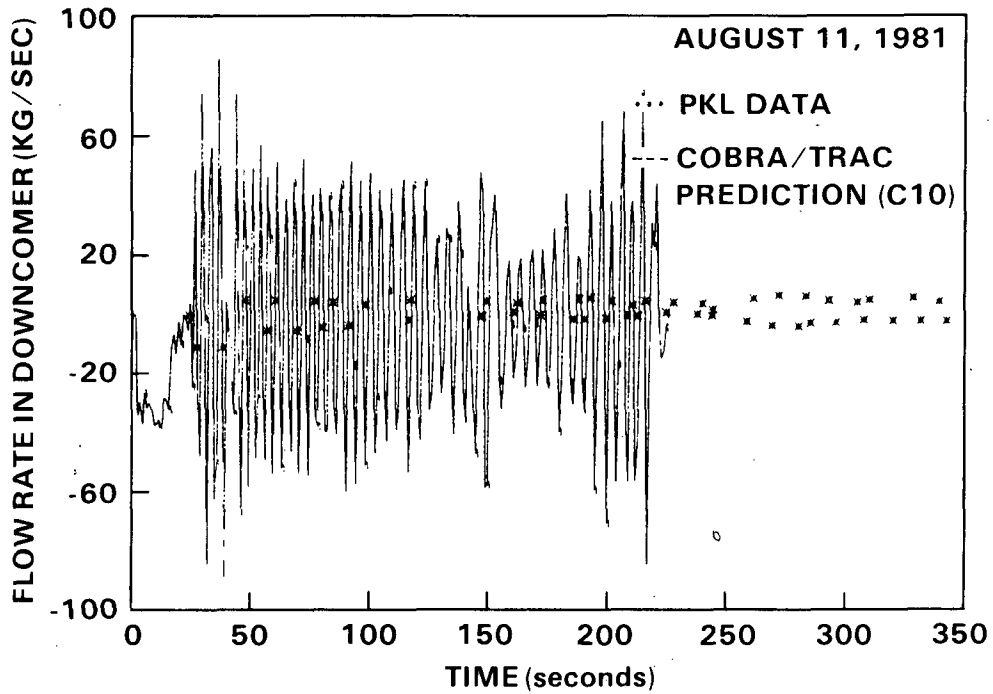


FIGURE 2.9-8. Flow Rate in the Downcomer (at the Lower Boundary Node).

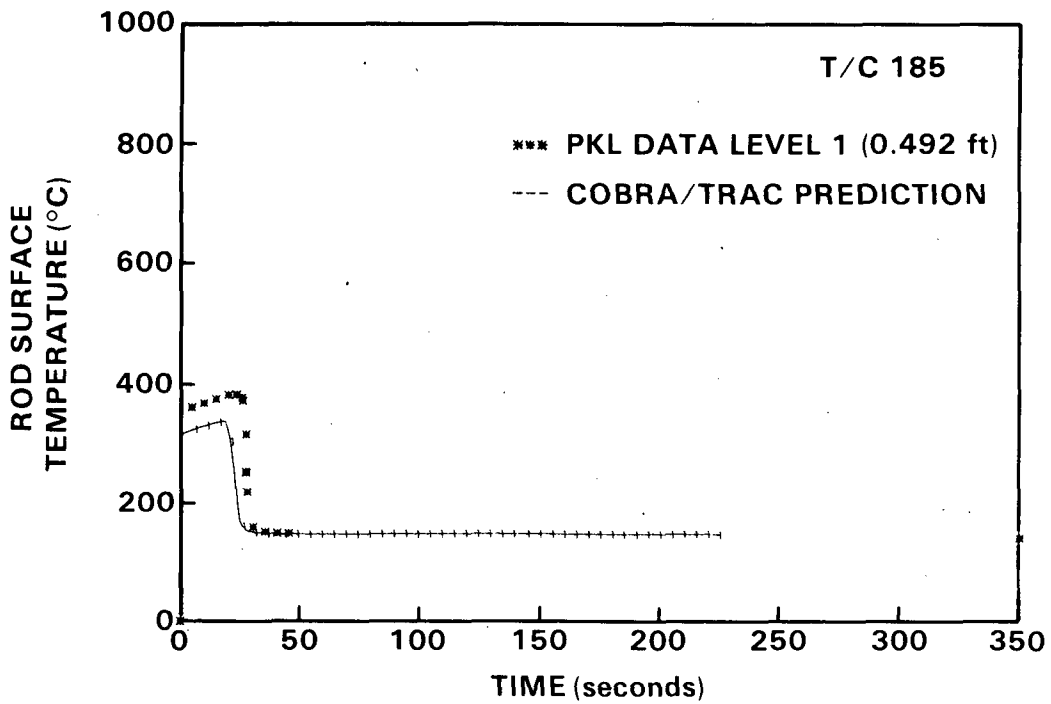


FIGURE 2.9-9. Rod Surface Temperature at Level 1

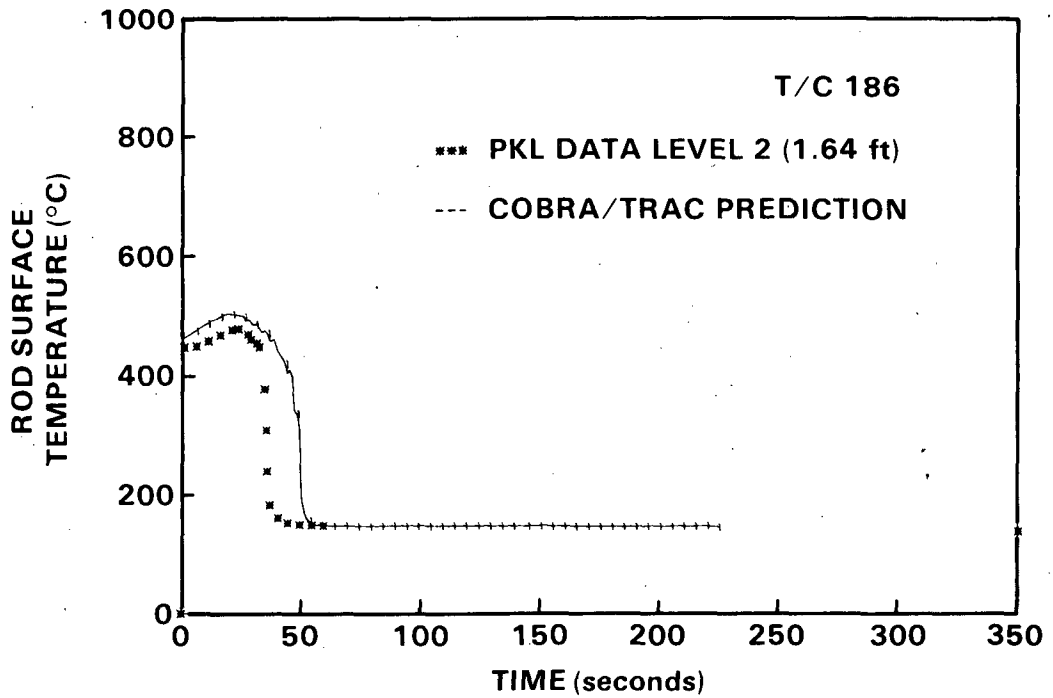


FIGURE 2.9-10. Rod Surface Temperature at Level 2

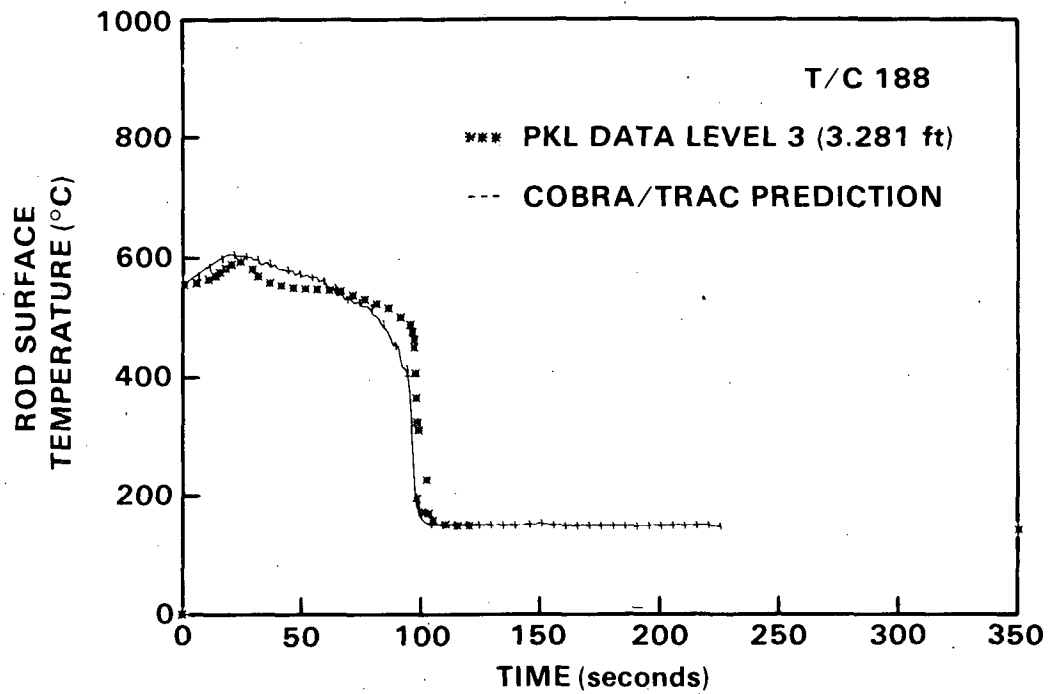


FIGURE 2.9-11. Rod Surface Temperature at Level 3

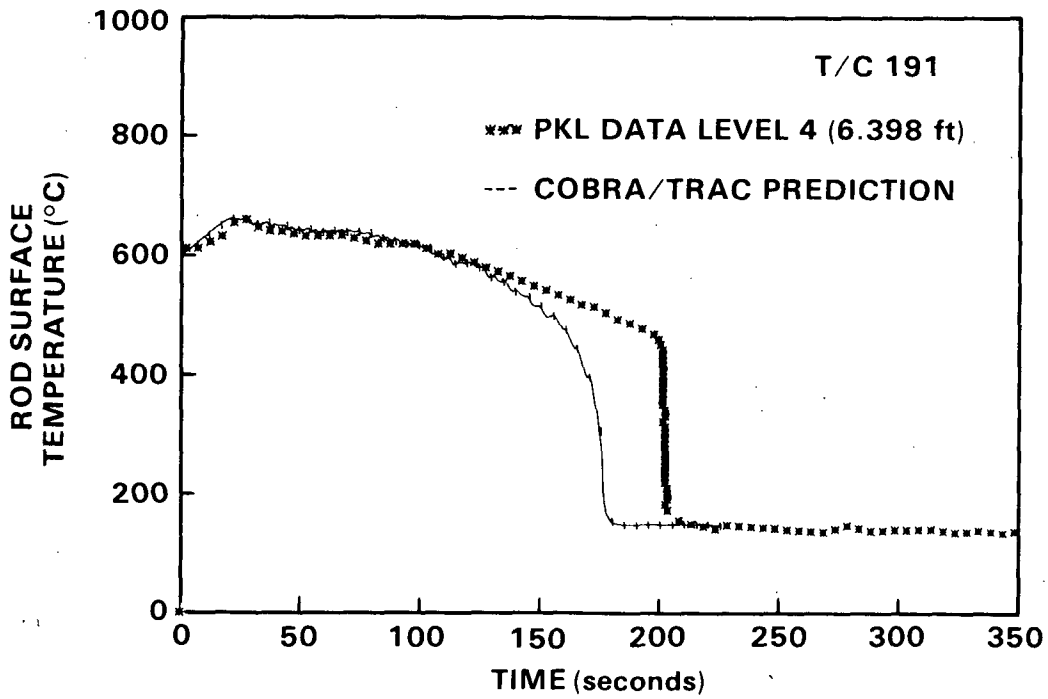


FIGURE 2.9-12. Rod Surface Temperature at Level 4

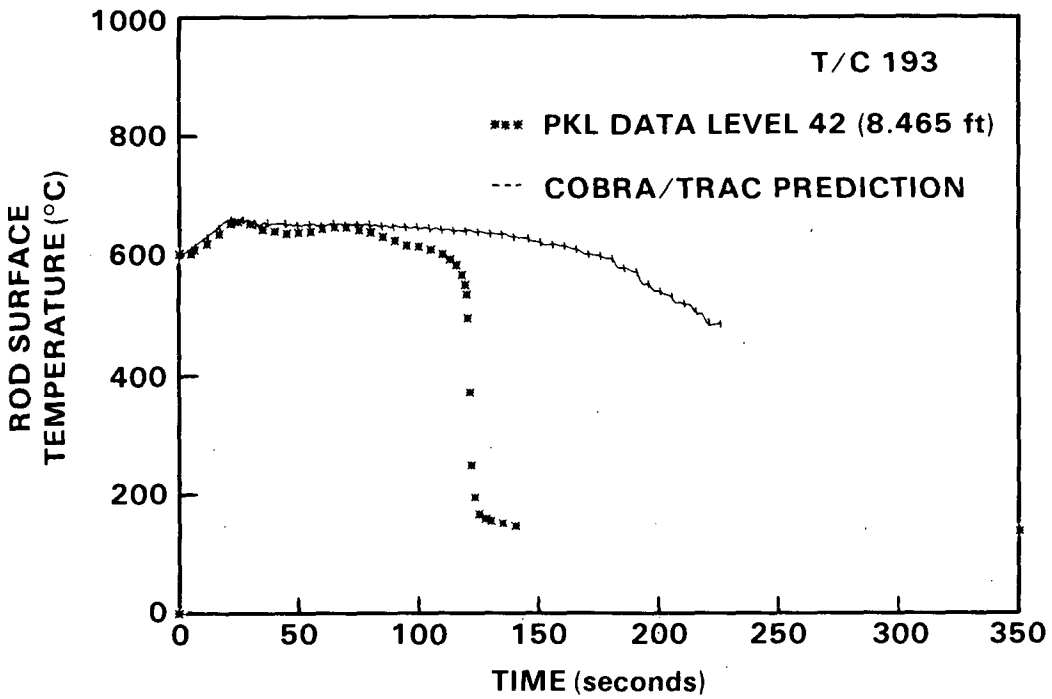


FIGURE 2.9-13. Rod Surface Temperature at Level 42

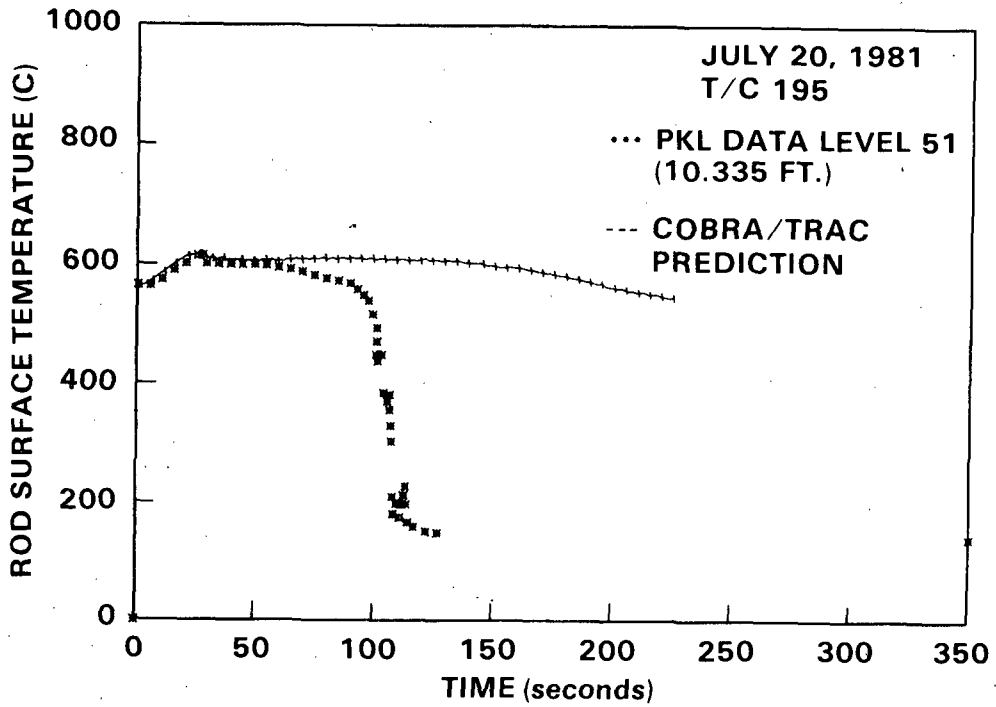


FIGURE 2.9-14. Rod Surface Temperature at Level 51

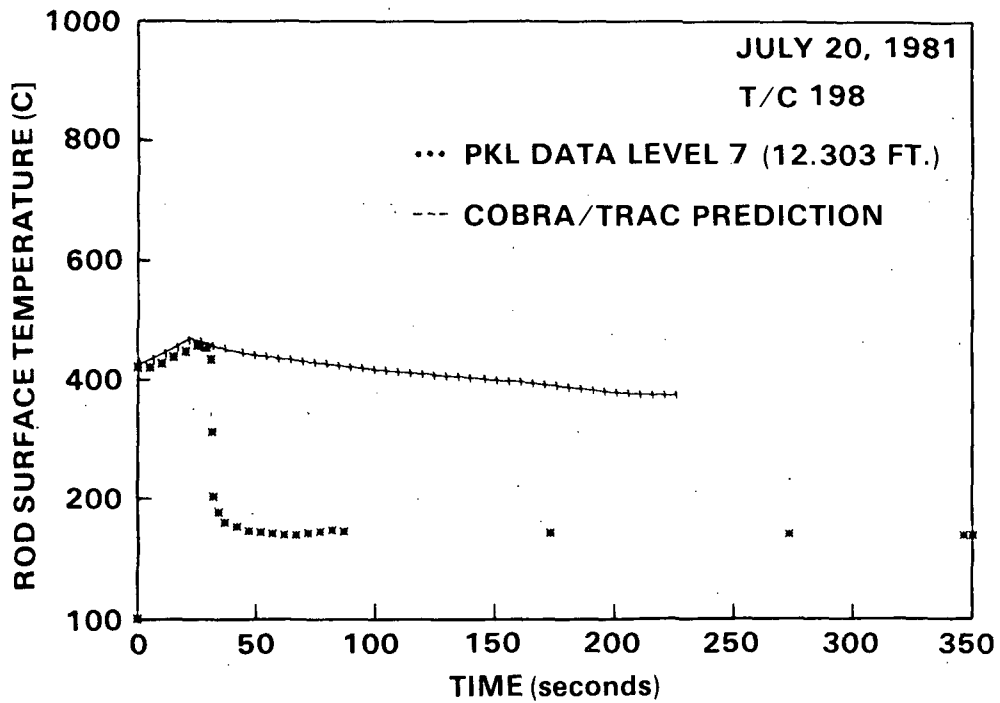
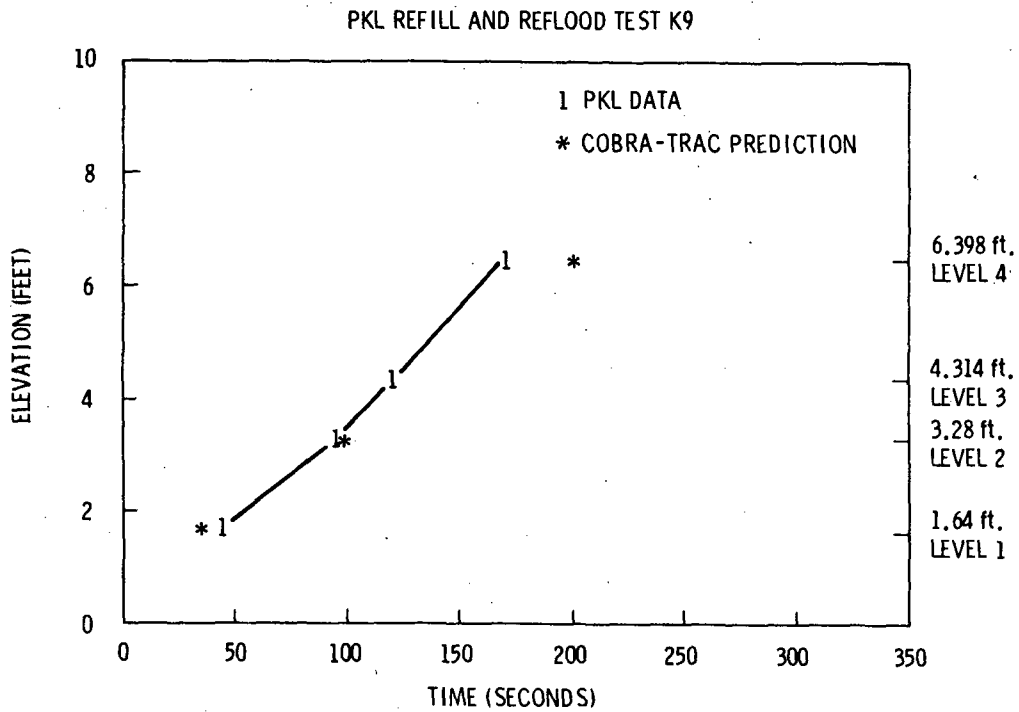
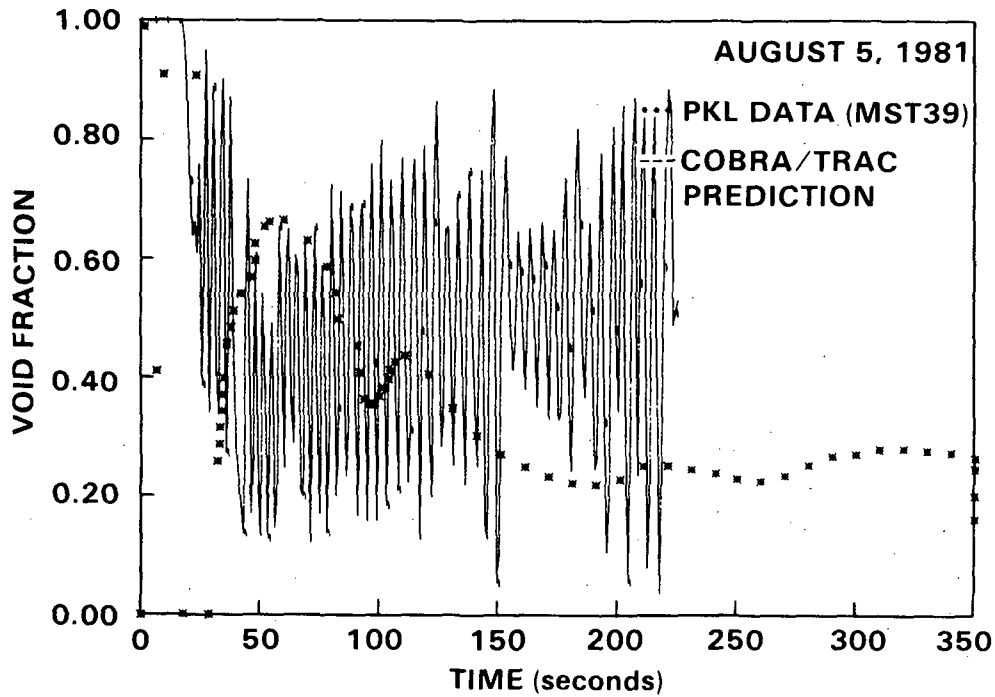


FIGURE 2.9-15. Rod Surface Temperature at Level 7



**FIGURE 2.9-16.** Quench Front Envelope



**FIGURE 2.9-17.** Void Fraction in the Core, (Channel 3, Nodes 3-5)

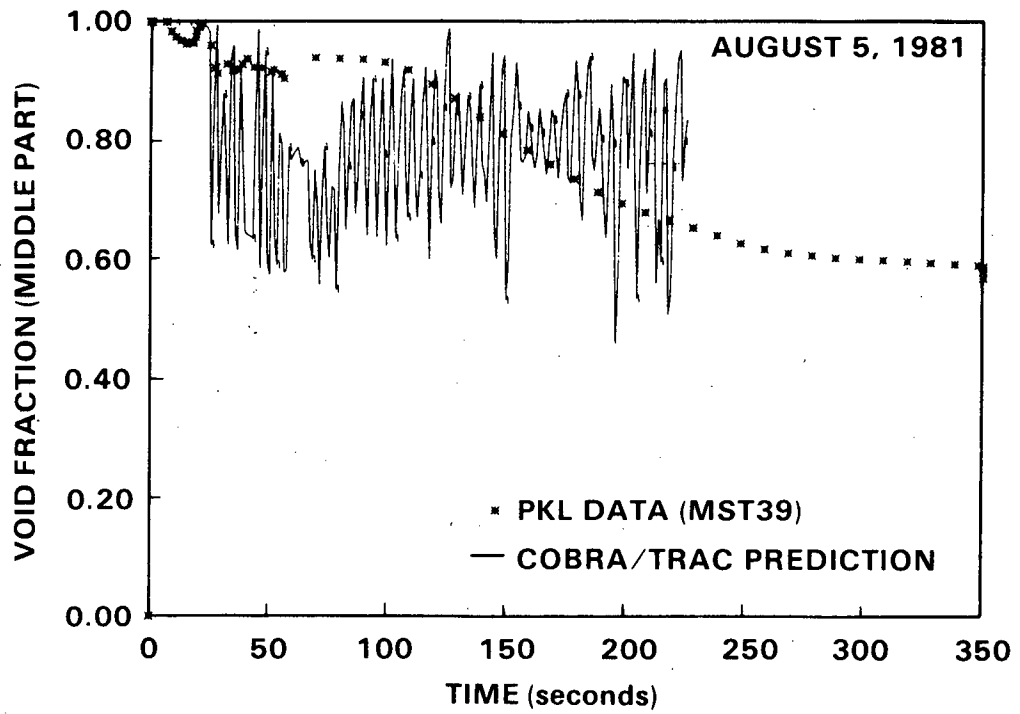


FIGURE 2.9-18. Void Fraction in the Core, (Channels 3-4, Node 5-9,2)

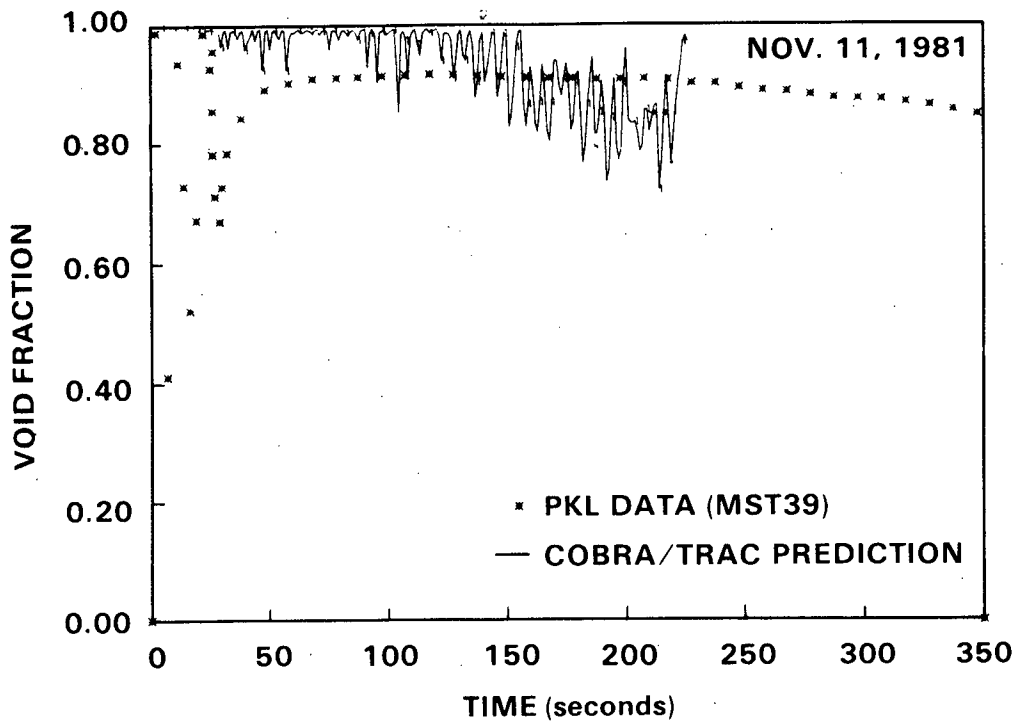


FIGURE 2.9-19. Void Fraction in the Core

## 2.10 CYLINDRICAL CORE TEST FACILITY GRAVITY REFLOOD EXPERIMENT C1-2

A COBRA/TRAC simulation of a gravity feed reflood experiment conducted in the JAERI cylindrical core test facility (CCTF) (Ref. 21) was made to assess the code's ability to predict gravity feed reflood transients. This simulation tested the code's ability to predict the system transient response and feedback to the thermal-hydraulic behavior of the core during reflood. Steam binding caused by steam flow through the hot legs, steam generators and pumps occurred in the test and was modeled in COBRA/TRAC. The effects of evaporation of drops carried over from the core into the steam generators, de-entrainment of liquid drops in the upper plenum, downcomer filling behavior and transient carryover and reflood in the core were also modeled.

### 2.10.1 Description of Experiment

The large-scale experiment CCTF test C1-2 (Run 011) was chosen for this simulation. The CCTF was designed to model a full-height core section and the intact and broken loops of a PWR. The facility contained a nonnuclear core of 2000 electrically heated fuel rod simulators arranged in a rectangular array and placed within a cylindrical vessel. The test vessel included a downcomer, lower plenum, core region and upper plenum with associated internals. The intact loop represented the three intact loops of a PWR and included a steam generator and pump simulator with associated piping. The broken loop also contained a steam generator and pump simulator. The test was initiated by turning on the power to the core with the vessel filled with steam except for 0.86 m of saturated water in the lower plenum. The rods heated up virtually adiabatically in the core's steam environment. Fifty-three seconds after power was applied to the fuel rod simulators, accumulator injection into the lower plenum was initiated. When the liquid level reached the bottom of the core at 69 sec, the accumulator injection was switched to the cold leg for the remainder of the transient. The core power decay was initiated at 67 sec. At 78 sec, accumulator injection ended and low pressure coolant injection (LPCI) was initiated. All heater rods were quenched by 588 sec.

A schematic of the CCTF system is shown in Figure 2.10-1. The scaled dimensions for the various components of the system are provided in Table 2.8. The CCTF dimensions are compared to the dimensions of a PWR to

2.106

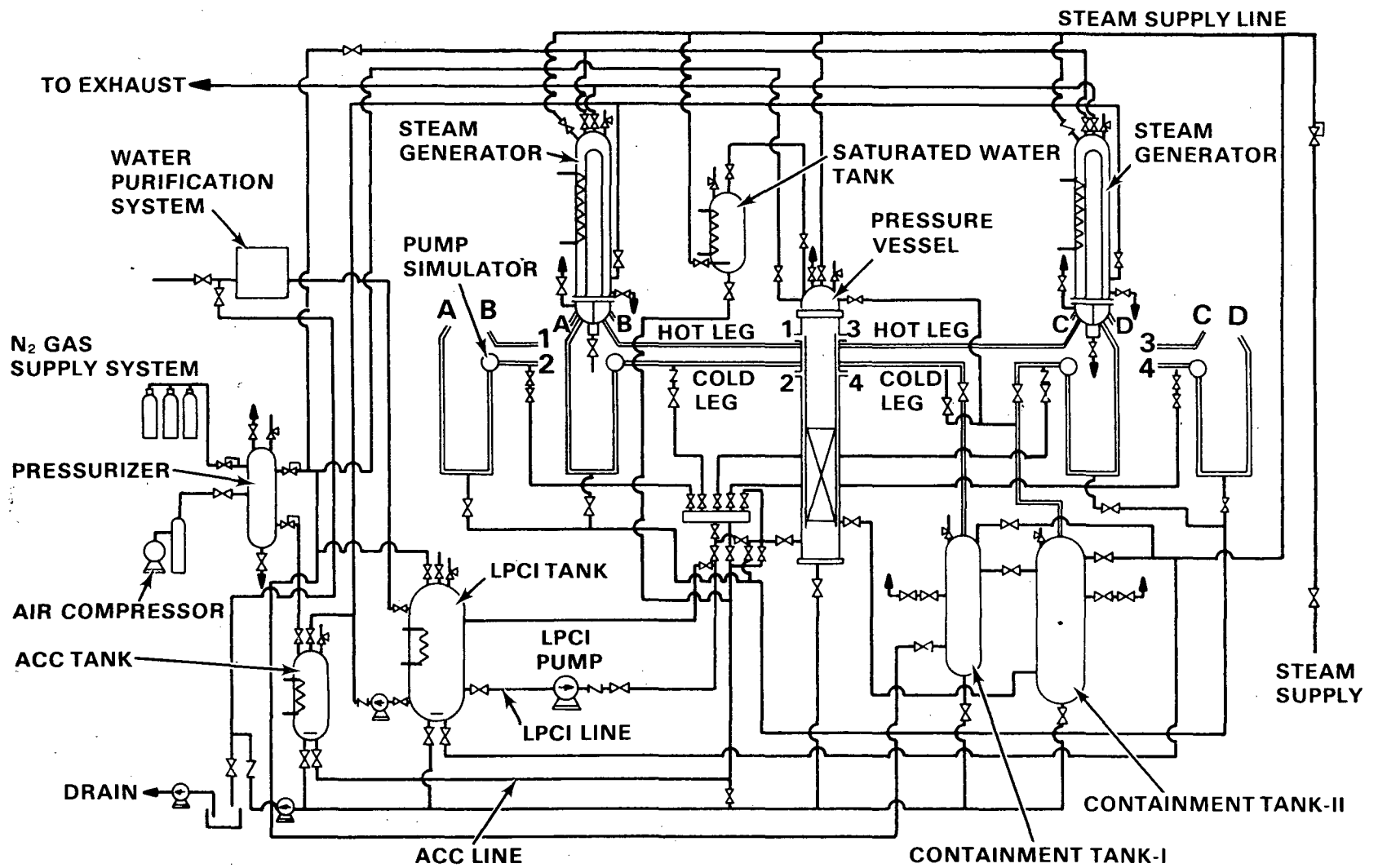


FIGURE 2.10-1. Schematic of Cylindrical Core Test Facility

TABLE 2.8. Component Dimensions of Cylindrical Core Test Facility

COMPONENT		PWR	JAERI	RATIO
PRESSURE VESSEL				
Vessel Inside Diameter	(mm)	4394	1084	
Vessel Thickness	(mm)	216	90	
Core Barrel Outside Diameter	(mm)	3874	961	
	(mm)	3760	929	
Thermal Shield Outside Diameter	(mm)	4170		
Thermal Shield Inside Diameter	(mm)	4030		
Downcomer Length	(mm)	6066	6066	1/1
Downcomer Gap	(mm)	114.3	61.5	
Downcomer Flow Area	(m <sup>2</sup> )	4.23	0.197	1/21.44
Lower Plenum Volume	(m <sup>3</sup> )	29.6	1.38	1/21.44
Upper Plenum Volume	(m <sup>3</sup> )	43.6	2.04	1/21.44
FUEL (HEATER ROD) ASSEMBLY				
Number of Bundles	(--)	193	32	
Rod Array	(--)	15 x 15	8 x 8	
Rod Heater Length	(mm)	3660	3660	1/1
Rod Pitch	(mm)	14.3	14.3	1/1
Fuel Rod Outside Diameter	(mm)	10.72	10.7	1/1
Thimble Tube Diameter	(mm)	13.87	13.8	1/1
Instrument Tube Diameter	(mm)	13.87	13.8	1/1
Number of Heater Rods	(--)	39372	1824	1/21.58
Number of Nonheating Rods	(--)	4053	224	1/18.09
Core Flow Area	(m <sup>2</sup> )	5.29	0.25	1/21.2
Core Fluid Volume	(m <sup>3</sup> )	7.95	0.813	1/21.2
PRIMARY LOOP				
Hot Leg Inside Diameter	(mm)	736.6	155.2	1/4.75
Hot Leg Flow Area	(m <sup>2</sup> )	0.426	0.019	1/22.54
Hot Leg Length	(mm)	3940	3940	1/1
Pump Suction Inside Diameter	(mm)	787.4	155.2	1/5.07
Pump Suction Flow Area	(m <sup>2</sup> )	0.487	0.019	1/25.77
Pump Suction Flow Length	(mm)	7950	7950	1/1

give an idea of the modeling scale. The dimensions for the vessel are shown in Figure 2.10-2. The configuration of the rods in the core are shown in Figure 2.10-3. The core is divided into the three main power zones: low, intermediate and high. The lower power zone consists of zones M2 through M4 shown in Figure 2.10-3. The intermediate power zone consists of zones M6 through M9, and M5 is the high power zone. The axial power profile is shown in Figure 2.10-4 along with the locations of rod thermocouples. The test conditions are summarized in Table 2.9.

### 2.10.2 COBRA/TRAC Model Description

A diagram of the COBRA/TRAC model of CCTF is shown in Figure 2.10-5. The system was modeled with appropriate one-dimensional components for the intact and broken loops, including steam generators.

The CCTF vessel was modeled using a one-dimensional representation of the core, lower plenum, downcomer and upper plenum. A diagram of the vessel model is shown in Figure 2.10-6. The flow paths through orifices, support columns and guide tubes in the upper plenum were also modeled. Twelve 1-ft long nodes were used in the core and downcomer. The heater rods were modeled using a single average rod heat transfer model. The thermal capacitance of the vessel and core barrel wall were modeled with heat slabs to obtain the effects of hot walls on downcomer penetration. The pump flow resistances were modeled by specifying a constant loss coefficient at the appropriate locations in the loop piping. ECC water injection was modeled using fill components in the cold leg piping. The containment was modeled by specifying a constant pressure at the end of the broken cold leg and hot leg piping.

### 2.10.3 Discussion of Results

An oscillatory reflood behavior was computed throughout the test. The period of the oscillation was on the order of 2 sec. The amplitude of the oscillation was largest at the initiation of reflood and diminished as the transient proceeded.

Comparisons between predictions and the experimental data are shown in Figures 2.10-7 through 2.10-19. Figures 2.10-7 through 2.10-14 show

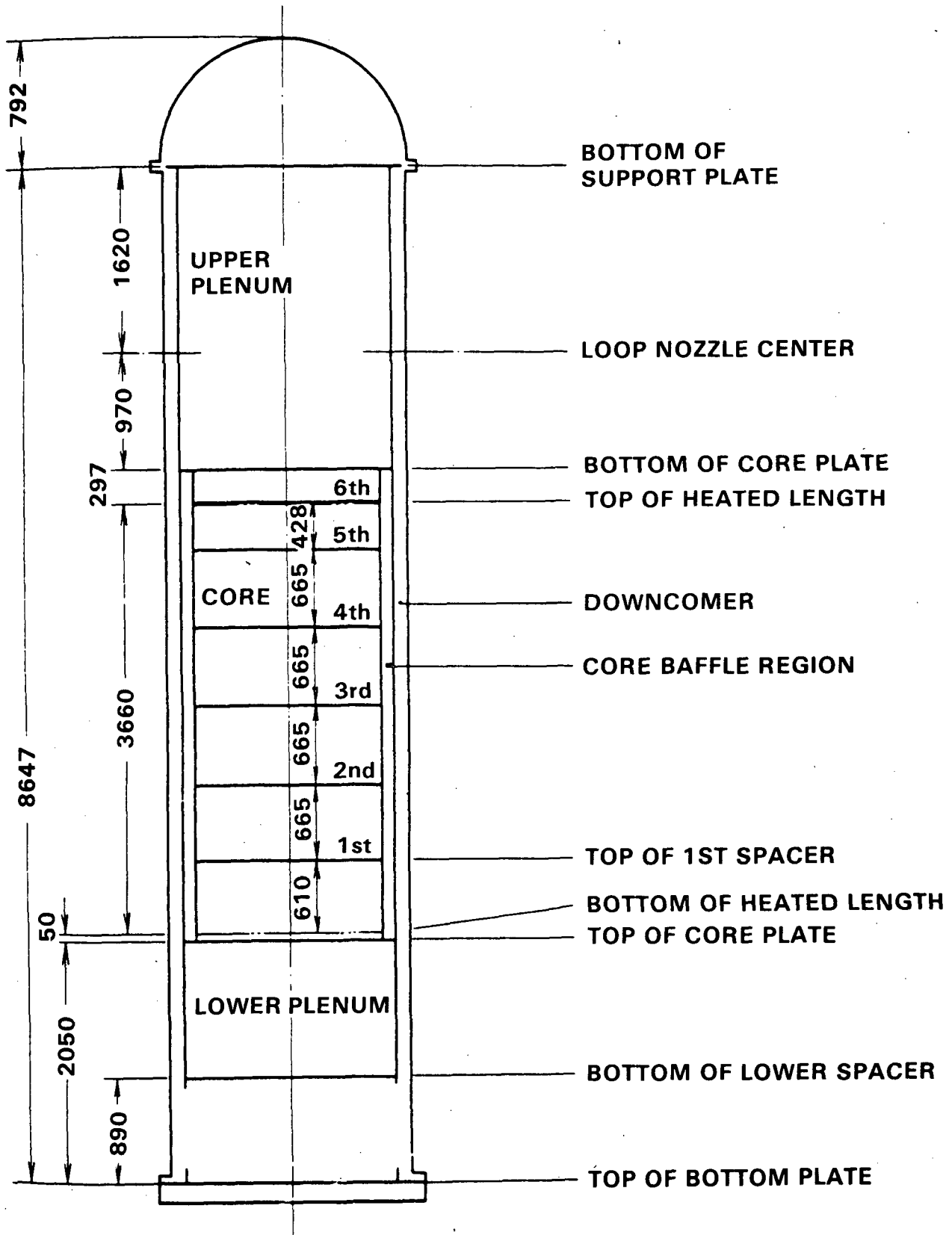


FIGURE 2.10-2. Diagram of CCTF Pressure Vessel

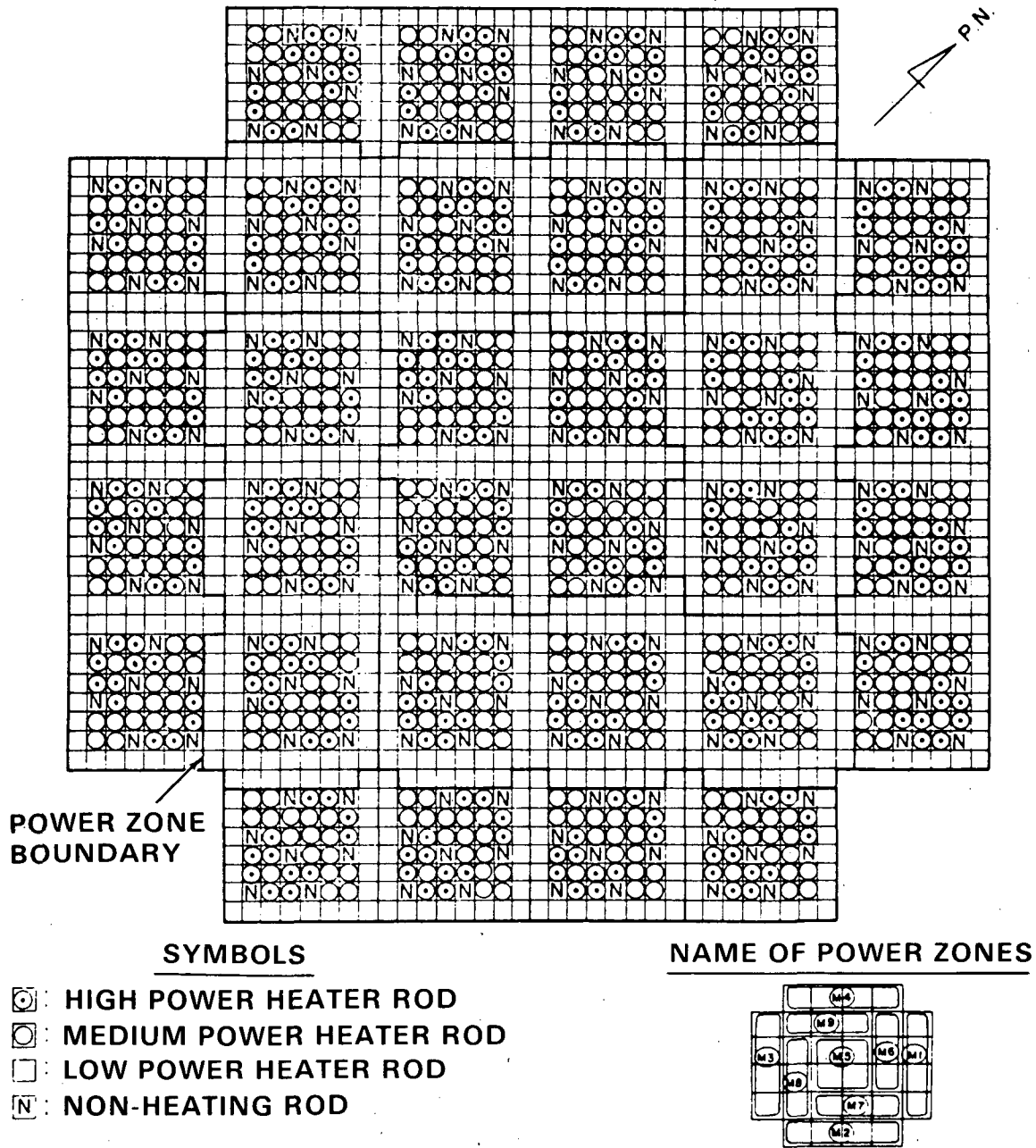


FIGURE 2.10-3. Cross Section of CCTF Core

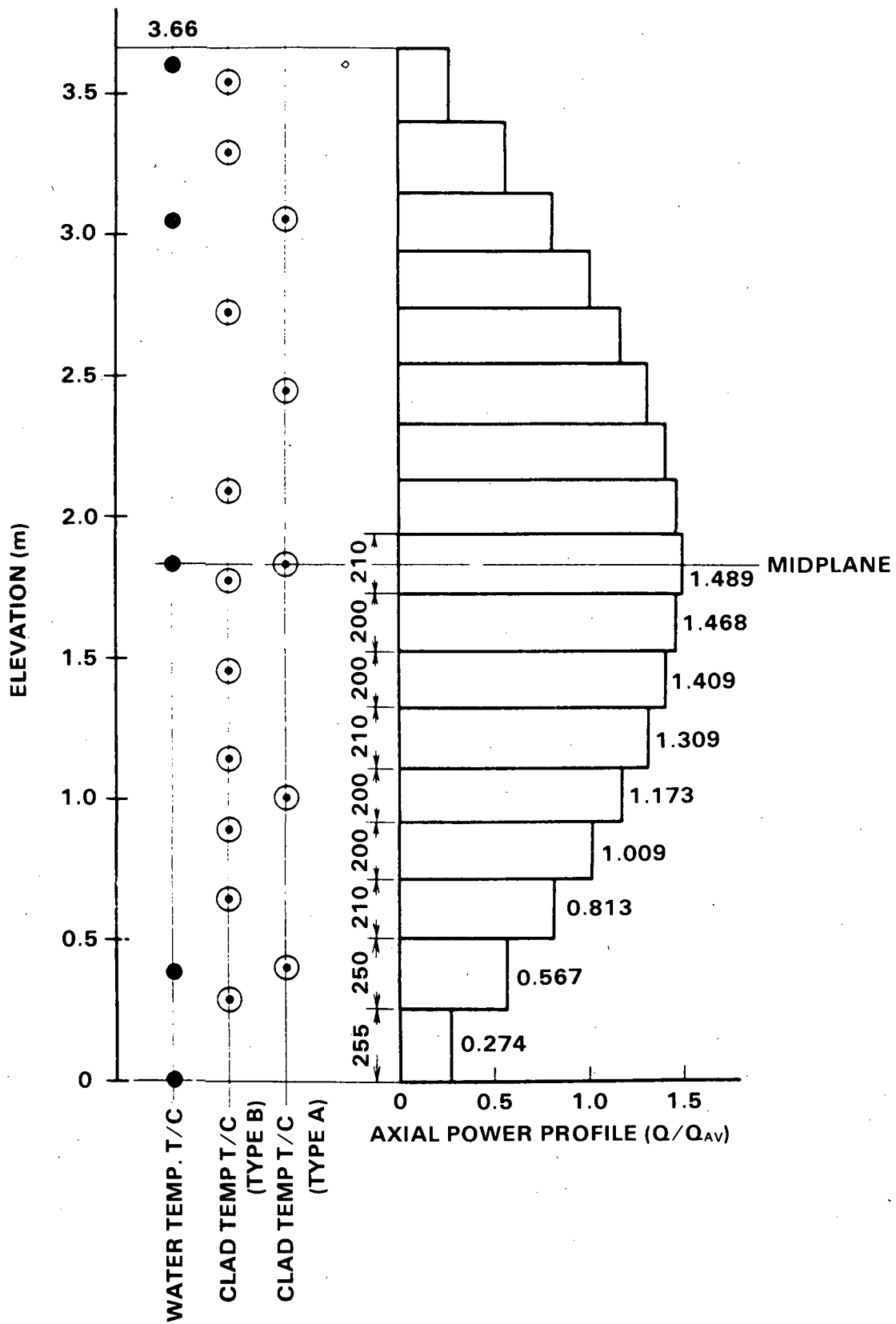


FIGURE 2.10-4. Axial Power Profile and Thermocouple Elevations for Heater Rods in CCTF Core

TABLE 2.9. Summary of Conditions for CCTF Test (1-2)

1. TEST TYPE: TEST C1-2 (CCTF MAIN TEST NO. 20)
2. TEST NUMBER: RUN 011
3. DATE: July 4, 1979
4. POWER: A: TOTAL: 9.36 MW; B: LINEAR: 1.4 KW/M
5. RELATIVE RADIAL POWER SHAPE:  
 A: ZONE: A B C  
 B: RATIO: 1.07 : 1.0 : 0.82
6. AXIAL POWER SHAPE: CHOPPED COSINE
7. PRESSURE (KG/CM<sup>2</sup>a):  
 A: SYSTEM: 2.07\*, B: CONTAINMENT 2.06  
 C: STEAM GENERATOR SECONDARY: 50
8. TEMPERATURE (DEG.C):  
 A: DOWNCOMER WALLS 187, B: VESSEL INTERNALS 120  
 C: PRIMARY PIPING WALLS 118, D: LOWER PLENUM LIQUID 113  
 E: ECC LIQUID 39, F: STEAM GENERATOR SECONDARY 263  
 G: CORE TEMPERATURE AT ECC INITIATION 506
9. ECC INJECTION TYPE: C  
 A: COLD LEG, B: LOWER PLENUM, C: LOWER PLENUM + COLD LEG
10. PUMP K-FACTOR: ~15 (UNCERTAIN)
11. ECC FLOW RATFS AND DURATION:  
 A: ACCUMULATOR 264 M<sup>3</sup>/HR FROM 0 TO 25 SECONDS  
 B: LPCI 30.9 M<sup>3</sup>/HR FROM 25 TO 674 SECONDS  
 C: ECC INJECTION TO LOWER PLENUM: FROM 0 TO 16 SECONDS  
 (VALVE OPENING AND CLOSING TIMES ARE INCLUDED IN THE INJECTION DURATION)
12. INITIAL WATER LEVEL IN LOWER PLENUM: 0.86 M.
13. POWER CONTROL: ANS x 1.2 + ACTINIDE (30 SEC AFTER SCRAM)
14. EXPECTED BOCREC TIME FROM ECC INITIATION 12 SEC
15. EXPECTED PEAK TEMPERATURE AT BOCREC 600 C

\* Since system pressure drops below containment pressure in initial stages of ECC injection, condensation in the vessel was set to zero when this occurred to simulate air intake from containment.

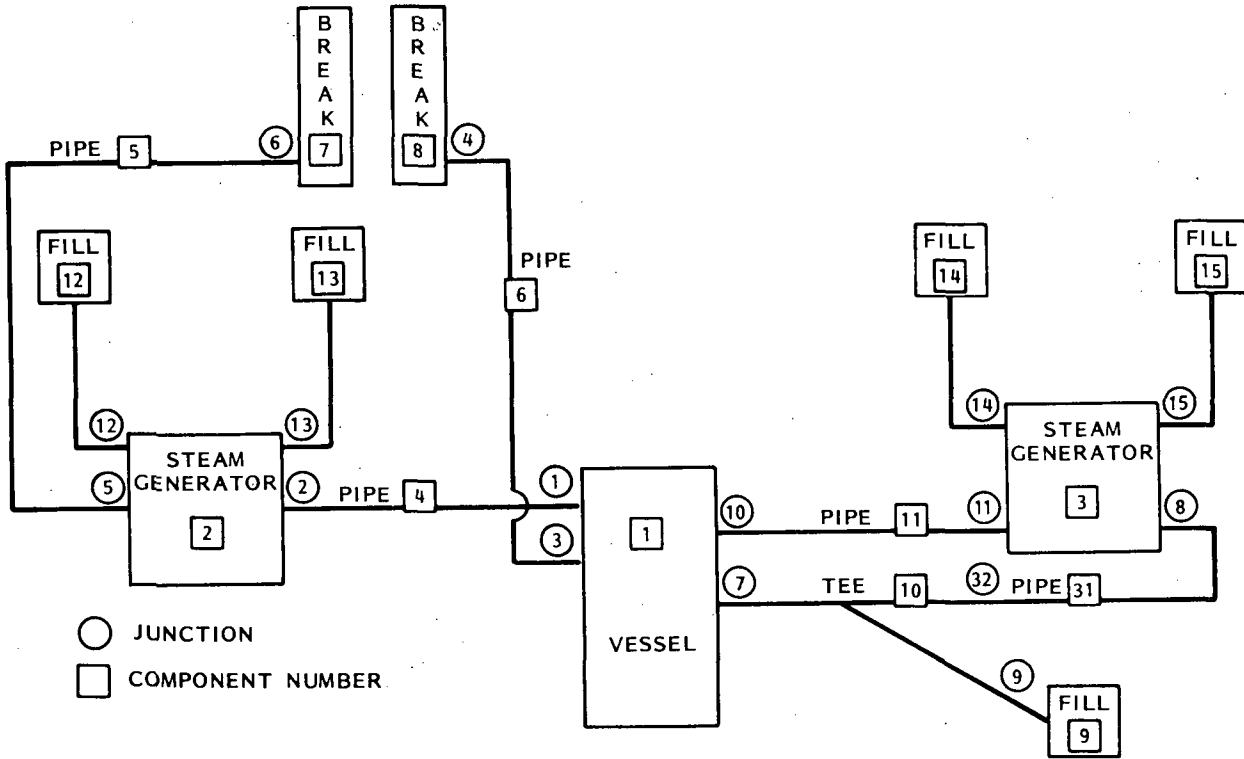
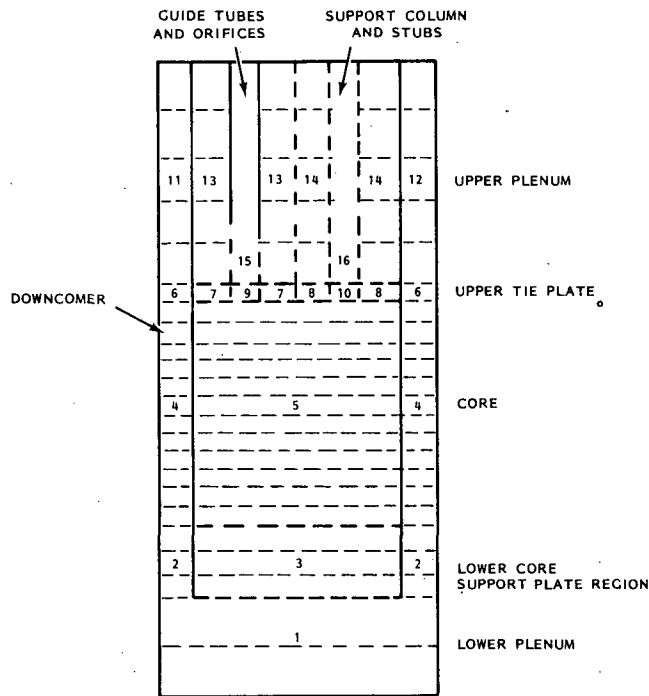


FIGURE 2.10-5. Schematic of COBRA/TRAC Model of CCTF



1 CHANNEL NUMBERS

FIGURE 2.10-6. Vessel Mesh for CCTF

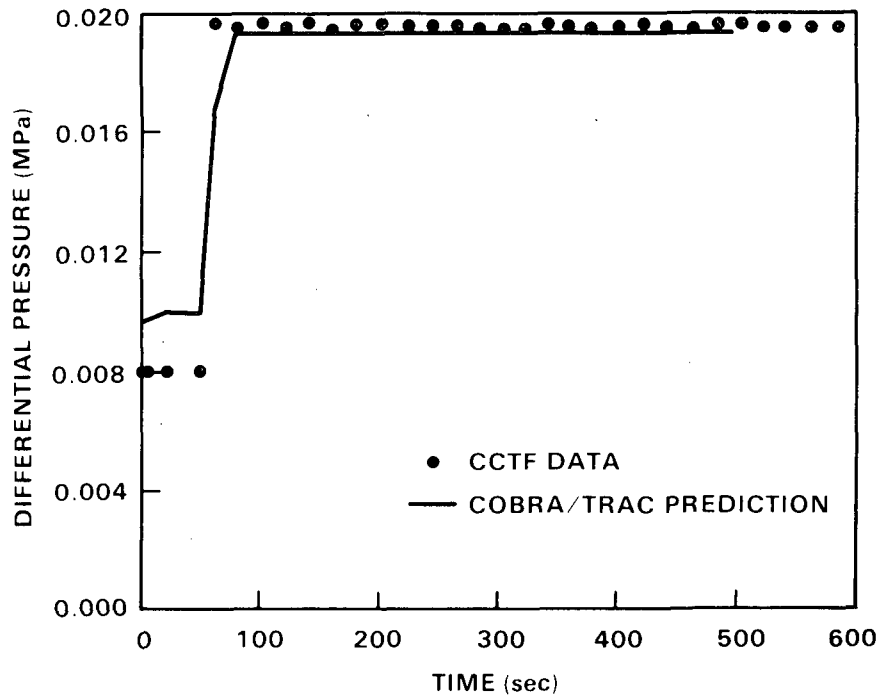


FIGURE 2.10-7. Differential Pressure in the Lower Plenum

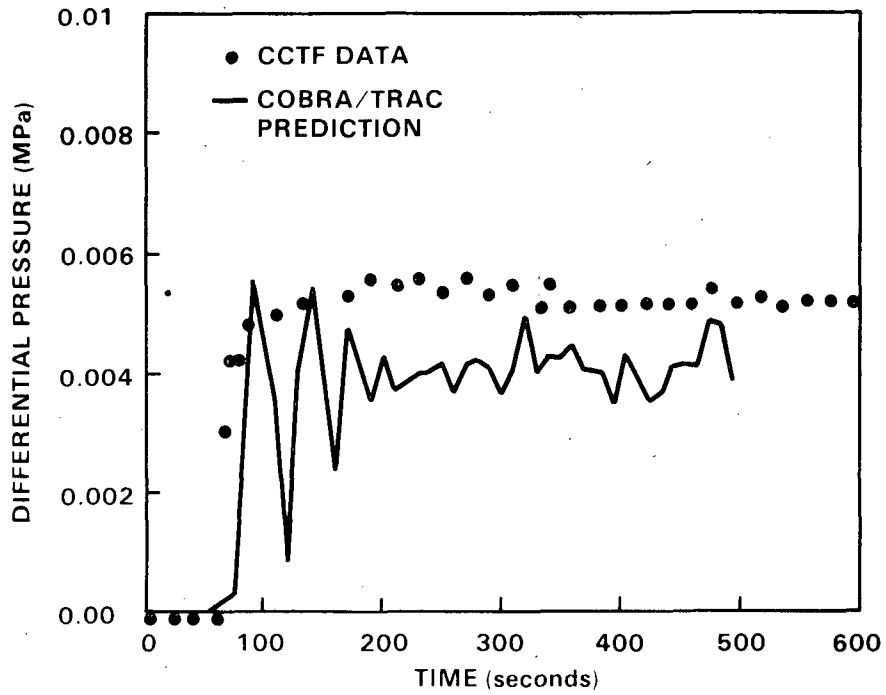


FIGURE 2.10-8. Differential Pressure Between the 0 and 2-ft Elevations in the Core

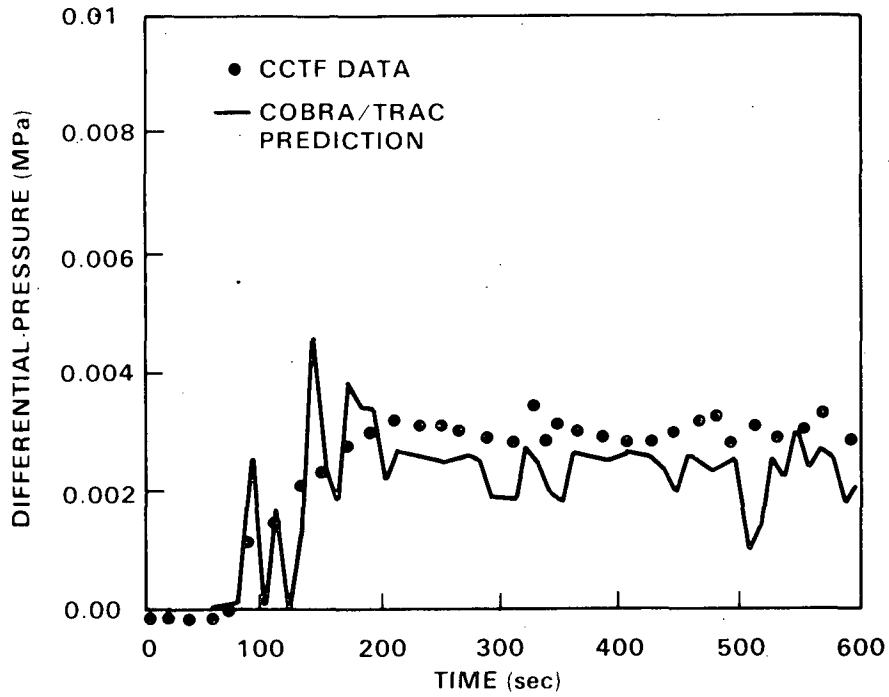


FIGURE 2.10-9. Differential Pressure Between 2 and 4-ft Elevations in the Core

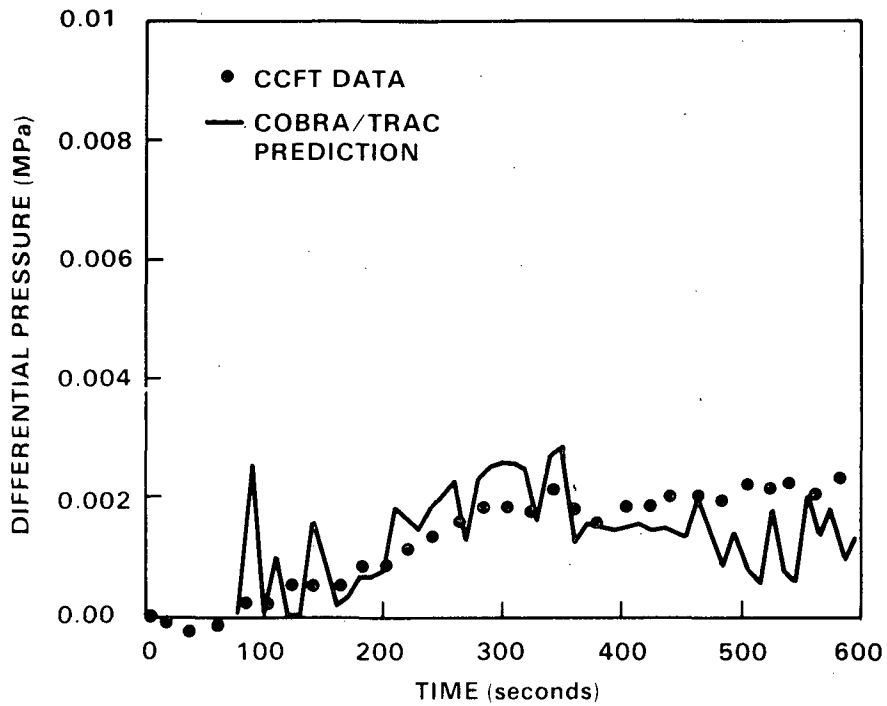


FIGURE 2.10-10. Differential Pressure Between the 4 and 6-ft Elevations in the Core

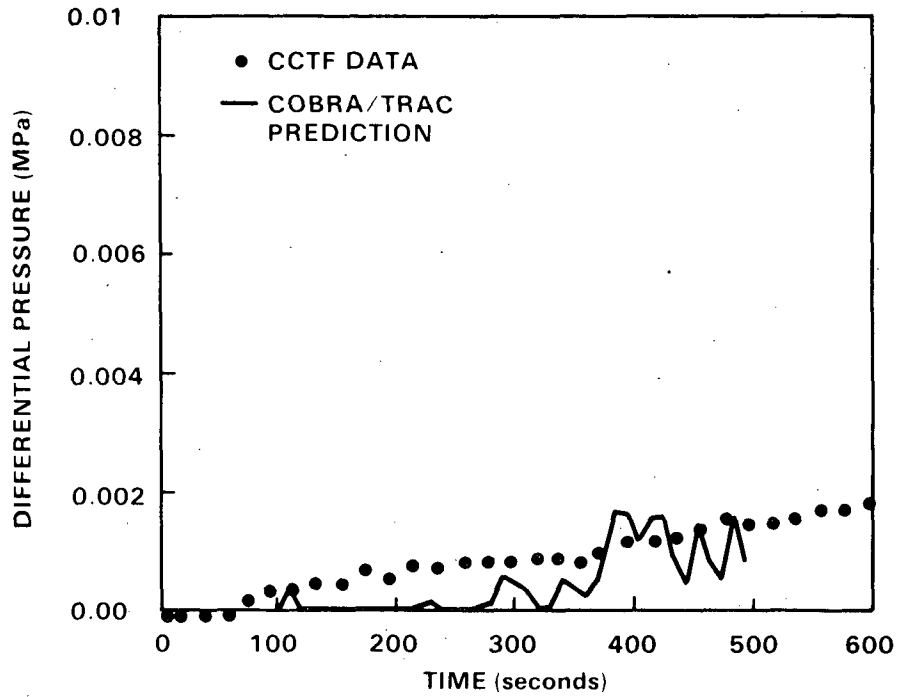


FIGURE 2.10-11. Differential Pressure Between 6 and 8-ft Elevations in the Core

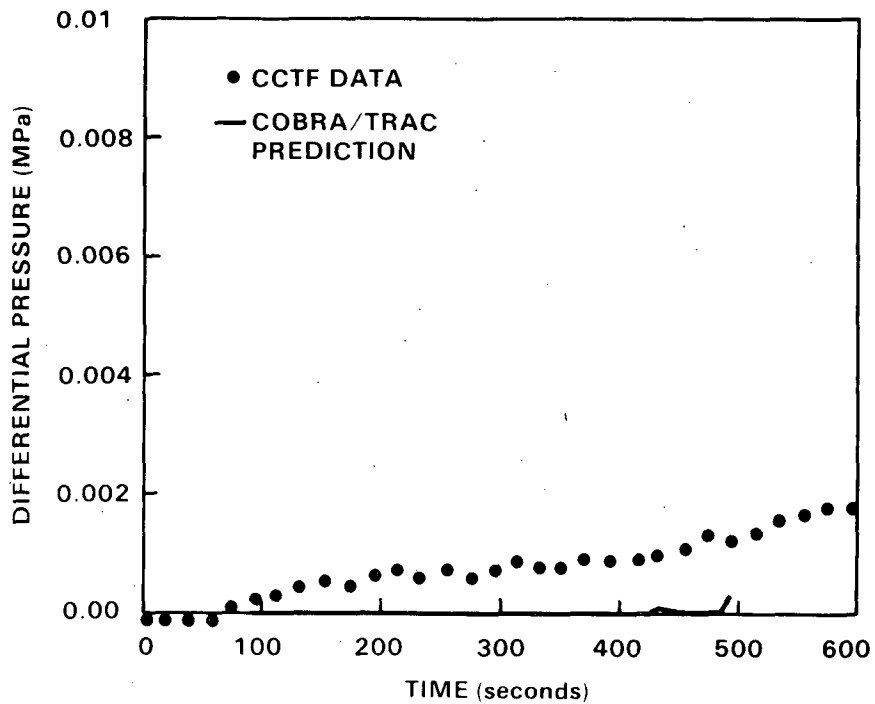


FIGURE 2.10-12. Differential Pressure Between the 8 and 10-ft Elevations in the Core

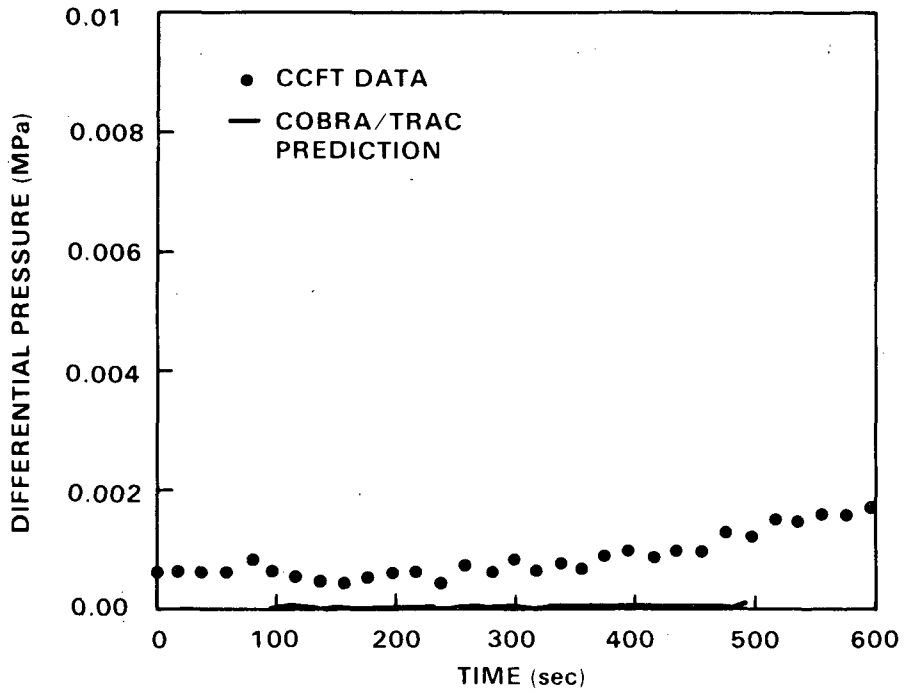


FIGURE 2.10-13. Differential Pressure Between 10 and 12-ft Elevations in the Core

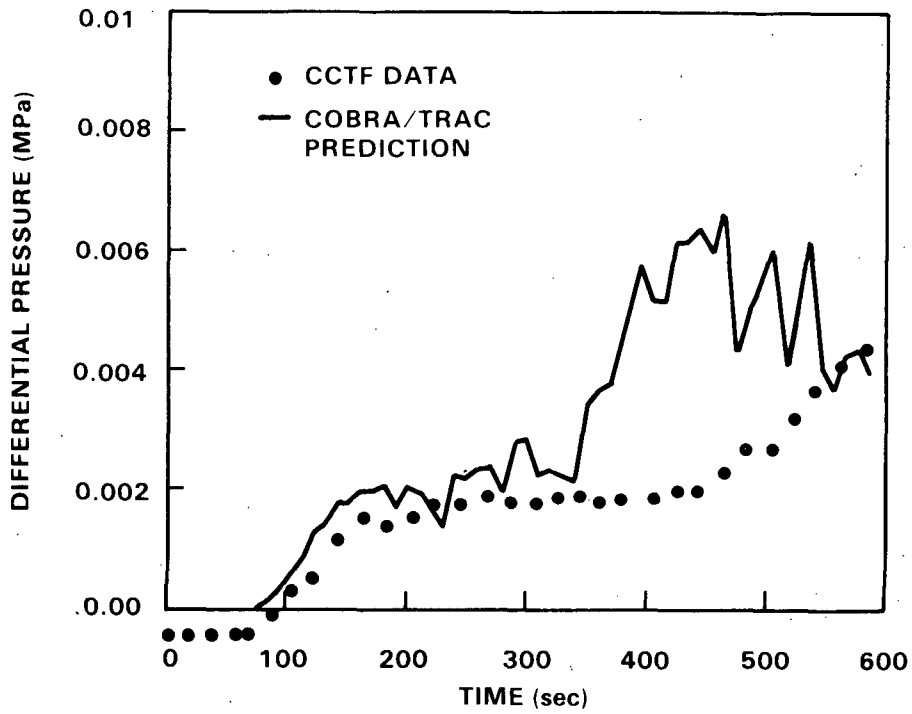


FIGURE 2.10-14. Differential Pressure in the Upper Plenum

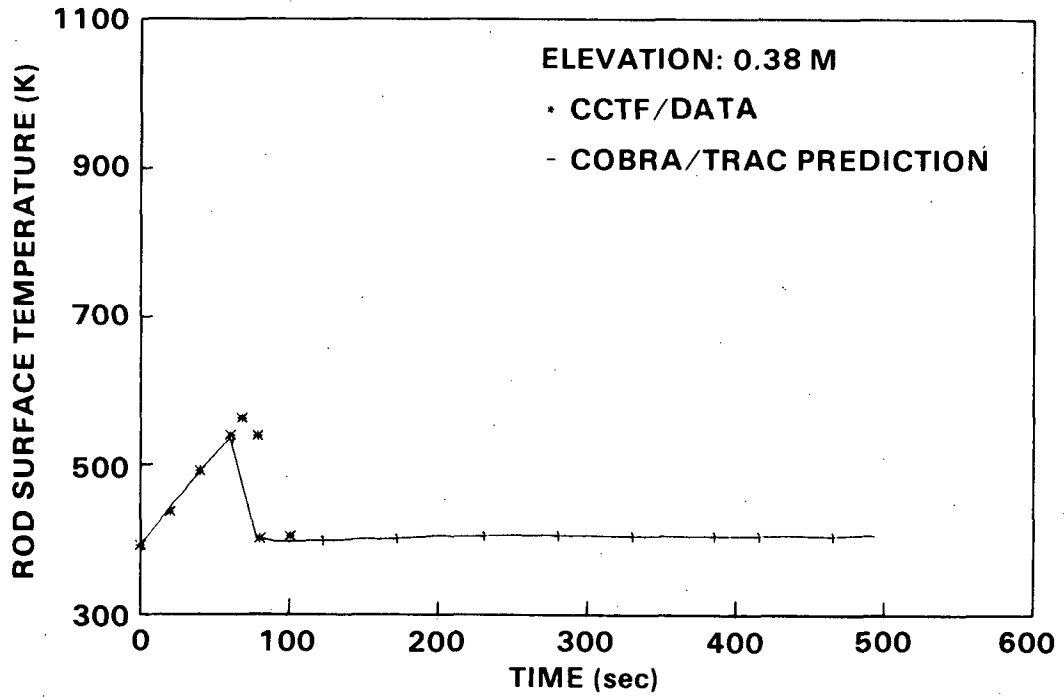


FIGURE 2.10-15. Temperature at 0.38 m Elevation

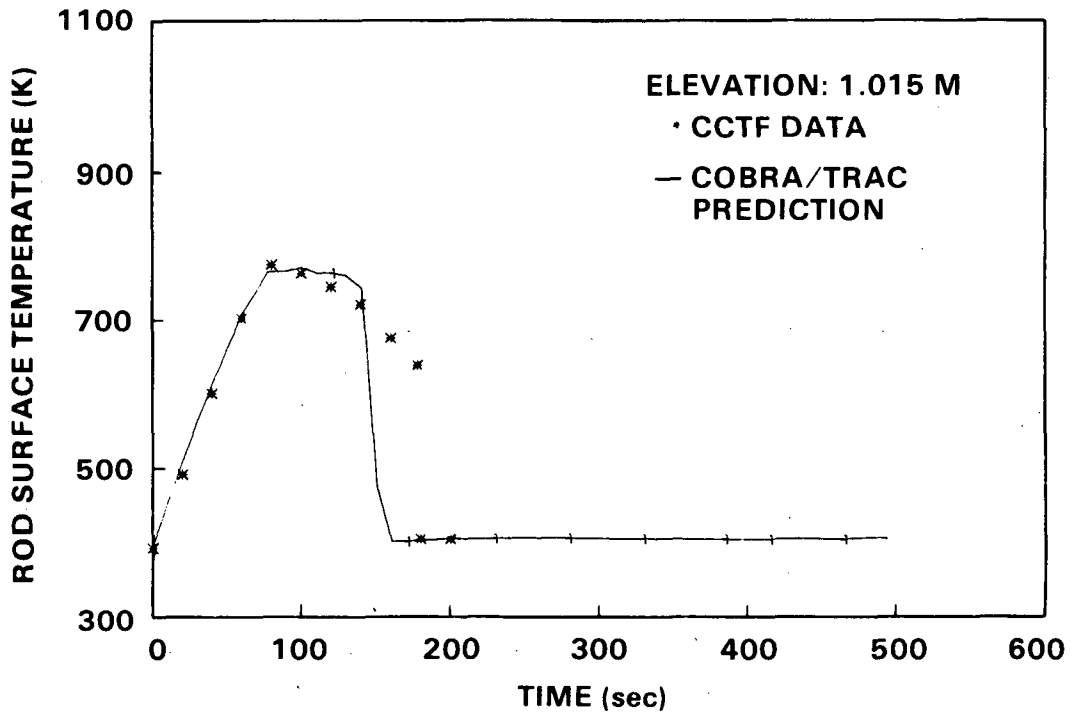


FIGURE 2.10-16. Temperature at 1.015 m Elevation

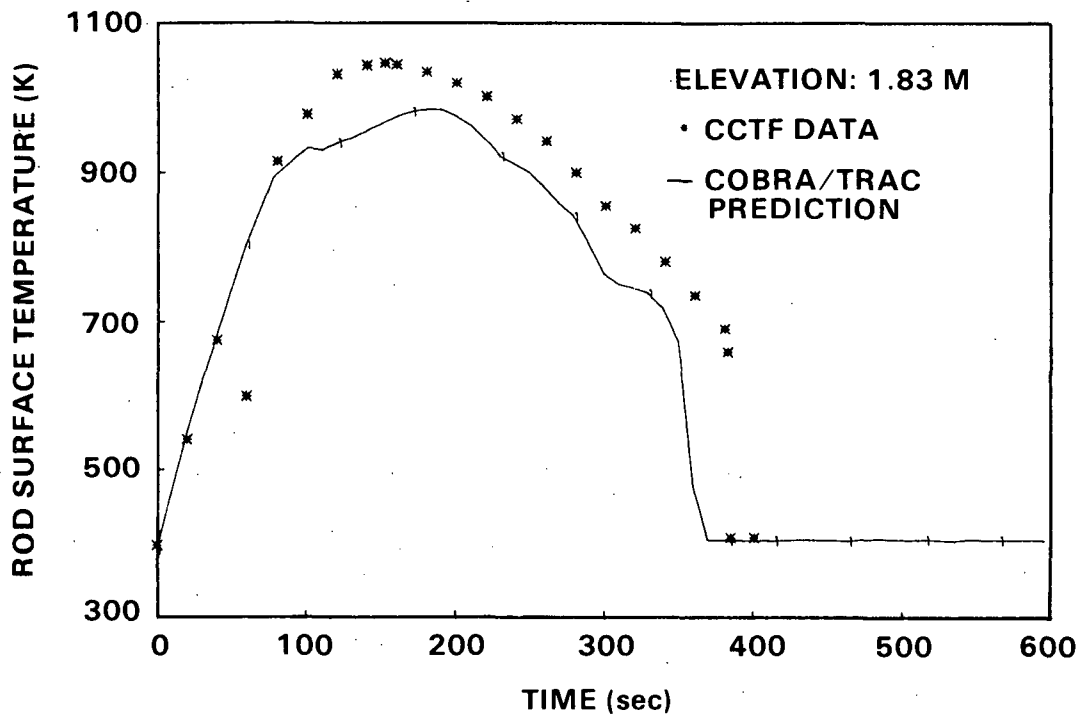


FIGURE 2.10-17. Temperature at 1.83 m Elevation

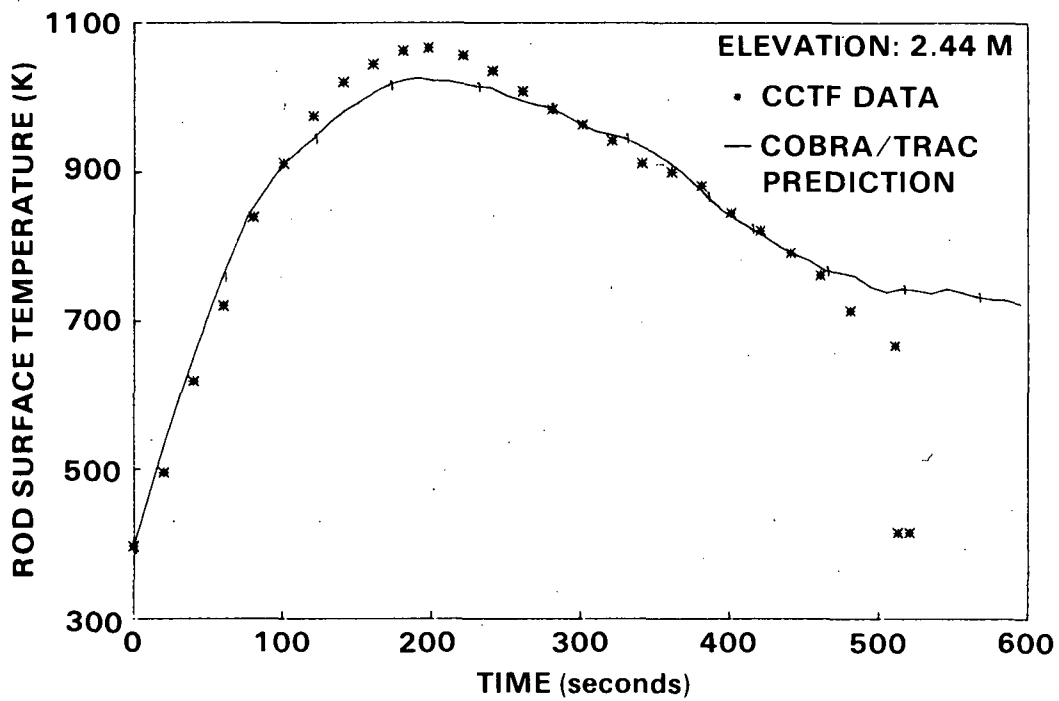


FIGURE 2.10-18. Temperature at 2.44 m Elevation

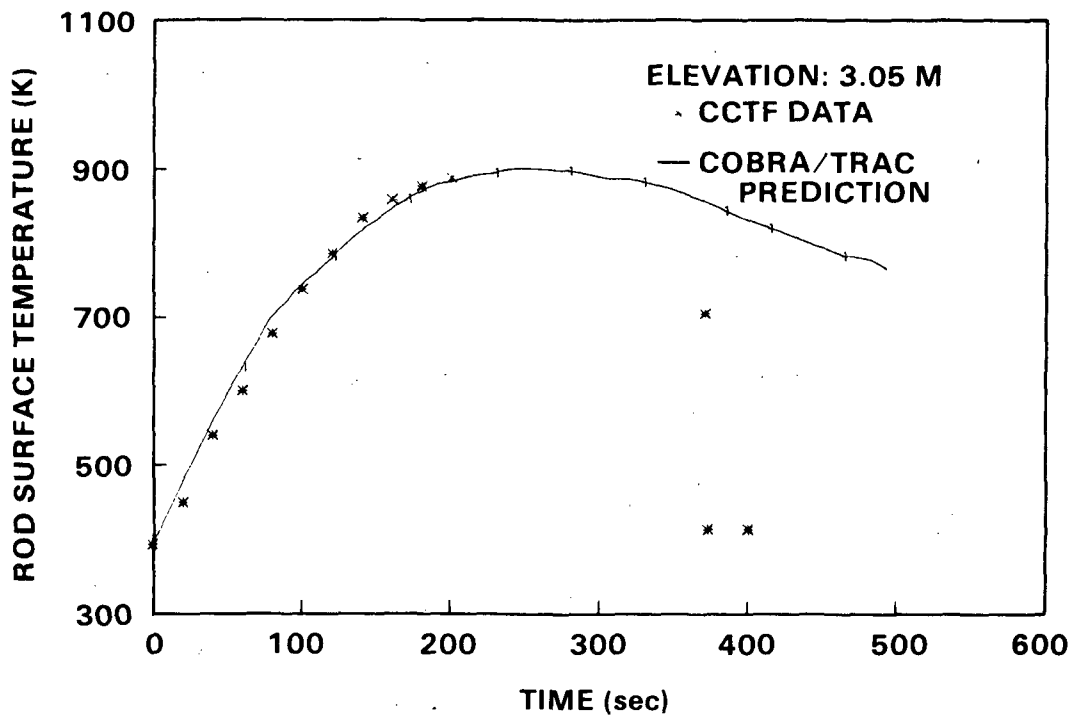


FIGURE 2.10-19. Temperature at 3.05 m Elevation

comparisons of predicted differential pressures in the lower plenum, core and upper plenum. (Comparisons with downcomer differential pressures are not shown. These data were used to obtain a corrected ECC injection rate since discussion with other investigators indicated that the reported values may be in error. The temperature of the injected water was also uncertain since there appears to have been segments of piping filled with saturated water between the ECC water supply and the simulated reactor vessel. This caused a significant period of saturated water injection into the vessel before subcooled water actually reached it. The fill rates and temperatures were corrected to account for these uncertainties. The flows were corrected based on the downcomer filling rate, so any comparison between the code predictions of the downcomer liquid level ( $\Delta P$ ) and the measured data would be, of necessity, very good.)

Differential pressures for the lower plenum are shown in Figure 2.10-7. The prediction is slightly higher than the data due to the difference in location between the pressure taps and computational mesh cell centers. Otherwise, the comparison is very good and indicates that the lower plenum filled at the right time and at about the right rate.

Comparisons of differential pressures (void fractions) in the core are shown in Figures 2.10-8 through 2.10-13. The comparisons below 6 ft are all good, indicating that the interfacial shear and vapor generation models are predicting about the right void fraction in the core. The computed liquid level is much more oscillatory than the data indicates. The oscillation has a period of about 2 sec. The plotting interval used to generate Figure 2.10-8 was too large (10 sec) to show the correct period for the oscillation, but the general magnitude is about right. Very large oscillations occur shortly after water first enters the core. The magnitude diminishes later on in the transient. It is uncertain whether oscillations of such magnitude actually occurred in the test and the measurement system was not able to detect them, or if heat transfer or flow regime transitions in COBRA/TRAC are responsible for generating them. It is likely that the answer is somewhere in between. Work is in progress to understand exactly what the driving mechanism for the oscillations are, to see if they are physical or numerical.

The differential pressure in the top portions of the core indicate that COBRA/TRAC may be under-predicting the liquid content of the flow in the core. The differential pressures for the upper plenum are shown in Figure 2.10-14. The liquid level in the upper plenum is well predicted out to about 320 sec. At that point a sudden increase in the differential pressure is predicted that is not seen in the data. Part of this increase is caused by the liquid level reaching and submerging the hot leg outlets. The remainder is caused by excessive carryover from the core. This comparison indicates that the liquid carryover and de-entrainment in the upper plenum were correctly predicted during the first 320 sec of the transient.

Heater rod surface temperature comparisons are shown for five elevations in the core in Figures 2.10-15 through 2.10-19. Predictions at the four lower elevations are very good both on peak clad temperature and quench time. The peak temperatures are slightly underpredicted at the middle two elevations. This may be the result of excessively large flow oscillations. The peak clad temperature of the highest elevation, shown in Figure 2.10-19, is predicted but the turnaround time is overpredicted and the rod is cooling too slowly. This is probably a result of the underprediction of the liquid content of the flow at this elevation.

## 2.11 NORTHWESTERN UNIVERSITY COUNTERCURRENT FLOW FILM CONDENSATION EXPERIMENT

This simulation analyzed the steam-water countercurrent condensation tests (Ref. 22) in a vertical test section at Northwestern University. The experimental tests investigated the condensation rates for countercurrent flow in a vertical channel approximately 3/20th the size of a nuclear reactor downcomer. The simulations of the Northwestern experiment were initiated to assess the interfacial heat transfer and drag coefficient equations used for countercurrent film flow.

### 2.11.1 Description of Experiment

The major components of the test facility (test section, upper and lower plenums) were designed and constructed of aluminum and transparent polycarbonate. A diagram of the test section and adjoining entrance and exit plenums is shown in Figure 2.11-1. The test section dimensions were 3.81 cm wide, 38.1 cm deep, and 96.5 cm high. The upper plenum consisted of a water inlet plenum designed to form a liquid film on the test section wall and a steam exit plenum. The steam entrance and water exit plenums were incorporated into a lower plenum. The design of the steam entrance plenum assured a uniform flow distribution.

There were six steam flow measurement stations within the test facility. They were located in the inlet and outlet steam feed tubes and at 30.48-cm intervals within the active portion of the test section starting 2.54 cm above the lower plenum connection flange. The steam flow rates were measured using a steam venturi for the measurements outside the test section and with heated pitot tubes within the test section. The water flow rates were measured only at the entrance and exit of the test facility by means of flow meters. The inlet and exit temperatures of both the steam and water were also measured.

The tests were performed from set initial flow conditions at a pressure of 1 atmosphere and with the test section tilted 7 degrees from vertical. The test section was tilted to reduce the effects produced by flow down the edges of the flow channel. Forty-nine tests were run varying the steam flow from 0.074 to 0.084 kg/s, the water flow from 0.80 to 1.78 kg/s, and the

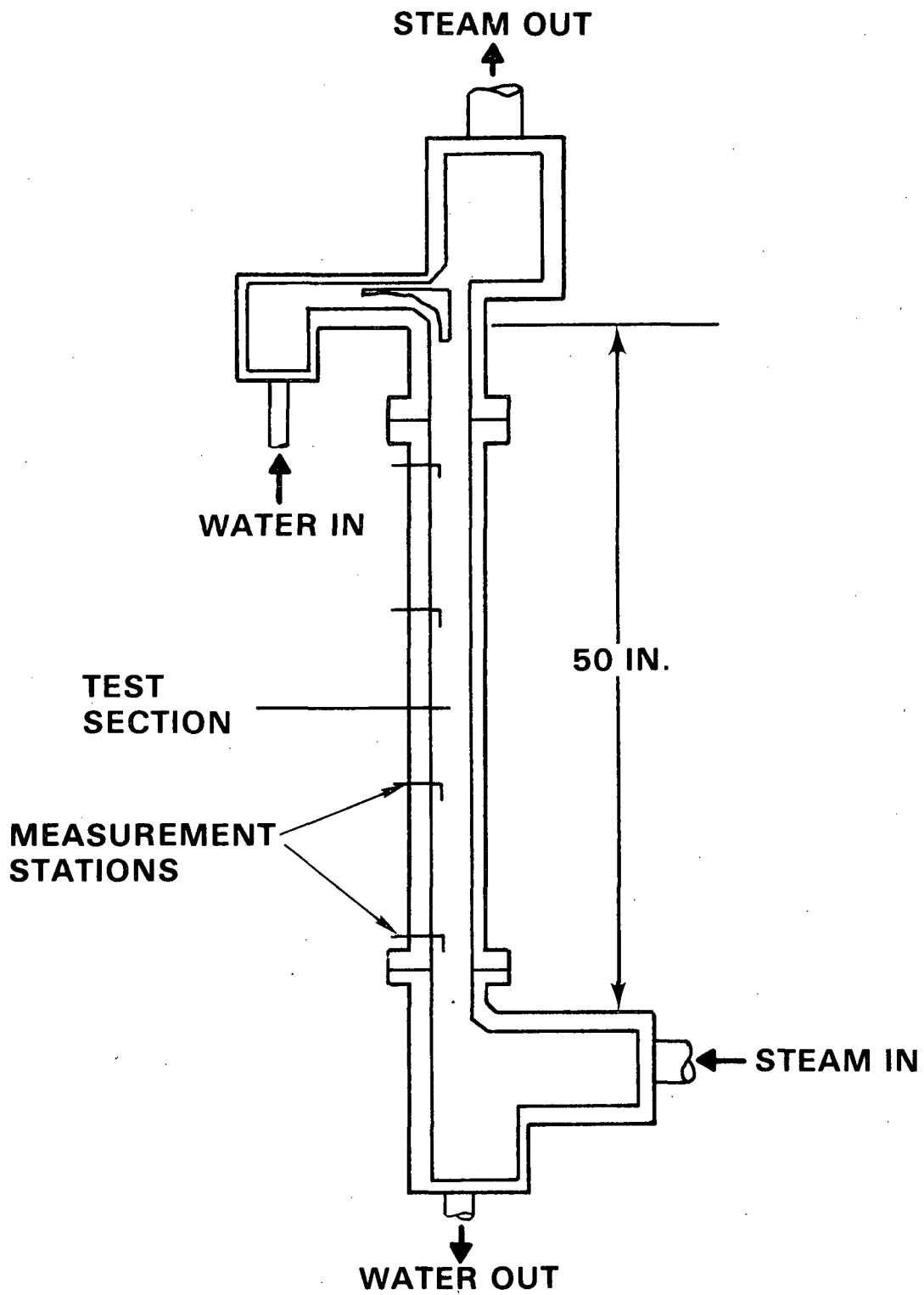


FIGURE 2.11-1. Vertical Test Apparatus for Countercurrent Flow Film Condensation Experiments

temperature of the incoming water from 35 to 71°C. An attempt was made to keep the inlet steam temperature constant throughout the test series but it also varied from 129.9 to 141.6°C.

Prior to each test the test section was preheated with steam flow. After preheating, a steady two-phase flow was established throughout the test section. This was accomplished by adjusting the water flow and temperature to the desired values for a given run and then adjusting the steam flow rate and temperature to their prescribed values. Once a steady-state condition was established, ten 20-sec steam flow data scans were performed over the 3.30 cm steam flow width. Upon completion of the data scans, a computer compiled and calculated the integrated mass flow rate for each pitot tube, the average steam and water temperatures at the entrance and exit locations. The local heat transfer coefficient at the pitot tube locations was also computed from the measured data.

#### 2.11.2 COBRA/TRAC Model Description

Figure 2.11-2 shows a detailed noding diagram for this problem. The system was modeled using 7 components and 6 junctions. The vessel component contained two channels with 3 and 11 fluid nodes in the lower and upper channels. The lower channel was added only as a water accumulation plenum and did not exist on the actual test section. The steam and water were injected by FILLS 1 and 3 into the simulated test section at the appropriate elevations. The steam exited through PIPE 6, which was connected to the top of the second vessel channel. A water flow boundary condition was imposed at the bottom of channel one to drain away the excess water accumulation if necessary. A one-dimensional nodalization was used in this simulation to test the film flow correlations within a mesh cell.

The entire test system, except for the water fill and pipe, was initialized to the inlet steam conditions for experimental test case no. 1. The water and pipe fill were initialized at their respective values. At time zero both the steam and water flow were initiated and the system achieved a steady-state condition after about 2.5 sec. Condensation was set to zero in the three lower channel nodes. This was done because in the actual experiment these water accumulation nodes did not exist.

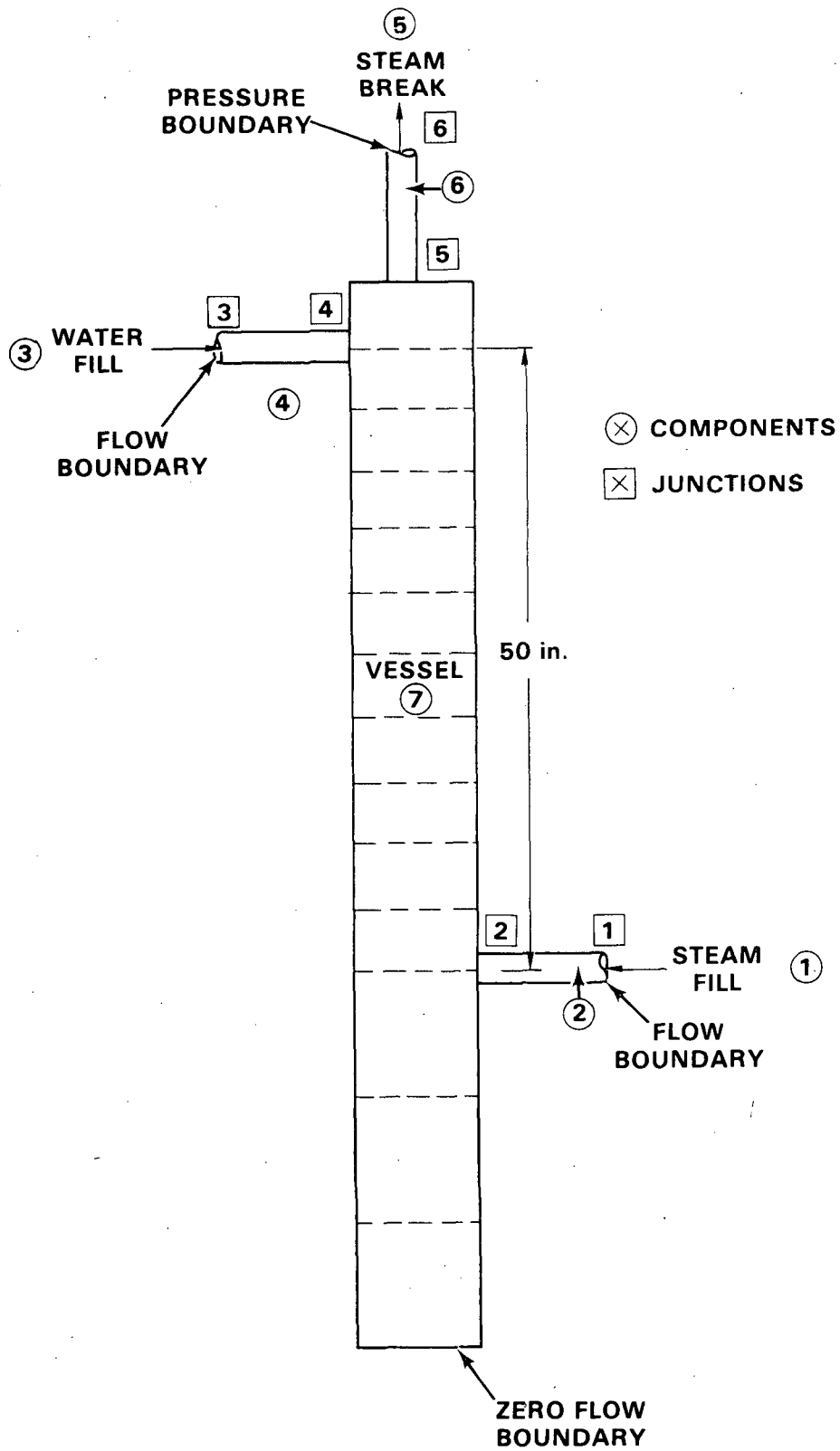


FIGURE 2.11-2. COBRA/TRAC Model for NWU CCFF Condensation Tests

### 2.11.3 Discussion of Results

Figure 2.11-3 shows a comparison of the calculated steam flow and the measured steam flow at various axial locations for test case number 1. The three sets of experimental data are from three tests having the same boundary conditions. Two of the data sets were run on the same day while the third set was performed on a different day. An acceptable comparison is shown between the prediction and the experimental data. A comparison between the predicted exhaust effluences and those reported in the experimental data was made. COBRA/TRAC predicted a steam exit temperature of 234°F instead of the measured 240°F, and a water exit temperature of 204°F instead of the measured 200°F. This difference indicates that COBRA/TRAC is condensing a little too much steam.

It can be concluded that the liquid/vapor interfacial heat transfer coefficient models for film flow are acceptable and can be used for simulations of this type. This simulation was run on cycle 8 of COBRA/TRAC. Since the same interfacial heat transfer correlations are used in the final code version, no major change in the results is expected.

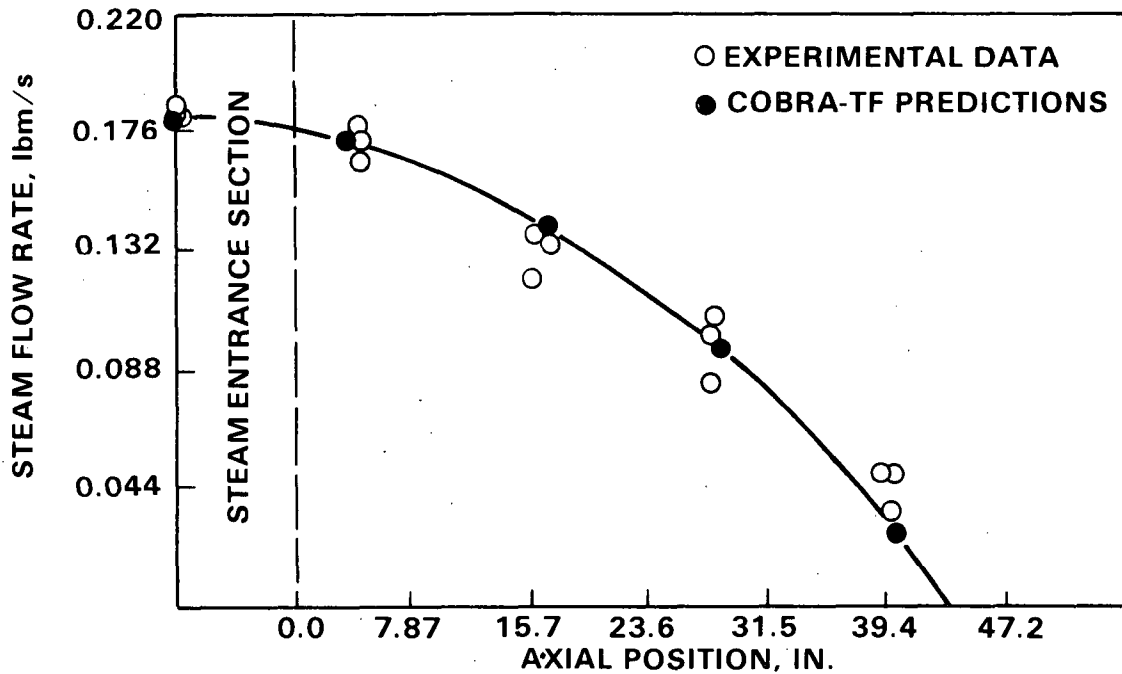


FIGURE 2.11-3. Steam Flow Rate as a Function of Axial Position

## 2.12 RPI FLAT PLATE PHASE DISTRIBUTION EXPERIMENT

Simulations have been run for two experiments in the Rensselaer Polytechnic Institute (RPI) phase separation series (Ref. 23). The purpose of these simulations was to test the ability of the code, with a three-dimensional turbulence model, to predict the void distribution in a recirculating two-dimensional, two-phase flow.

One of the most difficult aspects of a multidimensional turbulent two-phase flow to predict accurately is the phase distribution. Experiments (Ref. 24,25) have shown that the dispersed phase tends to migrate to regions of high continuous-phase turbulent intensity. It has been theorized (Ref. 26) that the turbulent normal stresses are primarily responsible for this behavior. Thus, it appears that any code used for phase distribution predictions needs a reasonable turbulence model.

The turbulence model currently available in COBRA/TRAC is a three-dimensional mixing length model. The mixing length is variable and parametric values must be supplied by the user. Both the turbulent (Reynolds) stresses and the turbulent heat flux are included in the model, as well as the viscous shear stresses.

### 2.12.1 Description of Experiment

The experimental apparatus, shown in Figure 2.12-1, consisted of a two-dimensional thermoplastic test section, measuring 1/2 in. x 12 in. x 36 in. An air-water mixture was injected at the bottom and withdrawn from outlets near the top. Steady-state tests were conducted with various flowrates and inlet qualities. Runs were made both with and without 24 simulated fuel rods of 1/4 in. diameter and 1/2 in. pitch. In addition, the mass withdrawal method was varied: in some cases all mass was removed from one side of the test section; in others it was equally split between the two horizontal outlets. The local void fraction was measured at 20 locations in the test section using a gamma densitometer system.

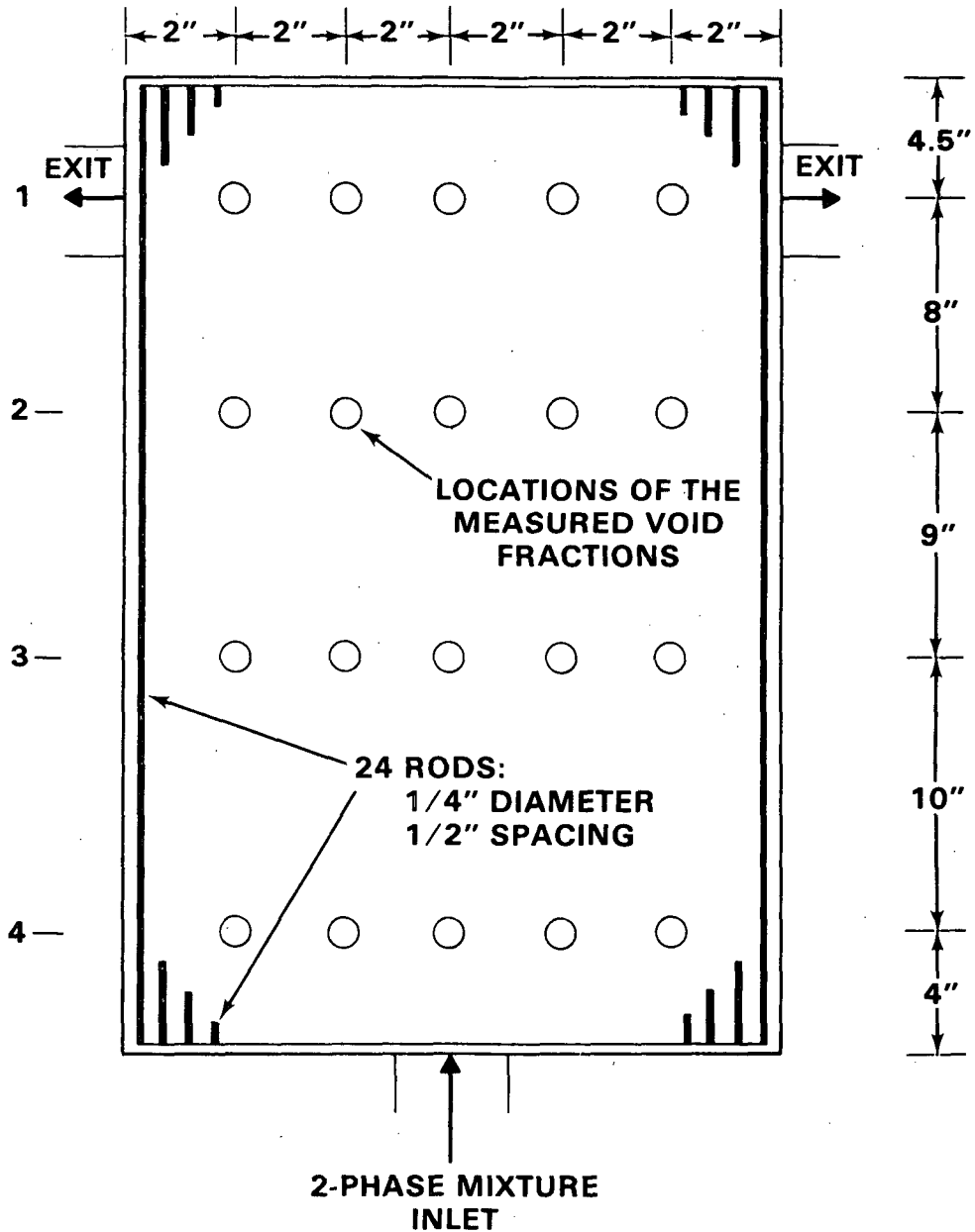


FIGURE 2.12-1. RPI Phase Separation Experimental Apparatus

Two of the symmetric runs with rods in were chosen for initial simulation. These runs had the same inlet quality but different flow rates.

RPI Test # 8:  $\dot{m} = 206.53$  lbm/min,  $x = 0.257\%$

RPI Test # 10:  $\dot{m} = 318.82$  lbm/min,  $x = 0.257\%$

The quality 0.257 corresponds to an inlet void fraction of approximately 0.6.

### 2.12.2 COBRA/TRAC Model Description

The COBRA/TRAC model is shown in Figure 2.12-2. Since the experiments being simulated were symmetric, only half of the test section was modeled. The vessel component, a short PIPE and a BREAK were used. The vessel mesh was comprised of 12 levels with five cells on each level for a total of 60 computational cells. This mesh was chosen to minimize the number of mesh cells while providing sufficient resolution of velocity and void profiles necessary for the computation of the turbulent shear stresses.

The air and water mixture was simulated using saturated steam and water at 40.7 psia. At this pressure the gas/liquid density ratio is the same as in the actual experiment. Boundary conditions for the simulations were flow and enthalpy at the inlet and pressure at the break. Each simulation was run as a transient from a standing start with initially no vapor in the test section. The mass flow rate was ramped from zero to its full value in 0.2 sec and the transient continued until the change in the dependent variables was sufficiently small to indicate that a steady state had been achieved.

### 2.12.3 Discussion of Results

Simulation results for the steady-state void fraction distribution are presented in Figures 2.12-3 through 2.12-6. Void profiles are shown for the four axial locations where data were taken. The solid curves give the experimental results and the dashed lines are the code prediction. Figures 2.12-3 and 2.12-4 show results obtained without using the turbulence model while Figures 2.12-5 and 2.12-6 depict the same simulations with the turbulence model.

Figure 2.12-3 shows results from RPI test #8, which had the lower flow rate. The experimental results clearly show the affinity of the vapor phase

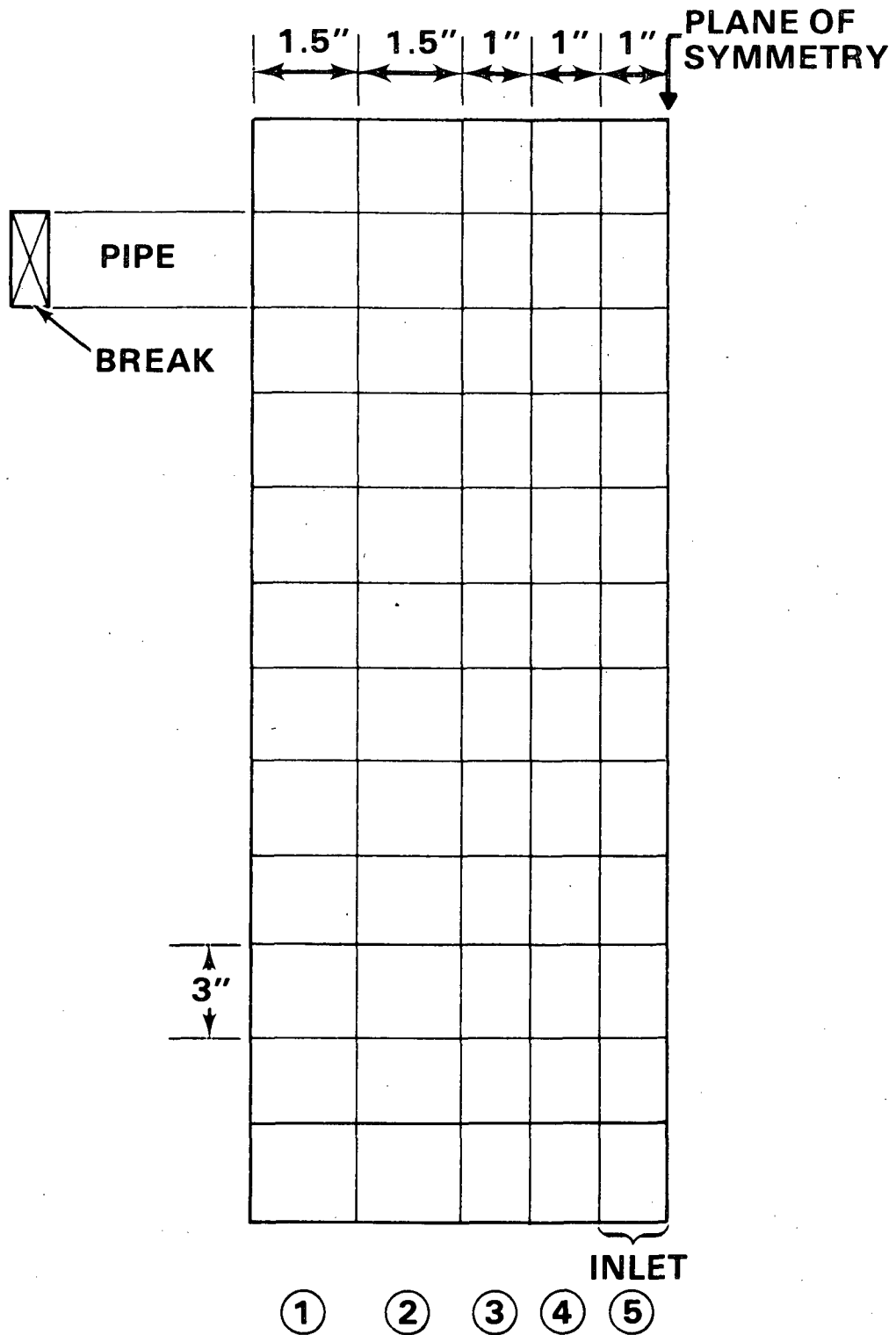


**FIGURE 2.12-2.** COBRA/TRAC Model of the RPI Phase Separation Experiment Test Section

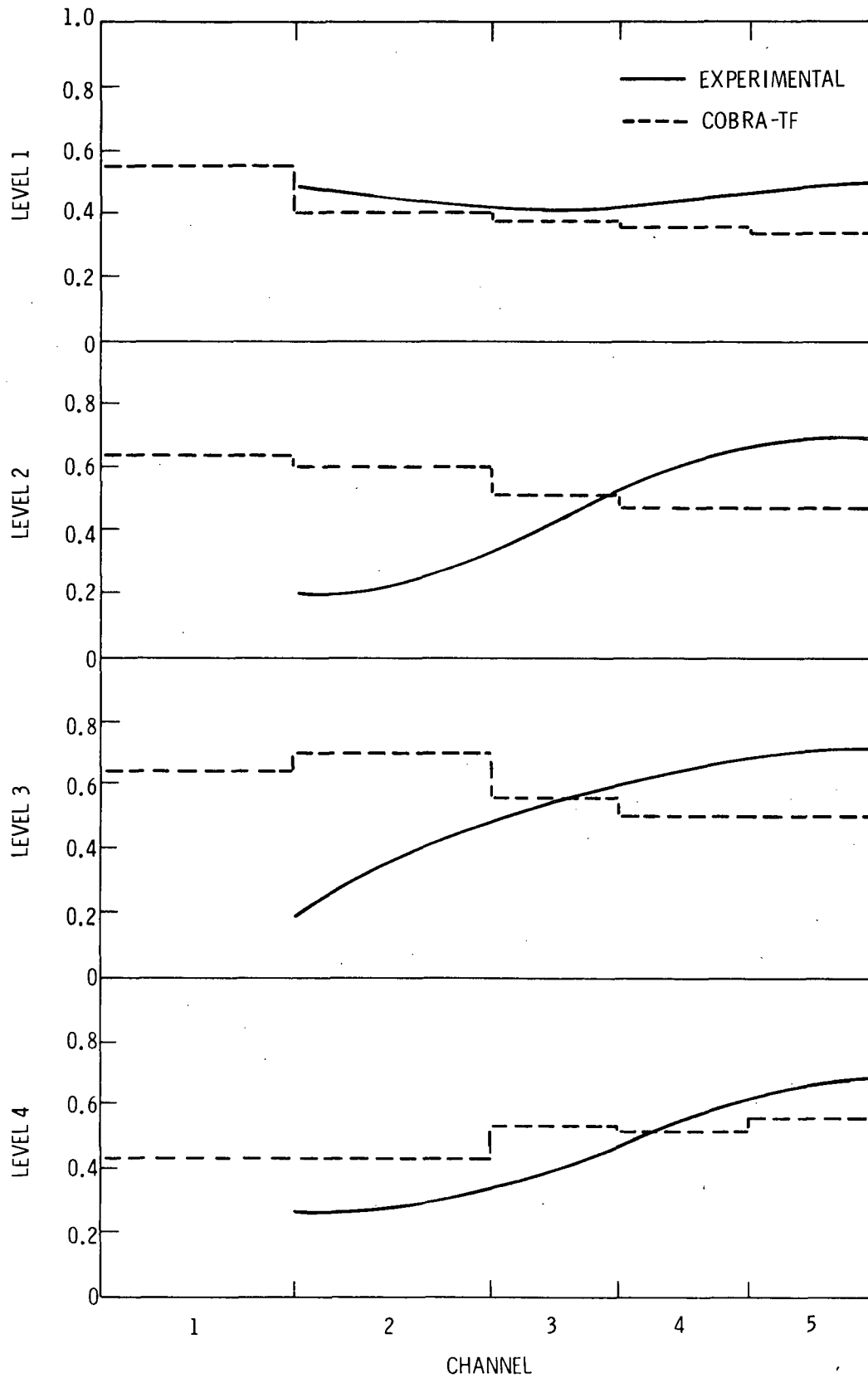


FIGURE 2.12-3. Void Distribution for RPI Test #8 Predicted by COBRA/TRAC without the Turbulence Model

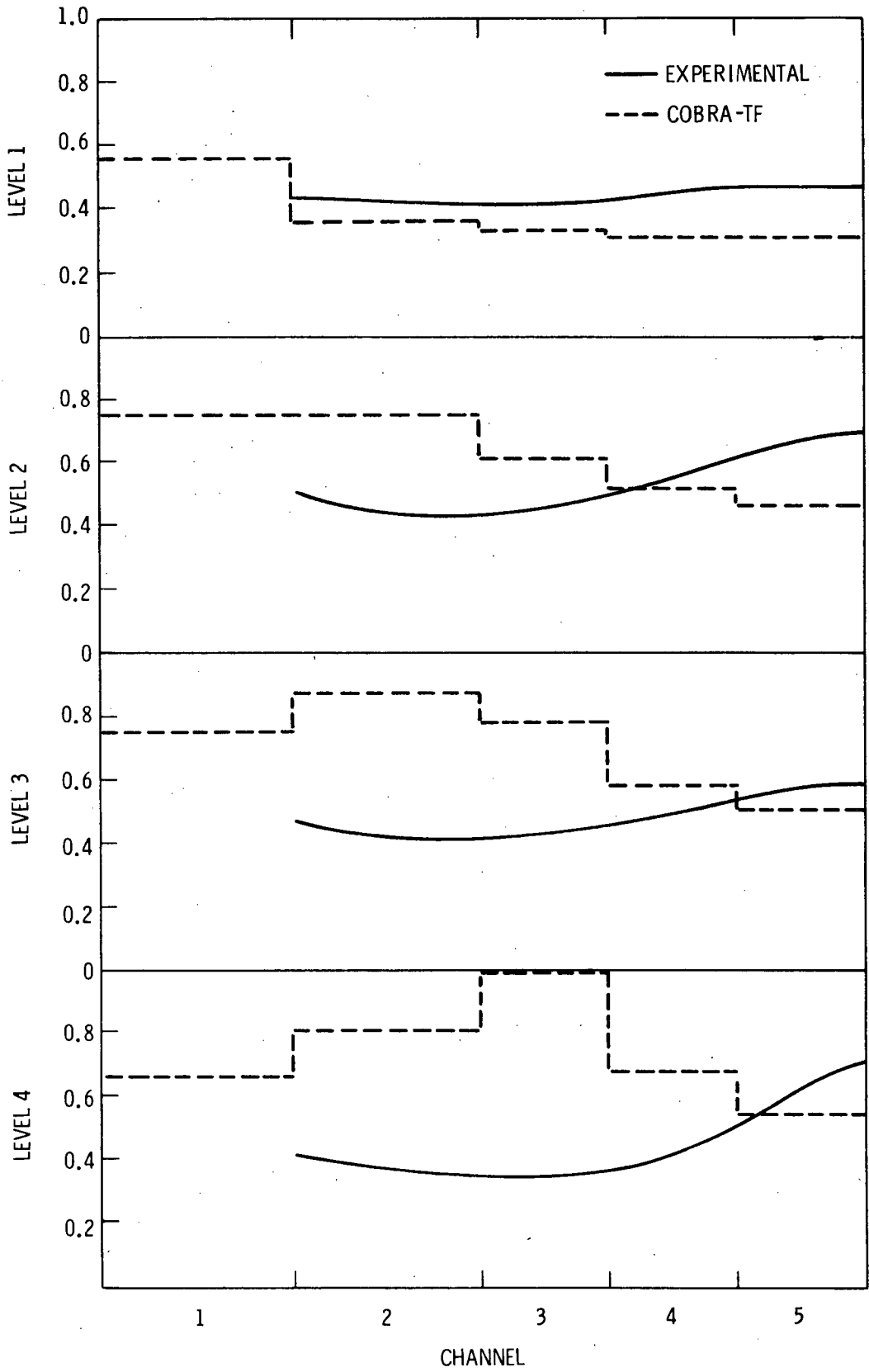
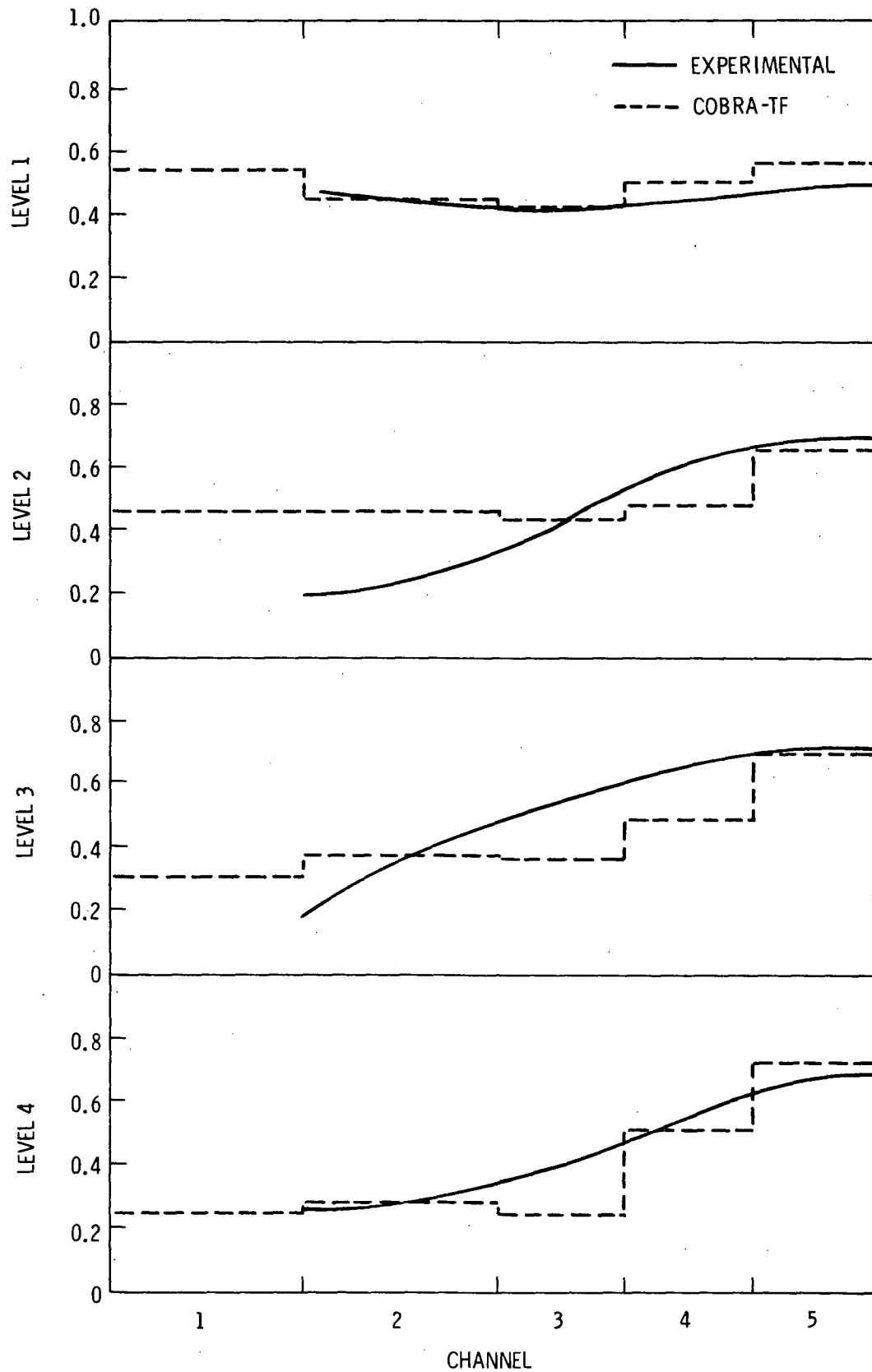
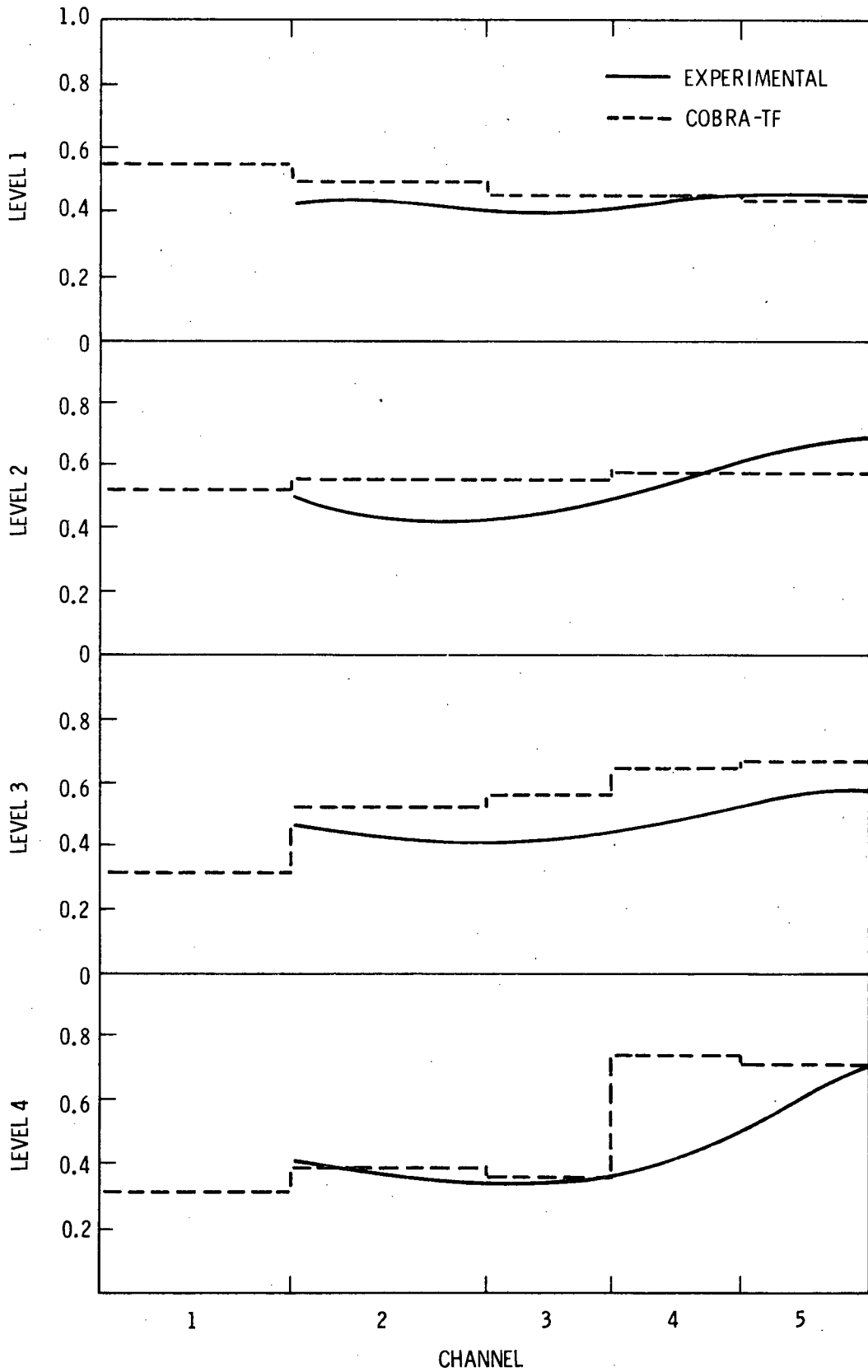


FIGURE 2.12-4. Void Distribution for RPI Test #10 Predicted by COBRA/TRAC without the Turbulence Model



**FIGURE 2.12-5.** Void Distribution for RPI Test #8 Predicted by COBRA/TRAC with the Turbulence Model



**FIGURE 2.12-6.** Void Distribution for RPI Test #10 Predicted by COBRA/TRAC with the Turbulence Model

for the highly turbulent region near the jet centerline. At level 4, near the bottom of the test section, the computed results show the correct trend, but the profile is more uniform than the experimental profile. The prediction is worse at levels 2 and 3 where the computed solution shows too much vapor on the left side of the test section and not enough on the jet axis. The prediction at level 1, near the top of the test section, is fairly good, although the values near the jet centerline should be higher.

COBRA/TRAC results for test #10, which has the higher flowrate, are shown in Figure 2.12-4. The experimental results show slightly flatter void profiles than in test #8, but the trend toward maximum void fraction at the jet centerline is still obvious. The code prediction without turbulence modeling shows just the opposite trend, greatly overpredicting the amount of vapor on the outlet side of the test section.

Figure 2.12-5 shows the code prediction with the turbulence model for test #8. The turbulence model has improved the results significantly, especially at levels 1, 3 and 4. Even at level 2, where the prediction is not quite as good, the code at least predicts the correct trend toward maximum void fraction at the jet centerline. This simulation was performed using a mixing length of 0.25 in. in channels 1 through 4, and a value of 0.5 in. in channel 5. Trials with a single constant value of 0.3 in. gave similar results, but the prediction at levels 1 and 2 was not as good.

Code predictions for test #10 with turbulence are given in Figure 2.12-6 which shows results obtained for a constant mixing length of 0.33 in. Comparison of Figure 2.12-6 with Figure 2.12-4 shows a marked improvement at all axial levels when turbulence is used.

The steady state was attained after three seconds of transient time for all runs. The execution speeds and average time step sizes for the four runs are given in Table 2.10.

In summary, COBRA/TRAC uses a three-dimensional turbulence model based on mixing length theory. The simulations presented above indicate that the model can significantly improve calculations where detailed phase distribution information is desired and reasonably fine noding is justified. Although the

TABLE 2.10. Execution Speeds and Average Time Steps for Calculations of RPI Phase Separation Tests

<u>RUN</u>	<u>Execution Speed (sec/<math>\Delta t</math>-cell)</u>	<u>Average Time Step (sec/<math>\Delta t</math>)</u>
RPI-8 (no turbulence)	3.90(10) <sup>-3</sup>	6.06(10) <sup>-3</sup>
RPI-10 (no turbulence)	3.86(10) <sup>-3</sup>	4.38(10) <sup>-3</sup>
RPI-8 (with turbulence)	4.04(10) <sup>-3</sup>	5.57(10) <sup>-3</sup>
RPI-10 (with turbulence)	3.97(10) <sup>-3</sup>	3.95(10) <sup>-3</sup>

model can easily accommodate a spatially varying mixing length, the results given in this report were obtained using a constant value for the entire test section, except near the jet axis. It is reasonable to assume that additional experimentation with a variable mixing length could further improve the calculation. This simulation was run on cycle 10 of COBRA/TRAC.

## 2.13 BENNETT TUBE CRITICAL HEAT FLUX EXPERIMENTS

Experiments investigating dryout and post-CHF heat transfer (Ref. 27) were simulated to assess the code's ability to calculate both the dryout point and heat transfer to dispersed flow beyond the dryout point. (The dryout point is defined as the axial location where liquid is no longer in contact with the tube wall.) Since heat transfer to a vapor droplet mixture is much lower than heat transfer to continuous liquid, the dryout point can be identified by a sharp increase in wall temperature. COBRA/TRAC's calculation of liquid film dryout is compared to the dryout point measured in the Bennett Tests (indicated by a sharp increase in wall temperature) and to the dryout point predicted by the Biasi CHF correlation.

### 2.13.1 Description of Experiment

The Bennett Tests were a series of experiments carried out in the Harwell High Pressure Two Phase Heat Transfer Loop. The main objectives of the tests were to measure surface temperature profiles in the region beyond the dryout point and to investigate the behavior of the dryout interface.

An electrically heated Nimonic alloy tube served as the test section. The tube was 0.497 in. I.D., 0.625 in. O.D., and 19 ft long. Nimonic alloy was used because of its low temperature coefficient of electrical resistivity, which provided a nearly uniform heat flux with large axial temperature variation. The tube geometry eliminated the problems encountered with spacers and offered a more straightforward means of comparison with theoretical models.

To prepare for each test the system was brought to the specified pressure (nominally 1000 psia) and inlet temperature with the test section power just below that required for CHF. The power was then increased until the top-most thermocouple showed a rapid increase in temperature, indicating CHF. Conditions were allowed to reach steady state. The temperatures, power, flow and exit pressure were recorded by a data logging system. The power was again increased until the next thermocouple exhibited a rapid increase in temperature. The readings were taken again. This procedure was repeated until the maximum temperature of the rod approached 1400°F. Power was then decreased and readings made as each successive thermocouple exhibited a rapid decrease in temperature.

#### 2.13.2 COBRA/TRAC Model Description

A simple COBRA/TRAC model was used to simulate the Harwell Loop for this series of experiments. The model consisted of a PIPE, a BREAK and a VESSEL component. A diagram of the model is shown in Figure 2.13-1.

The vessel component modeled the test section of the Harwell Loop. The vessel consisted of 20 cells in three vertically connected channels. Channels 1 and 2, each containing nine 1-ft long cells, modeled the heated length. A rod of tube geometry with heat transfer to the fluid on the inside surface simulated the heated Nimonic tube. Properties of the Nimonic 80A alloy used in the simulation do not change with temperature. Material properties were not important in this simulation since the tests were at steady state and the only parameter of interest was the wall surface temperature. A uniform power profile was used in both the axial and radial directions. Channel 3 of the vessel, with two 1-ft cells, provided the exit length and was connected to the pipe component.

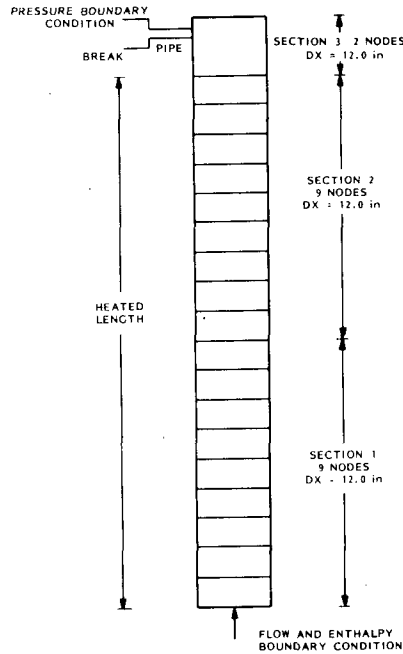


FIGURE 2.13-1. COBRA/TRAC Mesh for Bennett Tests

The remainder of the Harwell loop was modeled by boundary conditions to the vessel component. A mass flow, enthalpy boundary condition at the bottom of channel 1 was used to model the subcooled water entering the test section. The pressure at the top of the test section was specified by the break component. The break was connected to the top cell of channel 3 by a pipe component.

### 2.13.3 Discussion of Results

There were 37 different Bennett Tests simulated by COBRA/TRAC. Test conditions and the results of dryout point calculations are shown for nine of the tests in Table 2.11. These nine tests have been chosen to show a wide range of mass flux and heat flux combinations. The measured dryout point, the dryout points calculated by COBRA/TRAC, and the Biasi correlation are listed. The average error in the Biasi correlation and in the COBRA/TRAC calculation are similar, but the maximum error in the calculated dryout point is much less than that for the Biasi correlation. The uncertainty in the measured dryout location is 6 to 12 in. because thermocouples are located 6 to 12 in. apart.

TABLE 2.11. Summary of Bennett Test Conditions and Results of Dryout Point Calculations

Test	Mass Flux (Mlb/hr-ft <sup>2</sup> )	Heat Flux (MBtu/hr-ft <sup>2</sup> )	Dryout Location (in)	Error ( $\Delta Z$ )	
				Biasi	COBRA-TF
5359	0.29	0.173	140	-20	- 8
5336	0.49	0.260	140	-44	- 8
5273	0.75	0.292	140	- 8	+26
5250	1.00	0.290	164	+ 4	+16
5294	1.44	0.348	164	+ 4	+16
5313	1.87	0.381	170	+10	+10
5310	1.88	0.358	185	+19	+ 7
5379	2.80	0.542	140	- 8	+16
5397	3.82	0.584	164	<u>-24</u>	<u>+ 4</u>
			Avg error =	15.7	12.3
			Max error =	44	26

COBRA/TRAC uses the Biasi correlation for CHF when the mass flux is greater than 30 gm/cm<sup>2</sup>-sec and the flow regime is not annular film flow. In the Bennett tests the liquid does form an annular film on the tube surface. Instead of limiting the heat flux by the Biasi correlation, COBRA/TRAC uses forced convection to the liquid film until the film is completely vaporized or entrained. The results shown in Table 2.11 indicate that the film dryout approach is an improvement over the Biasi correlation, at least for film dryout CHF.

The entrainment rate is important in determining dryout of a liquid film. COBRA/TRAC uses separate models for entrainment and de-entrainment that result in a net entrainment rate. Figure 2.13-2 shows the effect of entrainment on film dryout in test no. 5373. The entrained liquid fraction increases rapidly at 6 to 8 ft from the bottom of the heated length indicating a large positive entrainment rate. The entrainment rate decreases gradually as the entrained liquid becomes a large fraction of the total liquid mass from

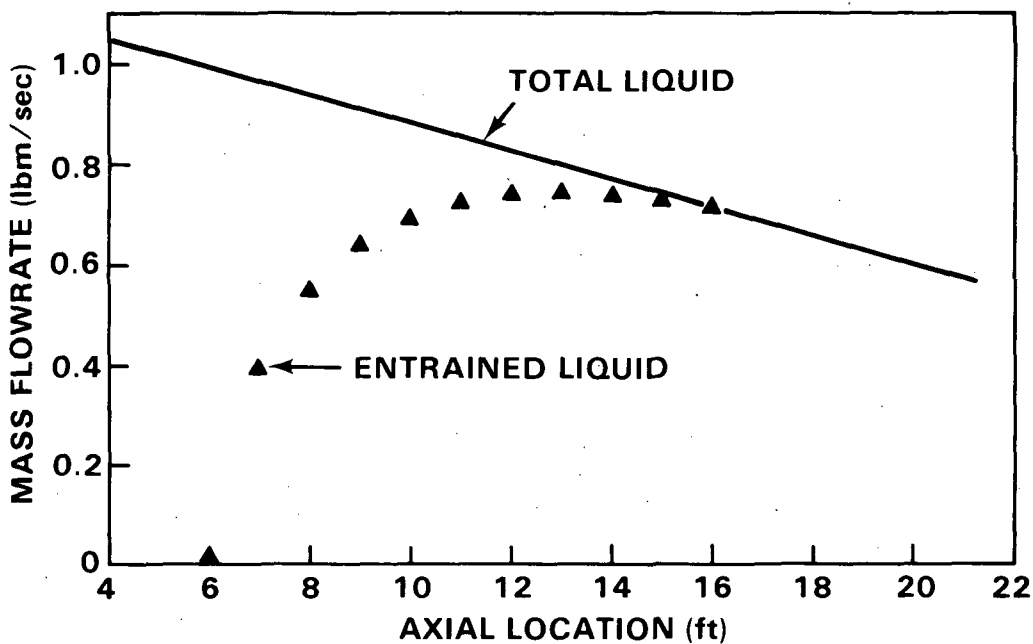


FIGURE 2.13-2. Entrained Liquid in Bennett Test No. 5373

8 to 12 ft. From 13 ft to the dryout point at 16 ft, continuous liquid has become a small fraction of the total liquid mass flow. The de-entrainment rate is larger than the entrainment rate and liquid droplets are deposited on the liquid film. Net de-entrainment near the dryout point of the annular film is typical of all the Bennett Tests.

The COBRA/TRAC calculation of CHF is compared with the Biasi correlation and the Bennett Test measurements as a function of equilibrium quality at the dryout point in Figures 2.13-3 through 2.13-6. In each figure, measured data, COBRA/TRAC calculations and a line representing the Biasi correlation are plotted for a series of tests at a single mass flux.

Equilibrium quality for each of the Bennett experiments was calculated as follows:

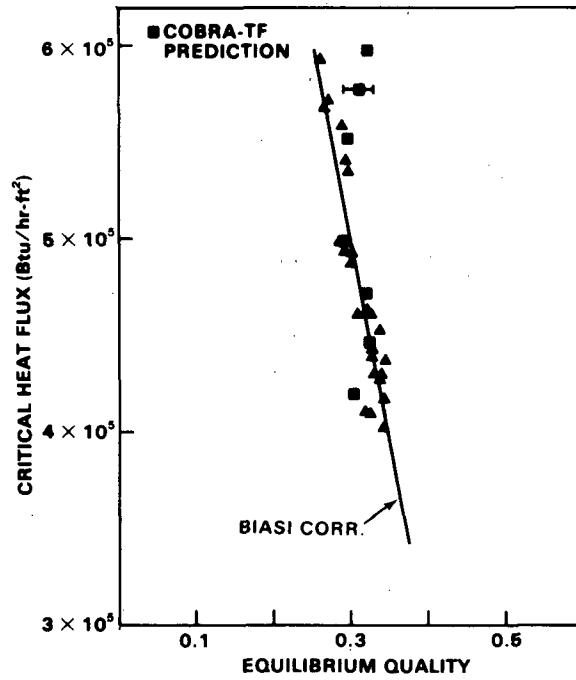


FIGURE 2.13-3. Bennett Test Critical Heat Flux vs. Equilibrium Quality (at Mass Flux =  $2.84 \times 10^6$  lbm/hr-ft<sup>2</sup>)

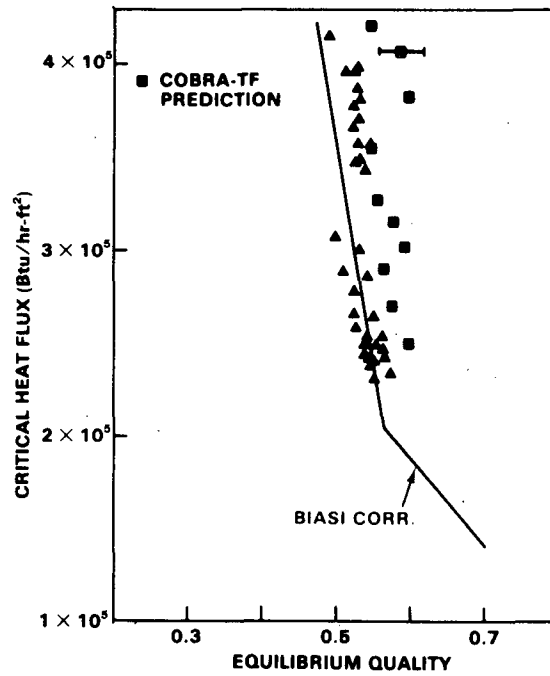


FIGURE 2.13-4. Bennett Test Critical Heat Flux vs. Equilibrium Quality (at Mass Flux =  $1.0 \times 10^6$  lbm/hr-ft<sup>2</sup>)

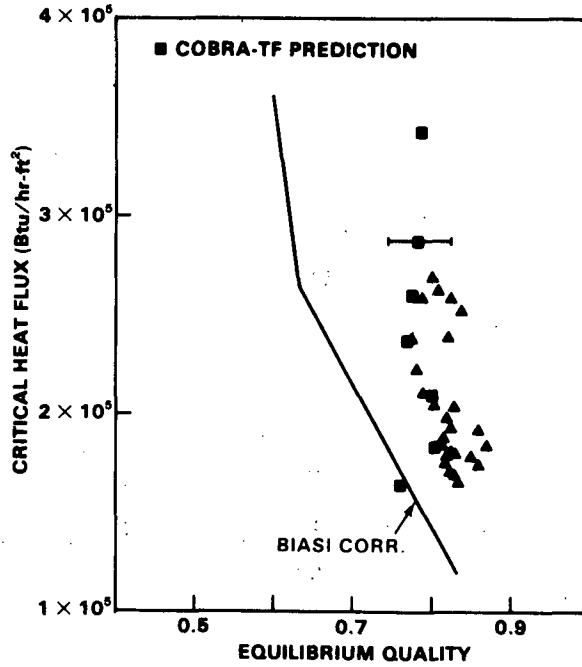


FIGURE 2.13-5. Bennett Test Critical Heat Flux vs. Equilibrium Quality at Mass Flux =  $0.49 \times 10^6$  lbm/hr-ft<sup>2</sup>)

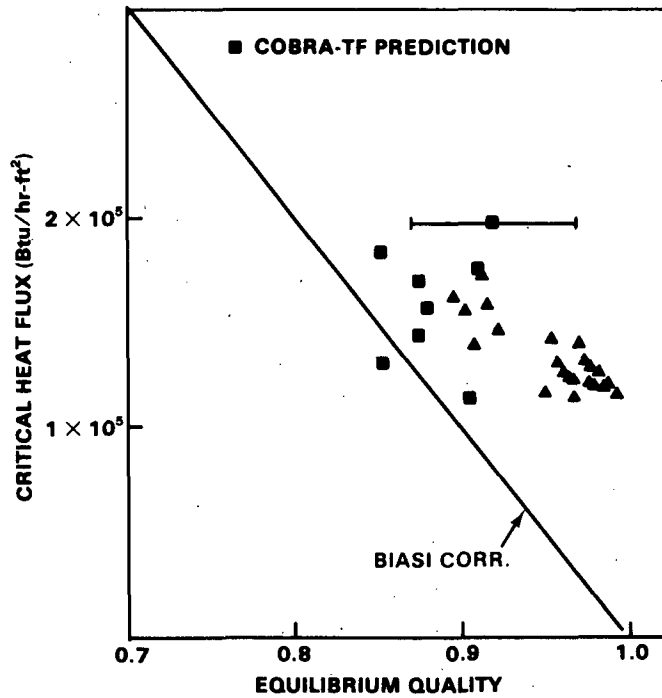


FIGURE 2.13-6. Bennett Test Critical Heat Flux vs. Equilibrium Quality (at Mass Flux =  $0.29 \times 10^6$  lbm/hr-ft<sup>2</sup>)

$$x_{eq} = \frac{m_{vapor}}{m_{total}} = \frac{q'' P_w L}{m_{total} \Delta h} \quad (2.5)$$

where  $x_{eq}$  = equilibrium quality at the dryout point  
 $m_{vapor}$  = vapor mass flow rate at the dryout point (lb/hr)  
 $m_{total}$  = total mass flow rate (lb/hr)  
 $q''$  = heat flux (Btu/hr-ft<sup>2</sup>)  
 $P_w$  = wetted perimeter of the tube (ft)  
 $L$  = distance from bottom of heated length to dryout point (ft)  
 $\Delta h$  = change in enthalpy from test section inlet to saturated steam at dryout point (Btu/lb)

This equation is valid since the test section is at steady state and the heat flux is uniform over the length of the tube. The largest uncertainty in the equation is the location of the dryout point. In this analysis, dryout is assumed to occur halfway between the thermocouple indicating a sharp increase in temperature and the thermocouple immediately below it. Most dryout points occur at or above 140 in. from the bottom of the heated length in a region of the test section where thermocouples are less than 6 in. apart so that the uncertainty in equilibrium quality is less than 5%.

The COBRA/TRAC quality is simply the mass flow rate of vapor divided by the total mass flow rate at the dryout point. The dryout point is defined as halfway between the first axial node in dispersed flow film boiling and the axial node immediately below it. Dryout, therefore, always occurs at a cell boundary. The mass flow rates from the fluid cells above and below were linearly averaged to get mass flow at the cell boundary. The uncertainty due to the axial node size was indicated on each of the four plots by an error bar on one of the calculated data points.

According to Biasi, CHF is a function of mass flux, pressure, hydraulic diameter and quality. A discontinuity in slope is present in the Biasi correlation prediction because the correlation uses the maximum of two equations. One equation is for low quality and the other for high quality CHF. The Biasi correlation is described in detail in Volume 1, Section 4.2 of the COBRA/TRAC manual.

When compared with measured data in Figures 2.13-3 through 2.13-6 neither the Biasi correlation nor the COBRA/TRAC calculation is clearly better at predicting CHF. In Figure 2.13-3 both methods agree well with the measured data, the Biasi correlation doing slightly better. Figure 2.12-4 also shows the Biasi correlation in better agreement with measured data than COBRA/TRAC. On the other hand, COBRA/TRAC calculations are in better agreement with measured data than the Biasi correlation in Figures 2.13-5 and 2.13-6. If a trend can be established, it is that the Biasi correlation does better for high mass flux, low quality dryout, while COBRA/TRAC does better for low mass flux, high quality dryout conditions.

Axial wall temperature profiles for the nine tests listed in Table 2.11 are shown in Figures 2.13-7 through 2.13-15. Each figure shows the calculation as a solid line and the temperature recorded by each thermocouple on the test section represented by an asterisk. Both the measured and calculated dryout points are easily identified in all the temperature profiles as a sharp increase in wall temperature. The portion of the profile of most interest is above the dryout point where wall heat flux is transferred to a mixture of superheated steam and dispersed liquid droplets. This type of heat transfer is referred to as dispersed flow film boiling or post-CHF heat transfer.

Dispersed flow film boiling heat transfer is calculated as follows. The primary heat transfer mode is forced convection to the superheated steam. The steam superheat is then determined by the interfacial heat transfer rate to the entrained droplets as part of the hydrodynamic solution.

The wall temperature profile above the dryout point is a direct indication of how well COBRA/TRAC predicts post-CHF heat transfer because the test section is at steady state with a uniform heat flux. Nine temperature profiles are shown because of the wide variation in the behavior of the temperature profile. For example, wall temperature may continue to increase with distance above the dryout point, indicating nonequilibrium conditions, as in tests 5359 and 5336 (Figures 2.13-7 and 2.13-8) or it may decrease with distance above the dryout point, indicating near equilibrium conditions as in

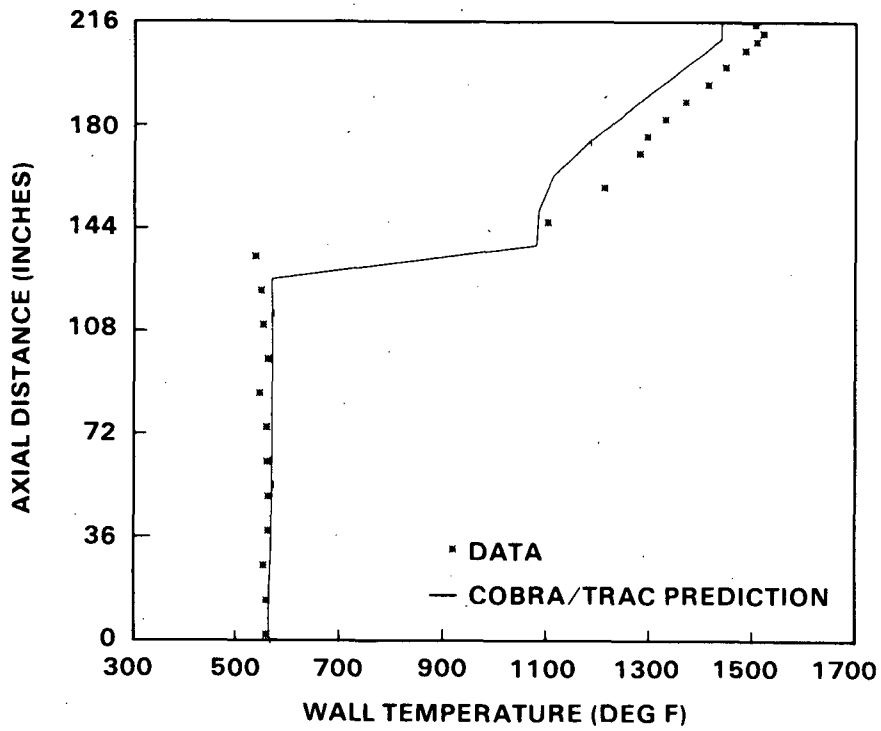


FIGURE 2.13-7. Bennett Test 5359 Axial Temperature Profile

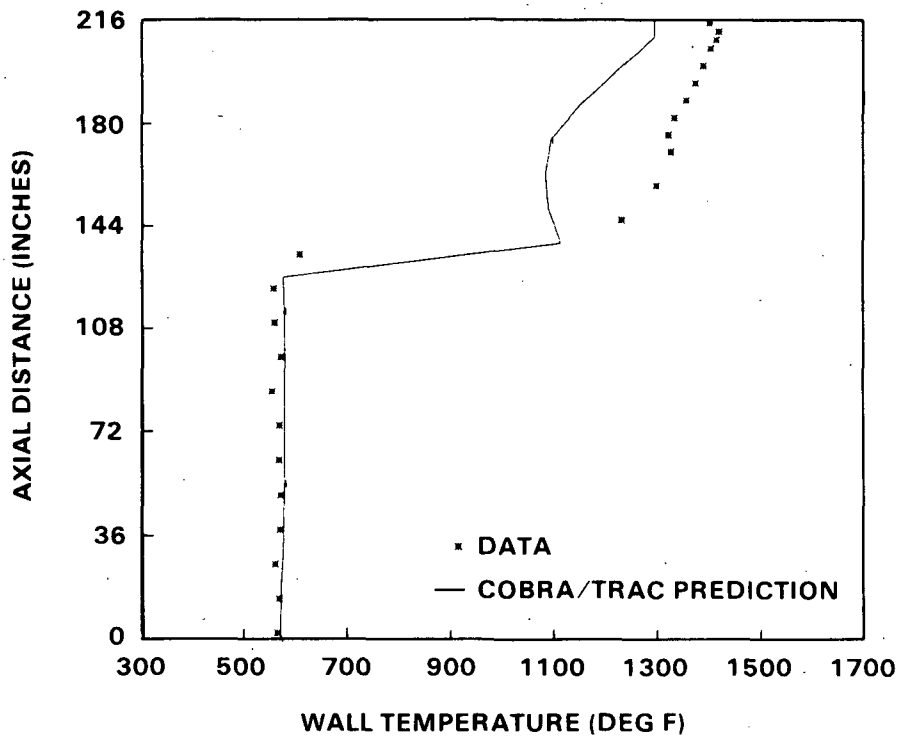


FIGURE 2.13-8. Bennett Test 5336 Axial Temperature Profile

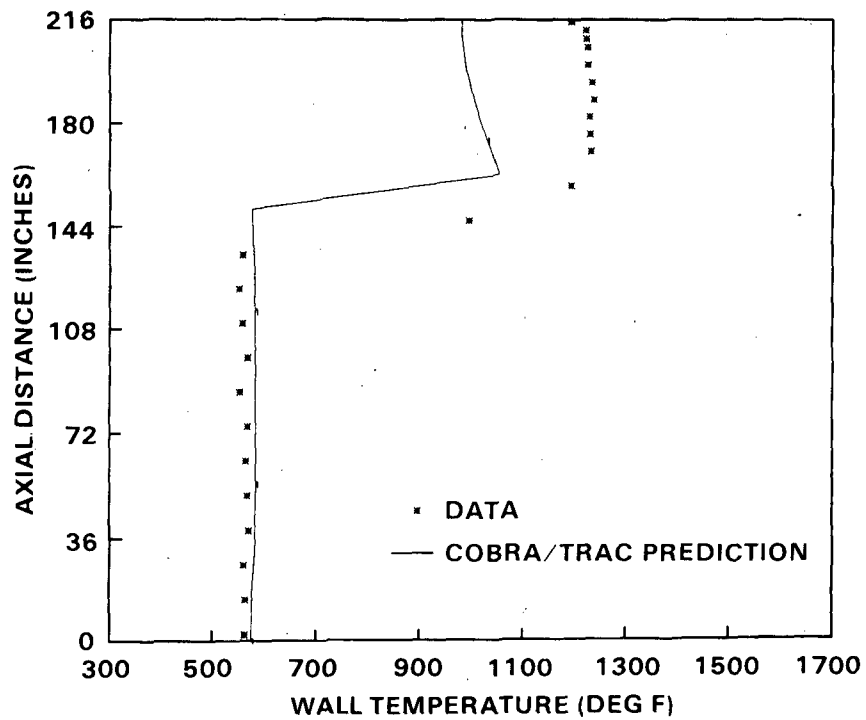


FIGURE 2.13-9. Bennett Test 5273 Axial Temperature Profile

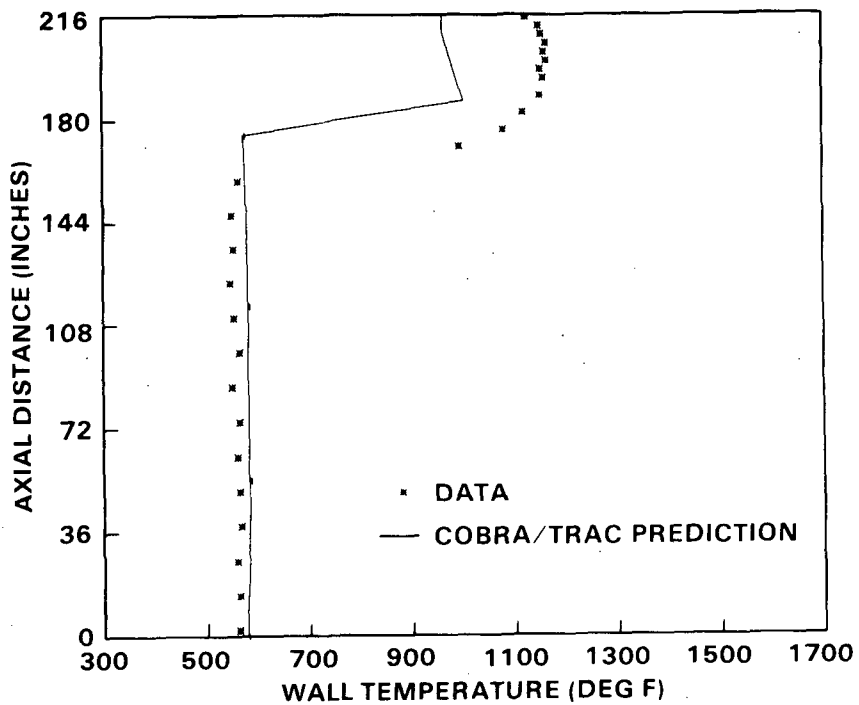


FIGURE 2.13-10. Bennett Test 5250 Axial Temperature Profile

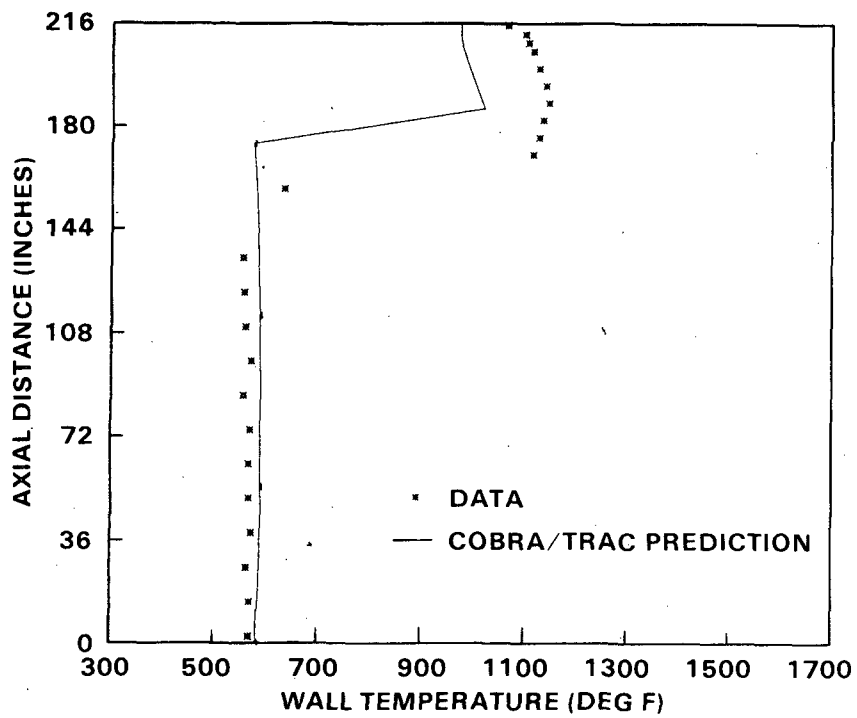


FIGURE 2.13-11. Bennett Test 5294 Axial Temperature Profile

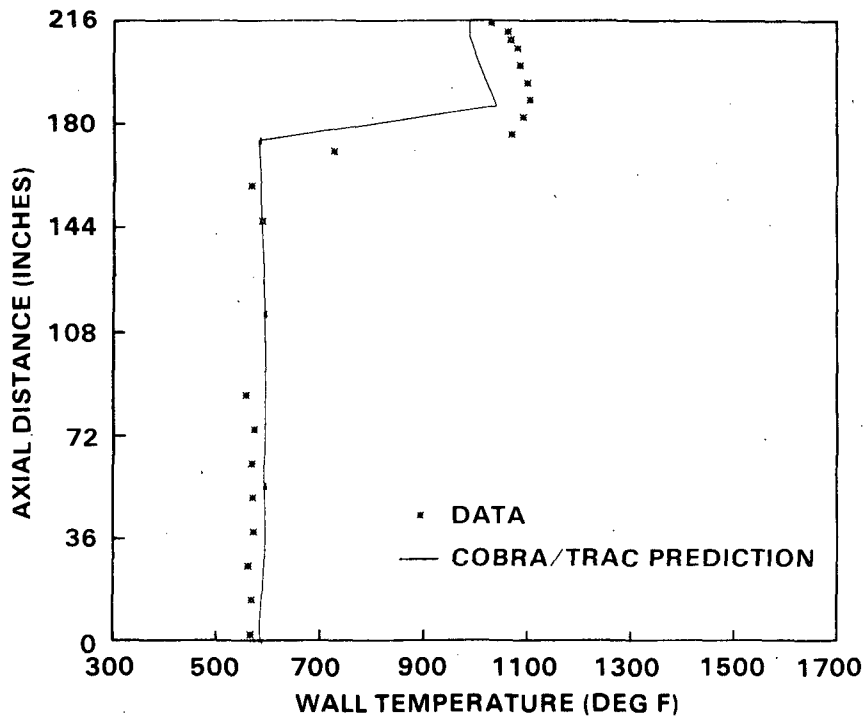


FIGURE 2.13-12. Bennett Test 5313 Axial Temperature Profile

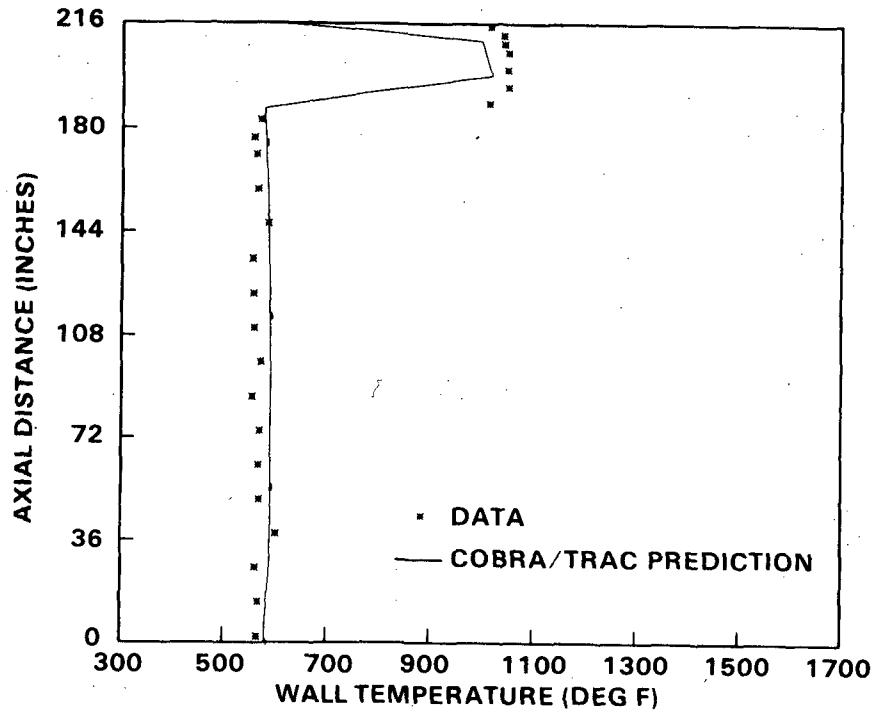


FIGURE 2.13-13. Bennett Test 5310 Axial Temperature Profile

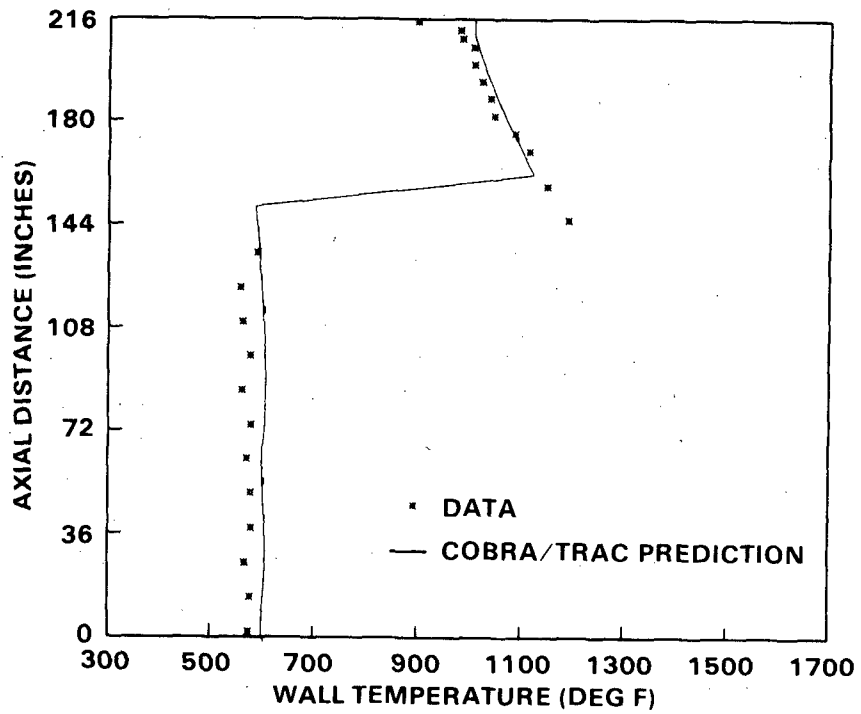


FIGURE 2.13-14. Bennett Test 5379 Axial Temperature Profile

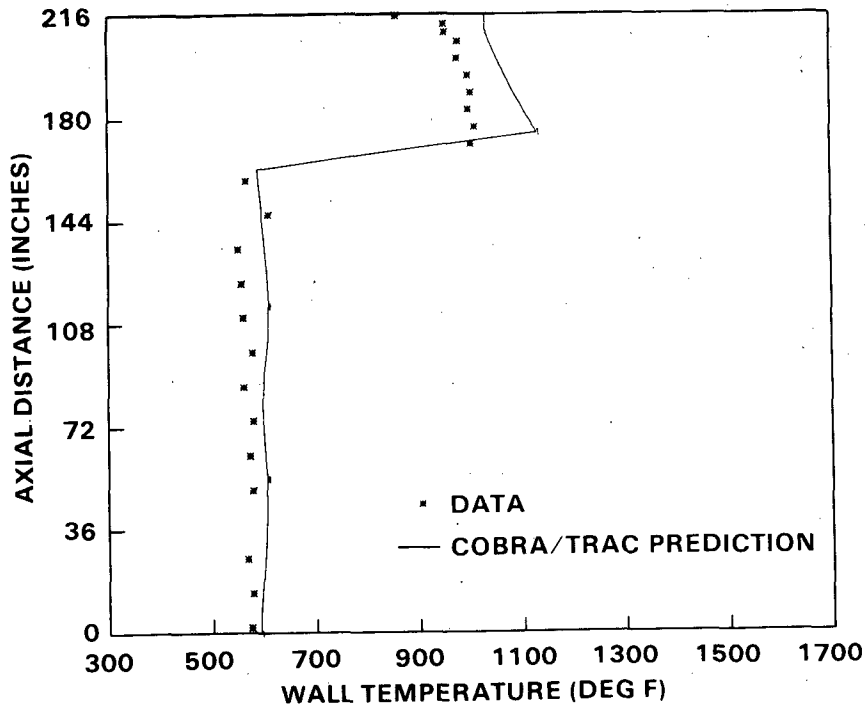


FIGURE 2.13-15. Bennett Test 5397 Axial Temperature Profile

tests 5379 and 5397 (Figures 2.13-14 and 2.13-15). The wall temperature may increase and then decrease as in tests 5250, 5294, and 5313 (Figures 2.13-10, 2.13-11 and 2.13-12) or remain relatively constant as in test 5273 and 5310 (Figures 2.13-9 and 2.13-13). Generally, COBRA/TRAC calculates wall temperatures that are too low and decrease too much with axial distance from the dryout point, except for tests 5379 and 5397. The maximum difference between measured and calculated post-dryout wall temperature is 220°F in test 5273. The behavior that COBRA/TRAC has the most trouble simulating is increasing and then decreasing temperature above the dryout point. The code completely misses the increasing part of the profile and predicts a temperature gradually decreasing with distance above the dryout point.

The post-CHF wall temperature is dependent on vapor superheat. Superheat, in turn, is a function of the dryout point, droplet size, slip velocity and the interfacial heat transfer correlation. The fact that calculated wall temperatures are too low and decrease too rapidly indicates that an excessive amount of interfacial heat transfer is leading to a low vapor temperature. Similar results have been noted in the upper elevations of

the FLECHT reflood tests with low flooding rate. COBRA/TRAC simulation of the Bennett Tests has shown that the film dryout approach is an improvement over the Biasi correlation for predicting the dryout location when annular film flow is present. Using forced convection to the liquid film and not limiting heat flux to the CHF calculated by the Biasi correlation has reduced the average error and significantly reduced the maximum error in calculating dryout location. Plotting CHF as a function of equilibrium quality has shown that the calculation is sometimes better and sometimes inferior to the Biasi correlation. A clear choice cannot be made as to which method predicts the dryout equilibrium quality more reliably.

The Bennett test simulations also have shown that post-dryout heat transfer is a difficult process to model. Wide variation in the behavior of the wall temperature profiles indicate that some refinement of the dispersed flow film boiling heat transfer regime is required to reduce uncertainty in the calculated wall temperature profile.

## 2.14 FRIGG FORCED CONVECTION TESTS

FRIGG forced convection tests (Ref. 28) were simulated to assess the ability to predict axial void fraction distribution. Axial void distribution is affected primarily by the flow regime selection logic, by the physical models for interfacial friction within each flow regime and by the vapor generation models for subcooled and nucleate boiling heat transfer. The purpose of these simulations was to assess these models. The code's performance is measured by comparing the calculated axial void fraction distribution with the void fraction distribution measured by gamma ray attenuation in the FRIGG loop.

### 2.14.1 Description of Experiment

The forced convection tests are part of the FRIGG loop project, an experimental investigation of the hydrodynamic and heat transfer conditions in a boiling water reactor (BWR) channel. The experiments are the result of a joint effort between AB Atomenergi (now Studsvik Energiteknik AB) and ASEA, carried out from 1967 to 1968 in the laboratories of the Nuclear Power Department of ASEA in Vasteras, Sweden. The purpose of the project was to verify that the Marviken BWR could be run at rated power with proper safety margins against burnout or instability. These experiments also established a basis for calculational methods to be used for other reactors. Forced convection experiments have been done to supplement measurements taken in the natural circulation experiments.

The loop was made up of an electrically heated test section connected to a steam separator. Liquid from the separator recirculated to the forced circulation pump. The pump forced water into the heated test section at a constant flow rate. Steam from the separator flowed through a spray condenser which maintained the system pressure at 50 bar. The condensed steam was further cooled in a heat exchanger before returning to the test section as feedwater. Inlet subcooling was controlled by changing the feedwater flow rate. A simplified flow diagram is shown in Figure 2.14-1.

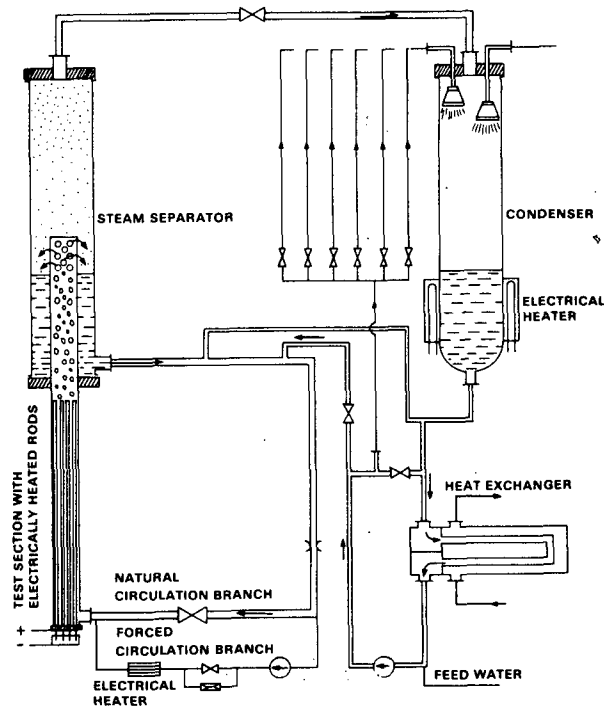


**FIGURE 2.14-1.** Simplified Diagram of FRIGG Forced Convection Loop

The test section consisted of a uniformly heated 36-rod cluster with a 4.4-m heated length. The heater rod diameter was 13.8-mm and an unheated center rod of 20 mm outer diameter was present. Prototypic reactor grid spacers were used.

A gamma ray attenuation device measured the void fraction in the test section. The device was mounted on an elevator to measure void fraction as a function of axial level. The standard error of the measurements was 2.5%.

#### 2.14.2 COBRA/TRAC Model Description

The COBRA/TRAC model for the forced circulation FRIGG loop consisted of three components: a vessel, a pipe and a break. The vessel contained two vertical channels with 14 fluid nodes. A schematic diagram of the model is shown in Figure 2.14-2. A one-dimensional mesh was used and code predictions are compared to the bundle average void fraction at each axial level.

Forced circulation flow into the bottom of the heated length was provided by a vessel boundary condition. The boundary condition specified the enthalpy and mass flow rate of water into the first node of the vessel. Section 1 of

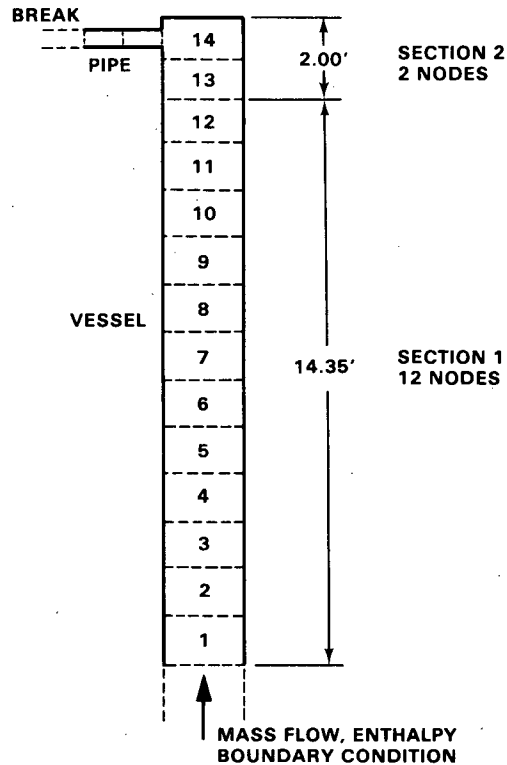


FIGURE 2.14-2. COBRA/TRAC Model of FRIGG Forced Convection Loop

the vessel modeled the heated length of the test section. The fluid nodes were thermally connected to an average rod simulating the 36 heater rods. Loss coefficients were used to model the eight grid spacers in eight of the fluid nodes of section 1. Section 2 of the vessel modeled the area of the test section above the heated length. At the top of the section a pipe connected the vessel to a break component. The break component modeled the pressure boundary condition imposed on the test section by the remainder of the FRIGG loop.

### 2.14.3 Discussion of Results

Test conditions of the FRIGG forced circulation tests simulated by COBRA/TRAC are summarized in Table 2.12. The tests are identified by numbers 313020, 313018 and 313016. (These are code numbers of the steady state void distribution measurements reported in Appendix 1 of the FRIGG loop project documentation.) Inlet subcooling, inlet mass velocity, and total power were experimentally measured. The COBRA/TRAC input parameters in Table 2.12 are calculated from the measured quantities.

TABLE 2.12. Summary of FRIGG Forced Circulation Test Conditions

	Test Number		
	<u>313020</u>	<u>313018</u>	<u>313016</u>
Inlet Subcooling (°C)	22.4	3.7	19.3
*Inlet Enthalpy (Btu/lbm)	448.34	487.92	454.71
Inlet Mass Velocity (kg/m <sup>2</sup> -sec)	1159	1124	1208
*Inlet Mass Flow rate (lbm/sec)	36.81	35.70	38.37
Total Power (kW)	4415	4390	2910
*Linear Heat Rate (kW/ft)	8.544	8.495	5.631

\*Denotes parameters used in COBRA/TRAC input

A comparison of calculated and measured axial void distribution for each of the FRIGG runs simulated is shown in Figures 2.14-3, 2.14-4 and 2.14-5. The difference between measured and calculated void fraction is less than 5%.

In test 313018, liquid enters the test section only 3.7°C subcooled. According to COBRA/TRAC calculations, subcooled boiling takes place only in the first node of the heated length. Vapor generation in the remainder of the test section is due to nucleate boiling. Assuming that the subcooled boiling model provides reliable results for the first node, agreement between calculated and measured void distribution indicates proper calculation of the flow regime and interfacial drag forces. Figure 2.14-3 shows how well the calculated and measured axial void distribution agree.

In test 313020, the inlet subcooling is increased to 22.4°C. COBRA/TRAC calculates a transition from subcooled to nucleate boiling seven feet from the bottom of the heated length. The plot of void fraction as a function of axial distance in Figure 2.14-4 shows a rapid increase of void fraction with axial distance at the seven-foot level. This simulation indicates that the subcooled boiling model combined with the subcooled liquid interfacial heat transfer model, flow regime map, and interfacial shear models accurately predict the void fractions in a boiling channel.

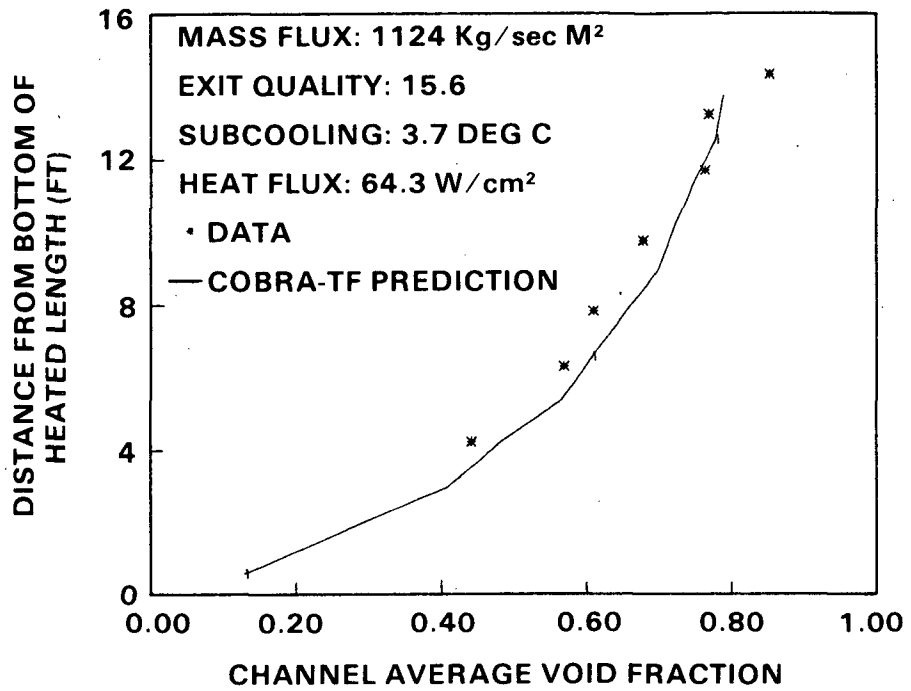


FIGURE 2.14-3. FRIGG Forced Convection Test 313018

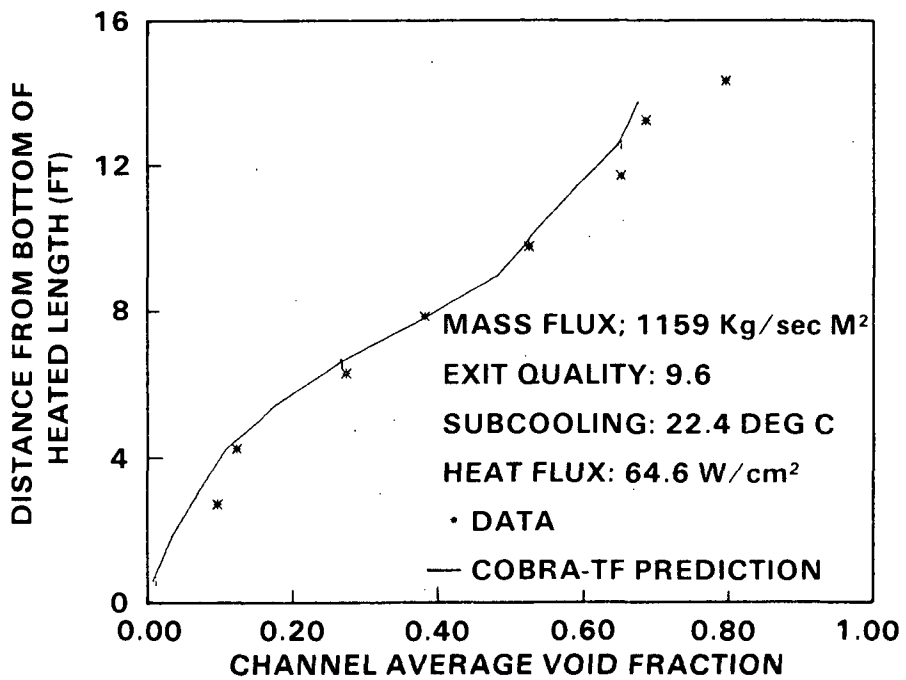


FIGURE 2.14-4. FRIGG Forced Convection Test 313020

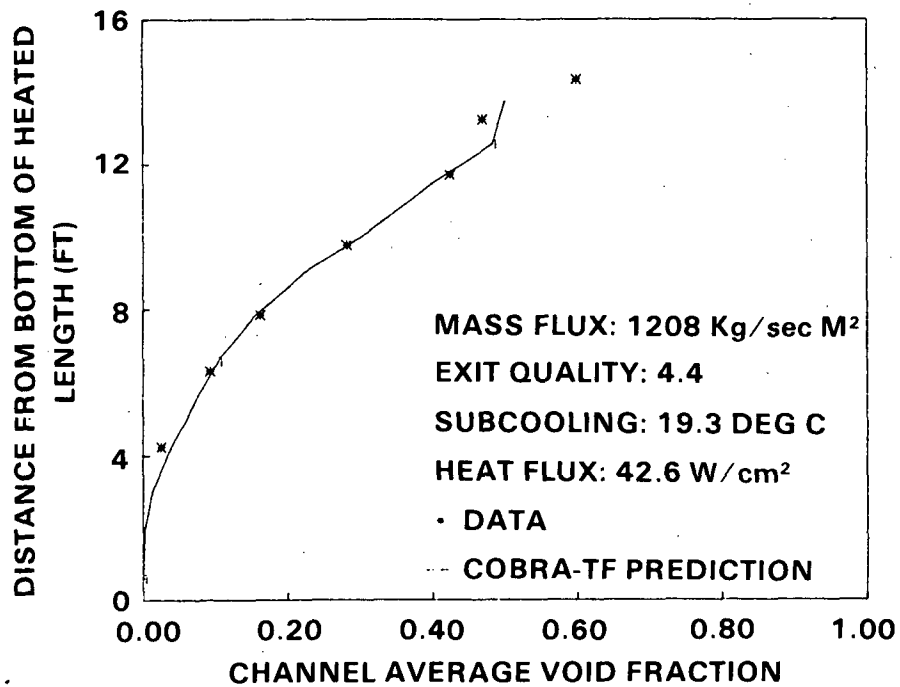


FIGURE 2.14-5. FRIGG Forced Convection Test 313016

Test 313016 has a larger mass flux and a lower heat flux than the other simulations. Water enters the test section 19.3°C subcooled. Transition from subcooled to nucleate boiling heat transfer is calculated to occur at 9.6 ft from the bottom of the heated length. Figure 2.14-5 shows a rapid increase in void fraction from 8 to 12 ft from the bottom of the heated length.

The excellent predictions for void fraction in the subcooled region indicate that the subcooled boiling model is performing satisfactorily, as are the interfacial models and flow regime selection logic. These simulations were run on cycle 10 of COBRA/TRAC.

## 2.15 FRIGG NATURAL CIRCULATION TESTS

COBRA/TRAC simulations of FRIGG (Ref. 28) natural circulation experiments have been done to assess the code's ability to calculate axial void distribution in the heated length, two-phase flow pressure drop and the natural circulation flow rate. The calculated axial void distribution is compared to the void distribution measured by gamma ray attenuation. COBRA/TRAC's calculation of two-phase flow pressure drop is assessed by comparing measured and calculated inlet flow rate as a function of rod power. In natural circulation the inlet flow rate is determined by the force balance between the driving head in the downcomer and pressure losses in the heated length. Hydrostatic and single-phase pressure losses are well understood and have been tested in other simulations. Comparing the measured and calculated inlet flow rate determines the credibility of the two-phase flow pressure drop models used in COBRA/TRAC.

### 2.15.1 Description of Experiment

The FRIGG Loop project is an experimental investigation of hydrodynamic and heat transfer conditions in a boiling water reactor (BWR) channel. The experiments are the result of a joint project between AB Atomenergi and ASEA, carried out from 1967 to 1968 in the ASEA laboratories in Vasteras, Sweden. The purpose of the project was to establish a basis for calculational methods to verify that BWR's can be operated at rated power with proper safety margins against burnout or instability.

The loop is made up of an electrically heated rod bundle connected to a steam separator. Liquid from the separator recirculates through the downcomer to the bottom of the rod bundle. Steam from the separator is condensed in a spray condenser and cooled in a heat exchanger before returning to the top of the downcomer as feedwater. Inlet subcooling is controlled by the loop heat exchanger. The loop pressure of 50 bar is maintained by the spray condenser. Water from the downcomer flows into the heated length by natural circulation. A diagram of the loop is shown in Figure 2.15-1.

The axial void distribution is measured by gamma ray attenuation. An elevator is used to move the device along the length of the rod bundle. A

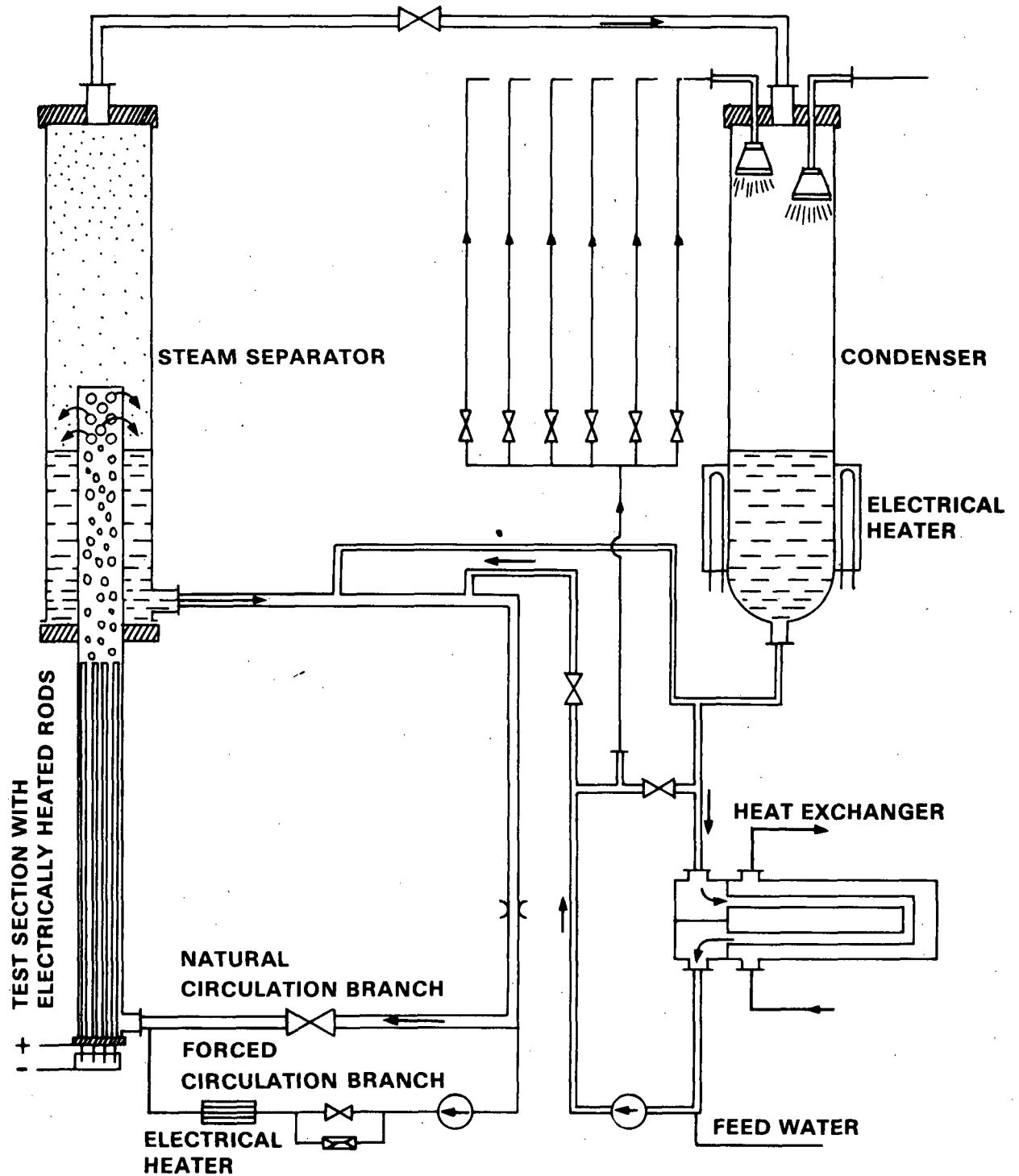


FIGURE 2.15-1. Simplified Flow Diagram of FRIGG Natural Circulation Loop

venturi meter with fast response measures mass velocity in the downcomer. Local pressure is measured in the separator with a calibrated manometer.

### 2.15.2 COBRA/TRAC Model Description

A diagram of components in the COBRA/TRAC model is shown in Figure 2.15-2. The test section and separator are modeled by the VESSEL component. The downcomer and feedwater inlet are modeled using TEE and FILL components.

The vessel component consists of 8 channels and a total of 28 cells. Channels 4 through 8 model the separator. The two-phase mixture from the test section flows through the gap between channels 6 and 7. Continuous liquid and liquid droplets fall into channel 5 and recirculate through the downcomer.

The test section is modeled by vessel channels 1, 2, and 3. One rod, simulating the 36-rod bundle, is thermally connected to channel 2. Heat transfer to the grid spacers and vessel wall is neglected.

The 8 grid spacers in the heated length are modeled by a loss coefficient in each of the 8 cells of channel 2. A loss coefficient is also used in channel 3 to account for area changes in the upper tie plate.

Two boundary conditions are used to specify the rest of the loop. A pressure-enthalpy boundary condition at the top of the vessel models the connection to the condenser of the FRIGG loop. Feedwater into the downcomer is modeled by a FILL component. The FILL specifies the flow rate and temperature of the feedwater.

### 2.15.3 Discussion of Results

Table 2.13 summarizes the test conditions simulated by COBRA/TRAC. The test numbers used are code names of the steady state void distribution measurements reported in Appendix 1 of (Ref. 28). Test numbers 313030A, 313030B and 313030C refer to a series of simulations with conditions similar to test 313030. Each simulation in the series has a different rod power, which yields inlet mass velocity as a function of rod heat flux.

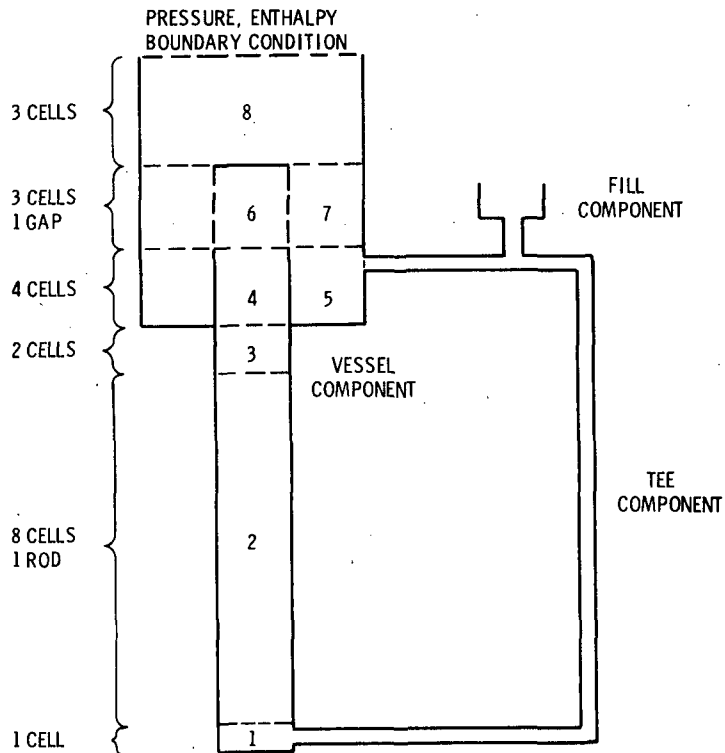


FIGURE 2.15-2. COBRA/TRAC Model of FRIGG Natural Circulation Loop

TABLE 2.13. Summary of FRIGG Natural Circulation Test Conditions

<u>Test #</u>	<u>Feedwater Temperature (°K)</u>	<u>Heat Flux (W/cm<sup>2</sup>)</u>	<u>Rod Power (kw/ft)</u>
313037	506	43.90	5.8086
313034	446	21.98	2.9040
313030	519	66.70	8.8291
313030A	519	90.0	11.88
313030B	519	30.0	3.96
313030C	519	10.0	1.32

Calculated vapor void fraction is compared to measured data as a function of axial distance for tests 313030, 313034 and 313037 in Figures 2.15-3, 2.15-4 and 2.15-5. The maximum difference between calculated and measured void fraction is 20% at four meters from the bottom of the heated length in test 313037. Standard error in the measured data is reported as 2.5%. Generally the code calculates a void fraction curve that fits the measured data well.

A comparison between measured and calculated mass velocity as a function of rod power is shown in Figure 2.15-6. The four calculated data points in the figure correspond to test numbers 313030, 313030A, 313030B, and 313030C. The estimated accuracy in measured mass velocity is  $\pm 20 \text{ kg/m}^2\text{s}$ . COBRA/TRAC calculations at 30.0, 66.6, and 90.0  $\text{W/cm}^2$  agree well with the measured data. The maximum difference between calculated and measured mass velocity is 80  $\text{kg/m}^2\text{s}$  at a heat flux of 10  $\text{W/cm}^2$ . Mass velocity changes rapidly with heat flux around 10  $\text{W/cm}^2$  and a difference of 80  $\text{kg/m}^2\text{s}$  is considered reasonable.

At a heat flux of 90  $\text{W/cm}^2$  the liquid film in contact with the heater rod has become unstable. COBRA/TRAC assumes an unstable film exists when the pressure differential acting over the crest of a wave exceeds the surface tension holding the wave to the film. The calculated inlet mass velocity at 90  $\text{W/cm}^2$  is extremely sensitive to the model used for interfacial friction when an unstable film is present.

The friction factor used in COBRA/TRAC for unstable films is the maximum of a film flow correlation by Henstock and Hanratty (Ref. 29) and five times the stable film friction factor recommended by Wallis (Ref. 30). The value of five times the stable film friction factor is derived from experimental observation of pressure drop for stable and unstable films (Ref. 31). At the onset of instability, the system pressure drop increases suddenly. The change is due to increased roughness of the liquid film caused by large, unstable waves on the film surface. The Henstock and Hanratty correlation by itself fails to predict the sudden increase in pressure drop at the onset of instability. When compared to the measured values in Figure 2.15-6, the COBRA/TRAC correlation for unstable film friction factor results in less than a 3% error in mass velocity.

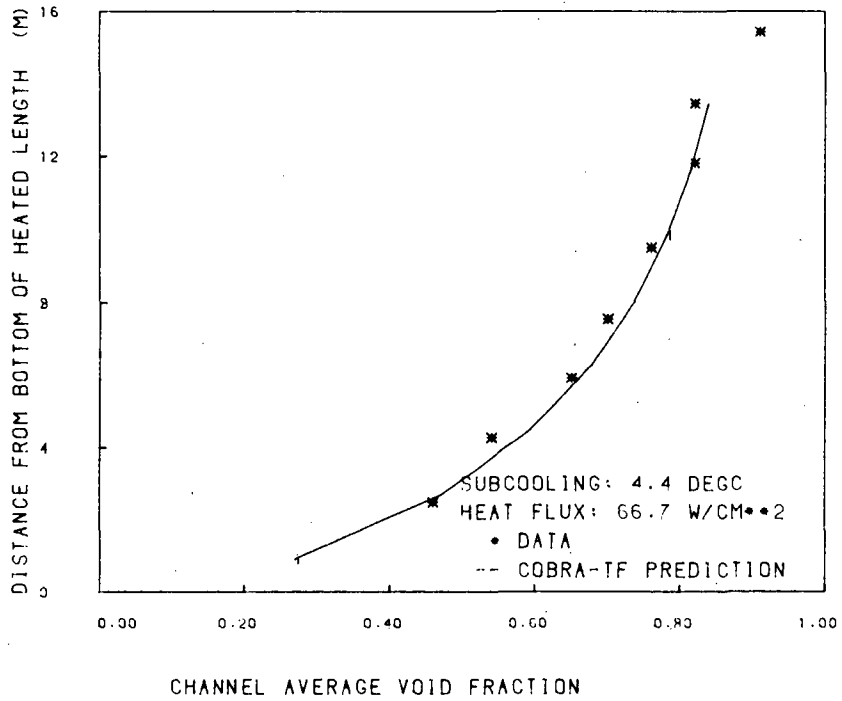


FIGURE 2.15-3. FRIGG Natural Circulation Test 313030

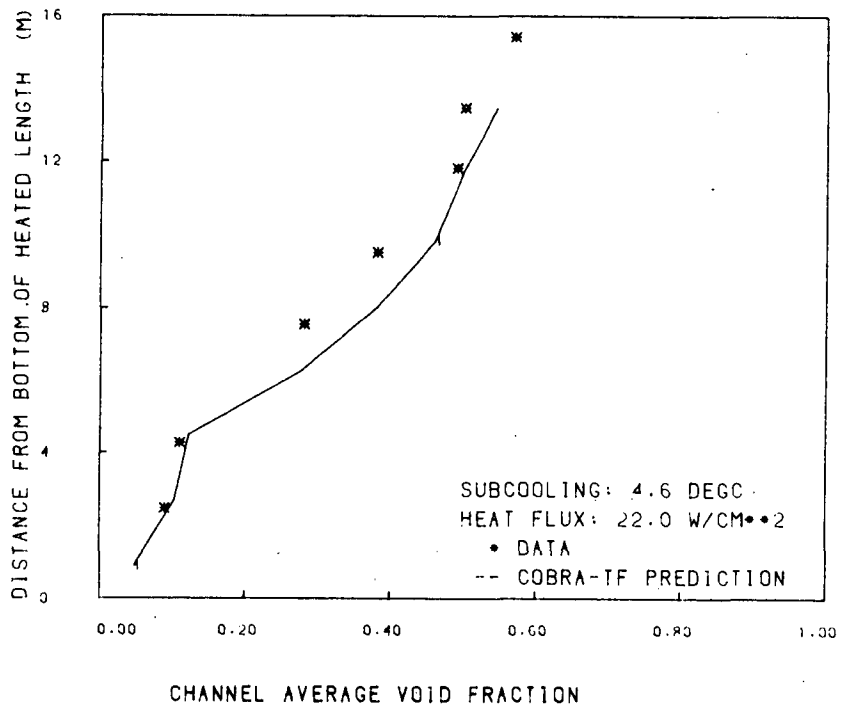


FIGURE 2.15-4. FRIGG Natural Circulation Test 313034

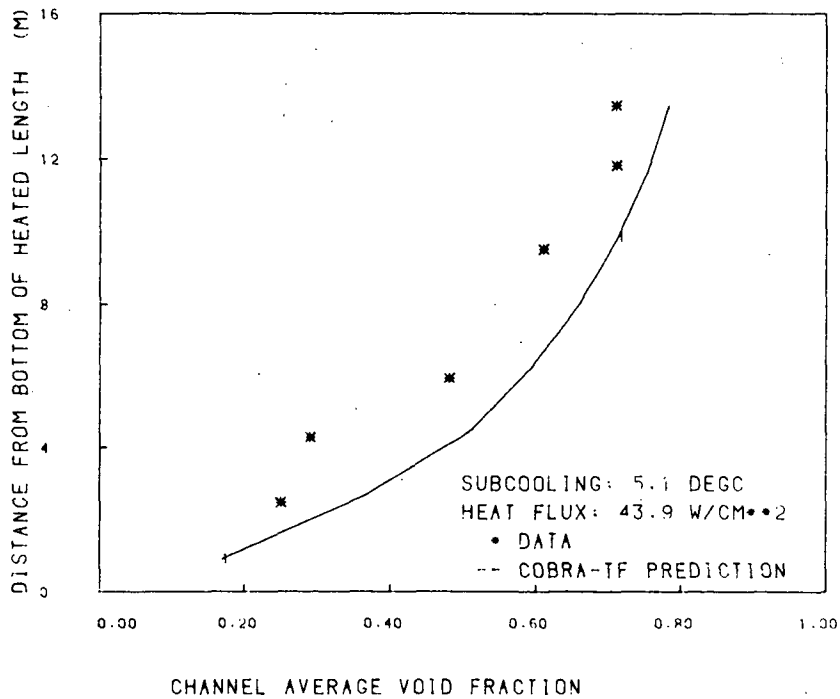


FIGURE 2.15-5. FRIGG Natural Circulation Test 313037.

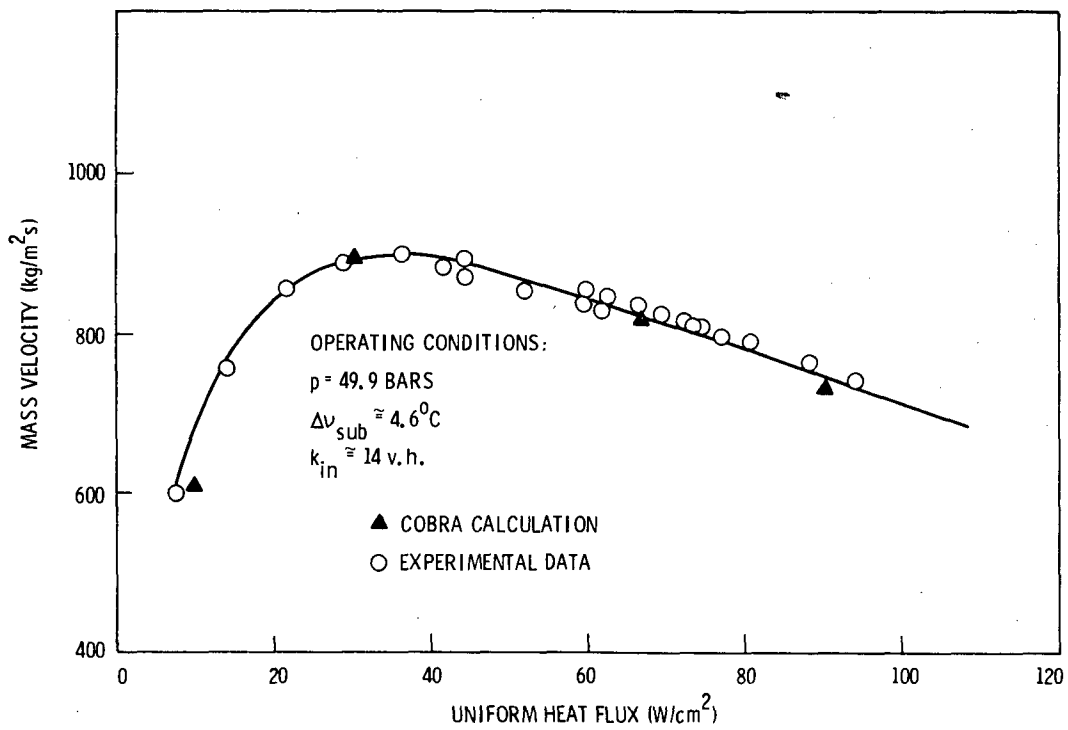


FIGURE 2.15-6. FRIGG Natural Circulation Mass Velocities

These results indicate that the methods used for modeling interfacial shear, two-phase wall shear, two-phase form losses, entrainment and subcooled boiling are adequate for a boiling channel. These simulations were run on cycle 10 of COBRA/TRAC.

## 2.16 SEMISCALE MOD3 TEST S-07-6

Test Series 7 in the Semiscale Mod 3 configuration was performed to investigate blowdown and reflood transients. Test S-07-6 (Ref. 32) was a 200% cold leg break with emergency coolant injection in the intact cold leg. The entire primary system was modeled for the simulation of test S-07-6. The purpose of the simulation was to demonstrate the capability of the COBRA/TRAC code to calculate the flow and heat transfer in the system during the blowdown and reflood transient.

### 2.16.1 Description of Experiment

The semiscale MOD-3 system consisted of a pressure vessel with simulated reactor internals, (including 25-rod core and external downcomer assembly) and two complete primary loops. The intact loop, (which simulated three loops of a 4-loop plant) consisted of a steam generator, pump and pressurizer. The broken loop consisted of a steam generator, pump and rupture assembly on the piping for the inlet cold leg to the downcomer. The primary ECC system was modeled with high and low pressure injection pumps on the intact loop, and an ECC accumulator isolated by a pressure activated check valve. The rupture assembly vented the break to a pressure suppression tank pressurized to 0.25 MPa that simulated the containment.

The initial conditions for the test simulated steady-state reactor operating conditions. The transient was initiated by subjecting the system to a double-ended cold leg break. At initiation of blowdown, power to the primary pumps was reduced and the pump speed was regulated to simulate coastdown. Power to the electrically heated core was controlled to simulate the ANS +20% power decay curve. The ECC system was activated at appropriate times in the transient. The high pressure coolant injection pumps were started at 3 seconds (at a system pressure of 15.21 MPa) and ran throughout the test. The low pressure injection pumps were activated at 31.5 seconds

after blowdown (at a system pressure of 1.0 MPa). The accumulator check valve opened at 19 seconds after blowdown, and emptied ECC water into the intact loop cold leg.

The performance of the system during test S-07-6 was monitored with 235 detectors, with an effective sample rate of 1.917 points per second. Data was taken for fluid temperature, material temperature, pressure, volumetric flow rate and density throughout both loops and within the pressure vessel and external downcomer. The transient lasted ~460 seconds.

#### 2.16.2 COBRA/TRAC Model Description

The Semiscale system was modeled in COBRA/TRAC with 29 components.<sup>(a)</sup> The model consisted of an intact loop, a broken loop, the ECC system and the pressure vessel and downcomer. The pressure vessel and downcomer were modeled with the VESSEL component, and the rest of the system was modeled with the one-dimensional components.

A diagram of the one-dimensional system components is shown in Figure 2.16-1. The intact loop model consisted of the hot leg (TEE 1) with the pressurizer (PRIZER5) attached to the tee branch, a steam generator (STGEN2, with secondary modeled by FILL 30 and BREAK 31), piping between the steam generator and pump (PIPE3), a Semiscale pump (PUMP4), and the cold leg, (TEE9). The ECC components connect to the intact cold leg through the tee branch. The ECC components were modeled by an accumulator (ACCUM18), a pressure-controlled valve (VALVE32), piping from the accumulator to the cold leg (TEE16), and piping from the low pressure and high pressure injection pumps (TEE17). The injection pumps were modeled as simple mass sources (FILL33 and FILL34).

<sup>(a)</sup> The published references for the semiscale system do not provide enough data on the physical characteristics of the system to construct an adequate model for COBRA/TRAC. The input data describing the one-dimensional components of the system was obtained from a TRAC-P1A input deck. The vessel and downcomer was modeled in COBRA/TRAC using data obtained from working drawings of the semiscale system.

2.166

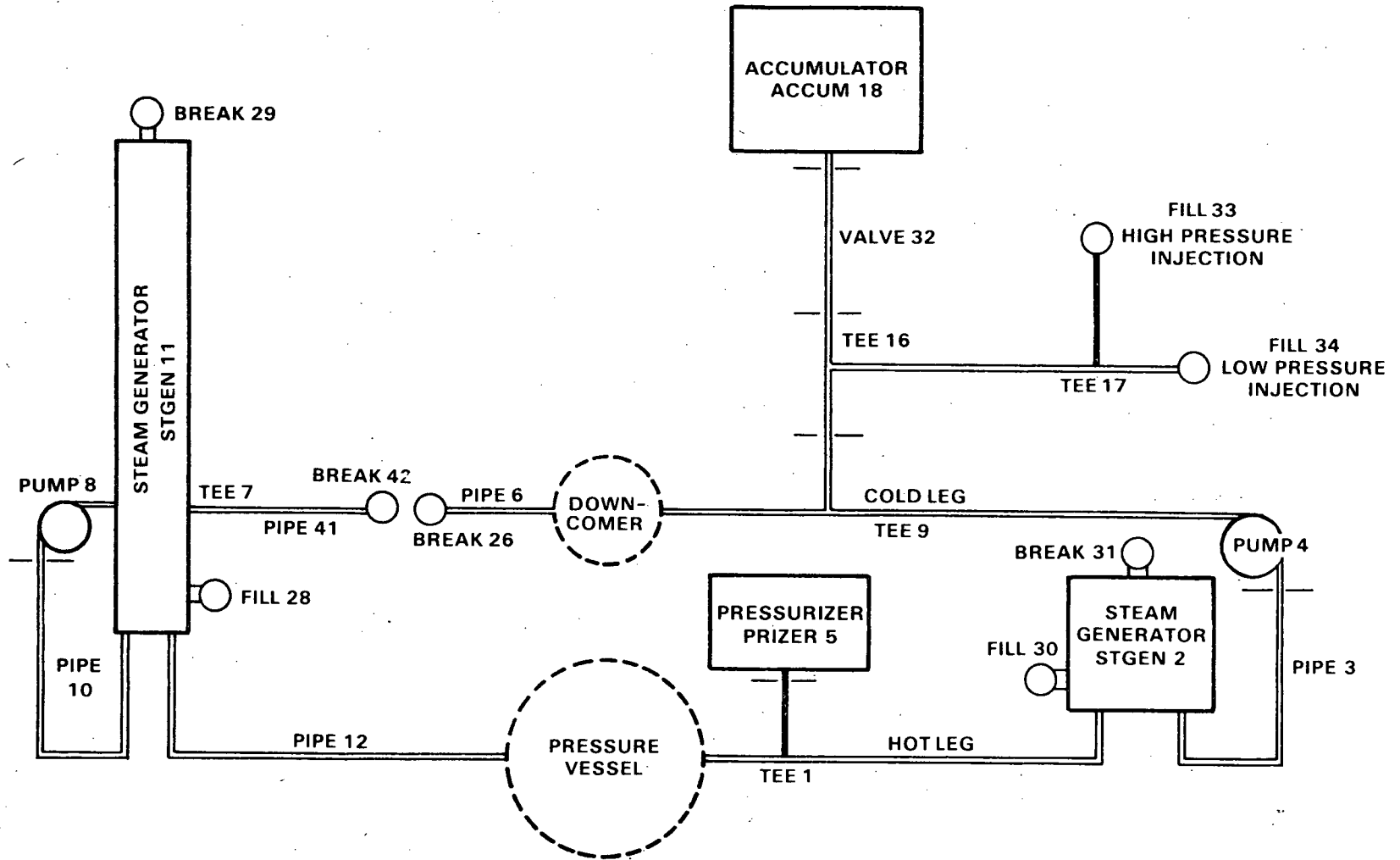


FIGURE 2.16-1. COBRA/TRAC Model of Semiscale MOD 3 System

The broken loop model consisted of the hot leg pipe (PIPE12), a steam generator (STGEN11, with secondary modeled by FILL28 and BREAK29), piping from the steam generator to the pump (PIPE10), a Semiscale pump (PUMP8), and piping between the pump outlet and the break assembly (TEE7). The pump side of the break assembly was modeled with a pipe (PIPE41) and a break (BREAK42); the downcomer side of the break assembly was modeled with a separate pipe and break (PIPE6 and BREAK26).

The vessel component modeled the pressure vessel and downcomer with the multisection channel-splitting logic. A diagram of the VESSEL model is shown in Figure 2.16-2. The model consists of 36 channels in 10 axial sections. There are 116 computational cells in the component. The fluid volumes and flow areas are modeled at values as close as possible to the actual volumes and flow areas in the Semiscale vessel and downcomer. The heater rods in the core and the solid structures in contact with the fluid are modeled using the heat conductor models in the VESSEL module. A one-dimensional mesh is used except in regions where more channels are required to allow piping connections or to allow convection paths.

Test S-07-6 began from a steady-state condition intended to simulate a reactor at full power. The system pressure was at 15.21 MPa, with the core generating  $1.97 \text{ MW}_{th}$ , and the system was at equilibrium. The simulation was run in a steady-state configuration (i.e., without the ECCS components and with the break assembly modeled as an unbroken straight pipe) for 20 seconds until the calculation achieved stable equilibrium conditions consistent with the test initial conditions. Table 2.14 compares measured steady-state test conditions with the calculated conditions at 20.0 seconds, just before blowdown was initiated.

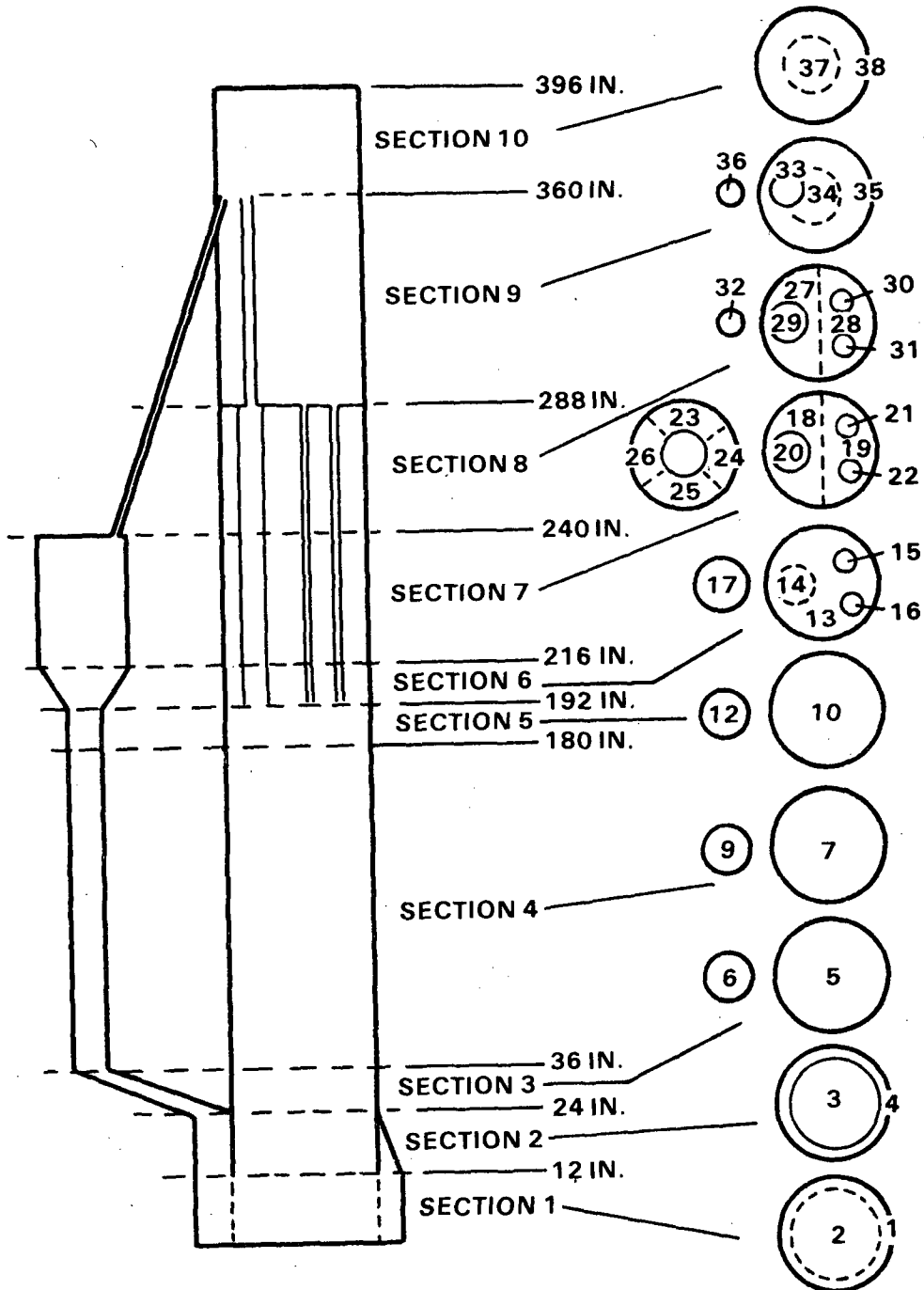


FIGURE 2.16-2. COBRA/TRAC Model of Semiscale Pressure Vessel and Downcomer for Test S-07-6

TABLE 2.14. Initial Conditions for Semiscale Test S-07-6

Parameter	Test Value	COBRA/TRAC Value (at 20 seconds)
Core power (MW)	1.97	1.94
System Pressure (MPa)	15.21 (2163 psia)	16.82 (2393 psia)
Cold leg temperature (K)		
Intact loop	559	559
Broken loop	558	562
Hot leg temperature (K)		
Intact loop	594.3	593.7
Broken loop	593.9	593.5
Loop Temperature Difference (K)		
Intact loop	35.3	34.6
Broken loop	35.9	31.4
Core volumetric flow rate (l/sec)	14.26	13.16

The blowdown was initiated by restarting the calculation with the broken loop cold leg component replaced by the break components modeled as shown in Figure 2.16-1 and the ECCS components added to the intact loop. Forcing functions on core power and the pump speed values were used to model the core power and pump behavior in the transient.

The steam generator secondaries were isolated at the initiation of blowdown. This was somewhat difficult to model accurately with the TRAC steam generator module. Even though the main feedwater was shut off, the secondary side of the steam generators continued to recirculate, providing an unknown, but not insignificant, secondary flow rate for heat transfer. This was modeled by providing a reduced but nonzero flow in the FILLS modeling the steam generator secondaries.

### 2.16.3 Discussion of Results

Results for the first 70 seconds of the calculation for S-07-6 are shown in Figures 2.16-3, 2.16-4 and 2.16-5. (In these graphs, the solid line is the calculation, the asterisks show the data points.) Figure 2.16-3 is a plot of

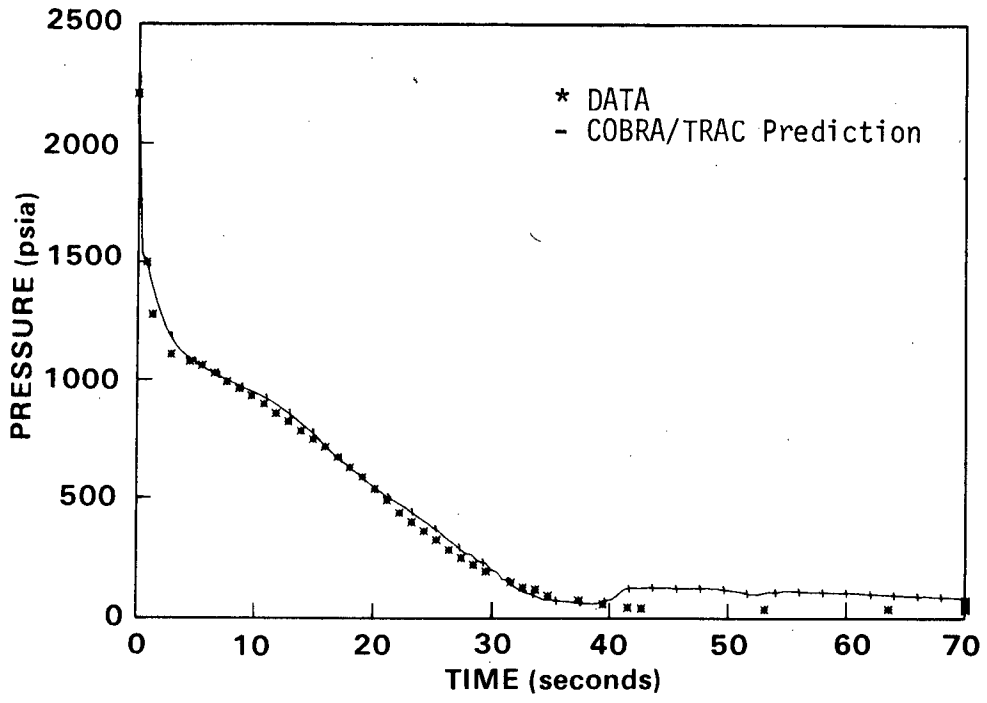


FIGURE 2.16-3. Upper Plenum Pressure

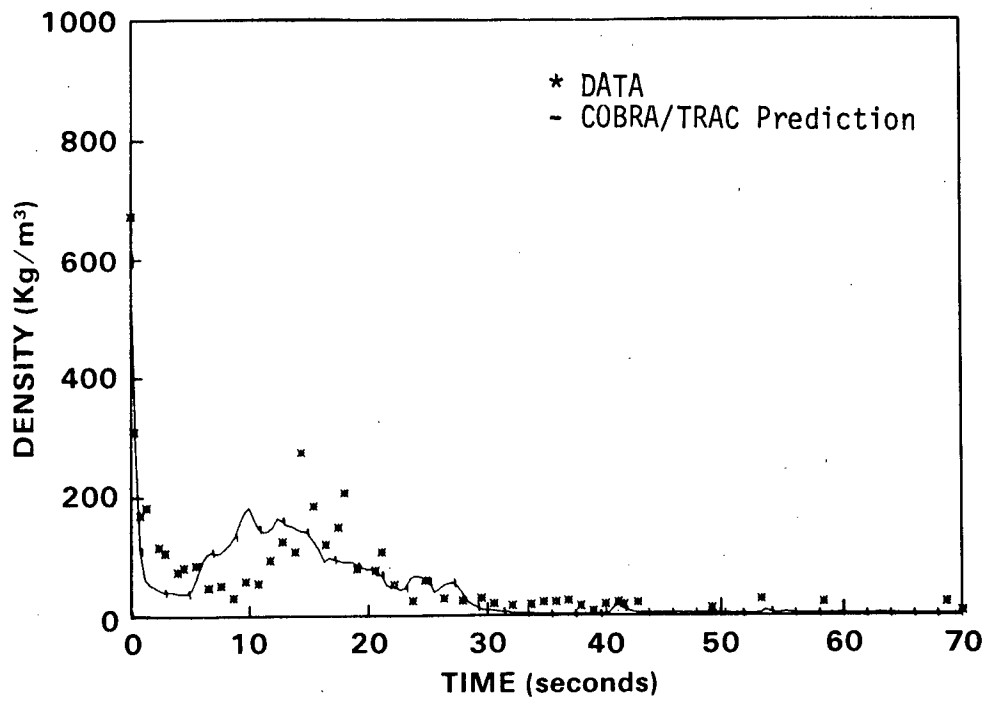


FIGURE 2.16-4. Density at Top of Core

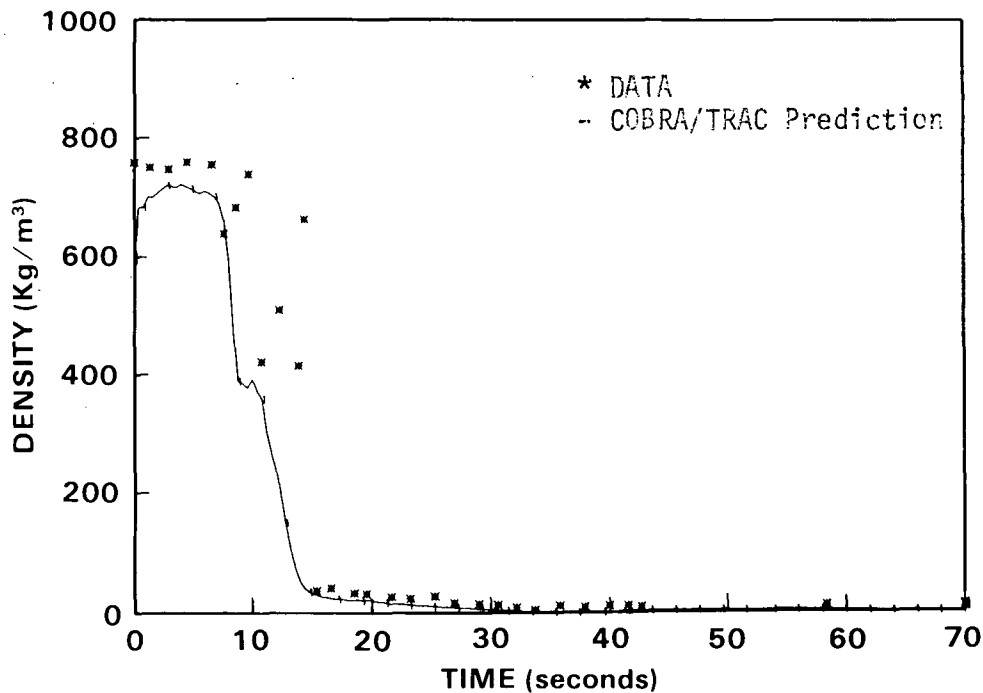


FIGURE 2.16-5. Density in Upper Head

the calculated pressure in the vessel upper plenum versus the measurements obtained in the experiment. In the blowdown portion of the transient, the calculation follows the data very well. After 40 seconds, however, errors in the input caused too much vapor to be generated by heat transfer from the hot walls in the downcomer, and the pressure was too high. Figure 2.16-4 is a plot of the density calculated at the top of the core-heated length compared with the measured values. The calculation is in good agreement with the data. A similar plot for density in the vessel upper head (Figure 2.16-5) is also in agreement with the data.

These results indicate that the COBRA/TRAC code is capable of calculating accurately the behavior of a system undergoing severe blowdown transients. Good data comparisons require that the system geometry and operating conditions be modeled correctly.

Developing an accurate and efficient model of the Semiscale system has proved to be nearly as important as solving the equations in the code correctly. The large heat transfer surface area-to-volume ratio makes the

system extremely sensitive to small errors in the modeling input, and the inadequate documentation of the Semiscale system has made construction of an accurate model difficult.

The results for the blowdown portion of the transient (i.e., out to 40 seconds) show that the code is calculating the two-phase hydrodynamics quite well. Later on, however, when the behavior in the downcomer is dominated by heat transfer from the walls, inaccuracies in the modeling result in the wrong heat transfer coefficients, and the calculation no longer matches the data. This simulation was run on cycle 10 of COBRA/TRAC.

## 2.17 SEMISCALE MOD2A TEST S-UT-2

Test S-UT-2 performed on Semiscale MOD-2A (Ref. 33) was designed to simulate the transient behavior of a scaled PWR system under a small break LOCA (SBLOCA) condition and to study the effects of having emergency core coolant (ECC) injected into the upper head. Test S-UT-2 was a small (10%) communicative cold leg break loss-of-coolant experiment performed with upper head injection. The data from this test was intended for use in assessment of computer codes developed for full-scale PWR transient calculations.

The purpose of the computer simulation of test S-UT-2 was two-fold. It verified the capability to model an integrated system with all representative loop components of a PWR present. In addition, it permitted study of the capability to predict the system response during a SBLOCA and the effects of upper head injection (UHI) on core behavior.

### 2.17.1 Description of Experiment

The MOD-2A system was designed as a small-scale model of the primary system of a four-loop PWR nuclear generating plant. The system incorporated the major components of a PWR, including steam generators, vessel, pumps, pressurizer and loop piping. The intact loop was scaled to simulate three loops in a PWR, while a broken loop simulated the single loop in which a break was postulated to occur. Geometric similarity was maintained between a PWR and MOD-2A, (e.g., in the design of a 25-rod, full-length (3.66-m) electrically heated core, a full length upper head and upper plenum, the component layout, and relative elevations of various components). Equipment in the upper head of the MOD-2A vessel was designed to simulate the fluid flow paths found in a PWR with the capability of injecting ECC into the upper head.

A diagram of the Semiscale Mod-2A system, as configured for Test S-UT-2, is shown in Figure 2.17-1 with major components identified. The break was located in the broken loop cold leg between the pump and the vessel and was communicative in nature. The break orifice is shown in detail in Figure 2.17-2. The break size was  $0.228 \text{ cm}^2$ , which is volumetrically scaled to represent 10% of the area of a cold leg pipe in a PWR. In order to be

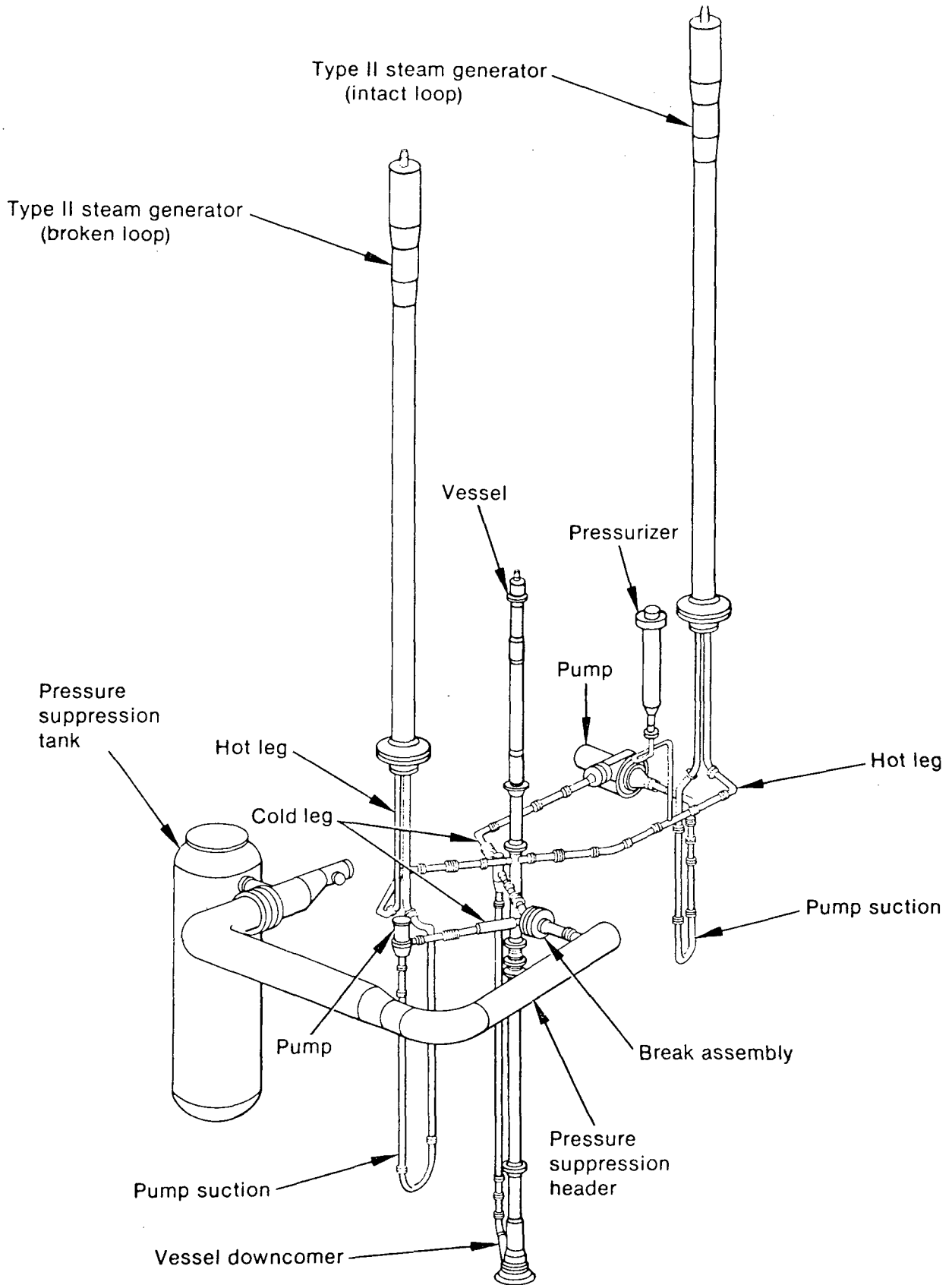
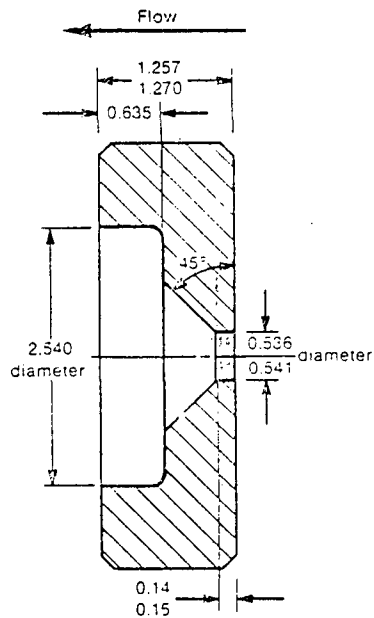


**FIGURE 2.17-1. Semiscale MOD-2A System for Small Break LOCA**



All dimensions in cm

FIGURE 2.17-2. Detail of Small Break Orifice in Test S-UT-2

representative of an orifice-like break in a PWR pipe, the orifice was designed as sharp-edged with a length-to-diameter ratio of 0.27.

Internally heated electric rods are used to simulate the nuclear rods of a PWR. The rods are geometrically similar to nuclear rods with a heated length of 3.66 m and an outside diameter of 1.072 cm. The axial power profile for the rods has a step cosine shape with a 1.55 peak-to-average power factor. Twenty-three heated rods were powered uniformly. Two diagonal rods were unpowered. The total core power was 1.91 MW which yielded a maximum linear heat generation rate of 35.19 kW/m. Penetrations into the upper head consist of a perforated ECC injection tube, a bypass line from the top of the downcomer, a simulated control rod guide tube, and two simulated support columns.

The test was initiated from steady state conditions by rupturing discs downstream of the break orifice to breach the system pressure boundary. Transient core power control and the intact and broken loop pump speed controllers were initiated by a pressure trip 1 sec after the pressurizer

pressure reached 12.41 MPa. The pressure suppression system (PSS) tank pressure was held initially at 1030 kPa, then ramped down to 280 kPa from 50 to 90 sec and held there for the remainder of the test. (This was done to keep the downstream drag screen measurement within range while keeping the flow choked at the break orifice.) Both intact and broken loop steam generator feedwater and steam valves were sequenced to close 1 sec after the pressurizer pressure reached 12.41 MPa.

The system pressure decreased continuously throughout the test. The high-pressure injection system (HPIS) pump began injecting ambient temperature water into the intact loop cold leg 2 sec after rupture. The system voided from the upper elevations downward, and by 200 sec the loops had cleared of liquid while liquid remained in the vessel and downcomer below the cold leg elevation. Between 30 and 90 sec, water in the pump suction of each loop formed a seal, preventing steam flow around the loops. This caused a depression of the vessel liquid level and a brief period of dryout and minor temperature excursions throughout most of the core. These hot spots were re-wet after the loop seals voided.

When the pressure dropped to 2.98 MPa at 345 sec, the intact loop accumulator began injecting water into the cold leg. Heater rod cladding temperatures followed system saturation temperature until the end of the test. The low pressure injection system (LPIS) began injecting water at 2395 sec at a system pressure of 1.15 MPa.

#### 2.17.2 COBRA/TRAC Model Description

Figure 2.17-3 shows the COBRA/TRAC model of the semiscale MOD-2A system used for Test S-UT-2. The intact and broken loops and the upper head injection systems were represented by one-dimensional components. The pressure vessel and downcomer was represented by a VESSEL component. The high pressure and low pressure injection systems were modeled as mass sources by two FILL components. The UHI system and intact loop accumulator were modeled by the ACCUM components. The steam generator model includes the primary side U-tube and the secondary side tube region. The steam separator, steam dome and downcomer were not explicitly modeled due to the limitation of the one-dimensional component steam generator model. To provide a reasonable

2.177

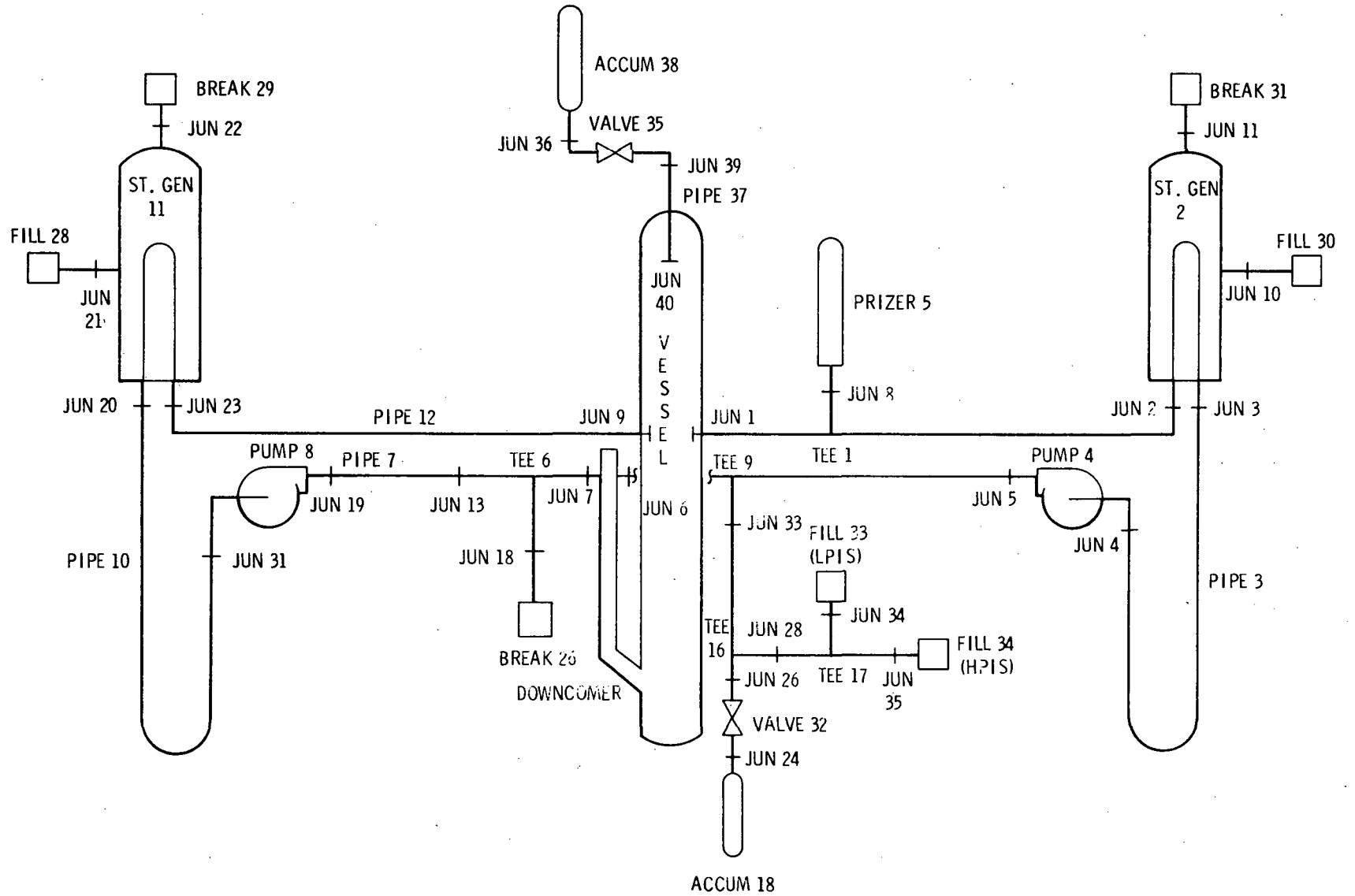


FIGURE 2.17-3. COBRA/TRAC Model of Semiscale MOD2A System

secondary side boundary condition, the feedwater flow rates and temperatures were adjusted to account for the recirculation flow. Steam discharge pressure histories were set to the measured values to minimize the errors associated with the heat transfer characteristics between the primary and secondary loops, since the downcomer and steam separator were not explicitly modeled.

Figure 2.17-4 shows the detailed noding diagram of the vessel component. The vessel is divided into 10 vertical sections. Section 1 models the lower plenum which contains two channels (1 and 2) separated by a gap (G1). Channel 1 is an annular volume that connects to the downcomer and channel 2 is directly below the core.

Sections 2 and 3 model the core inlet and lower part of the downcomer. Section 2 contains channels 3 and 4 and rods 3 and 4. The rods are modeled to account for heat transfer through the metal walls and insulation liners. Section 4 contains the vessel core, the heated rods inside the core and the downcomer. Section 5 models the upper core plate. Sections 6, 7 and 8 model the upper plenum, downcomer inlet and downcomer bypass line. The two support columns are modeled by a single channel (channels 15, 21 and 30 stacked one on top the other through sections 6, 7 and 8). Channel 15 communicates with the core at the lower end of the support column, and channel 30 with the upper head at the upper end. The guide tube is modeled by stacking channels 14, 20, 29 and 33. It also communicates with the core at the lower end. Its open upper end is inside the upper head.

Sections 9 and 10 model the upper head. Channels 35 and 38 represent the upper head injection (UHI) tube. The tube is perforated to allow water from the UHI accumulator to be injected into the upper head. These openings are modeled by gaps 4 and 5.

Except through guide tube and support columns, there is no connection for fluid flow between channels 27 and 34. The noding for the break nozzle is shown in Figure 2.17-5.

### 2.17.3 Discussion of Results

With the given core power level, pressurizer saturation temperature, pump speed and steam generator secondary boundary conditions as input, the calculation was started. Steady-state conditions were assumed to be

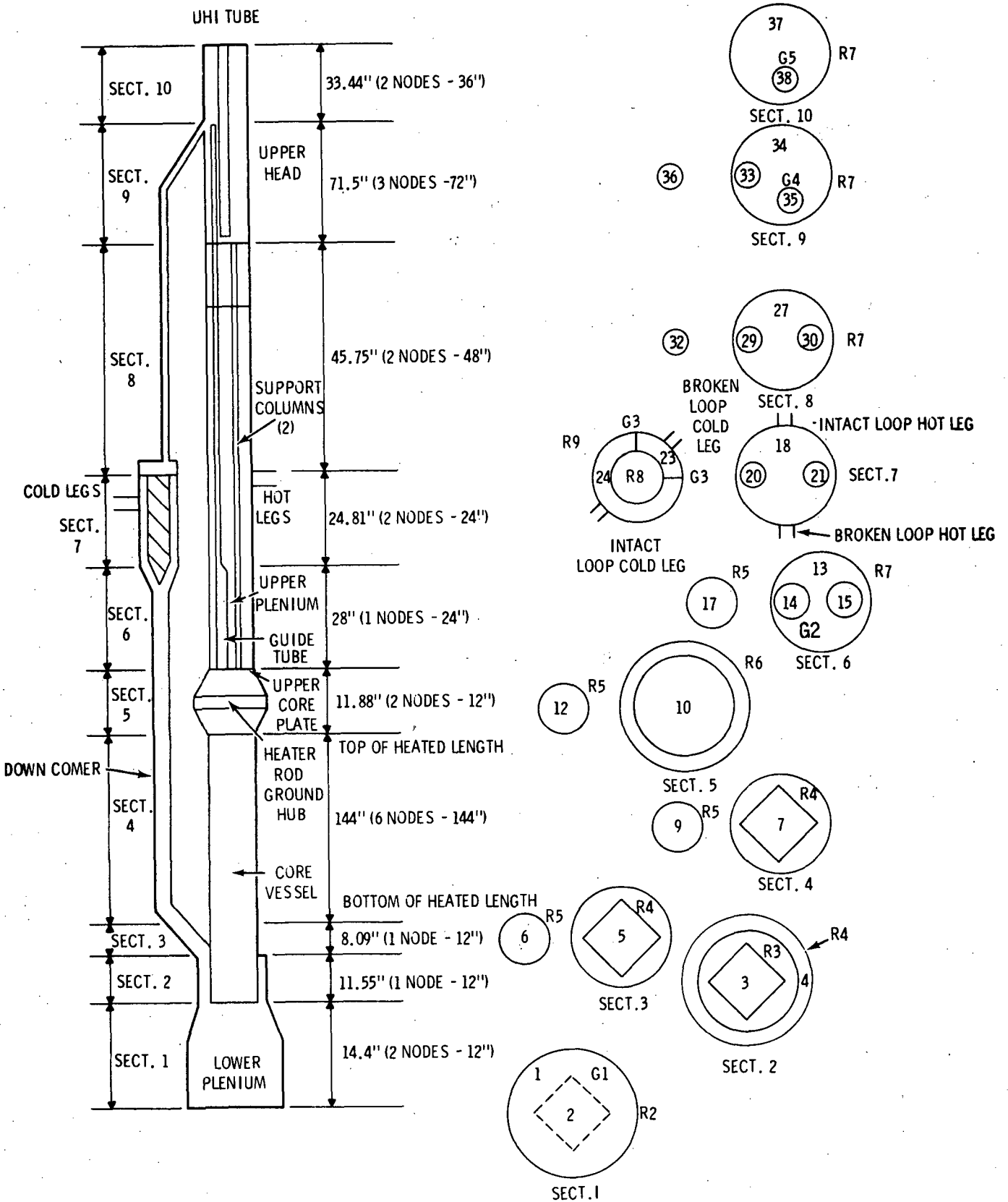


**FIGURE 2.17-4. COBRA/TRAC Model of Semiscale Pressure Vessel and Downcomer for Test S-UT-2**

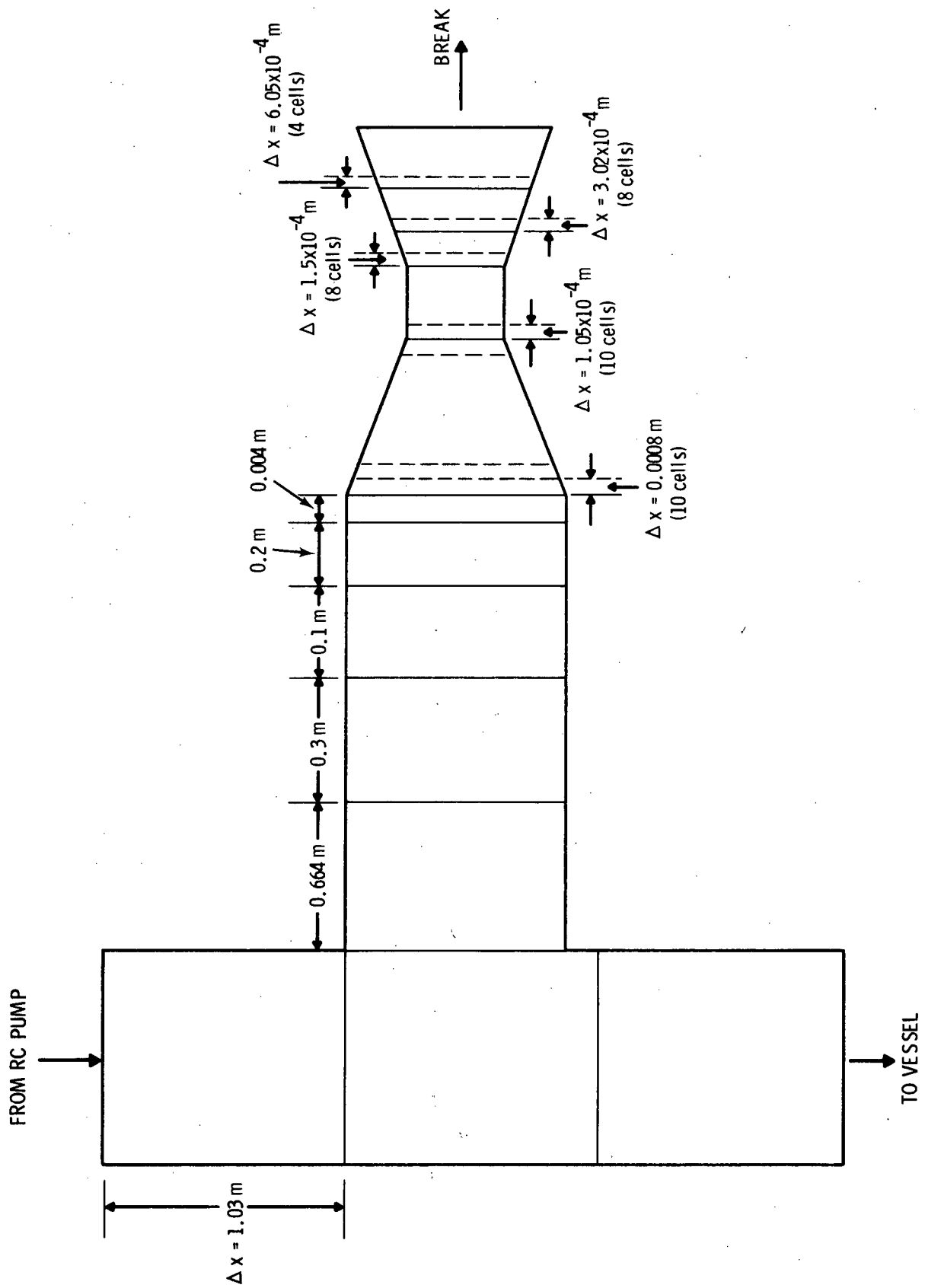


FIGURE 2.17-5. COBRA/TRAC Noding of Break Nozzle

established when all major parameters reached steady values. The steady-state parameters established before the blowdown was started are listed in Table 2.15.

The calculated steady-state values do not exactly match the measured values. It is believed that the discrepancies were caused by the modeling of the steam generators. The steam generators were modeled without the steam separator and downcomer, therefore errors in the computed recirculation rate caused errors in the prediction of the temperature drop across the U-tubes. This caused errors in the core enthalpy and flow rate. The system pressure mismatch was apparently caused by the pressurizer modeling.

After steady-state conditions were established, the blowdown was started. The calculated results are given in Figures 2.17-6 through 2.17-12.

Figure 2.17-6 gives the system pressure as a function of time. The calculated pressure follows the initial rapid depressurization with reasonable accuracy. After the initial depressurization, the curve starts to diverge gradually from the measured values, and the calculation gives a higher pressure as the transient progresses. This deviation is due to an incorrect prediction of the break mass flow rate predicted by TRAC.

Figure 2.17-7 gives the collapsed liquid level in the vessel downcomer as a function of time. The shift relative to the measured data is probably due to too much heat transfer from the steam generator secondary to the primary side; i.e., higher system pressure, which suppresses the core liquid level through hot leg connections and keeps the downcomer liquid high for a longer period. However, the decrease of downcomer liquid level from pump seal clearing and subsequent liquid level equalization with the core were predicted in the calculated results.

The pump suction clearing occurred at about 120 sec for the broken loop and 230 sec for the intact loop; compared to about 90 sec for both loops from measurements. This also contributed to the delayed behavior of the downcomer liquid level history.

TABLE 2.15. Initial Conditions for Semiscale Test S-UT-2

	<u>COBRA/TRAC</u> <u>Value (at 20s)</u>	<u>Test</u> <u>Value</u>
System pressure (psia)	2310	2250
Core inlet flow ( $lb_m/s$ )	21.4	23.2
Core $\Delta H$ (Btu/ $lb_m$ )	82.6	78.2
Intact loop steam generator primary side $\Delta T$ (K)	28.8	34.1
Broken loop steam generator primary side $\Delta T$ (K)	35.0	31.6

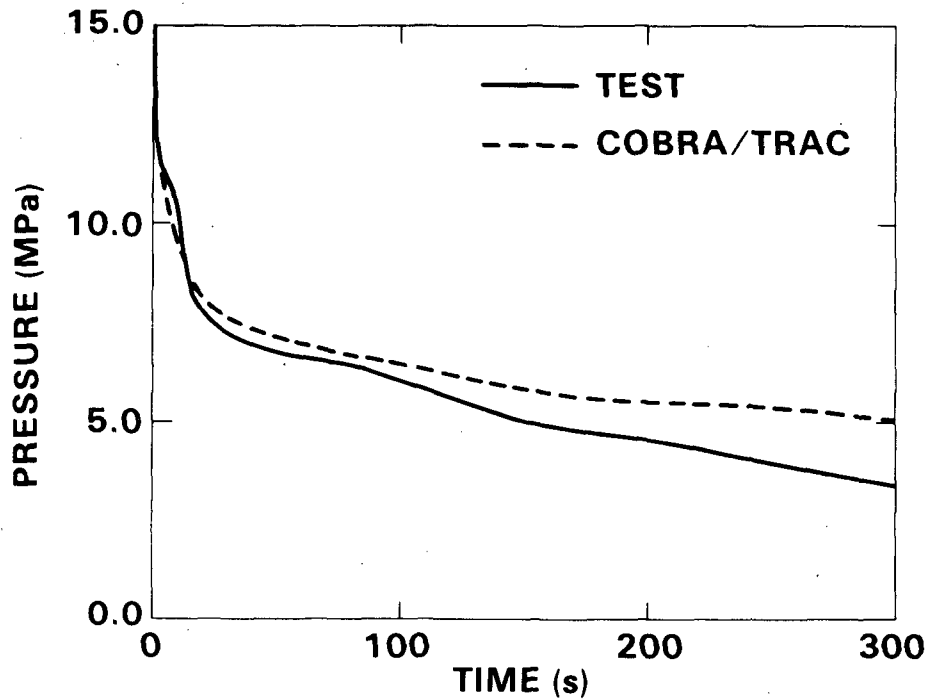


FIGURE 2.17-6. System Pressure

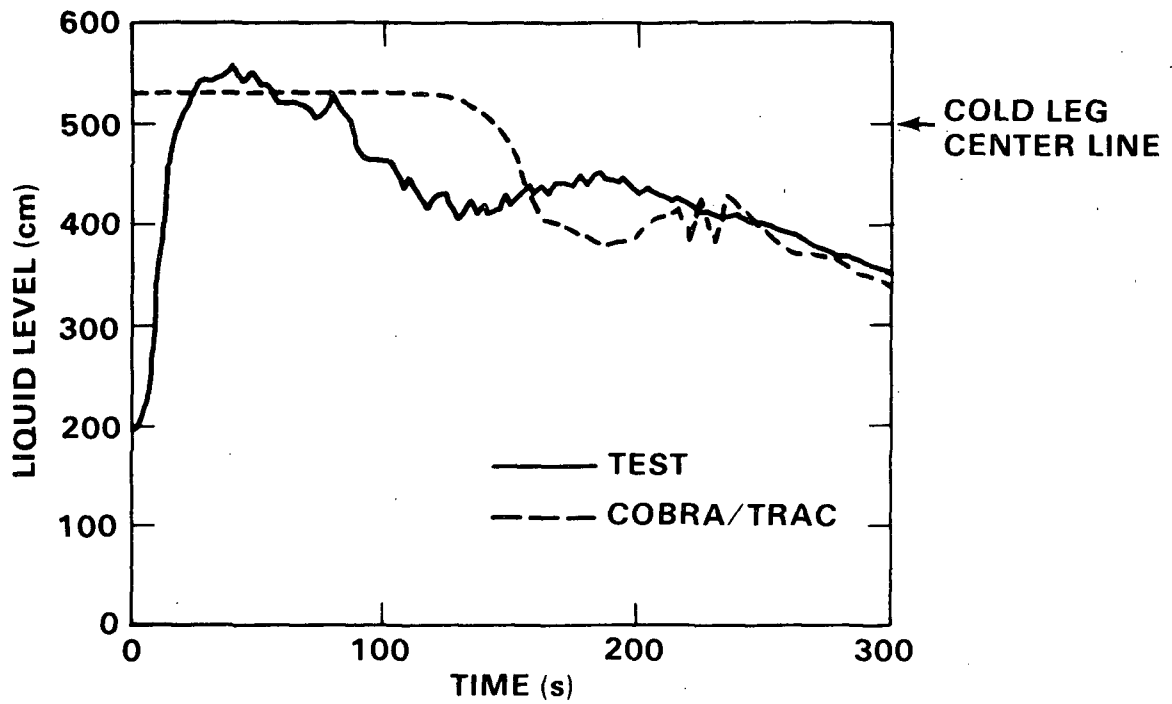


FIGURE 2.17-7. Collapsed Liquid Level in Semiscale Downcomer Pipe

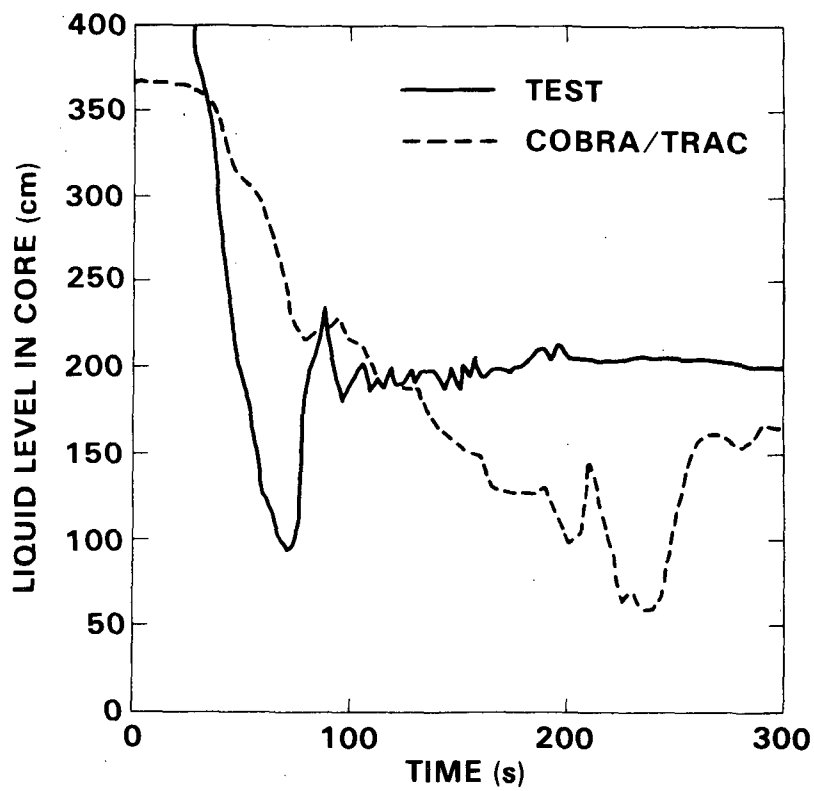


FIGURE 2.17-8. Collapsed Liquid Level in Semiscale Core

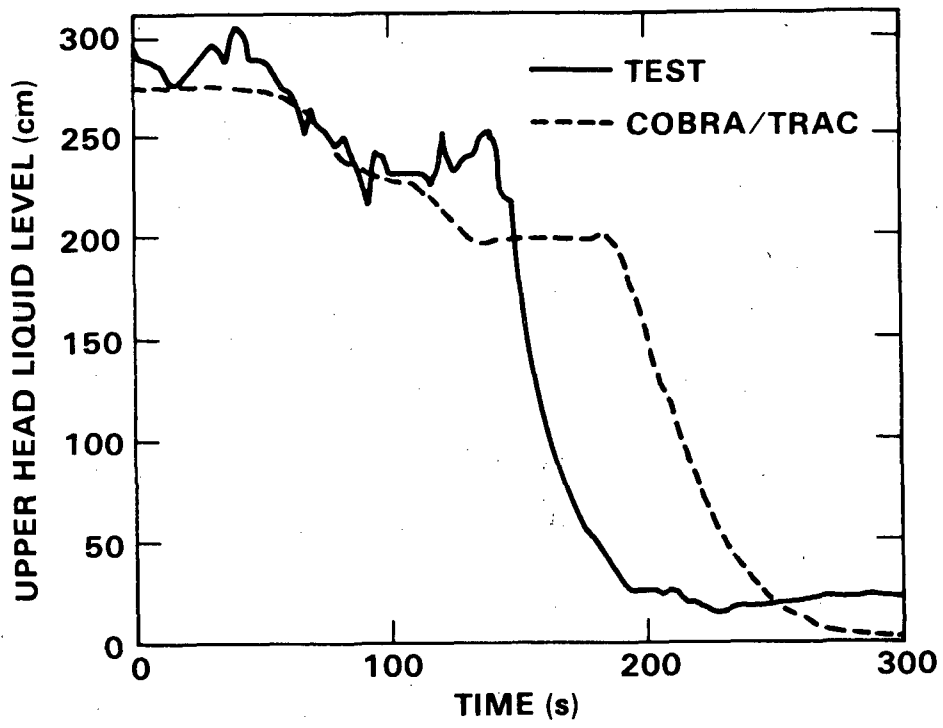


FIGURE 2.17-9. Collapsed Liquid Level in Upper Head

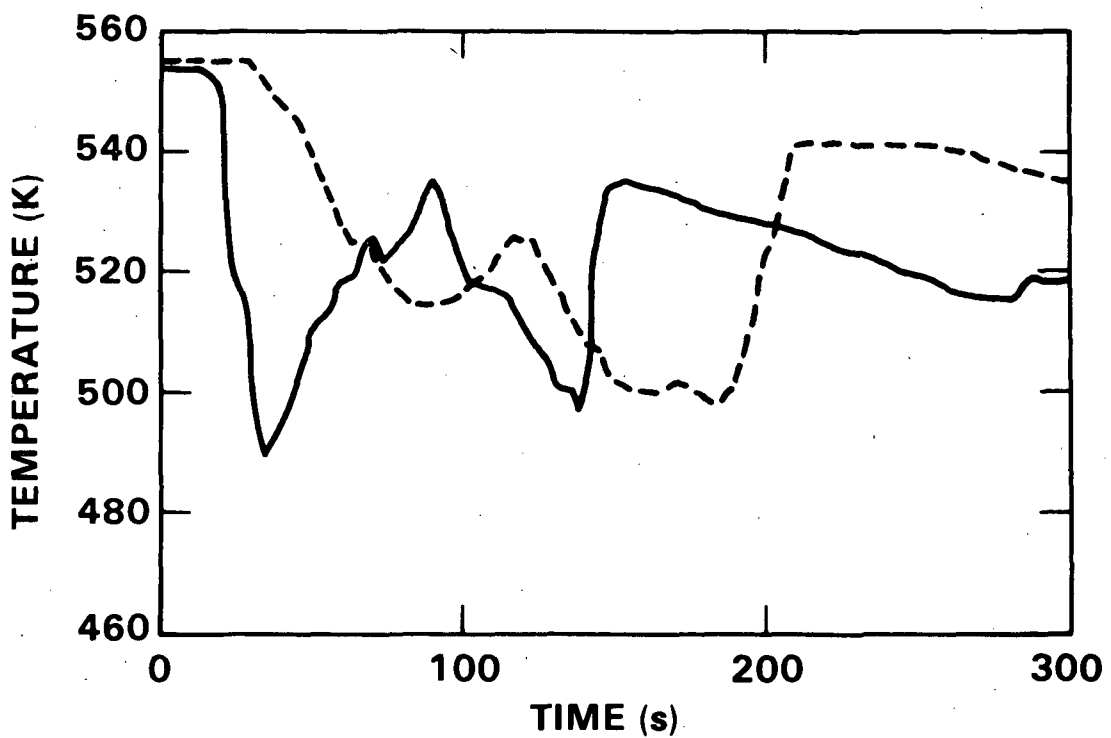


FIGURE 2.17-10. Upper Head Fluid Temperature

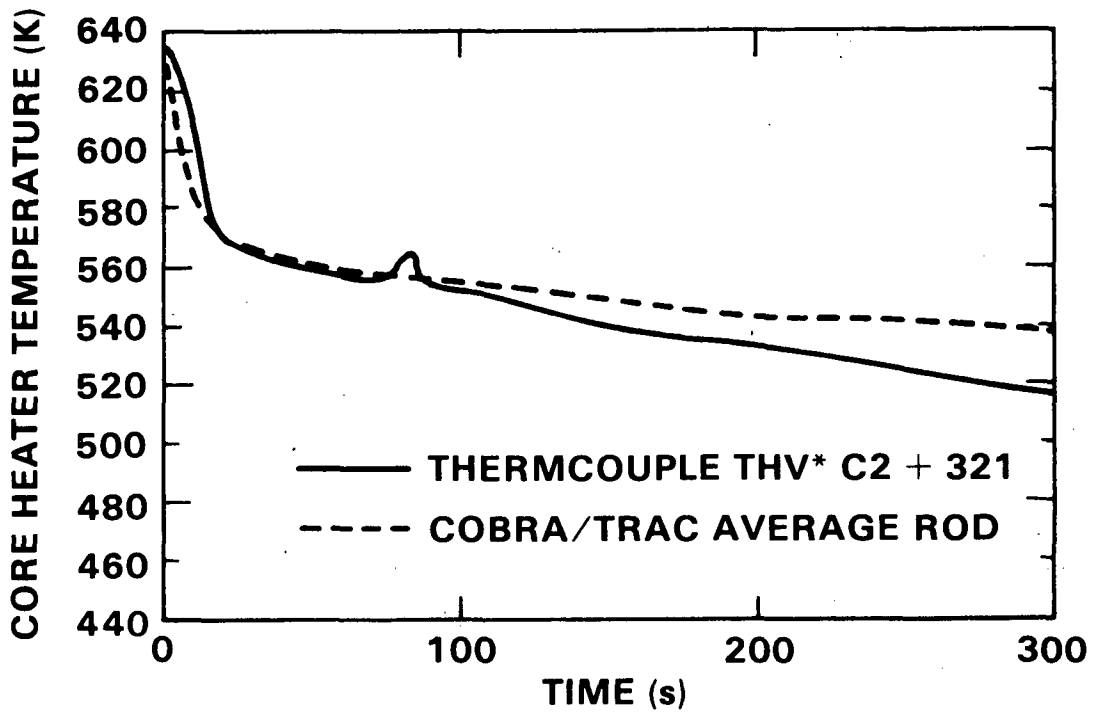


FIGURE 2.17-11. Rod Temperature at the Core Mid-Plane

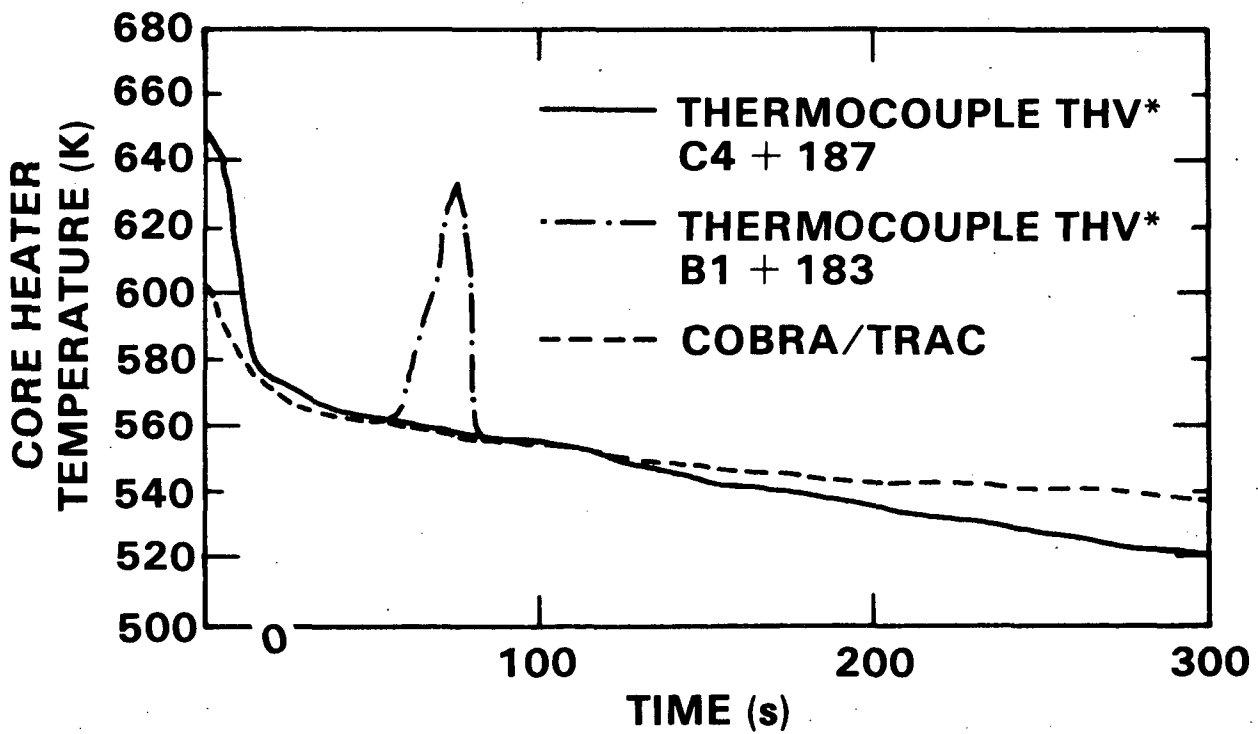


FIGURE 2.17-12. Rod Temperature Near Top of Core

Figure 2.17-8 gives the core liquid level as a function of time. COBRA/TRAC calculated more liquid in the core than the test showed because of the higher heat transfer from the steam generators and the delayed pump suction clearing. In addition, the core level recovery due to clearing of pump suction occurred late in the transient. The higher liquid level from the beginning of blowdown up to 100 sec is mainly due to the slower blowdown caused by high energy input from the steam generators and a poor break flow prediction. Figure 2.17-9 gives the upper head liquid level. In this region, the calculation follows the measurements reasonably well. The higher system pressure resulted in a slower and longer drain of the upper head accumulator (the accumulator injection was terminated at about 185 sec instead of the measured 140 sec), causing the delayed drop shown in the curve. Figure 2.17-10 gives the upper head fluid temperature as a function of time. The temperatures were plotted for the fluid at 122 cm above the bottom of the upper head. Condensation due to the cold UHI water and subsequent heatup due to the steam upflow from the guide tube are illustrated by the repeated fluctuations in the fluid temperature. The fluid temperature after UHI was terminated essentially followed the saturation temperature curve. Because of the higher system pressure, the fluid temperature is also higher during this period.

Figures 2.17-11 and 1.17-12 give the heater rod clad temperatures at two different elevations, one at about the mid-plane, another close to the outlet. Comparisons were made between an average rod as calculated by COBRA/TRAC and thermocouple measurements of selected rods. Again the trend is consistent with the calculated higher system pressure. In the thermocouple measurements some rods experienced dryout and others did not. The code calculation for the average rod did not show dryout. There are two possible causes for this inconsistency. The CHF correlations in the code may not be adequate for the calculations of the dryout heat transfer. This, however, is unlikely because the code has been tested on other sample cases and showed good comparison on rod temperature calculations under similar conditions. Another possibility is that because of the calculated slower blowdown there was a sufficient inventory of liquid inside the core to prevent the dryout from occurring.

Different cell arrangements in the break nozzle were tested. Some with more cells than the one presented in Figure 2.17-5, some with less. All of them gave about the same amount of break flow during the initial stage of blowdown. Therefore, the prediction of break flow is a result of modeling deficiencies in the TRAC implicit pipe component and not in the nodalization at the break.

It was found that lowering the secondary feedwater temperature in the steam generator (below  $T_{sat}$ ) increased the core maximum uncoverly. In the current one-dimensional steam generator model, the feedwater temperature input is fixed rather than a function of time, and the recirculation flow is input rather than consistently calculated. The inaccuracies this introduced in the calculation may have caused the calculated core liquid level to differ from the measured value.

In general, given the constraints of modeling the steam generators and the break flow the results from the COBRA/TRAC calculation produced the correct trends of the data. Important phenomena such as pump suction clearing, upper head condensation and heatup, the downcomer liquid level equalization, and the core liquid level recovery, were demonstrated by the calculation. The shifted (with respect to time) behavior of different components all could be explained by the heat transfer deviations from secondary to primary loops due to the steam generator model and by the error in the calculated break mass flow rate.

To correct the deficiency caused by the simplified steam generator model, the same simulation has been repeated with the one-dimensional steam generator model replaced by a three-dimensional model using the VESSEL module. The VESSEL module is capable of explicitly simulating the steam generator downcomer, the steam dome and the steam separator. With this improvement, the heat balance between the primary and secondary loops during transient should be calculated more accurately. A new break model has also been implemented that should provide an improved prediction of break mass flow. Results of this more recent calculation will be reported in a different document. This simulation was run on cycle 8.

## 2.18 WESTINGHOUSE UPPER HEAD DRAIN TEST

The Westinghouse Drain Test facility was designed to simulate the upper head of a pressurized water reactor (PWR) vessel with upper head injection (UHI). A COBRA/TRAC simulation of the drain test assessed the code's ability to predict upper head draining in a UHI system. Performance was evaluated by comparing the calculated draining rate, temperature and pressure with experimentally measured proprietary data. The results of this simulation were used to develop the model for the upper head for simulation of a PWR vessel with UHI.

### 2.18.1 Description of Experiment

The UHI reactor vessel was designed to deliver water to the upper head of the vessel during a loss-of-coolant accident. The objective of the Westinghouse Drain Test was to demonstrate that the upper head will drain of water. Designers predict that the hydrostatic head forces water from the upper head into the core. At the same time, steam flows from the core and upper plenum through the control rod guide tubes to the upper head of the vessel.

The Westinghouse Drain Test facility consisted of a full-scale PWR guide tube with the upper plenum, upper head volume and support columns to simulate the vessel on a per guide tube basis. Two pipes were used as the support columns. The pipes were orificed to simulate one full-scale and one-half scale support column since a PWR vessel contains one and one-half support columns per guide tube. A steam chamber simulated the upper plenum of the core during the reflood stage of a loss-of-coolant accident. Saturation conditions were maintained by a continuous flow of steam through the chamber. A check valve in the exhaust line prevented air from entering the test section during testing.

The upper head and support columns were initially filled with subcooled water. A plug valve at the top of the guide tube and flapper valves at the bottom of the support columns were opened simultaneously to begin the test. Water from the upper head drained through the support column to the upper plenum as steam from the upper plenum rose through the guide tube to the top.

of the upper head. The test was terminated when the water level in the upper head reached the top of the support columns.

### 2.18.2 COBRA/TRAC Model Description

Although only the vessel component was needed in this simulation a PIPE component is required in every COBRA/TRAC model. The pipe in this model connected a FILL component to the top of the vessel component. A zero velocity boundary condition on the FILL component prevented flow through the pipe. The net effect of the PIPE component was to add 0.03% to the volume of the upper head.

Thermal non-equilibrium was an important feature in this simulation because saturated steam comes into contact with subcooled water at the top of the guide tube. Heat transfer to the wall of the vessel was ignored. The carbon steel test section was heated with steam flow before each test, and the test was completed in a relatively short period of time. Heat transfer between the wall and the fluid was negligible.

The COBRA/TRAC model of the Westinghouse Drain Facility consisted of 28 cells in five channels. A schematic diagram of the model is shown in Figure 2.18-1. Channels 1 and 3 model the guide tube. Area changes due to intermediate guide plates were modeled by loss coefficients. The loss coefficients used were calculated from the area change, thickness of orifice and hydraulic diameter of the channel. The full and half-scale support columns were combined into channel 2. The flow area of the channel was the sum of the flow areas for the two support column tubes.

Since two support columns were being modeled by one channel, the loss coefficients for the support columns were combined. Each support column had an experimentally measured loss coefficient. The loss coefficient for input was calculated to produce the same pressure drop for the same total mass flow through the two support columns. Channels 4 and 5 modeled the upper head. A pressure and enthalpy boundary condition below channels 1 and 2 modeled the steam chamber of the test facility.

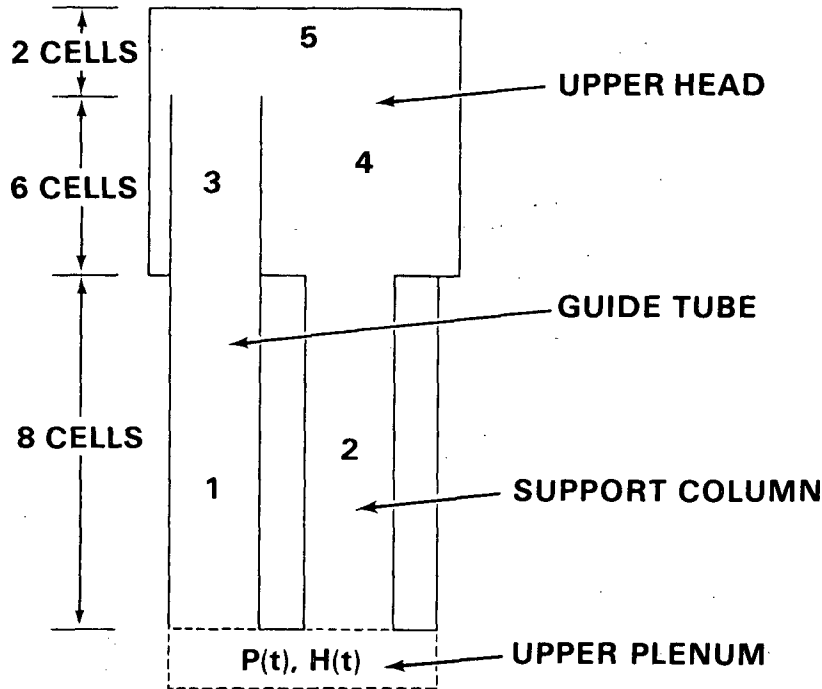
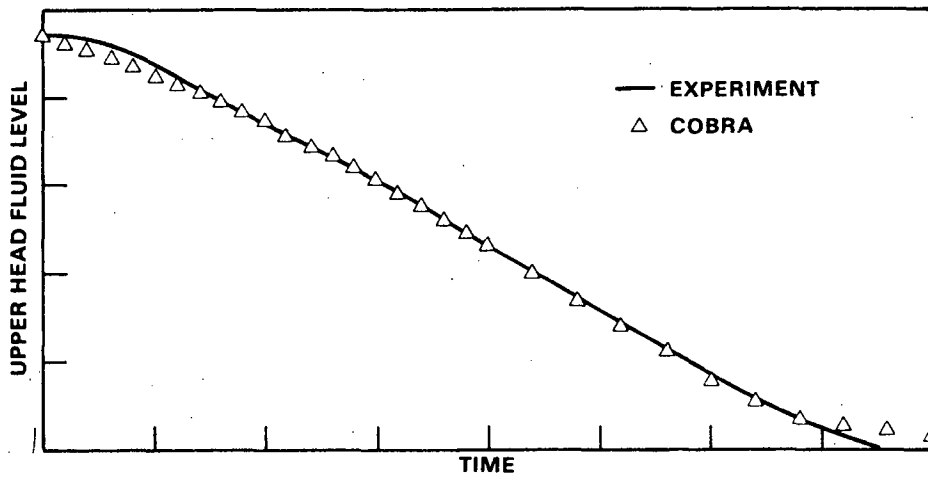


FIGURE 2.18-1. COBRA/TRAC Model of Westinghouse Upper Head Test Section

### 2.18.3 Discussion of Results

COBRA/TRAC calculations of drain rate, temperature at the top of the support columns, and pressure at the top of the guide tube are compared with measured data from the Westinghouse Drain Test in Figures 2.18-2, 2.18-3 and 2.18-4. (The numbers have been removed from the axes because the information is proprietary.)

Drain rate is reported as upper head fluid level versus time in Figure 2.18-2. The maximum difference between calculated and measured fluid level is 3% of the initial level at the beginning of the transient. Approximately half of the difference is accounted for by a small amount of liquid that fell into the guide tube at the beginning of the transient. Liquid fell into the guide tube because the orifice at the top of the guide tube was modeled by a loss coefficient without an area reduction. The loss coefficient provided the right pressure drop, but the velocity was wrong. The calculated vapor velocity out the top of the guide tube was much lower than that in the experiment. The lower velocity allowed a small amount of



**FIGURE 2.18-2.** Westinghouse Drain Test #5; Upper Head Liquid Level vs. Time

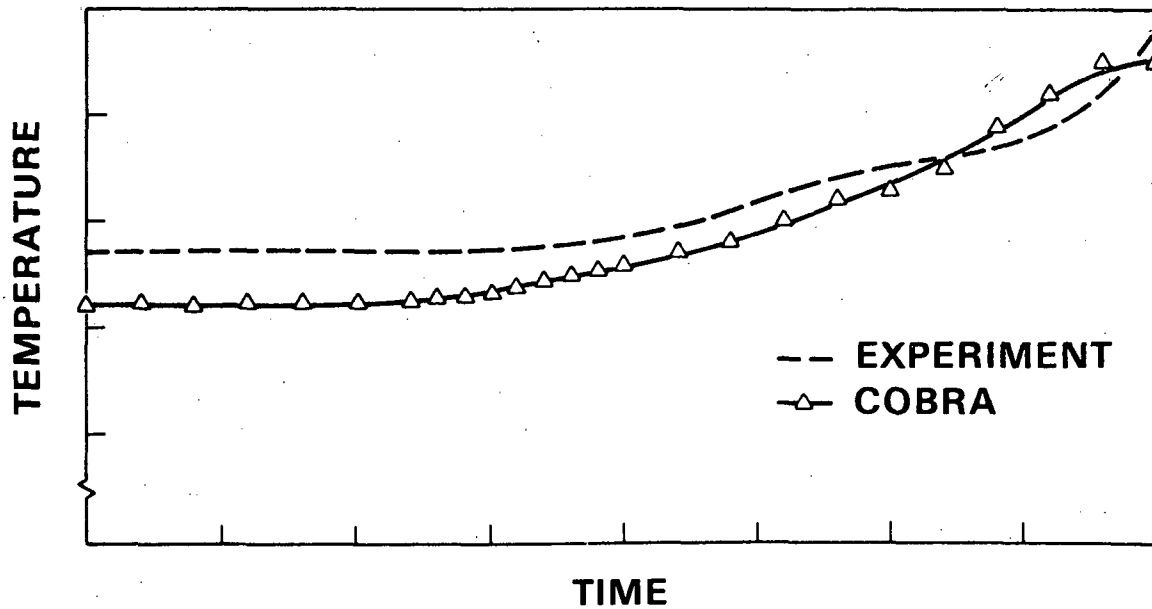


**FIGURE 2.18-3.** Westinghouse Drain Test #5; Fluid Temperature at Top of Support Columns

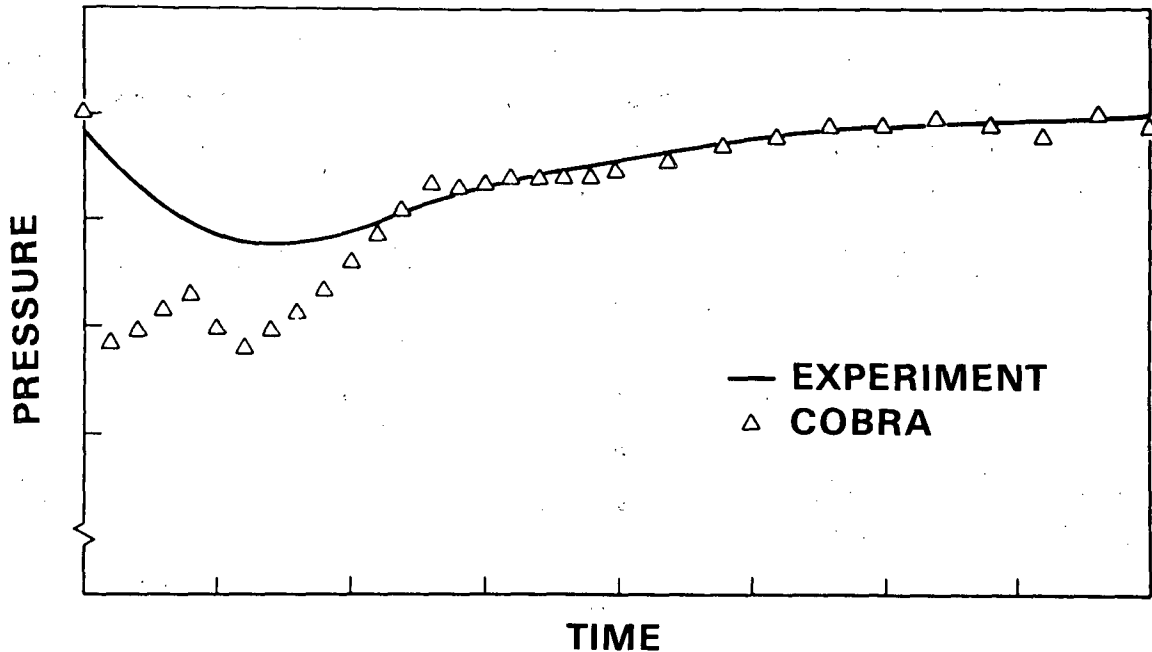


FIGURE 2.18-4. Westinghouse Drain Test #5; Pressure at Top of Guide Tube

liquid to fall into the guide tube. An area variation can be used to model the orifice, but the increase in vapor velocity would severely limit the time step size.

Figure 2.18-3 shows the fluid temperature at the top of the support columns as a function of time. The maximum difference between measured and calculated temperature is 5°F at test initiation. The reason for the difference is a 10°F temperature gradient from the top to the bottom of the upper head. COBRA/TRAC was initialized with the average upper head liquid temperature. The temperature at the top of the support columns was actually 5°F higher than the average temperature. The calculated temperature approached the measured temperature as the transient proceeded.

Pressure at the top of the guide tube is shown in Figure 2.18-4. The calculation of pressure over the first third of the transient does not agree with the measured pressure. The maximum difference between measured and calculated values is 21%. The difference is caused by the location of the pressure measuring device in the upper head. The pressure tap was located at the top of the upper head directly above the support columns. COBRA/TRAC

computes the pressure above the guide tube as an average over the entire area of the upper head. Since saturated steam was condensing in the subcooled liquid of the upper head it is likely that a local pressure in the upper head is considerably different than an averaged value.

The liquid level was below the top of the guide tube in the final two-thirds of the transient. Condensation no longer played a significant role in determining the pressure above the guide tube. Figure 2.18-4 shows that when the liquid level fell below the top of the guide tube the measured and calculated pressures above the guide tube agreed well. The maximum difference between measured and calculated pressure above the guide tube in the final two-thirds of the transient was less than 2%.

The calculation of drain rate, pressure and temperature in the upper head agrees well with measured data from the Westinghouse Drain Test. These results indicate that the model used in this simulation can predict the behavior of upper head draining in the simulation of a complete PWR with UHI.



## REFERENCES

1. Liles, D. R., et al., Los Alamos Scientific Laboratory, "TRAC-PD2, An Advanced Best Estimate Computer Program for PWR LOCA Analysis," USNR Report NUREG/CR-2054, April 1981.
2. Lovell, T. W., "The Effect of Scale on Two-Phase Countercurrent Flow Flooding in Vertical Tubes," M.S. Thesis, Thayer School of Engineering, Dartmouth College, Hanover, New Hampshire, June 1977.
3. Hsieh C., S. G. Bankoff, R. S. Tankin and M. C. Yuen, "Countercurrent Air/Water and Steam/Water Flow above a Perforated Plate," Final Report, NUREG/CR-1808, Northwestern University, November 1980.
4. Crowley, C. J. and J. A. Block and C. N. Cary, Downcomer Effects in a 1/15-Scale PWR Geometry, Experimental Data Report, CREARE, Inc., NUREG-0281, 1977.
5. Carbiener, W. A., et al., Steam-Water Mixing and System Hydrodynamics Program Quarterly Progress Report, July 1 - September 30, 1977, BMI-NUREG-1987, Battelle-Columbus Laboratories, Columbus, Ohio, 1977.
6. Carbiener, W. A., et al., Steam-Water Mixing and System Hydrodynamics Program, Quarterly Progress Report, January 1 - March 31, 1977, BMI-NUREG-1972, Battelle Columbus Laboratories, Columbus, Ohio, 1977.
7. Collier, R. P., et al., Steam-Water Mixing and System Hydrodynamics Program, Quarterly Progress Report, July 1 - September 30, 1977, NUREG/CR-0526, BMI-2011, Battelle-Columbus Laboratories, Columbus, Ohio, 1978.
8. Rust, K. and P. Ihle, Warmeübergang und KuhlmitteIstromung beim Fluten blockierter Anordnungen, Kernforschungszentrum Karlsruhe, Republic of West Germany, 1980.
9. Ihle, P., Flooding Experiments in Blocked Arrays, FEBA, Recent Results and Future Plans, presented at the Eighth Water Reactor Safety Research Information Meeting, October 27-31, 1980, Gaithersburg, Maryland, 1980.
10. Rosal, E. R., L. E. Hochreiter, and M. F. McGuire, "FLECHT Low Flooding Rate Cosine Test Series Data Report," WCAP-8651, Westinghouse Electric Corporation, 1975.
11. Rosal, E. R., C. E. Conway, and M. C. Kocpinevich, "FLECHT Low Flooding Rate Skewed Test Series Data Report," WCAP-9108, Westinghouse Electric Corporation, 1977.
12. Phillips, L. E., letter to U. S. Standard Problem Participants transmitting "Standard Problem No. 9 (FLECHT-SEASET) Specification Report." Nuclear Regulatory Commission, 1979.

13. Hochreiter, L. E., et al., Power FLECHT-SEASET Unblocked Bundle, Forced and Gravity Reflood Task: Task Plan Report. NRC/EPRI/Westinghouse Report No. 3, 1978.
14. Mohr, C. L., et al., "Prototypic Thermal-Hydraulic Experiment in NRU to Simulate Loss-of-Coolant Accidents," PNL-3681 NUREG/CR-1882, Pacific Northwest Laboratory, Richland, Washington, 1980.
15. Mohr, C. L., et al., "Loss-of-Coolant Accident Simulations in the National Research Universal Reactor, Safety Analysis Report," PNL-3093 NUREG/CR-1208, Pacific Northwest Laboratory, Richland, Washington, 1981.
16. Banner, J. O., et al., Materials Test-2 LOCA Simulation in the NRU Reactor. NUREG/CR-2509, PNL-4155. Pacific Northwest Laboratory, Richland, Washington. Prepared for U.S. Nuclear Regulatory Commission, 1982.
17. Russcher, G. E., et al., LOCA Simulation in the NRU Reactor: Materials Test-1. NUREG/CR-2152, PNL-3835. Pacific Northwest Laboratory, Richland, Washington, Prepared for the U.S. Nuclear Regulatory Commission, 1981.
18. Brand, B., R. Kirmse, and W. Winkler, Refill and Reflood Experiment in a Simulated PWR Primary System (PKL). Specification, 1979. OECD-CSNI LOCA Standard Problem No. 10. Kraftwerk Union Report R513.
19. Brand, B., R. Mandl, and H. Schmidt, PKL Refill and Reflood Experiment Selected Results from Test K9, 1979, Kraftwerk Union Report R51/22/79.
20. Kirmse, R. E., Status of PKL Activities. Presented at 6th Meeting of the CSNI Working Group on Emergency Core Cooling in Water Reactors, 1979.
21. Hirano, K., et al., "Quick-Look Report on Large Scale Reflood Test-2 - CCTF C1-2 (Run 011)," JAERI-memo 8530, Japan Atomic Energy Research Institute, October 1979.
22. Cook, D. H., Local Condensation Rates for the Countercurrent Stratified Flow of Steam and Water in a Vertical Channel, M. S. Thesis, Northwestern University, Evanston, Illinois, 1979.
23. Lahey, R. T. Jr., Two-Phase Phenomena in Nuclear Reactor Technology. Quarterly Progress Report No. 8, NUREG/CR-0418, Rensselaer Polytechnic Institute, Troy, New York, 1978.
24. Serizawa, A., et al., "Turbulent Structure of Air-Water Bubbly Flow-II. Local Properties." Int. J. Multiphase Flow. 2(3):235-246, 1976.
25. Lahey, R. T. Jr., et al., Subchannel and Pressure Drop Measurements in a Nine-Rod Bundle for Diabatic and Adiabatic Conditions. Technical Report No. GEAP-13049, General Electric Company, San Jose, California, 1970.

26. Sim, S. K., Analysis of Phase Distribution Mechanisms in Turbulent Two-Phase Pipe Flow. M. S. Thesis, Rensselaer Polytechnic Institute, Troy, New York, 1977.
27. Bennett, A. W., et al., Heat Transfer to Steam-Water Mixtures Flowing in Uniformly Heated Tubes in Which the Critical Heat Flux has Been Exceeded. UKAEA Report No. AERE-R5373, 1967.
28. Nylund, O., et al., Hydrodynamic and Heat Transfer Measure on a Full Scale Simulated 36-Rod Marviken Fuel Element with Uniform Heat Flux Distribution. ASEA and AB Atomenergi Report FRIGG-2, R4-447/RTL-1007, 1968.
29. Henstock, W. H., and T. J. Hanratty, "The Interfacial Drag and the Height of the Wall Layer in Annular Flows." AICHE Journal, Vol. 22, No. 6, pp. 990-1000, 1976.
30. Wallis, G. B., "Annular Two-Phase Flow, Part I: Simple Theory," Journal of Basic Engineering, (March 1970).
31. Dukler, A. E., Flow Regime Transitions for Vertical Upward Gas Liquid Flow: A Preliminary Approach Through Physical Modeling. NUREG-0214, Progress Report, 1977.
32. Esparza, V., et al., Experiment Data Report for Semiscale MOD-3 Integral Blowdown and Reflood Heat Transfer Test S-07-6 (Baseline Test Series), NUREG/CR-0467, TREE-1226, EG&G Idaho, Inc., Idaho National Engineering Laboratory, prepared for U.S. Nuclear Regulatory Commission and U.S. Department of Energy, January 1979.
33. Blakely, J. E. et al., "Quick Look Report for Semiscale MOD-2A Test S-UT-2", EG&G-SEMI-5333, Idaho National Engineering Laboratory, 1981.



APPENDIX A

DESCRIPTION OF CODE VERSIONS

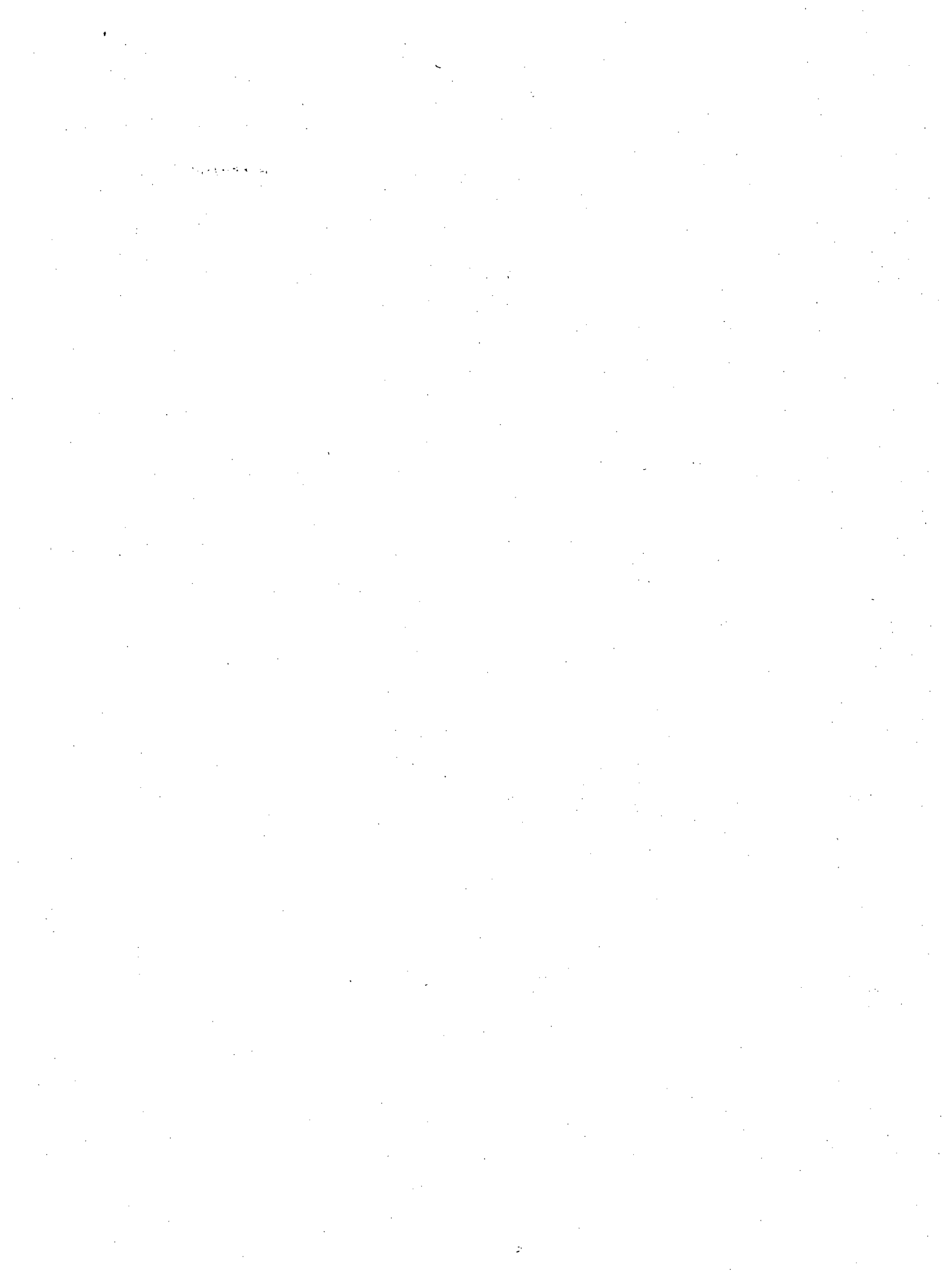


APPENDIX A  
DESCRIPTION OF CODE VERSIONS

Many versions of the code were created during the development of COBRA/TRAC. A brief description of the major code versions is presented in Table A.1 to inform the reader of the major differences between the various code versions.

TABLE A.1. Description of Code Versions

<u>Code Version</u>	<u>Description</u>
Cycle 8 ~Jan 1981	Consisted of TRAC P1A and COBRA-TF. The hydrodynamic models were nearly completely developed in this version and have changed very little since. This version contained an early form of the rezoning quench front rod model.
Cycle 10 ~June 1981	Same as cycle 8 except the fuel rod conduction rezoning models were rewritten. The dynamic gap conductance model was added in this version.
Cycle 11 ~Jan 1982	Liquid turbulence model added. TRAC P1A was replaced with TRAC PD2. An improved top quench front model was incorporated. The overlay structure of the code was changed to accommodate larger problems.
Cycle 12 ~Sept 1982	Vapor turbulence model added. Metal water reaction heat source added. Miscellaneous corrections.
Cycle 13 ~Nov 1982	Cleaned up version for release.



DISTRIBUTION

No. of  
Copies

No. of  
Copies

OFFSITE

ONSITE

335 U.S. Nuclear Regulatory  
Commission  
Division of Technical  
Information and Document  
Control  
7920 Norfolk Avenue  
Bethesda, MD 20014

50 Pacific Northwest Laboratory  
MJ Thurgood (43)  
Publishing Coordination ( 2 )  
Technical Information ED ( 5 )

5 James Han  
U.S. Nuclear Regulatory  
Commission  
7915 Eastern Ave.  
M/S 1130-SS  
Silver Spring, MD 20910



<b>NRC FORM 335</b> (11-81)		<b>U.S. NUCLEAR REGULATORY COMMISSION</b> <b>BIBLIOGRAPHIC DATA SHEET</b>		<b>1. REPORT NUMBER (Assigned by DDC)</b> NUREG/CR-3046, Vol. 4 PNL-4385	
<b>4. TITLE AND SUBTITLE (Add Volume No., if appropriate)</b> COBRA/TRAC - A Thermal Hydraulics Code for Transient Analysis of Nuclear Reactor Vessels and Primary Coolant Systems - Vol. 4: Developmental Assessment and Data				<b>2. (Leave blank)</b>	
<b>7. AUTHOR(S)</b> M.J. Thurgood, T.E. Guidotti, G.A. Sly, J.M. Kelly, R.J. Kohrt, K.R. Crowell, C.A. Wilkins, J.M. Cuta, S.H. Bian				<b>5. DATE REPORT COMPLETED</b> MONTH   YEAR November   1982	
<b>9. PERFORMING ORGANIZATION NAME AND MAILING ADDRESS (Include Zip Code)</b> Pacific Northwest Laboratory PO Box 999 Richland, Washington 99352				<b>DATE REPORT ISSUED</b> MONTH   YEAR March   1983	
<b>12. SPONSORING ORGANIZATION NAME AND MAILING ADDRESS (Include Zip Code)</b> Division of Accident Evaluation Office of Nuclear Regulatory Research U.S. Nuclear Regulatory Commission Washington, DC 20555				<b>6. (Leave blank)</b>	
<b>13. TYPE OF REPORT</b> Computer Code Manual				<b>PERIOD COVERED (Inclusive dates)</b>	
<b>15. SUPPLEMENTARY NOTES</b>				<b>8. (Leave blank)</b>	
<b>16. ABSTRACT (200 words or less)</b> The COBRA/TRAC computer program has been developed to predict the thermal-hydraulic response of nuclear reactor primary coolant systems to small and large break loss-of-coolant accidents and other anticipated transients. The code solves the compressible three-dimensional, two-fluid, three-field equations for two-phase flow in the reactor vessel. The three fields are the vapor field, the continuous liquid field, and the liquid drop field. A five-equation drift flux model is used to model fluid flow in the primary system piping, pressurizer, pumps, and accumulators. The heat generation rate of the core is specified by input and no reactor kinetics calculations are included in the solution. This volume documents the major data comparisons made with COBRA/TRAC during the process of code development. These data comparisons were extremely useful in detecting programming errors and defining deficiencies in the code's physical models. The data comparisons presented in this volume document the results obtained on developmental versions of the code. A separate document will be released at a later date containing data comparisons run on the final released version of the code.				<b>10. PROJECT/TASK/WORK UNIT NO.</b>	
<b>17. KEY WORDS AND DOCUMENT ANALYSIS</b>				<b>11. FIN NO.</b> FIN B2391	
<b>17b. IDENTIFIERS/OPEN-ENDED TERMS</b>				<b>14. (Leave blank)</b>	
<b>18. AVAILABILITY STATEMENT</b> Unlimited		<b>19. SECURITY CLASS (This report)</b> Unclassified		<b>21. NO. OF PAGES</b>	
		<b>20. SECURITY CLASS (This page)</b> Unclassified		<b>22. PRICE</b> \$	





**UNITED STATES**  
**NUCLEAR REGULATORY COMMISSION**  
WASHINGTON, D.C. 20555

OFFICIAL BUSINESS  
PENALTY FOR PRIVATE USE, \$300

FOURTH-CLASS MAIL  
POSTAGE & FEES PAID  
USNRC  
WASH. D. C.  
PERMIT No. G-67